UNIVERSITY OF SOUTHAMPTON

FACULTY OF ENGINEERING, SCIENCE AND MATHEMATICS

Institute of Sound and Vibration Research

Independent Component Analysis and source analysis of Auditory Evoked Potentials for assessment of Cochlear Implant users

by

Norma Castañeda Villa

Thesis for the degree of Doctor of Philosophy

June 2009

UNIVERSITY OF SOUTHAMPTON

ABSTRACT

FACULTY OF ENGINEERING,
SCIENCE AND MATHEMATICS
INSTITUTE OF SOUND AND VIBRATION RESEARCH

Doctor of Philosophy

INDEPENDENT COMPONENT ANALYSIS AND SOURCE ANALYSIS OF AUDITORY EVOKED POTENTIALS FOR ASSESSMENT OF COCHLEAR IMPLANT USERS

by Norma Castañeda Villa

Source analysis of the Auditory Evoked Potential (AEP) has been used before to evaluate the maturation of the auditory system in both adult and children; in the same way, this technique could be applied to ongoing EEG recordings, in response to acoustic specific frequency stimuli, from children with cochlear implants (CI). This is done in oder to objectively assess the performance of this electronic device and the maturation of the child's hearing. However, these recordings are contaminated by an artifact produced by the normal operation of the CI; this artifact in particular makes the detection and analysis of AEPs much harder and generates errors in the source analysis process. The artifact can be spatially filtered using Independent Component Analysis (ICA); in this research, three different ICA algorithms were compared in order to establish the more suited algorithm to remove the CI artifact. Additionally, we show that pre-processing the EEG recording, using a temporal ICA algorithm, facilitates not only the identification of the AEP peaks but also the source analysis procedure. From results obtained in this research and limited dataset of CI vs normal recordings, it is possible to conclude that the AEPs source locations change from the inferior temporal areas in the first 2 years after implantation to the superior temporal area after three years using the CIs, close to the locations obtained in normal hearing children. It is intended that the results of this research are used as an objective technique for a general evaluation of the performance of children with CIs.

Content

List of figures

List of tables

Academic Thesis: Declaration Of Authorship

I Norma Castañeda Villa declare that this thesis and the work presented in it are my own and has been generated by me as the result of my own original research.

Independent Component Analysis and source analysis of Auditory Evoked Potentials for assessment of Cochlear Implant users

I confirm that:

1. This work was done wholly or mainly while in candidature for a research degree at this University;

2. Where any part of this thesis has previously been submitted for a degree or any other qualification at this University or any other institution, this has been clearly stated;

3. Where I have consulted the published work of others, this is always clearly attributed;

4. Where I have quoted from the work of others, the source is always given. With the exception of such quotations, this thesis is entirely my own work;

5. I have acknowledged all main sources of help;

6. Where the thesis is based on work done by myself jointly with others, I have made clear exactly what was done by others and what I have contributed myself;

7. Either none of this work has been published before submission, or parts of this work have been published as: [please list references below]:

Signed:

Date: 02 July 2010…….

Acknowledgements

My sincere thank to my supervisor, Dr Christopher James for his excellent direction, encouragement and ideas throughout my research. His support and continuous guidance enabled me to complete my research successfully. I am also highly thankful to Prof Paul White for his valuable suggestions throughout this study. My gratitude also goes to my colleagues and staff members of Signal Processing and Control Group at ISVR.

I want to thank Prof. Juan Manuel Cornejo, Prof. Pilar Granados and all my Mexican colleagues from UAM-I for all their help, support, and interest whilst I was in UK. I also wish to thank my friends in Mexico and now in many parts of the world who always encouraged me to follow. Especially, I would like to give thanks to Dr Miguel Rodriguez for providing me access to Curry software, fundamental in the last part of my research. I was supported by grants from PROMEP No. PROMEP/103.5/06/2055, UAM: 35062 and UAM's scholarship.

I would like to express my gratitude to my parents and sisters for all their advice and unconditional support every day, not only during the last four years but also during all of my life.

Norma Castañeda Villa

List of symbols and Abbreviations

General notation

$\mathbf{A}$	Mixing matrix
$\mathbf{D}$	Dissimilarity matrix
$\mathbf{W}$	De-mixing matrix
$\mathbf{M}$	Whitening matrix
$\mathbf{Q}$	Rotation matrix
$\mathbf{S}$	Separability matrix
$\mathbf{G}$	Spherig matrix
$\mathbf{C}$	Covariance matrix
$\mathbf{R}$	Correlation matrix
$\mathbf{A}^{\mathrm{T}}$	Transpose of matrix $\mathbf{A}$
$\mathbf{A}^{+}$	Pseudo-inverse of matrix $\mathbf{A}$
$\mathbf{I}$	Identity matrix
$\mathbf{V}$	Orthogonal matrix
$\mathbf{E}$	Orthonormal matrix
$\mathbf{P}$	Permutation matrix
$\mathbf{\Lambda}$	Diagonal matrix
$\boldsymbol{s}(t)$	Continuous time signal sources
$\boldsymbol{x}(t)$	Continuous time signal measurements
$\hat{\boldsymbol{s}}(t)$	estimate sources
$\mathbf{s}$	Vector of source signal
$\mathbf{x}$	Vector of measurement signals
α	Angle of rotation
σ	Standard deviation
$H(X)$	Entropy of variable X
$J(X)$	Negentropy of variable X
$I(X, Y)$	Mutual Information between variable X and Y
X	Random variable
$E\{X\}$	Expected value of variable X
I_q	Cluster quality index
$P_X(X)$	Probability density function of variable X

$P(X, Y)$	Joint probability density function between variables X and Y
SE_B	Bootstrap estimate of the standard error
dij	Dissimilarity or distance between i and j
Δij	Similarity between i and j
rij	Correlation coefficient between i and j
τ	Time delay
$\langle . \rangle$	Time average
$Kurt$	kurtosis
Am	Amari index
h	height in a dendrogram
N	Number of parameters
k	constant

Source analysis notation

$\boldsymbol{E}$	Electrical field
$\boldsymbol{B}$	Magnetic field
$\boldsymbol{J}$	Neural currents density
$\boldsymbol{H}$	Magnetic field due to macroscopic currents
$\boldsymbol{D}$	Electric displacement
$\boldsymbol{G}$	Green's function
$\boldsymbol{P}$	current dipole moment
$\mathbf{r}$	Location of the current
$\boldsymbol{V}$	Electrical potential
V	Sphere volume
σ	Electrical conductivity
ρ	Charge density
ε	Permittivity
μ	Permeability
S	Dipole
θ, φ	Angle of orientation of dipole
∇	Gradient

Abbreviations

AC	Alternating current
ACE	Advanced Combination Encoder
ACNS	American Clinical Neurophysiology Society
A-D	Analog to Digital
AEP	Auditory Evoked Potentials
BEM	Boundary Element Method
BOLD	Blood oxygenation level-dependent
BSS	Blind Source Separation
CAR	Common Average Reference
CE	Confidence ellipsoid
CI	Cochlear Implant
CIS	Continuous interleaved sampling
CT	Computer Tomography
D-A	Digital to analog
DC	Direct current
DSP	Digital Signal Processor
ECD	Equivalent Current Dipole
EEG	Electroencephalogram
EOG	Electrooculography
EP	Evoked Potential
ERP	Event related potential
FFT	Fast Fourier Transform
fMRI	functional Magnetic resonance imaging
HA	Hearing Aid
HOS	High order Statistics
i.d.d.	Independent identically distributed
IC	Independent Component
ICA	Independent Component Analysis
MEG	Magnetoencephalography
MGFP	Mean Global Field Power
MI	Mutual Information
MICA	Multidimensional ICA

MLE	Maximum likelihood estimation
MRA	Multi-resolution analysis
PAN	Pre-Auricular and Nasion electrodes system
PCA	Principal Components Analysis
pdf	Probability density function
Res. Dev.	Residual Deviation
SIR	Signal to interference ratio
SNR	Signal to noise rate
SOS	Second order Statistic
SPEAK	Spectral peak extraction
SVD	Singular Value Decomposition
TDSEP	Temporal Decorrelation Source Separation
WT	Wavelet Transform

Chapter 1.

Introduction

The overall objective of this research is to develop a procedure to evaluate objectively the maturation of the auditory system of children with cochlear implants (CIs). The benefits of this electronic device, which assists in the rehabilitation of deaf people, are assessed by the technique know as Independent Component Analysis (ICA) followed by source analysis of the Auditory Evoked Potentials (AEP).

Different methods of measuring the effectiveness of a CI in deaf children have been devised of late, however most of these are subjective methods (Pure Tone Average Audiometry, language comprehension and language production scores [99;122]). It is important to have an objective method to follow the maturation of the auditory system of an implanted child-CI as a complete system; this procedure could help in monitoring the quality of the sound generated by the CI on uncooperative subjects, such as children. Furthermore this method should be suitable to be implemented in a practical clinic. Multi-channel AEP recordings and source analysis have been used to objectively study the maturation of the auditory system in young children. The child-CI system could be studied in the same way, however this is problematic as normal operation of the CI generates an electrical artifact; the CI artifact generally masks, either partially or totally, the brain auditory response and so results in errors in the both the analysis and source analysis of the auditory response.

To solve this problem ICA is applied prior to the source analysis step of AEPs. Assuming linear and instantaneous volume conduction in the brain, the use of ICA algorithms for source separation from EEG data is plausible. The goal of ICA is to recover independent sources using only sensor observations, which in our case is the scalp EEG from children CI users; the sources to be extracted are the AEPs and the CI artifact. The measurements at the electrodes $\boldsymbol{x}(t)$ are given by are a linear mixture of

the independent sources $\boldsymbol{s}(t)$, such that $\boldsymbol{x}(t)=\mathbf{A}\boldsymbol{s}(t)$. $\mathbf{A}$ is the mixing matrix which depends on the conductivity characteristics of the brain and where the electrodes are placed. ICA calculates the de-mixing matrix, $\mathbf{W}$, from the observations $\boldsymbol{x}(t)$ and estimates the original sources as $\hat{\boldsymbol{s}}(t)=\mathbf{W}\boldsymbol{x}(t)$. ICA tells us what parts of the scalp are most responsible for the activity (auditory in our case), identified by a spatial projection of the Independent Components (ICs) onto the electrodes. The columns of $\mathbf{W}^{-1}$ are used to give the topographic maps (spatial weighting of the activity) that are used to facilitate the source analysis process.

Multi-channel AEP recordings provide temporal resolution for the chronological aspects of brain plasticity. However, looking for a complete indicator of the auditory neuroplasticity in children with CIs, it is necessary to increase the spatial resolution for the source analysis, in order to solve the so-called inverse problem. This problem (the search of unknown source or sources underlying the scalp measurements) is solved by first finding a solution of the forward problem (how the electric potentials measured at the scalp arise from known sources). The electrical potential is computed using the quasi-static approximation of Maxwell's equations (which state the fundamentals of electricity and magnetism); where the potential is obtained by solving Poisson's equation with proper boundary conditions. Subsequently, to assess the auditory neuroplasticity in children with CIs, the changes of the source analysis of the AEPs attributed to the length of time of use/implantation of the CI on the child will be used in this research.

The contributions of this research include: (1) the application of ICA to not only reduce the CI artifact (spatial filtering) but also to identify the AEP in children with CIs (source extraction); (2) to identify the most adequate ICA algorithm, as well as its parameters, for this type of biomedical signal analysis. Moreover, (3) to obtain a method for the robust identification of ICs with *physiological meaning* as well as the ICs associated with the CI artifact using the concept of Mutual Information and Cluster Analysis. Finally, (4) this research provides a basis for a practical, clinical procedure to assess the benefits of a CI following the changes of the (modelled) Equivalent Current Dipoles (ECD) of the AEPs, attributed to the length of time of use/implantation of the CI on the child.

This thesis is organized in the following way; Chapter 2 gives a review of the Audiological topics used in this research, including Auditory Evoked Potentials, auditory system maturation and Cochlear Implants, and describes the development of the auditory system after cochlear implantation. The description of the protocol for AEP recording, as well as a review of some signal processing techniques used to recover and analyse these biomedical signals are included in Chapter 3. Chapter 4 presents a brief overview of the statistical concepts necessary to understand the technique of BSS by ICA, used in the pre-processing of the AEPs. Moreover, it explains the theory of BSS in general and ICA in particular, and reviews the principal differences between three popular ICA algorithms (*FastICA, Infomax* and *TDSEP-ICA*). Chapter 5 describes the procedure used to select the optimal parameters of these three ICA algorithms mentioned above, for robust AEP component estimates. Chapter 6, which complements the previous chapter, shows the results of the assessment of the variability and performance of those algorithms applied to auditory response estimations. A novel procedure to choose ICs with physical and physiological meaning using Mutual Information, as similarity measure between estimates, and Cluster Analysis is included in chapter 7. Chapter 8 shows the results of using ICA not only to de-noise the AEP of children with CIs but also to assess the maturation of the auditory system in these children, using the topographic map of the ICs related with the auditory response. The basic theory of source analysis, beginning with the Maxwell's equations and following with an explanation of how the parameters for source analysis of the AEP were selected in this research are included in chapter 9; results of the changes in the location of the sources of the auditory response in accordance with the time of implantation are shown in this chapter. The final chapter, chapter 10, is dedicated to the principal conclusions and future work of this research.

During this research the following papers and abstract have been accepted in different specialist journal and conferences.

Journal Paper

N. Castaneda-Villa, J.M. Cornejo, and C. J. James. "*Independent Component Analysis for robust assessment of auditory system maturation in children with cochlear implants*" Cochlear Implant International Journal. Published Online: Feb 2009.

N. Castañeda-Villa and C. J. James "*Independent component analysis for Auditory evoked potentials and cochlear implant artifact estimation: a comparison between High and Second order statistic algorithms*". (In preparation)

Conference papers

C.J. James and N. Castañeda-Villa. *"ICA of auditory evoked potentials of children with cochlear implants: component selection"*. 3rd International Conference MEDSIP 2006 Advances in Medical, Signal and Information Processing, 17-19 July, Glasgow, Scotland.

N. Castañeda-Villa and C. J. James. *"Objective source selection in Blind Source Separation of AEPs in children with Cochlear Implants"* 29th Annual International Conference of the IEEE Engineering in Medicine and Biology Society, 23-26 August 2007, Lyon France.

N. Castañeda-Villa and C. J. James. *"Differences in source analysis accuracy of AEP generators following FastICA and TDSEP-ICA de-noising"* 4th International Conference MEDSIP 2008 Advances in Medical, Signal and Information Processing, 14-16 July 2008 Santa Margherita Ligure, Italia.

N. Castañeda-Villa and C. J. James *"The selection of optimal ICA algorithm parameters for robust AEP component estimates using 3 popular ICA algorithms"* 30th Annual International Conference of the IEEE Engineering in Medicine and Biology Society "Personalized Healthcare through Technology" 20-24 August 2008 Vancouver, British Columbia.

Conference Abstracts

N. Castaneda-Villa, J.M. Cornejo-Cruz, and C. J. James. *"Assessment of the neurological maturation in children with CIs: Identification of AEPs by ICA"*. 10th International Conference on Cochlear Implants and Other Implantable Auditory Technologies, 10-12 April 2008, en San Diego, California, US (Poster).

N. Castaneda-Villa, J.M. Cornejo, P. Granados and C. Tirado. *"Cochlear implant fitting using middle latency auditory evoked potentials"* 11th International Conference on Cochlear Implants in Children, Charlotte NC, USA, 11-14 April 2008 (Oral Presentation)

N. Castañeda, C. James and J.M. Cornejo. *"Objective assessment of CI users by source analysis of LLAEPs peak P_1"* 12th International Conference on Cochlear Implants in Children, 17-20 June, 2009 Seattle, Washington.

Chapter 2.

An overview of Audiological topics

Two major audiological topics are included in this research: Auditory Evoked Potentials (AEPs) and Cochlear Implants (CIs). An AEP is the response of the auditory system (in the brain) produced by a sound [58], this response is suitable to be measured on the scalp with the appropriate techniques such as averaging out the spontaneous electroencephalography (EEG) [100]. The clinical applications of the AEPs are diverse, such as: estimation of the auditory sensitivity in very young children, frequency specific estimation of the auditory sensitivity in older children and adults, and to evaluate the maturation of the auditory system.

After setting forth the theory of AEPs, the general concepts of EEG and Evoked Potentials (EPs) in general, a description of the way to evaluate the maturation of the auditory system using AEPs is incorporated. A description of the apparatus used in the rehabilitation of deaf people known as CI is included; its main parts, as well as the principal stimulation strategies used by this electronic device to emulate the human cochlea, are then explained. Finally, a description on the auditory system maturation after cochlear implantation is incorporated.

2.1 The EEG

The EEG is the recording of the spontaneous electrical activity of the brain; this activity is recorded from electrodes on the scalp [11]. The changes in the characteristics of the EGG (amplitude and frequency) reveal the subject’s state of consciousness; for example, EEG signals with large amplitude and low frequency content are typical during deep sleep and widespread EEG signals with oscillation near to sinusoidal are characteristic in eyes closed waking. More advanced techniques used in clinical EEG can identify neurological disorders such as Alzheimer's disease, epilepsy, brain tumor and sleep disorders [100].

EEG analysis is usually described in terms of frequency bands. Most of the common cerebral signals are in the range of 1-30 Hz; in clinical settings activity below or above this range is generally considered an artifact. Examples of wave pattern recognized on EEG are: delta (up to 3 Hz), theta (between 4 and 7 Hz), alpha (8-12 Hz), beta (13 to 20 Hz) and gamma (20 to 30 Hz). Most of the EEG waves have an inverse relationship between amplitude and frequency, for example alcohol or drugs consumption may cause a reduction in the frequency and an increase in the amplitude of EEG waves [98].

Delta tends to be the highest in amplitude and slower wave, its location is frontal in adults and posterior in children; this wave could reveal subcortical lesions in the elderly. Theta waves are seen normally in young children, there location may involve many lobes of the brain and can be lateralized or diffuse [98]. Alpha waves are widely used in the clinical practice; these waves are usually identified in a relaxed awake subject, its amplitude is typically 20-50 μV with location in posterior regions of head. Other alpha waves may occur in comatose subjects with cerebral lesion or with patients under halothane anesthesia [100]. Beta waves have a frontal and symmetrical distribution and low amplitude, they are present in the EEG signal when the subject is concentrating; these waves are accentuated by drug consumption such as barbiturates.

The basic EEG equipment recommended by the American Clinical Neurophysiology Society (ACNS) includes electrodes, connecting wires, amplifiers, a computer control module, and a display device [11]. Each electrode is connected to one input of a differential amplifier and a reference electrode is connected to the other input. In a digital EEG system, the amplified signal is digitized by an analog to digital (A-D) converter (sampling rate between 256 and 512 Hz and resolution of 12 bits or more), after the signal is passed through an anti-aliasing filter. For standard recordings the settings for the low pass filter should be no higher than 1 Hz (-3dB) and the high pass filter should be no lower than 70 Hz (-3dB). The recorded EEG can be visualized on a computer screen or on paper [10]. Different type of EEG activity occurs simultaneously at diverse locations on the head and so encourage the use of multiple electrodes for simultaneous recordings.

The type of electrodes used in the EEG recordings is fundamental to acquire a good signal; recording electrodes should be free of acquired inherent noise and they should not attenuate signals between 0.5 and 70 Hz [11]. Disk and needle are some of the types of electrodes used in the EEG recording. Needle electrodes are made from a bar of stainless steel, whilst disk electrodes are made from silver silver-chloride or gold; the diameter of disk electrodes can vary from 4 to 10 mm, smaller diameter electrode are optimal to be used with infants. The most commonly used electrodes in AEPs recordings are the disk electrodes, silver-chloride electrodes are recommended for recording very slow auditory responses. All the electrodes are designed to conduct electrical activity at the frequency range of the AEPs.

In order to increase the quality of the recordings, it is necessary to introduce an electrolyte (electrically conductive medium) between the scalp and the electrode. Different electrolytes for EEG are commercially available; gels, conductive pastes and creams. Most of the disk electrodes contain a hole so that the electrolyte can be added after the electrode has been attached on the head.

Electrode attachment is checked by the interelectrode impedances; this impedance is measured applying a small electrical AC current (30 Hz) to one of the electrodes, and determining the amount of current reaching a second electrode. The interelectrode impedance will be lower if the skin has been cleaned or rubbed to remove surface oil and superficial layers of the epidermis; it is possible to use alcohol or acetone for this purpose. Interelectrode impedances can be reduced to below 3 kΩ if the skin preparation and electrode selection is done well; impedances should not exceed 5 kΩ. The quality of the AEPs recordings is highly dependent on low and balanced electrode impedances. The ACNS recommends checking the impedances as a routine prerecording procedure and rechecking it during the recording when the wave patterns might start to appear artifactual.

Most electrode sites in AEPs measurement can be designed by a specific system of electrode positioning which has been recommended for the ACNS; this standardized electrode placement system is know as the International 10-20 system [12].

2.1.1 International 10-20 electrodes system

The International 10-20 system uses particular anatomical landmarks (nasion inion and left and right preauricular points) to locate different sites for a given subject. The total distance between nasion (bridge of nose) and the inion (the occipital protuberance) is divided into 10% and 20% intervals. The point at the initial 10% of the distance away from the nasion is the electrode site 'Fpz'; this is generally used as ground in AEP recordings, the electrode site 'Fz' towards the rear an additional 20% of the total distance nasion to inion is the frontal midline, the site 'Cz' towards the back by another 20% is the coronal midline, etc.

This system is for 21 electrodes (see Figure 2.1); but it is designed so it can be used with additional electrodes (the extended 10-20 system). The nomenclature for the electrode positions is alphanumeric, consisting of one or two letters derived from names of underlying lobes of the brain, or other anatomic landmarks as auriculars and mastoids; this nomenclature provides a system of coordinates for positioning a designated electrode. The system places odd numbers for electrodes on the left hemisphere and even numbers on the right; a "z" identifies the electrodes in the middle line; two other relevant sites are the left and right mastoids (M1 and M2, respectively).

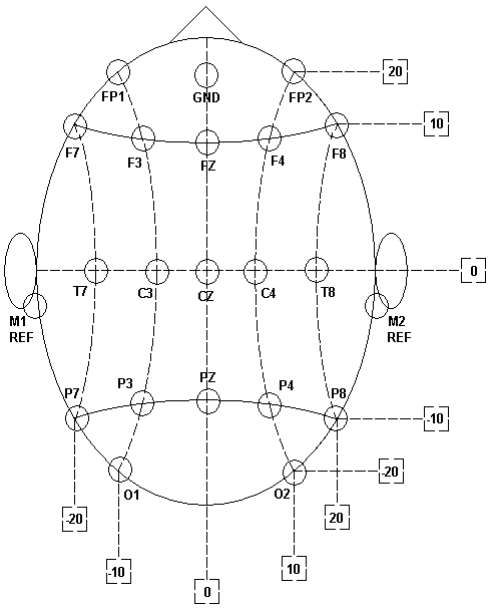

Figure 2.1 Electrode distribution in accordance with the standard international 10-20 system for the 21 electrodes; Fpz is generally used as ground and M1-M2 linked as reference in multi-channel AEPs recordings [32].

The number of electrodes needed is based on the type of activity to be recorded, the population studied, and the number of channels available. The American EEG Society [11] considers that the minimum number of channels required showing the areas producing most normal and abnormal EEG patterns are 16 simultaneous recording; another factor to decide the number of electrodes is the montage used.

The term ‘montage’ refers to the particular combination of electrodes examined at a specific point in the time; that to record the activity from all areas of the scalp. Montages are designated for 16, 18 and 20 channels [13]. Two standard montages can be used in EEG, bipolar and referential; bipolar montages are also so called differential. In a referential montage, the recording of the EEG from each single electrode is made with a neutral reference, whilst for a bipolar montage; two areas of the brain are recorded through two independent electrodes.

The analysis and interpretation of the EEG could be a problem when the signal is contaminated by artifacts. An artifact is electrical activity which is not part of the EEG. The most common artifacts come from the recording equipment, such as random fluctuations of the signal at 50 or 60 Hz (line noise) or problems with the electrodes. Line noise is generally identified by high voltage which produces saturation of the differential amplifiers; such behaviour is uncharacteristic of the brain activity.

2.1.2 EEG Artifacts

A general classification of EEG artifacts could be biological or external artifacts; blinking, cardiac and muscular artifacts are examples of the first type whilst high electrode impedances, line and background noise are examples of the second type. A frequent artifact is related to problems with the electrodes, broken electrodes or improperly attached to the head. Cardiac artifact is interference resulting from the heart QRS complex or pulse artifact which is a consequence of the blood pulsing through a vessel under an electrode; it could occurs due to the expansion and contraction of the scalp arteries [40]. Before the analysis and interpretation of the EEG, these artifacts must be eliminated; EEG artifact removal is dealt with in part in Chapter 4.

Whilst what has been discussed so far can be termed spontaneous EEG, another particular aspect of the EEG is Evoked Potentials, which involve the measurement of spontaneous EEG activity time-locked to the repetitive presentation of a specific stimulus; generally either auditory, visual, or somatosensory.

2.2 Evoked Potentials

According to the ACNS [14] an EP (some time known as an Event related potential, or ERP) is an electrical potential recorded from a human or animal following presentation of a stimulus. An EP can be used to assess peripheral sensory function and to evaluate the function of sensory pathways in the central nervous system. These potentials can be Auditory, Visual and/or Somatosensory, which have clinical applications to the diagnosis of diverse neurological disorders. Figure 2.2 shows the human cortex division, visual and auditory stimuli are integrated by the occipital and the temporal lobe respectably; the frontal lobe controls motor functions whilst the parietal lobe processes somatosensory stimuli.

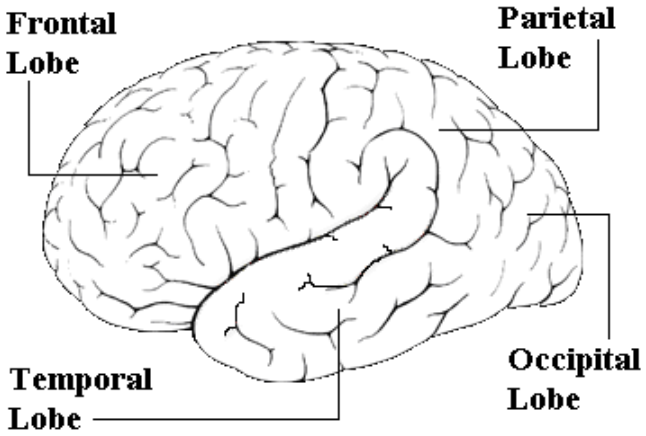

Figure 2.2 Human cerebral cortex division; each lobe is specialized in processing different stimuli; the temporal lobe integrates auditory stimuli whilst the occipital lobe integrates visual stimuli. Motor functions depend on the frontal lobe and the parietal lobe processes somatosensory stimuli [100].

Although the EP amplitude is small (from less than one to several μVs), the potentials are time-locked with the stimuli, then it is feasible to use a coherent average to recover them from background noise. Additionally to the basic EEG equipment mentioned before the clinical evoked potential equipment includes an averager; this should average several epochs or trials of EEG in order to recover the EPs. The onset

of the averaging sweep should be synchronised with stimulus production; depending on the type of EPs to record, two or four channels are usually required. A mechanism to reject artifacts is indispensable; the criterion for artifact rejecting is generally simply by amplitude (those trials that exceed the limits of the A-D converter are excluded from the averaging process). The replication of the EP is essential to demonstrate that responses are consistently repeatable and therefore are of neuronal origin and not artifact.

The EPs in children in particular have demonstrated a great clinical utility because of the possibility to objectively assess the development of neurological function is these subjects. All types of standard EPs have been shown to mature and develop during infancy and childhood; such as Auditory Brainstem Evoked Potentials (ABR), Visual Evoked Potentials (VEP) and Somatosensory Evoked Potentials (SEP) these have been established as clinically useful in infants and children [14].

2.3 Auditory Evoked Potentials

An Auditory Evoked Potential is the response of one or more parts of the auditory system (which consists of the ear, the auditory nerve and the auditory cortex) which is evoked by an acoustic stimulus [58]. Since the stimulus is sound, the response occurs somewhere in the auditory system; on analyzing the characteristic of the response (generally amplitude and latencies of the waveforms), it is possible to establish the region or regions in the auditory system which generated the response.

The principal sounds used to elicit AEPs are clicks, tone-bursts, tone-pips (see Figure 2.3) and speech. The standard auditory stimuli used in AEP are clicks; these stimuli are brief wideband sounds of varying amplitude (intensity level) but constant polarity and duration. Click improves synchronous neural activity and is effective to generate rapid evoked responses. Their repetition time generally used in infants to evoke an auditory response is 10/sec. Tone-bursts are pure tones enveloped with a trapezoid and tone-pips are pure tone enveloped with a rhomboid. The typical frequencies selected in both stimuli are the frequencies included in the audiometric range (tones at octave frequencies from 125 to 8000 Hz). These stimuli are optimal to

generate slow evoked responses. The selection of envelope characteristics (rise-decay and plateau times) and the specific frequency tone is based on the objective of the test.

In general the repetition time should be as fast as possible, in order to reduce the test time but without sacrificing the quality of the auditory response. The fundamental principle is that fast repetition times generate rapid auditory response whilst slow repetition times evoke slow responses. There are not standard numbers of stimuli (repetitions) in AEPs measurement; this number depends on the amplitude of the response and the amount of background noise in the recording; fewer repetitions are necessary with larger signals and/or smaller noise.

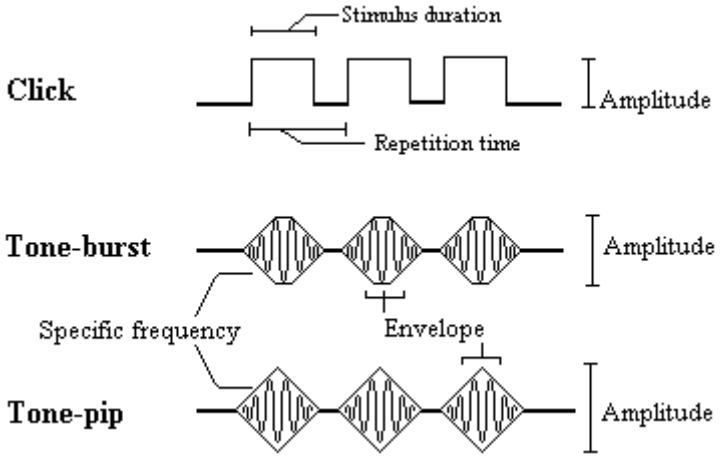

Figure 2.3 Principal stimuli used to elicit AEPs, stimulus clicks are wideband sounds whilst tone-burst and tone-pips are specific frequency sounds. The stimulus' duration, the repetition time as well as the amplitude and frequency of those sounds produce different components of the AEPs.

The stimuli are usually delivered to the subjects under test either through headphones or speakers; in the case of children it is important to adapt the headphones to assure a proper fit and to avoid collapse of the external auditory canal. The intensity levels (amplitude) of the stimuli are calibrated in dB_{SPL} (decibels Sound Pressure Level), where the sound pressure of a sound is measured relative to a reference pressure value (20 μPa). The instruments used to calibrate the intensity level of the stimuli are sound level meter, microphones and an artificial ear.

The AEPs are generally recorded in an attenuated sound room such as an anechoic chamber, to ensure that the subject being tested is not influenced by external or internal reflected sound or noise. An anechoic chamber is a shielded room designed

to attenuate sound and/or electromagnetic signals. Anechoic chambers absorb sound echoes produced by internal reflections of a room; additionally, the anechoic chambers also provide a shielded environment for Radio Frequency and microwaves [62].

As mentioned before, the scalp recording of the AEPs require three or four electrodes placed according to the International 10-20 system [10], the electrode connected to the positive input of the differential amplifier is generally the Cz electrode. In humans, AEPs must consist of at least 15 reproducible waveforms (see Figure 2.4). The analysis of the AEPs is based on latency and amplitude criteria. In general, the amplitude of each wave of the AEPs is a function of the intensity level of the stimuli such that sounds with a higher intensity produce a larger auditory response. The latency (time at which each one of the waves of the AEP appear after the stimulation) is shorter with higher intensities. The AEPs can be classified in accordance with their latency, such as Short Latency Auditory Evoked Potentials or ABRs, Middle Latency Auditory Evoked Potentials (MLAEPs) and Long Latency Auditory Evoked Potentials (LLAEPs) [58]; it is the latter type that are used in this research.

The peaks of AEPs are labelled with Roman numeral for ABR and capital P's and N's for MLAEP and LLAEP. ABRs, associated with the eighth cranial nerve and the auditory brainstem, are followed by the MLAEP which neural generators are in the upper brainstem and/or the auditory cortex. It is now possible to identify the LLAEP which includes the *slow* and the *late* cortical auditory response, Figure 2.4 shows only the *slow* waveforms; the LLAEP is originated in the auditory cortex [10].

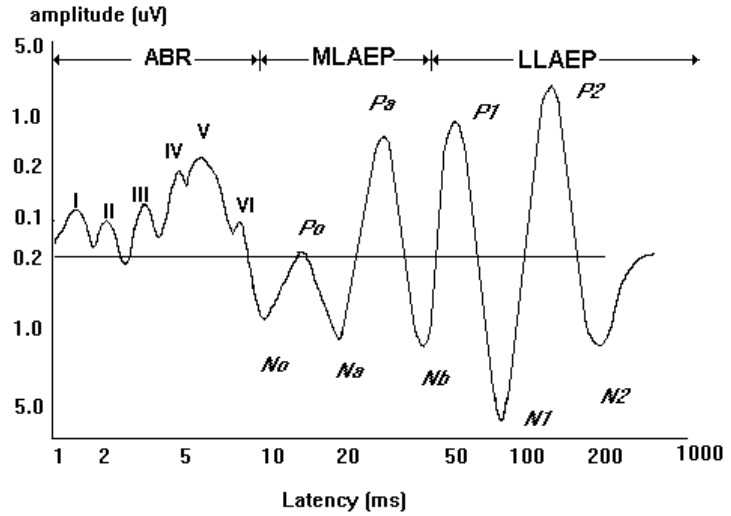

Figure 2.4 Auditory Evoked Potential classification: Auditory Brainstem Response (ABR), Middle Latency Auditory Evoked Potential (MLAEP) and Long Latency Auditory Evoked Potential (LLAEP); Cz electrode connected to the positive input of the differential amplifier [15].

The clinical applications of these potentials are varied, for example: newborn auditory screening [14], the objective determination of auditory thresholds in infants and children who are difficult to test with standard audiometric techniques [21], monitoring of anaesthesia levels and evaluation of the auditory system maturation [44;58;132]. Recently, AEPs have been used to evaluate Hearing Aids (HA) and CIs [84;111;112] as well as to investigate mental disorders such Schizophrenia and Alzheimer's disease [57;113]. The following paragraphs set forth each one of the AEPs mentioned; including their measurement parameters, main characteristics, generators and clinical applications.

A. ABR

The first components or generator of the AEPs occur between 1 and 10 ms post stimulus. This potential is known as the ABR and is produced by a brief sound, a click of varying intensity, constant polarity and duration (0.1 ms) and typically a stimulus rate of 10/sec. The number of stimuli necessary to recover this response is variable, from 500 to 4000; fewer stimuli are needed with normal hearing and quite subjects and at high intensities.

The electrode montage conventionally used in ABR recording is with the negative input of the differential amplifier connected to the mastoid of the stimulus

side (ipsilateral recording), whilst the positive input of the differential amplifier connected to the vertex (Cz electrode) or the midline forehead near the Fz site; the ground can be localized in the forehead (Fpz) or on the contralateral mastoid.

ABR is one of the most common audiological tests recently used because of its reliability and independence from the patient's state of arousal. It is possible to identify five or six peaks in ABR; each peak is labelled with a Roman numeral from I to V or VI. The ABR is generally used to determinate auditory thresholds in very young children or those difficult to test by traditional methods; as well as to detect neurological abnormalities in the auditory nerve and the brainstem.

The neural generators of the ABR waveforms (see Figure 2.4) begin with the distal and proximal portion of auditory nerve (wave I and II), wave III is originated in the cochlear nucleus whilst the superior olivary complex generates wave IV, finally wave V is associated with the lateral lemniscus [105].

B. MLAEP

At between 10 and 50 ms the MLAEP is recorded; clicks or brief duration pure tone stimulus as tone-bursts are appropriate stimuli to evoke this response. The repetition time is generally 7.1/sec and the number of stimuli is variable, depending on size of the response and background noise.

The nomenclature used to label the peaks of the MLAEP is a capital letter "P" for positive voltages and a capital letter "N" for negative voltages (considering the vertex as positive). The sequence of peaks and valleys is denoted alphabetically; N_a, P_a, N_b and P_b (see Figure 2.4). The MLAEP is recorded with electrodes placed at Cz and M1 or M2 electrodes (contralateral to the stimuli). The number of stimuli to elicit a clear response is approximately 1000.

The principal clinical applications associated with this potential are frequency-specific estimation of auditory sensitivity in both older children and adults and as an indicator of levels of anaesthesia [82]. The generators of the MLAEP are in the

thalamus and primary auditory cortex. The P_a peak arises from the posterior temporal lobe and the thalamic medial geniculate body could be the generator of the N_a components. There is controversy about the possible generators for the rest of the MLAEP [58].

C. LLAEP

The LLAEP appears from 50 to 250 ms after stimulation; tone-bursts are used to elicit this response, the stimuli duration depends on the application but is generally 10 ms for the rise-decay time and 30 ms for the plateau and a stimulus rate of 1.1/sec [58].

The amplitude of these waves is larger than ABR and MLAEP amplitudes, about 3-10 μV or larger (see Figure 2.4). As before, the peaks of LLAEP are labelled with capital letters "P" and "N" for positive and negative peaks respectively; the sequence of waves is denoted by numbers, P_1, N_1, P_2 and N_2. These waves are known as *slow* cortical waves because they appear before the late cortical waves (for example the P_{300}) [82]. *Slow* cortical waves are elicited by a repetitive stimulus of at least one stimulus per second; the changes of these waves are best studied using the latency of peaks because the amplitude is much more variable between subjects.

The LLAEP is a response from the central auditory system and optimally responds to tone-burst stimuli of relatively long duration, greater than 5ms. The LLAEP is also named the "obligatory potential" because is determined by the physical characteristics of the stimulus, such as amplitude and frequency as well as stimulus duration and repetition time [67]; this implies that a slight change in certain stimulus characteristic can modify the response. The LLAEP, along with the ABR and MLAEP, are all exogenous responses [96], this means that are dependent on stimulus characteristics and are independent of the subject attending; in other words, it is not necessary that the subject performs a specific task such as for the P300 (oddball paradigm) [21]. LLAEP can be recorded from an awake subject who is very oblivious to the sound presented, because of this many researchers record these potentials whilst the subject is reading something or watching a TV program without sound [105].

Although LLAEP does not depend on a specific task or the patient's cooperation, it could be susceptible to subject condition and drugs.

This potential has been used in the diagnosis of neurological disorders, for example some waves of the LLAEP could be absent in mental disorders as Alzheimer's disease [57]. In Schizophrenia patients, N_1 latency could be increased whilst P_2 latency and N_1-P_2 inter-peak latency could be reduced [113]. LLAEP has been used to assess higher level auditory system functions [67] and as a frequency specific estimator of hearing sensitivity [119]. Purdy and Kelly, 2001 [111] used LLAEP as an objective technique for HA fitting in children. These authors compared aided (with HA) versus unaided (without HA) LLAEP waveforms; they identified the P_1 wave only when the children were wearing their HAs; the test stimuli in this research was a tone burst at 1000 Hz and 80 dB_{SPL} delivered binaurally.

The principal generator of LLAEP waves in adults is located within the temporal cortex, for example intracerebral and magnetic recordings in humans demonstrate that P_1 has an origin in the lateral portion of Heschl's gyrus whilst N_1 is originated in the auditory superior temporal cortex [85].

In the following sections the generators of P_1 are revised, general concepts about the maturation of the auditory system, and how AEPs have been used to evaluate the auditory system maturation is explained too.

2.4 Generators of the P_1 peak

This section explains the different generators or components (cerebral process) which constitute the peak between 50 and 150 ms of the LLAEP, known as the P_1 peak. At least six different cerebral processes contribute to form the P_1 peak. The following paragraphs describe the three "obligatory" components of this peak which depend on the physical and temporal features of the stimulus and by the general state of the subject [96].

A. Generator 1, with peak latency at 100 ms and maximally recorded from the fronto-central scalp, is generated in the cortex of the supratemporal plane. The degree of

frontal spread and of left-right asymmetry differs from subject to subject because of the variable orientation of the supratemporal plane between individuals. The amplitude of this element increases with increasing of stimulus intensity.

B. Generator 2 is composed by a positive wave at about 100 ms after stimulus and a negative wave at approximately 150 ms, generated probably at the superior temporal gyrus (see Figure 2.5) with maximum amplitude at the midtemporal electrodes. The radially oriented generator would be activated by connections from the primary auditory cortex and the thalamus. The effects of intensity and inter-stimulus interval are not clear in this element.

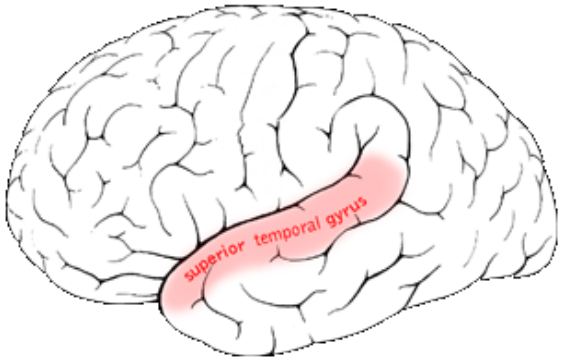

Figure 2.5 Superior temporal gyrus in the human brain [100].

C. Generator 3 is a vertex negative wave with peak latency at 100 ms post stimulus approximately; this element can be generated in the frontal motor and pre-motor cortex. The maximal amplitude of this component is at the vertex and the lateral central electrodes. Näätänen and Picton [96] suggest that the generator of this element is the cortical projection of a reticular process which facilitates motor activity. At stimulus intensities greater than 60 dB_{SPL} and inter stimulus interval greater than 4-5 s this component is easier to record.

D. The rest of the generators are related to the process of attention to the auditory stimulus; *generator 4* is the mismatch negativity, *generator 5* is the sensory- specific processing negativity and *generator 6* is a second element of the processing negativity [96]. These generators could be variations related to the attention of the subject; an unattended auditory stimulus could activate two areas of the cortex: the supratemporal plane (generator 1) and the superior temporal gyrus (generator 2); whilst an attendant

stimulus could facilitate interneural connections to increase the extension and degree of cortical activation.

2.5 Auditory System Maturation

One of the established ways to evaluate the maturation of the auditory system in children is by using the changes in latency and morphology of the AEP peaks [109;111;119]; maturation of the auditory system is dependent on the age of the subject and the auditory stimulation properties.

In ABR, various components mature in new born and preterm infants, such as wave shape, wave latency, inter-peak intervals and relative wave V/I amplitudes. The changes are more remarkable in infancy with peak latencies reaching near adult values at about 2 to 3 years of age; the ABR can be a measure of neurophysiological function and development.

Ponton, 1996 [107] described the LLAEP changes, in amplitude and latency from infancy to adulthood as a measurement of auditory cortex maturation. In the case of normal hearing children, from 5 to 9 years old, the typical response has a large positive peak around 100 ms (see Figure 2.6) labelled P_1 followed by a negative peak N_1, P_1-N_1 complex; the amplitude and latency of this positive peak decrease as a function of age. P1 peak is generated by thalamic and cortical sources.

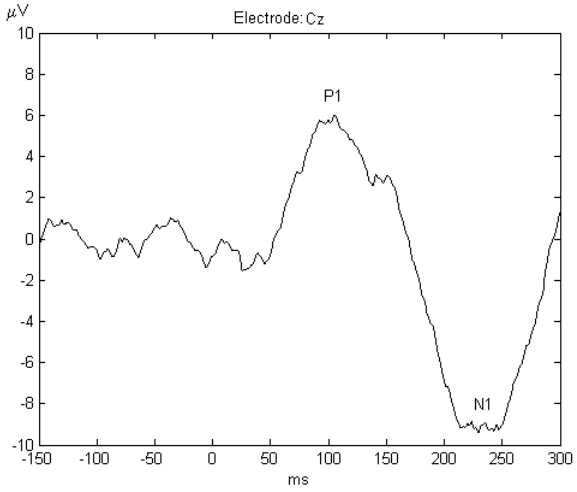

Figure 2.6 LLAEP waveform of a normal hearing child (7 y. o.), a positive peak around 100 ms (P_1) followed by a negative peak between 200 and 250 ms (N_1) characterize this waveform (N_1-P_1 complex).

This peak begins to spread out and finally divides into two positive peaks separated by a negative peak; from 10 years of age onwards, the LLAEPs are similar to an adult morphology.

The maturation of deeper layers of the auditory cortex may mature in the absence of sound stimulation whilst the maturation of superficial layers requires sound stimulation during a critical period [44].

2.6 Cochlear Implants

A CI emulates the principal function of the human cochlea, transforming an acoustic signal into pulses of electric current, to stimulate directly the auditory nerve [134]. The prime candidates for CIs must fulfil at least three conditions: they have severe hearing losses in both ears, their auditory nerve should be intact and functional and they have not benefitted significantly from HAs.

The CIs, surgically implanted, are divided into two principal parts, the external and the internal; the external part includes a microphone, a speech processor and a transmitter coil. The internal part includes a receiver and an array of electrodes, implanted in the base of the cochlea (see Figure 2.7).

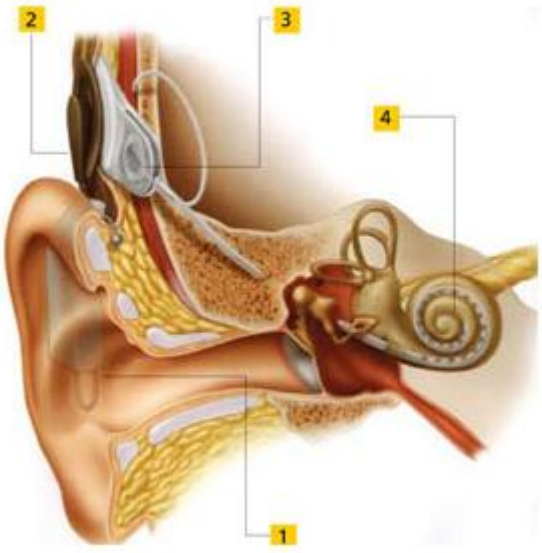

Figure 2.7 Parts of a cochlear implant: 1. Microphone and Speech Processor, 2. Transmitter coil, 3. Receiver, and 4. Electrode Array [7].

A. Speech processor

The speech processor is a *Digital Signal Processor* (DSP) chip that analyzes and codifies the sound signals. Once the microphone has received the sound, the speech processor should determine which electrodes must be activated. The *FFT* is the main strategy used to divide the signal into different frequency bands. In accordance with every each manufacturer of CIs, the parts of the speech processor could be different, but in general, it includes band-pass filters, envelope detectors, amplitude compressors and pulse modulators [114].

B. Electrodes and stimulation modes

The electrodes are made of a highly conductive material, such as platinum or iridium and are placed on a silicone rubber tip. In the 1970's, CIs were single-channel devices. These CIs included a band-pass filter at a frequency band relevant for speech (340-2700 Hz) and a modulator (16 kHz sinusoidal carrier) which is necessary for the inductive coupling across the skin; the improvement of the speech perception is achieved by the introduction of random patterns of neural discharges [114]. Nowadays, in accordance with manufacturers, the CIs can have 22 or 24 electrodes, which provide pitch perception and speech recognition to the users. In the case of CI with 24 electrodes, 22 electrodes are intra-cochlear and 2 electrodes are extra-cochlear or remote electrodes; the electrodes which are placed outside the cochlea function as ground electrodes. If one intra-cochlear electrode is stimulated with reference to a remote electrode, the stimulation is so called monopolar but if one intra-cochlear electrode is stimulated with reference to another intra-cochlear electrode the stimulation is termed bipolar [92].

C. Programming the speech processor

A trained audiologist is the professional responsible to program the CI for each user individually. The audiologists determine the Threshold (T) and Comfort (C) levels of electrical stimulation as well as the method that the CI transforms sound into electrical stimulation, in other words the audiologist must select the coding strategy most convenience for each CI user. The most important coding strategies are:

Continuous Interleaved Sampling, *Spectral peak extraction* and *Advanced Combination Encoder* [134].

i) *Continuous interleaved sampling (CIS).* In the CIS strategy, there is a pre-emphasis filter, after the microphone, which helps in the detection of weak consonants. The output of the pre-emphasis filter passes through band-pass channels which filter, compress and detect the envelopes of the speech; the envelope detection could be calculated by the *FFT* or using the *Hilbert Transform*. The output of band-pass channels modulates the amplitude of biphasic pulse trains. Modulated pulses from channels with low centre frequencies for the band-pass filter stimulate the apex of the electrodes array in the CI whilst modulated pulses from channels with high centre frequency stimulate basal electrodes in the implant; this stimulation mode replicates the tonotopic organization of a normal cochlea.

ii) *Spectral peak extraction (SPEAK).* In the *SPEAK* strategy, the signal transduced by the microphone is sent to a bank of 20 filters that have centre frequencies from 250 to 10 kHz. This strategy selects the output of the filters with the largest amplitude, to stimulate the corresponding electrodes; the number of maxima varies from 6 to 10. The stimuli are pulsed and the stimulation rate is approximately 250 Hz.

iii) *Advanced Combination Encoder (ACE).* This strategy combines the spectral maxima detection of *SPEAK* with higher stimulation rates, for example 14,400 pulse per second (pps), in order to avoid aliasing effects. The principal difference between *ACE* and the other strategies is that the number of maxima and electrode stimulated can be specified for each CI user. The number of maxima should be high enough to include all the fundamental spectral information of the signal but lower than the electrode used to conserve a high rate of stimulation.

A common characteristic of all these strategies is the interlacing of stimulus pulses across electrodes; this is to eliminate a vector summation of the electric fields from different electrodes simultaneously stimulated. The stimulation waveform of *CIS*, *SPEAK* and *ACE* strategies is pulsed which consists of square-wave biphasic pulses trains. As part of the process of fitting the CI, the Audiologist must select the

pulse rate, pulse duration and the range of frequencies for each band-pass filters. The general objective of these strategies is to stimulate the auditory nerve in such a manner that both the temporal and spectral characteristics of the acoustic signal are codified efficiently [102].

The eventual hearing performance of CI recipients depends on various factors; age at implantation, duration of deafness, number of electrodes inserted in the cochlea, and the therapy of rehabilitation, to name a few. The success of the implantation depends on the ability of the auditory system to extract useful auditory information from the electrical stimulation provided by the CIs [103]. There are different ways to evaluate this performance, for example, Pure-Tone Average Audiometry, Speech Scores and Language Scales, all of these tests are subjective [50]. The convenience of using LLAEP to asses the performance of these children is the objectivity; this is dealt with in the next section.

2.7 Auditory system maturation after cochlear implantation

Although the electrical stimulation of a CI, elicits the beginning of maturation of the auditory system in deaf children, this follows different patterns when compared to normal hearing children [108]. Ponton and Eggermont 1996 [107], observed prolonged P_1 latencies associated with auditory cortex immaturity in children fitted with CIs, and suggested that the delayed maturation is approximately equal to the period of deafness (see Figure 2.8). Although the latency of the P_1 decreases rapidly in these children, in an approximately exponential fashion, it is not equal to that of normal hearing children; the positive peak latency remains prolonged whilst the amplitude of this peak continues larger in children with CIs compared to age-matched normal hearing children. In some implanted children the LLAEPs consist of just the prominent P_1 peak, like that of the youngest normal hearing children.

Finally, the authors concluded that a CI is sufficient to restore at least some aspects of auditory system maturation. Eggermont and Ponton, 2000 [109] concluded later that LLAEPs are an efficient tool to describe the maturation of human central

auditory system and that the maturation of this system is a function of sound stimulation.

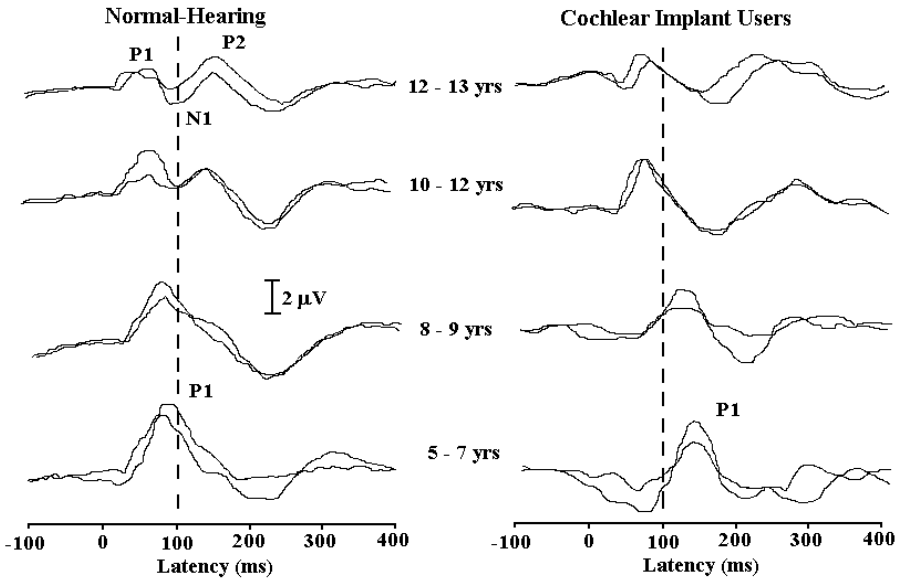

Figure 2.8 Development of LLAEP waveforms of normal hearing children. Between 5 and 9 years, the morphology of LLAEPs is similar in both normal hearing children and CI users. From 10 years old onwards, the response of normal hearing children is similar to the adult morphology (P_1-N_1-P_2 peaks) whilst the response of CI children remains dominated by a positive peak [108].

It is not known exactly what the age limits is to restore the maturation of the auditory system by implantation, however Eggermont *et al* [45] found that in two children implanted older than 8 y.o., their P_1 latencies were significantly longer than the rest of children fitted with cochlear implants (mean deafness 4 year 5 months), recorded in their study. Dorman *et al* [41] suggest that children implanted after 7 y. o. show abnormal waveforms and do not develop normal P_1 latencies even after years of implantation. These authors found that the auditory system maturation in children implanted before 3.5 y.o. is in the range of normal after 3-6 months post-implantation. Finally, these authors conclude the age of implantation is a significant factor in the development of oral speech and language function. They also infer that the plasticity of the auditory system is maximal for a period of about 3.5 years in childhood.

Since, the LLAEP peaks change from electrode to electrode and from subject to subject, looking for a better indicator of the maturation of the auditory system in children with CIs, Ponton *et al* [106] proposed maturation tracking by dipole source modelling. The problem is however, when the CI is working, there is an inherent

artifact, that can hide partially or totally the LLAEP and achieve an erroneous source analysis as a consequence.

Something important to highlight about the methodology used on the papers reviewed in this chapter is the fact that the auditory response from the CIs users is evoked by an electrical stimulus instead of the acoustic stimulus proposed in the next chapter.

2.8 Summary

This chapter included a review of audiological topics which are a fundamental part for this research. Mainly through a review of the general concepts about the EEG, including acquisition and common artifacts in this recording. The concepts of EPs and LLAEPs and an explanation of the way to evaluate the auditory system using LLAEPs were covered. Some general concepts about CIs were discussed too; including CI parts, speech processor characteristics and stimulation strategies. At the end of this chapter a review was given of some papers which describe the maturation of the auditory system after implantation.

The next chapter includes the details about the acquisition of the data set used in this research; consisting of the multichannel LLAEPs of 10 children with CIs, as well as the auditory response of twenty normal hearing children as a control group.

Chapter 3.

The experimental dataset

Multichannel AEP recordings were obtained from the Audiology Laboratory at the Universidad Autónoma Metropolitana-Izt, Mexico City. The Ethical Commission of the National Institute of Respiratory Disorder, Mexico City, approved the protocol to record the dataset used in this research. Normal hearing children and children CI users had their EEGs recorded after written informed consent had been obtained from their parents; a written explanation about the test was handed to parents of the children, some days before the test.

The experimental dataset consists of LLAEPs (see Chapter 2, section 2.1-2.3), since it is known that the multichannel recording of this auditory response is a useful tool for monitoring the development of the auditory system [106]. These potentials provide information about how the human brain processes acoustic information and how this processing could be modified in neurological disorders [105]. Taking this into account, this technique was employed as an objective method for evaluating the performance of children with CIs. The LLAEPs were used to evaluate how the brains of these children codify the stimuli generated by the CI, in accordance with the use of this electronic device.

This chapter begins with a description of the subjects (normal hearing children and children with CIs) who participated in this research (Section 3.1). Section 3.2 and 3.3 describe the test's recording parameters and stimulus characteristics, respectively. Section 3.4 shows some AEP waveforms from normal hearing children and children with CIs. The spectral characteristics of the CI artifact and various procedures used to some authors to remove this artifact are explained in Section 3.5. The last section of this chapter describes some AEP signal processing and analysis techniques which could be used to reduce the CI artifact.

3.1 Subjects

A control group of twenty normal hearing children consisting of 13 females and 7 males between 3 and 14 y.o. were tested; this group was divided according to their age into four groups (see Table 3.1) to facilitate the comparison between their AEPs and the auditory response of the children with CIs. The age range for children younger than 7 years was one year (Group 1 and 2) that to observe the auditory response changes over short time periods; the younger the children, the age-related differences in the auditory response are more marked [105]. The age range was two years for children from 7 to 9 years old (Group 3) and 4 years for group 4 (these divisions are the accepted over the age of 8 years and among teenagers [105]); each group had the same number of subjects (N=5).

Table 3.1 Normal hearing children were grouped according to age to facilitate comparison between their AEPs and the auditory responses of CI users.

Group	*N* (Male/Female)	Age range (years)	Mean age (years)
1	5 (3/2)	3-4	3.2
2	5 (1/4)	5-6	4.7
3	5 (2/3)	7-9	7.6
4	5 (1/4)	10-14	10.8

All the normal subjects have no personal or familiar history of disease of the ear or neurological disorders and they were not taking prescription medication at the time of the test. Their pure-tone threshold levels were $\leq$20 dB_{HL} for audiometric frequencies between 125 and 8 kHz. An otoscopy in both ears was performed before the test in order to discard wax or check for perforations in the eardrum, as well as for infection or inflammation in the ear canal.

Ten profoundly bilateral deaf pre-linguistic children between 3 and 12 y.o. (see Table 3.2) were tested before the CI surgery and at different periods after implantation. The aetiologies of the hearing losses of those children are diverse; including rubella in the first weeks of pregnancy, ototoxic drugs and meningitis, to mention only a few.

All the deaf subjects were fitted with HAs before implantation, but they did not receive any benefit from them. They had a low level in the Test of Auditory Perception Skill [50]; this test evaluates the comprehension, verbal reasoning, mature ability and spontaneous language production of child candidates for implantation.

The entire cohort of CI subjects, except one, are users of *Cochlear Nucleus 24* [7], using the ACE stimulation strategy (see section 2.4), a pulse width stimulus of 25 μs, and 5760 pps total stimulation rate; at the moment of each test they were using the control volume of their CIs set to the most comfortable level for each user. Subject 8 is a user of Clarion 1.2 CI (16 electrodes) developed by Advanced Bionics [8]; with a CIS stimulation strategy and 5200 Hz signal processing resolution.

Table 3.2 Ten children with CIs were recorded at different time after implantation in this research. M: male and F: Female; months (m) and years (y) after implantation when the studies were realized and the side of implantation (right or left) is indicated for each subject. *Subject 8 is a Clarion CI user.

Subject	CI implant side	Study 1	Study 2	Study 3	Study 4	sex	Age at implantation
1	Right	5m	1y		2y 6m	M	8y 3 m
2	Left	3m	1y			F	10y 5 m
3	Right	1y	1y 8m	5y 5m		M	7y 1 m
4	Right	4m	8m	1y 6m		F	3y 8 m
5	Right	1y 9m	2y 8m	5y 1m		M	4y 5 m
6	Right	2y 5m				F	4y 2 m
7	Right	1y 4m				F	5y 2 m
8*	Right	9m	1y 8m			F	3y 6 m
9	Left	5m				F	4y 3 m
10	Right	5m				M	5y 5m

3.2 Recording parameters

The ongoing EEG was recorded with 19 electrodes connected to a *Neuroscan, Synamps* system multi-channel amplifier [1]. This software-programmable amplifier includes 32 channels, 16-bit A-D conversion and a real-time digital filtering using high-speed DSPs; each channel is equipped with 28 monopolar and 4 bipolar channels. The *Synamps* system can acquire data in discrete epochs at sample rates up to 20 kHz for each of 32 channels, 50 kHz for each of 8 channels, or 100 kHz per each of 4 channels.

The EEG was sampled at 2 kHz and filtered between 0.1 and 500 Hz, $\pm$ 12 dB/octave. The analysis window consisted of a 450 ms window, including 150 ms of pre-stimulus data (pre-stimulus baseline longer than 100 ms are enough to average out residual noise [105]). 150 epochs were recorded, with 900 samples each; automatic artifact rejection was used if the signal exceeded $\pm$ 70 μV.

An internal calibration of the *Synamps* system was carried out before the EEG recordings; using a sinusoidal signal (1 V amplitude); amplified and averaged by the system with the same conditions mentioned above.

Medium and small Electro-Caps [6] were used as the EEG electrode application technique; they are made of an elasticated fabric. The silver silver-chloride electrodes on the caps, attached to the fabric, are positioned according with the International 10-20 electrodes system (see section 2.1.1). The diameter of the head of each subject was measured to determine the proper cap size to use; two cap straps were fitted to the torso of the subjects to avoid movement of the cap. The electrodes were attached to the scalp using an electro-gel which has been specifically formulated for the use with these Electro-Caps [6].

A monopolar recording montage was used, the reference electrodes were the linked mastoids (see Figure 3.1); together with linked earlobes, these references are the most commonly used in AEP recordings because it is possible to pick up activity

from the lateral and inferior aspect of the temporal lobe; Fpz was connected to ground.

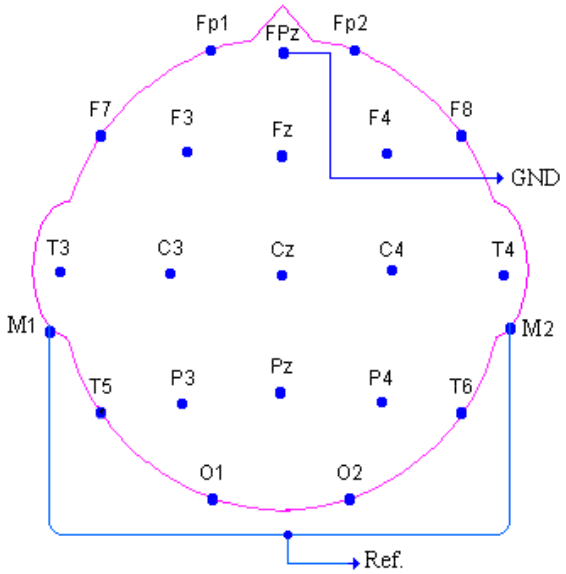

Figure 3.1 Electrode distribution according to the standard international 10-20 system for the 19 electrodes used in this research; Fpz is ground and M1-M2 linked is the reference.

The inter electrodes impedances were checked after placing the Electro-Cap and just before the recordings began; generally the impedances were balanced and below 5 kΩ. The impedances were rechecked during the recording if a pattern that might be artifactual appeared in the EEG recording.

Only 19 electrodes were used, as since the subjects were not under sedation it was considered important to reduce the testing time, and so decreasing the time to attach the electrodes was important (assuring balance inter electrodes impedances ≤5 kΩ). Using fewer electrodes could however have an effect on any accuracy of the source analysis of the P_1 peak later on. Nevertheless, the exact electrode positions for each of the subjects was digitized at the end of each test using a three-dimensional *Fastrak 3D* digitizer [2], these locations were determined relative to three landmarks (nasion, right and left auricula); these three landmarks were used to increase the accuracy of the AEP source analysis, specifically the source analysis of the positive peak, P_1, between 50 and 150 ms after the stimulation. This is discussed later on in this thesis (see Chapter 9).

3.3 Stimulation

The stimuli were generated by a software package called *STIM* which is part of the *Neuroscan* module [1]. The Sound Editor of this module has a dynamic range of 130 dB, with a programmable attenuation in 0.75 dB steps, 16 bit quality digital sampling, customizable digital filtering, mono or stereo processing, and a diversity of windowing options; for example Rectangular, Hamming and Hanning windows. Sounds can be synthesized as pure tones, clicks and noise; triggering is provided for external devices such as the *Synamps* system.

Tone bursts were used as stimuli, with rise and decay times of 10 ms and 30 ms plateau time (see Figure 3.2), an inter-stimuli interval of 1s was used. Three frequencies were selected: 500, 1000 and 2000 Hz with different audiometric intensity levels, 50 and 70 dB_{HL} for children with CIs and 60 and 80 dB_{HL} for normal hearing children.

The stimuli were windowed with a Hanning window and calibrated using a *Brüel & Kjær* 6cm^3 ear simulator type 4152 and a precision sound level meter type 2234 [4]. In the case of normal children, the stimulation was binaural via TDH-39 headphones and a speaker was used to stimulate children with cochlear implants. The speaker was localized one meter distant from the subject and with 0˚ azimuth.

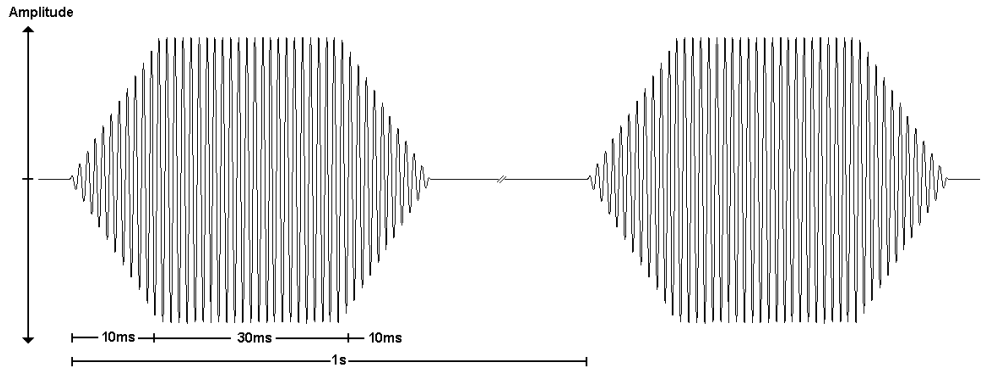

Figure 3.2 Tone burst with rise-decay time of 10 ms and a plateau time of 30 ms; the inter-stimuli interval is 1 s. The frequency of this tone burst is 500 Hz; the amplitude (intensity level) is variable and is calibrated in dB_{HL}.

Each test session included one recording of the spontaneous EEG without stimulation; then each frequency and each intensity level was replicated in order to be

sure about the reliability of the auditory responses. The total test time was approximately one hour, including positioning the electrodes. The following table summarises the principal parameters of the recordings.

Table 3.3 Summary of recording parameters; M1+M2 are left and right mastoids linked.

Parameter	**Value**	**Comment**
Electrode montage	19 monopolar electrodes	International 10-20 system
Low pass filter	500 Hz	-12 dB/oct
High pass filter	0.1 Hz	+12 dB/oct
Analysis window	450 ms	150 ms of pre-stimulus
Stimulus type	Tone burst	10-30-10 ms
Intensity Level	60-80/50-70 dB_{HL}	normal subject/CI user
Frequency stimuli	500, 1000 and 2000 Hz	
Transducer	Headphone/speaker	normal subject/CI user
Number of epochs	150	900 points/epoch
Repetition rate	1 pulse per second	
Electrode reference	M1+M2	
Artifact rejection	$\pm 70\ \mu V$	On line

All measurements were carried out in an anechoic room (3.5x3.0m). During the recordings the children were rested in a reclining chair, in half-light and were asked to relax with eyes closed; their mothers remained in the room during the entire test. The subjects were monitored using an infrared video camera; additionally their mothers had access to a microphone to communicate with the researchers.

Although some authors [58;105] recommend recording the auditory potential whilst the children are watching a video without sound, to best record the response; the AEP recorded in normal hearing children (see Figure 3.3) using the recording parameters described before does not suppress the P_1 peak and it is similar to the AEP reported by Wunderlich, *et al* [132;133] in a group of children in response to pure tones.

3.4 The AEP waveforms recorded

Figure 3.3 shows the average of the AEP waveforms at Cz electrode from the normal hearing children dataset (see Table 3.1), for Group 1, younger than 4 y.o. a broad positive peak with a maximum at 110 ms is recognized, in both Group 2 and 3 the P_1-N_1 complex can be identified, the latency of both peaks are shorter in Group 3 (younger than 8 y.o.) than in Group 2. Finally, the AEP waveforms of Group 4 (older than 10 y.o.), show a negativity followed by a positive and negative peak (N_1-P_1-N_1 complex), similar to the auditory response in adults.

The average latency of P_1 peak had a shift of 5.17 ms between Group 1 (138 ms) and Group 2 (132.83 ms), whilst the latency of P_1 (106.8 ms) in Group 3 is the shortest of those three groups. In group 4 a negative peak substitutes P_1 peak, this peak had an average latency of 88.1 ms. Both the age-related latencies changes of P_1 as well as the appearance of a negative peak instead of the positive P_1 peak, in older children, show the maturation of the auditory system in the control group; theses results are similar to other authors [107;108;132;133].

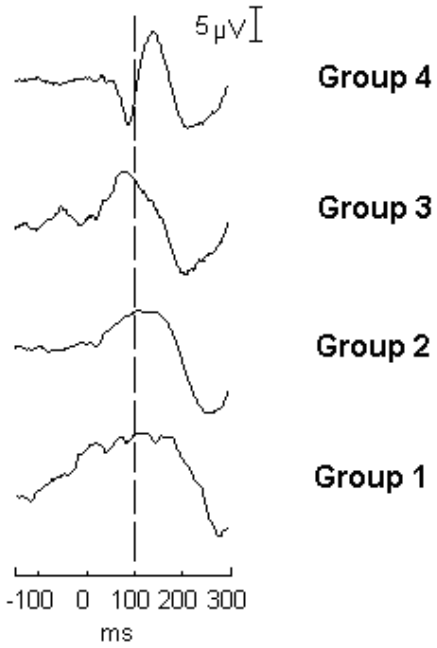

Figure 3.3 Average AEP waveforms at Cz electrode of normal hearing children for each one of the groups in Table 3.1. The latency of the positive peak decreases as a function of age. Group 4 presents a negative peak instead of the positive peak of the others groups; this is similar to the auditory response in adults.

Four recordings from children with CIs were excluded from the analysis in this research. The recordings from S8 (St1 and St2) were not included because, this subject is using a different CI, then this could introduce a bias in the interpretation of the results. At the time of the recording S4-St3 the subject had interrupted the use of her CIs for more than 6 months. Since the objective of this research is evaluate the changes of the AEP in accordance with the CI use, this recording is not consistent with the rest of the recordings where the subjects have been using without interruptions. During the recording S9-St1, the subject reported discomfort during the test; the recording has too few epochs because most of they were saturated and were automatically rejected

Figure 3.4 shows the AEPs for four different child CI users at Cz electrode and at different times after implantation, (a) S3-St1, (b) S3-St2, (c) S5-St2 and (d) S5-St1. It is possible to recognise a positive peak between 100 and 200 ms after stimuli. The latency of P_1 is 172, 173, 150 and 124 ms in (a), (b), (c) and (d), respectively. The N_1 peak was identified in all this recordings with latency between 200 and 300 ms.

In general, the latencies of P_1 peak in children with CIs are longer than in normal hearing children; the amplitudes are higher in implanted children than in normal children.

Appendix A includes the entire AEP recordings for both normal hearing children and children with CIs, the latency and amplitude of P_1 peak are included as well as general information about the subjects. The changes in the source analysis of this peak in accordance with the time using the CIs are shown later on in this thesis.

Figure 3.4 AEP waveforms at Cz electrode for four different children with CIs, (a) S3-St1, (b) S3-St2, (c) S5-St2 and (d) S5-St1. It is possible to recognize a positive peak between 100 and 200 ms after stimuli in all the recordings as well as a negative peak between 200 and 300 ms.

3.5 Cochlear implant artifact

The CI artifact in the EEG recording is the result of the coupling between the external and internal parts of the implant, a magnet maintains the attachment of the radio frequency antenna on the scalp for the digital communication between both parts; this artifact totally or partially obscures the AEPs, especially in the electrodes that are around the CI. Figure 3.5 shows 20 epochs of ongoing EEG recordings from a CI user where it is possible to visualize the CI artifact; the antenna is localised around the T4 and T6 electrodes.

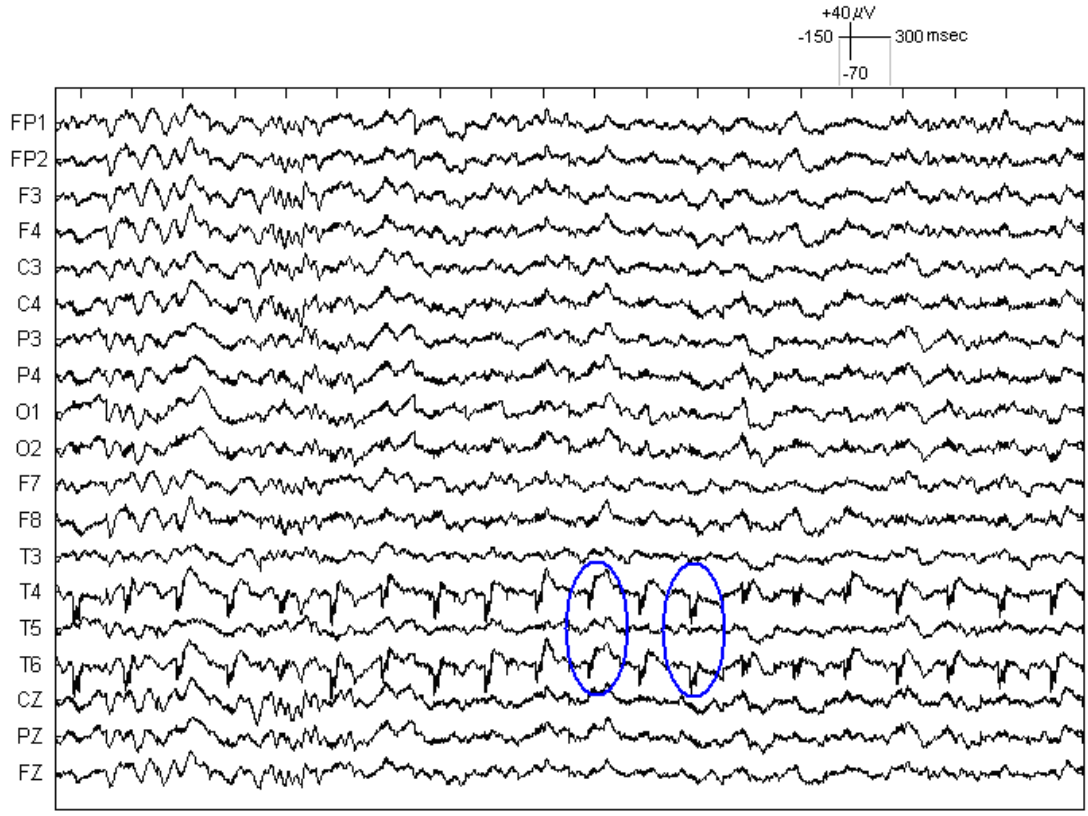

Figure 3.5 Twenty epochs of ongoing EEG recording from a CI user, a large cochlear implant artifact (blue ellipses) is present around T4 and T6 electrodes where the antenna of the implant is located.

There are different reasons why the CI artifact may appear in the AEP recordings, for example, the mode of stimulation of the CIs and localization of reference electrode of the AEP recording; Gilley *et al* [52] reported a greater incidence of the artifact in monopolar stimulation. This is not a new problem; many authors have already recorded this artifact previously in their AEPs recordings [39;102;118;130].

In AEP recordings from subjects without CIs, one strategy used to avoid the stimulus artifact produced by high intensity sound levels, is to utilize alternate polarity stimuli. However, the CI's speech processor does not encode the phase of the stimulus; because of this it is not a feasible alternative to solve the problem with CIs users.

Conventional filtering procedures are not appropriate because the AEP and the CI artifact have common low frequency spectral components (see Figure 3.6). This figure shows the magnitude of the FFT of both the AEP (blue) and the CI artifact

(red); it is possible to see that the two signal share frequency components lower than 10 HZ.

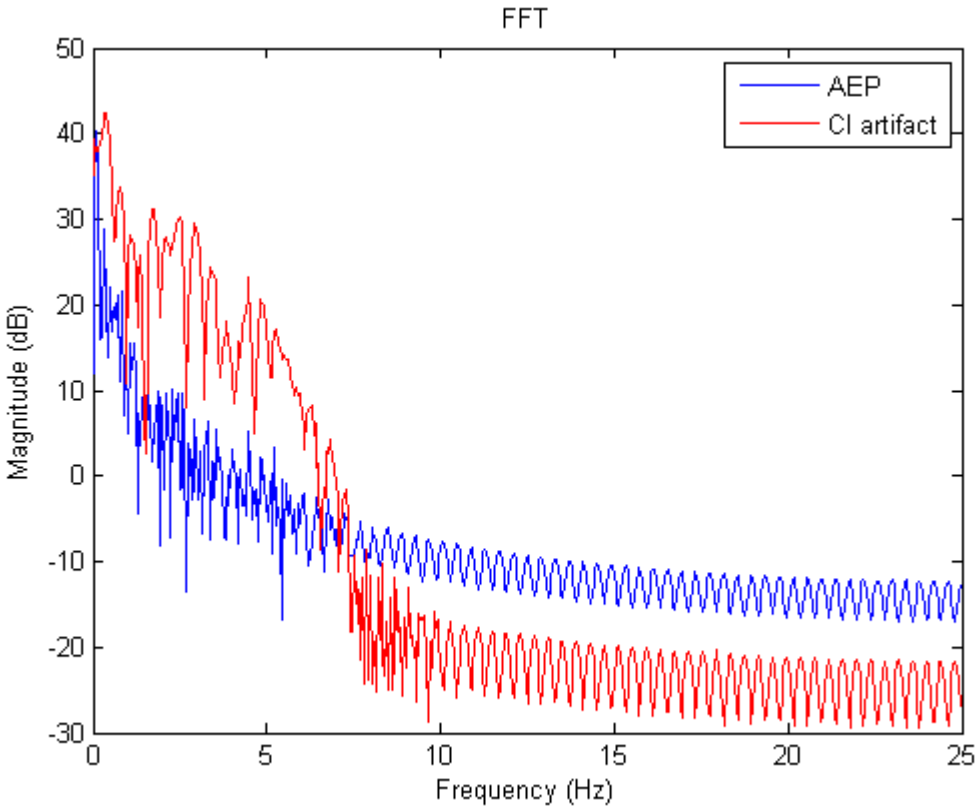

Figure 3.6 Magnitude of the FFT of both the AEP and the CI artifact, these singals have common low frequency components (<10 Hz).

Several solutions have been proposed to try to eliminate or reduce the CI artifact, for example Waring *et al* [130] removed the first part of the auditory response recorded from CI users to eliminate a large stimulus artifact that was recorded; this alternative is not guaranteed to preserve the auditory response and to eliminate only the CI artifact.

Another solution, proposed by Pantev *at al* [102] was to analyze only the contralateral hemisphere to the implant which is less contaminated by the artifact; the inconvenience of this proposal is the loss of contralateral information which is important to determinate hemispheric asymmetries in the response; additionally, the CI artifact could be spread out around all the electrodes. In a later publication Pantev *et al* [101] proposed to use a frequency-shift stimulus which produced a 10 times smaller artifact than the one originated by usual tone-burst stimulus, nevertheless the

artifact would still be present for which the authors then applied Principal Component Analysis to remove it.

Sharma *et al* [119] reported that the CI artifact hides the P_1 response to a speech syllable */ba/*; they moved the reference electrode of the AEP recording, so that the amplitude of the artifact was minimal; nevertheless, they suggest that it is necessary to develop signal processing techniques to minimize this artifact. The following section includes a review of the principal AEP signal processing techniques used to analyse AEPs as well as to remove the artifacts that confound their proper analysis.

3.6 AEP signal processing and analysis techniques

The AEP is several times smaller than the ongoing EEG, because of that it is necessary to do signal processing of the EEG to extract the auditory response from the EEG and then to obtain the signal characteristics (amplitude, latency and waveform) of clinical interest. AEP signal processing and analysis techniques have been on the increase in biomedical signal processing over the last few decades.

The principal techniques used in AEP signal processing and analysis are: Coherent averaging [21], Digital Adaptive Filtering [17;110], Regression Methods [34], Multi-resolution methods by Wavelet Transforms (WT) [19], Principal Components Analysis (PCA) [42] and Blind Source Separation (BSS) by Independent Component Analysis (ICA) [24;31;93]. Most of these techniques look for recovering the auditory response using the minimum number of epochs and keeping only good quality responses. These techniques have been used to develop procedures for automatic identification of the AEP peaks and to remove artifacts for the efficient analysis of the AEPs. The artifacts are produced by external and internal sources; external sources are, for example, line noise and interference from other medical equipments. Internal sources are caused by subject movements, muscle or cardiac activities and eye movements.

Coherent averaging is the traditional method to recover and then analyse the AEP from the spontaneous EEG; this procedure consists of averaging a different

number of epochs or trials of EEG. The *i*-th EEG epoch, $\boldsymbol{x}_i(t)$, in an AEP recording contains both the auditory response, $r(t)$, and the background EEG $\boldsymbol{e}_i(t)$

$$\boldsymbol{x}_i(t) = \boldsymbol{r}(t) + \boldsymbol{e}_i(t), \tag{3-1}$$

the coherent average estimates the auditory response as

$$\hat{\boldsymbol{r}}(t) = \frac{1}{N}\sum_{i=1}^{N}\boldsymbol{x}_i(t) = \boldsymbol{r}(t) + \frac{1}{N}\sum_{i=1}^{N}\boldsymbol{e}_i(t). \tag{3-2}$$

Assuming that the auditory response is the same at every stimulus presented and in contrast the background EEG is random, the average EEG decreases in proportion to the square root of the number of epochs [21]. Since the amplitude of the different types of AEP is variable the number of epochs to achieve a distinguish response is different for each type.

The function of a filter is to remove noise from a signal or to extract parts of the signal with certain frequency range. A digital filter performs numerical calculations to reduce noise or to enhance components of the signal. The applications of digital filters are diverse; one of the most common is to reduce or to remove artifacts. Another application of digital filters is enhancement and/or the extraction the characteristics of a signal of clinical interest; for example the processing of the EEG to extract signals as the AEP.

Digital filters which self-adjust their characteristics are known as adaptive filters; these filters consist of two parts: a digital filter with adjustable coefficients, and an adaptive algorithm which modifies the coefficients of the filter. Removing of ocular artifacts from EEG is one of the most popular applications of adaptive filters in EEG [60;61].

The time-frequency characteristics of the AEPs have been analysed using adaptive filters; these filters adjust their transfer function according to an additive input signal formed by the desired signal and noise (both the desired signal and noise are uncorrelated). The ABR signals are usually considered in three frequency bands: a

low band up to 240 Hz, a medium band between 240 and 483 Hz, and a high frequency band above 500 Hz [18]; an adaptable filter could be used for the peak identification of the components at each of these frequency bands. Pratt *et al* [110] indentified the ABR peaks using a digital filter at slow and medium frequencies, with the medium filter the peaks I, II and V were enhanced and the slow filter was used to enhance the peak V. After filtering, the peak identification was performance by analysis of the voltage and latency of the peaks.

When a digital adaptive filter is used, for example, to reduce the residual EEG or any other noise in the AEPs, it is necessary to choose a filter with a linear phase to preserve the latency of the auditory response [110]; this characteristic is one of the most important measures for clinical applications. A Wiener filter is an adaptive linear filter which reduces the amount of noise in a signal by comparison with an estimation of the desired noiseless signal. Two signals, $\boldsymbol{y}_k$ (noise) and $\boldsymbol{x}_k$ (signal and noise), are applied simultaneously to the Wiener filter, $\boldsymbol{x}_k$ is formed by a part which is correlated with $\boldsymbol{y}_k$ and another that is not. The output of the Wiener filter is an optimal estimate $\hat{\boldsymbol{s}}_k$, of the part of $\boldsymbol{x}_k$ which is correlated with $\boldsymbol{y}_k$. The filtering error, $\boldsymbol{e}_k$, is the difference between the estimated signal and the true signal with some delay.

In the adaptive ocular artifact filtering, the adaptive filter requires four ocular signals, from two electrodes placed near the external cantus of each eye (to record horizontal movements) and two electrodes placed closely above and below both eyes (to record vertical movements), the Fpz electrode is used as ground; this signals compose the Electrooculograms, EOGs. The contaminated EEG and the EOGs are used to obtain an estimate of the ocular artifact; this estimate is subtracted from the contaminated EEG to yield the de-noised EEG. The fraction of the ocular artifact removed from the adaptive filter depends on the degree of correlation between the EOG and its components in the EEG [72].

Gharieb *et al* [51] proposed to use the Wiener filter together with singular value decomposition (SVD) to reduce the number of epochs required to recover evoked potentials. SVD of a dataset of signals contains information about their energy, the number of sources and the noise level. The authors use the Wiener filter to

improve the *SNR* of simulated data with different levels of white Gaussian noise. After filtering, they apply SVD to identify the desired evoked potential.

Regression methods estimate and remove the portion of artifact that is present in the EEG using a least squares criterion; this technique has been used mainly to remove ocular artifacts from EEG [33;34]. A regression method calculates a coefficient (*B*) using the EOG, $\boldsymbol{y}_i$, and EEG, $\boldsymbol{x}_i$, measured voltages at time *i* as

$$B = \sum(\boldsymbol{y}_i - E\{\boldsymbol{y}\})(\boldsymbol{x}_i - E\{\boldsymbol{x}\}) / \sum(\boldsymbol{y}_i - E\{\boldsymbol{y}\}), \qquad 3\text{-}3$$

B calculates the proportion of EOG which is present in the EEG. *B* is used to correct the EEG using

$$c\boldsymbol{x}_i = \boldsymbol{x}_i - B(\boldsymbol{y}_i) - C\,, \qquad 3\text{-}4$$

$c\boldsymbol{x}_i$ is the corrected EEG and *C* the constant from the least squares formula

$$C = E\{\boldsymbol{x}\} - (B - E\{\boldsymbol{y}\}). \qquad 3\text{-}5$$

This method could need more than one clean EOG channel to correct the EEG [34]; the use of more complex equations than Equations 3.3 and 3.4 (i.d. *multiple* regression). There are different ways to calculate *B* in multiple regressions, the correction obtained by each regression is different [33].

In multi-resolution analysis (MRA) the components of a signal are partitioned into frequency bands of increasingly high resolution; at the end of the analysis the signal is decomposed into coarse and detail components [125]. MRA is implemented using low and high pass filters and subsampling. This technique has been used to study the elements of a signal and to filter signals; unwanted components are removed after signal decomposition and then the filtered signal is reconstructed using the inverse procedure of MRA.

The Wavelet Transform is a mathematical tool which provides information about the time, amplitude and frequency content of a signal; this is a commonly used

method in MRA. In WT the signal values are weighted by wavelet functions, all the wavelets are derived from a basic 'mother' wave, this wave has different properties: oscillatory, band pass and invertible. The WT has been used in the analysis of EEG as well as AEPs [17;19]. Decomposing the auditory response at different scales, results in diverse features of the response (frequency bands) that can be analyzed. The principal inquiries when the WT is used are the selection of the most appropriate WT algorithm and the mother wavelet convenient for the analysis.

PCA is another technique commonly used in signal processing, for example in dimensionality reduction, feature extraction, noise filtering and classification [30]. The aim of PCA is to obtain a small number of uncorrelated variables (principal components) of a signal (with zero mean), retaining as much information as possible from the original variables. PCA is usually implemented using SVD, finding an orthogonal basis for a given signal. The optimal solution for PCA is based on second order statistic (SOS), calculating the eigenvector and eigenvalues of the covariance matrix of the data. The first eigenvector gives the direction of the maximum variance of the signal; after the first component is extracted, the second component is extracted from the remaining variability, and so on until there is essentially no variance left [59]. PCA divides the signal into two subspaces: the signal subspace related to the largest components (an approximation of the noiseless signal) and the noise subspace associated with the minor components. PCA has demonstrated to be more efficient than regression methods to remove artifact such as ocular artifacts [89].

BSS by ICA is a statistical algorithm whose aim is to represent a set of mixed signals as a linear combination of statistically independent underlying sources or components [24]. Recently, ICA has been used to separate and remove artifacts in EEG data, such as eye movement, blinking, cardiac signals, muscle activity, and line noise [63;78;80;123;129]. ICA has been employed in the analysis of EEG and Magnetoencephalography (MEG) recorded using vibrotactile stimulus [128] and auditory stimulus [52;93;123] and in the detection of epileptic seizures [74-76]. The selection of the most appropriate signal processing techniques depends on the purpose of the processing and the characteristics in time and frequency of the desired AEPs.

AEP artifact removal

In the case of this research problem, the application of the signal processing techniques have one main objective, the reduction of the CI artifact (see Figure 3.4 and 3.5); in order to obtain a clear representation of the AEP and thus to enhance the accuracy source analysis of the P_1 peak. The implementation of some of the techniques mentioned above to remove the CI artifact could have some inconvenience as explained in the following paragraphs.

The implementation of regression methods to remove artifacts requires a good regression channel for each artifact source which is not usually accessible; for instance, Jung *et al* [80] indicated that regressing out muscle noise is not practical since signals from multiple muscle group require different reference channels. In the case of the CI artifact, it is not always the same for all the subjects (see Figure 3.4), and depend on the stimulation strategy used in each child; additionally, the effect of the CI artifact changes from electrode to electrode. Furthermore, it would be necessary to determine if it was not cancelling out information of the AEP together with the CI artifact.

PCA can not completely separate the ocular artifacts from EEG when they have similar correlation [93]. Jung *et al* [77;79] carried out a comparison between ICA and PCA to remove EEG artifacts, analysing the spectrogram of the EEG with out the artifactual components obtained with both techniques, the authors concluded the ICA removed only the EOG activity produced by eye movements whilst PCA additionally removed a portion of the theta EEG activity; the authors suggest that ICA recovers more brain activity in both simulated and real EEG data than PCA. In general ICA better estimates biomedical signals than PCA. It is important to highlight that PCA is used by many ICA algorithms to reduce the dimensionality of the data whilst maintaining as much as possible of the variation present in the original dataset.

One advantage of using ICA to remove the CI artifact instead of any other of the signal processing technique mentioned so far are that spectral analysis and WT are applied to AEP averages whilst ICA is applied to ongoing EEG making it possible to

reduce the number of epochs needed in the analysis and hence allowing a reduction in the overall recording time.

The amount of data that ICA needs for reliable decomposition of a signal depends on the number of channels. Since ICA is a statistical method, a large number of data points can improve the decomposition; however there is a compromise between the number of data points and the stationarity of the signal. Delorme and Makeig [40;79] recommended a number of points at least a few times the square of the number of channels (n) to obtain n stable decompositions; with the resolution of our data, 900 points per epoch, 50 epochs assures this criterion.

Furthermore, most of the signals processing techniques mentioned before remove only one type of artifact whilst ICA recovers components for each one of the artifact of the EEG as well as the auditory response. The use of ICA not only removes the AEP artifacts, including the CI artifact, but also recovers the auditory response, in order to objectively evaluate the performance of child CI user. This is what is proposed in this research.

3.7 Summary

This chapter included the specifications for the dataset recordings used in this research. Also, the recordings of the AEPs for groups of both normal hearing children and from children with implants were shown. The principal signal processing techniques used in the AEP analysis were reviewed and the use of ICA to remove the CI artifact and isolate the AEPs over any of the other of the techniques mentioned was proposed.

The next chapter includes an overview of the statistical topics necessary to understand the techniques of BSS by ICA used in the pre-processing step of the dataset before the AEPs source analysis stage. Moreover, this next chapter covers the theory of BSS by ICA in general and the principal differences between three of the more popular ICA algorithms (FastICA, Infomax and TDSEP-ICA) in particular.

Chapter 4.

Blind Source Separation and Independent Component Analysis

Blind Source Separation (BSS) is one of the many statistical techniques used in the pre-processing of biomedical signals. The recording of biomedical signals is essential to understand the function of physiological systems. However, these signals are easily distorted by noise and interference [30]. Because of this, a pre-processing step is fundamental to improve the signal quality and make easy the analysis for prognostic and diagnostic proposes. Recently, BSS by Independent Component Analysis (ICA) has been used to recover different biomedical signals, for example the components of Evoked Potentials, Electrocardiac and muscular signals [22;123;128], as well as to remove the classical artifacts of EEG, such as blinking, line-noise and other background noise [78;129].

As mentioned in Chapter 3, ICA is used here primarily to remove the CI artifact. This chapter will present some discussion on why the ICA algorithm is more convenient to remove this artifact from the EEG. The next chapter then assesses three popular ICA algorithms for AEP component estimates, as well as establishing the criteria for selection of their optimal parameters to reduce the CI artifact. Before that, it is useful to first define some statistical concepts used by ICA and provide some details about the three ICA algorithms assessed.

This chapter is divided into three parts; the first reviews some of the statistical concepts used in the theory of BBS and ICA, the second includes an explanation of the ICA technique, including the principal assumptions that are made on applying this

procedure, and finally, three ICA algorithms are listed which were used to extract the AEPs and the CI artifacts from the dataset used in this research.

4.1 Statistical concepts for BSS and ICA

BSS is a statistical technique which works on recovering a set of unobserved signals from sensors that are linear mixtures of unknown independent sources [24]. This technique is known as "blind" because: 1) the source signals are not observed and 2) only general information is available about the mixture.

The statement that different sensors receive different mixtures of the sources is exploited by BSS; that is spatial diversity. Spatial diversity means that BSS looks for structures across the sensors and not (necessarily) across time. BSS identifies the probability distribution of the measurements, given a sample distribution. The principal statistical concepts used by BSS and ICA are briefly explained in the following paragraphs.

All the characteristics of a random variable X are defined by its probability density function (pdf). The pdf is a function that assigns a probability density to each value of the random variable. A probability distribution has a density such that the probability in the interval [a, b] is given by

$$\int_a^b P_X(X)dX \ . \qquad 4\text{-}1$$

The joint probability density function of X and Y is the distribution of the intersection of both random variables; the joint probability of X and Y is written as

$$P_{X,Y}(X,Y). \qquad 4\text{-}2$$

Independence: if we consider two random variables, for example X and Y, independence intuitively means that information on the value of X does not give us any information on the value of Y. More formally, independence is defined by the probability densities; X and Y are independent if and only if their joint pdf is equal to the product of their individual pdfs, that is

$$P_{X,Y}(X,Y) = P_X(X)P_Y(Y). \quad 4\text{-}3$$

The pdf of *n* independent signals is shown by

$$P(s_1, s_2, ..., s_n) = \prod_{i=1}^{n} P(s_i). \quad 4\text{-}4$$

Random variables are independent and identically-distributed (*iid*) if each one has the same probability distribution as the others and all are mutually independent.

In order to solve the source separation problem it is necessary to identify the probability distribution of the data and to calculate a separating matrix (also called the de-mixing matrix, **W**), proposing a statistical model with two components: a mixing matrix (**A**) and the probability distribution of the data. **A** is a full rank matrix; it is square, invertible and its columns are assumed to be linearly independent.

The simplest BSS model using a vector notation is given by

$$\mathbf{x} = \mathbf{A}\mathbf{s}, \quad 4\text{-}5$$

where **s** is the vector of source signals (*n* is the number of sources) and **x** is the vector of measured signals (*m* is the number of sensors). This is a multiplicative model where the measured signals are the product of the mixing matrix **A** by the sources [25].

Sometimes it is more convenient to express the model in Equation 4.5 as a sum, a_i^j is the *j*-th element of the *i*-th column of the **A** matrix, then using a column notation the model is written as

$$x_j(t) = \sum_{i,j=1}^{n} a_i^j s_i(t). \quad 4\text{-}6$$

Where $\mathbf{s}_i$ is the *i*-th element of vector **s**. This is an additive model where the measured signals are a sum of the products of the columns of the mixing matrix by the sources [23].

A variety of ICA algorithms have been suggested in the literature, each one of these algorithms proposes a contrast function, which is a real function of the probability distribution of the data. The maximum likelihood estimation is a popular statistical method used for fitting a model to some data; therefore, it is used to find the contrast functions. Contrast functions can be defined using higher order statistics, for example the kurtosis.

***Kurtosis*:** measures the relative peakedness or flatness of a pdf, a distribution with a positive kurtosis is named *leptokurtic* (super-Gaussian); a distribution with a negative kurtosis is named *platykurtic* (sub-Gaussian). Kurtosis, *kurt*, is defined as

$$kurt = \frac{E\{X - \overline{X}\}^4}{\sigma^4} - 3, \qquad 4\text{-}7$$

where σ is the standard deviation of the random variable X; the constant term -3 makes the value zero for a normal distribution. High kurtosis value means more of the variance is due to infrequent extreme deviations.

Sources such as the AEPs and artifacts in EEG recordings have a positive kurtosis, and spontaneous brain activity (for example alpha waves) and power interference have a negative *kurtosis* value [22]. One restriction in some ICA algorithms is that sources must be non-Gaussian and that non-Gaussianity is measured by kurtosis.

Decorrelation of the source signals can be used to simplify the BSS problem (called *whitening* or *sphering* as a pre-processing step). This step, based only on second order statistic, eliminates redundancy or reduces noise in the data [30]. A whitening matrix **M** is chosen so that the covariance matrix of the source signals becomes the unit matrix; in whitening, measured signals are pre-processed using the following whitening transformation

$$\boldsymbol{x}_w(t) = \mathbf{M}\boldsymbol{x}(t). \qquad 4\text{-}8$$

The whitened signals are mutually uncorrelated and have unit variance, *i.e.*

$$\mathbf{R}_{x_w x_w} = E\left\{\mathbf{M}\boldsymbol{x}(t)\,\boldsymbol{x}(t)^{\mathrm{T}}\,\mathbf{M}^{\mathrm{T}}\right\} = \mathbf{M}\mathbf{R}_{xx}\mathbf{M}^{\mathrm{T}} = \mathbf{I}\,. \qquad 4\text{-}9$$

Whitening reduces the mixture to a rotation matrix **Q**, because it relates two spatially white signals $\boldsymbol{s}(t)$ and $\boldsymbol{x}_w(t)$ [24]. Then, the de-mixing matrix can be calculated as the product of the whitening matrix and the rotation matrix

$$\mathbf{W} = \mathbf{Q}\mathbf{M}\,. \qquad 4\text{-}10$$

The de-mixing matrix restores the maximal peakedness of the sources; the possible approaches to source separation restore the mutual independence of the signals. Hence, the estimation of the sources can be found by

$$\hat{\boldsymbol{s}}(t) = \mathbf{W}\boldsymbol{x}(t)\,. \qquad 4\text{-}11$$

Some BBS algorithms utilize concepts originating from information theory such as *entropy*, *negentropy* and *mutual information*. The different algorithms use these statistical concepts as a quantitative measure of non-Gaussianity of a random variable; BSS can be solved for example, by minimising the mutual information between two variables.

Entropy: is a measure of the uncertainty associated with a random variable. Entropy has to do with how much randomness there is in a signal or random event, in others words how much information is carried by the signal.

If we consider a random variable X with a probability density function $P_X(X)$, the entropy of this variable is defined by

$$H(X) = -E\{\log P_x(X)\} = -\int_{-\infty}^{\infty} P_X(X)\log P_X\,dX\,. \qquad 4\text{-}12$$

Since the entropy of the mixing matrix tends to increase, then the separated source signals should have minimum entropy. A Gaussian variable has the largest entropy among all random variables with the same variance.

Negentropy: is a statistical measure of 'distance' from Gaussianity of the random variable *X* and is defined as

$$J(X) = \int P_X(X) \log \frac{P_X(X)}{P_{X_G}(X)} dX \,, \qquad 4\text{-}13$$

where $P_{X_G}(X)$ is the probability density of a Gaussian variable with the same mean and variance as $P_X(X)$; negentropy is always nonnegative and is zero if and only if the probability distributions are identical.

Mutual information: (MI) is a measurement of the independence of two variables. Two random variables (*X* and *Y*) are independent when they have a low MI value; on the contrary, if the MI is high this means that the variables are dependent. Only if MI is zero can *X* and *Y* be strictly independent; the MI is always non-negative [87]. The MI between two random variables is defined as

$$I(X,Y) = \iint P_{X,Y}(X,Y) \log \frac{P_{X,Y}(X,Y)}{P_X(X) P_Y(Y)} dX dY \,, \qquad 4\text{-}14$$

where $P_X(X)$ and $P_Y(Y)$ are the individual pdf of *X* and *Y* respectively and $P_{X,Y}(X, Y)$ is the joint pdf of *X* and *Y*.

The joint entropy of two random variables is defined as

$$H(X,Y) = H(X) + H(Y) - I(X,Y) \,. \qquad 4\text{-}15$$

Through maximizing the individual entropies, $H(X)$ and $H(Y)$, and minimizing the MI $I(X, Y)$ between the two signals, it is possible to maximize the joint entropy (see Equation 4.15); that is a simple algorithm for BSS. An advantage of MI, over other techniques, to measure independence is that the whole dependence structure of the variable is being taken into account and not only the covariance, as is the case in PCA.

Principal Component Analysis (PCA): is a statistical technique used to decompose data into orthogonal components, PCA is generally implemented using SVD; after the first component is extracted, the second component is extracted from

the remaining variability, and so on until there is essentially no variance left. The resulting components are uncorrelated with each other (first order decorrelation) [59]. PCA computes the eigenvectors and eigenvalues for an estimated covariance matrix; the covariance matrix is the correlation matrix of the vector with the mean removed, *i. e.*

$$\hat{\mathbf{R}}_{xx} = E\left\{\boldsymbol{x}(t)\boldsymbol{x}^{\mathrm{T}}(t)\right\} = \mathbf{V}\boldsymbol{\Lambda}\mathbf{V}^{\mathrm{T}}, \qquad 4\text{-}16$$

where $\boldsymbol{\Lambda}$ is a diagonal matrix, containing the eigenvalues, and $\mathbf{V}$ is the corresponding *orthogonal* or *unitary matrix* consisting of the unit length eigenvectors. Next, the measured signal is projected in the estimated signal subspace and then rescaled such that each component has unit variance

$$\boldsymbol{x}_w(t) = \boldsymbol{\Lambda}^{-1/2}\mathbf{V}^{\mathrm{T}}\boldsymbol{x}(t). \qquad 4\text{-}17$$

PCA allows one to decompose mixed signals into two subspaces: the signal subspace corresponding to the principal components associated with the largest eigenvalues, and the noise subspace corresponding to minor components associated with the smallest eigenvalues.

The principal applications of PCA are: data compression, feature extraction, noise filtering and classification [30]. Although it has been argued that PCA may not be the most appropriate method to estimate the components of physiological data, it is used to *pre-whiten* the data set (see Equation 4.8), reducing the redundancy of the data and estimating the number of mutually independent components to be found by other techniques.

Resampling: Some authors propose using resampling techniques to evaluate the reliability of the BSS-ICA algorithms. Resampling is a statistical method to estimate, for example, the mean and the variance of a complete population by using subsets of the available data. The idea is resample the data and calculate the mean of this resample data to obtain the first *bootstrap mean*, the procedure is repeated to obtain the second resample data and compute the second *bootstrap mean*, in order to

have *B* bootstrap means. This represents an *empirical bootstrap distribution* of sample mean.

Bootstrap is a resampling technique used in data analysis; writing the measured signal as the vector $\boldsymbol{x}(t)=[x_1(t), x_2(t),..., x_m(t)]^T$ the aim of bootstrapping is to estimate some parameters of the complete population $\mathcal{X}$, such as its mean and variance [94]; the principal assumption is that the measuring signal is a good representation of the complete population. Then, *B* new bootstrap samples $\boldsymbol{x}(t)^{*b}=\left(x_1^{*b}, x_2^{*b},..., x_m^{*b}\right)$ with *l* size, are generated with *b*=1, 2, …, *B*, by taking *m iid* random variables from the empirical distribution $\hat{F}$. The estimator $\hat{\theta}_i^{*b}=\hat{\theta}_i\left(\boldsymbol{x}(t)^{*b}\right)$ is calculated for each bootstrap sample $\boldsymbol{x}(t)^{*b}$ [43]. Complete knowledge about the population is obtained from an empirical distribution function such as

$$\hat{F}(x)=\frac{1}{n}\sum_{i=1}^{n} I_{(-\infty,x]}\left(x_i\right). \qquad 4\text{-}18$$

A random variable from $\hat{F}$ takes values x_i with equal probabilities 1/*n*. *I* is the so-called indicator random variable which is defined to be equal to 0 for $x_i < x_1$, and equal to 1 for $x_i \geq x_n$. More advanced applications of the bootstrap involve estimating various measures of error, for example the bias of an estimator. The bootstrap estimate of the standard error of $\hat{\theta}_i^{*b}$ is calculate as

$$SE_B=\sqrt{\frac{1}{B}\sum_{i=1}^{B}\left(\hat{\theta}_i-\hat{\theta}_i^{*b}\right)^2} \qquad 4\text{-}19$$

4.2 Independent Component Analysis

ICA algorithms aim to decompose a set of mixed measurements as a linear combination of statistically independent underlying sources or components [31].

In the most simplistic formulation of the ICA problem, the (noise free) measured signals $\boldsymbol{x}(t)=[x_1(t), x_2(t),..., x_m(t)]^T$, are a linear mixture of unknown but statistically independent sources $\boldsymbol{s}(t)=[s_1(t), s_2(t),..., s_n(t)]^T$, *i.e.* $\boldsymbol{x}(t)=\mathbf{A}\boldsymbol{s}(t)$. The

square mixing matrix **A** is also unknown but invertible. ICA calculates the de-mixing matrix, $\mathbf{W}=\mathbf{A}^{-1}$, from the observations $\boldsymbol{x}(t)$ and estimates the original sources as $\hat{\boldsymbol{s}}(t)=\mathbf{W}\boldsymbol{x}(t)$.

ICA is different from popular methods such as PCA, in that ICA not only decorrelates the signals (2^{nd} order statistics) but also reduces higher order statistical dependencies; making the signals as independent as possible. The principal difference between PCA and ICA is that in ICA the components are not necessary geometrically orthogonal but are statistically independent; the independence is much stronger than simply uncorrelatedness.

The different ICA algorithms in the literature have various statements about the sources, channels and noise or artifacts. Some of the principal assumptions made on applying ICA to a measured signal such as EEG include:

i) The measured signals $\boldsymbol{x}(t)$ are a result of a linear mixing of different sources; volume conduction in the brain result in linear and instantaneous mixing, then EEG recordings at the electrodes are assumed to be a linear mixture of the underlying brain sources (AEP, alpha, beta activities, etc) and the artifact signals (blinking, muscle noise, CI artifact, etc). ICA assumes that different physical process tend to generate different statistically independent signals [9].

ii) Another restriction in standard ICA is that the number of underlying sources is usually less than or equal to the number of measurements ($n \leq m$). The dataset used in this research includes the recordings from 19 electrodes; the numbers of stable estimations expected are variable across subjects, but in general they could be one or two sources related to the auditory response, two to three linked to the CI artifact and one or two other artifacts such as blinking and line noise; then n will be a maximum of about 6-7 independent sources.

iii) The sources are non-Gaussian and the measured signal is stationary (over the short epoch measured). The CI artifact happens at the same time in each EEG epoch and is time-locked with the stimuli, therefore are considered stationary and with a non-Gaussian pdf

[52]. Furthermore, the ICA sources can be estimated but with certain indeterminacies; for example arbitrary scaling and permutation [25].

Figure 4.1 outlines the ICA algorithm including all the parts mentioned in this section. The electrical activity produced by different brain sources is recorded using the EEG; the EEG is a linear mixture of those sources and artifacts. Although the AEP and CI are temporally correlated they are spatially independent signals; since the CI artifact is generated by the array of electrodes and not by a brain source [52]. Using the EEG, ICA calculates the mixing matrix **A** which depends on the conductivity characteristics of the brain and where the electrodes are placed; the de-mixing matrix used to estimate the sources is $\mathbf{W}=\mathbf{A}^{-1}$.

Finally, ICA indicates what parts of the scalp are most responsible for the activity (auditory in our case) by interpolated topographic maps of the ICs. The columns of $\mathbf{W}^{-1}$, give the relative projection strengths of the respective components onto each of the scalp electrodes [40]. These topographic maps indicate the physiological origin of the estimated sources; for example: eye blinking, EP, muscle activity, etc.

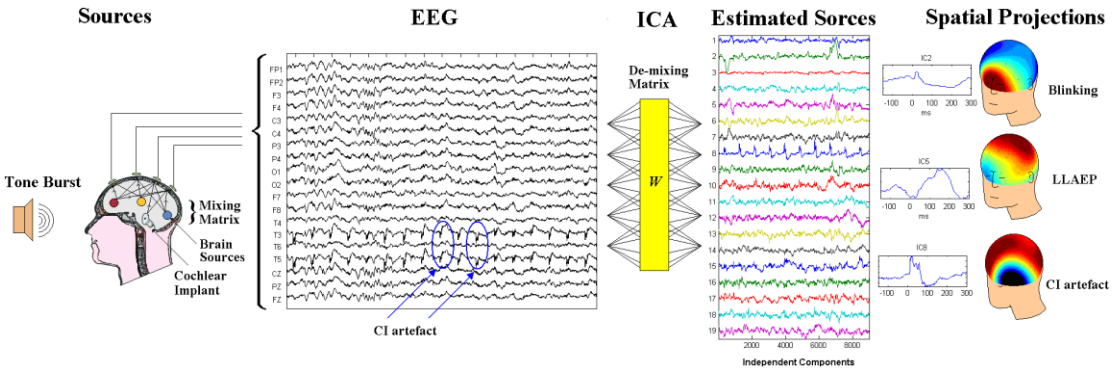

Figure 4.1 The EEG is used to calculate an estimate of the statistically independent brain sources; the CI artifact does not have a neurological origin, such as the brain sources do, then ICA can be applied in this case. ICA calculates the de-mixing matrix **W** used to estimate the sources; the spatial projections of the estimated sources are useful to identify the part of the scalp responsible for each estimate.

In the first stage of this research both the waveforms of the estimated sources and their spatial projections were used to identify the estimates related to the AEPs and the CI artifact.

4.3 ICA algorithms

Although a considerable amount of literature has been published on ICA algorithms, three algorithms can be classed as the most popular: *JADE*, *FastICA* and *Infomax* [16;26;71]. These algorithms have been modified, improved or extended by different authors; for example 30 ICA algorithms are included in the Matlab toolbox implemented by the group of Cichocki (ICALAB) [29].

One possible classification criterion of the different ICA algorithms could be the means of assessing independence used for each method and the assumptions made about the sources and the noise.

If only the second order statistics of the data are used, the algorithm is called Second order statistic (SOS) ICA, it is called high order statistics (HOS) ICA otherwise. Some general differences between the SOS and HOS are: in SOS methods the principal assumption is that the sources have some temporal structure, whilst the HOS methods minimize the *mutual information* between the source estimates. The HOS methods cannot be applied to Gaussian signals; as the method does not allocate more than one Gaussian source. Additionally, the SOS methods do not permit the separation of sources with identical power spectra shape, independent and identically distributed sources [30]. Two HOS ICA methods were assessed in this research *FastICA* [71] and *Infomax* [16] and one SOS ICA algorithm, a modification of *JADE* [26], called *TDSEP-ICA* [135].

The theory behind the three ICA algorithms is explained in the following. Most of the ICA algorithms have two common steps in their implementation:

i) Centring: subtract the mean of the mixed signal, which simplifies the ICA algorithm; $\mathbf{x} = \mathbf{x} - E\{\mathbf{x}\}$, where $E\{\mathbf{x}\}$ is the mean vector of the measurements; when the algorithm is finished the mean vector is added.

ii) Whitening: Find the whitening matrix (see whitening and PCA in section 4.1). The covariance matrix is calculated as $\mathbf{R}_{xx} = E\{\boldsymbol{x}(t)\boldsymbol{x}^{\mathrm{T}}(t)\}$, an eigen-value decomposition (EVD) is performed on it; the decomposition is given

by $\mathbf{R} = \mathbf{E}\Lambda\mathbf{E}^{\mathrm{T}}$ where **E** is the orthonormal matrix of eigen-vectors of **R**, and Λ is the diagonal matrix of eigen-values. Transforming the covariance matrix into an identity matrix, the whitening **M** matrix is calculated as

$$\mathbf{M} = \left(\Lambda^{1/2}\mathbf{E}^{\mathrm{T}}\right)^{-1}. \qquad 4\text{-}20$$

4.3.1 FastICA

FastICA, is a fast fixed-point iteration algorithm. As proposed by Hyvärinen and Oja [69-71] it calculates the required independent sources employing HOS. The algorithm is based on a fixed-point iteration scheme, the negentropy of the mixture is minimized such that uncorrelated and independent sources with as non-Gaussian distributions as possible are obtained. This approach makes the algorithm convergence faster than other ICA algorithms.

The authors introduce the following approximation of the negentropy [68]

$$J(y) \approx \sum_{i=1}^{p} C_i \left[E\{G_i(y)\} - E\{G_i(v)\} \right]^2, \qquad 4\text{-}21$$

where C_i is a positive constant, v is a Gaussian variable with zero mean and unit variance, the variable y is assumed to be of zero mean and unit variance, and G (.) is a non-linear function; p is the number of functions used in the approximation of the negentropy. In the case where only one non-linear function is used, the approximation becomes

$$J(y) \propto \left[E\{G(y)\} - E\{G(v)\} \right]^2. \qquad 4\text{-}22$$

The selection of G (.) depends on the problem; a comparison of the use of the following three functions, in AEP recordings from both normal hearing children and children with CI, is show later on in section 5.1

$$\text{(a)}\ G_1(y) = y^3. \qquad 4\text{-}23$$

$$\text{(b) } G_2(y) = \tanh(a_1 y). \qquad 4\text{-}24$$

$$\text{(c) } G_3(y) = y\exp\left(-a_2 \frac{y^2}{2}\right). \qquad 4\text{-}25$$

The default value for a_1 and a_2 is 1. After choosing an initial weight vector $\mathbf{w}$, the algorithm calculates the direction of $\mathbf{w}$ maximising the non-Gaussianity of the projection $\mathbf{w}^T\mathbf{x}$ (linear combination of the measured signals). Since the signal is already whitened, to make the variance of $\mathbf{w}^T\mathbf{x}$ unity it is sufficient to constrain the norm of the pseudo-inverse of the initial weight vector $\mathbf{w}^+$, to be unity, $\mathbf{w} = \mathbf{w}^+ / \|\mathbf{w}^+\|$; if the old and new values of $\mathbf{w}$ do not point in the same direction, the algorithm recalculates the direction of $\mathbf{w}$. Finally, the de-mixing matrix is given by $\mathbf{W} = \mathbf{w}^T\mathbf{M}$ and the estimations by $\hat{\mathbf{s}} = \mathbf{W}\mathbf{x}$.

4.3.2 Infomax (Information maximization)

Infomax, described by Bell and Sejnowski [16], is an ICA algorithm which finds independent signals by maximizing the joint entropy $H(y)$ (see Equation 4.13) of the outputs of a neural network, minimizing the MI among the output components. *Infomax* includes a linear pre-processing of the input data, $\mathbf{x_G}=\mathbf{G}\mathbf{x}$ called sphering, where $\mathbf{G}=(E\{\mathbf{x}\mathbf{x}^T\})^{-1/2}$ is a non orthogonal symmetrical decorrelator [91]. The de-mixing matrix $\mathbf{W}$, is found using stochastic gradient ascent, maximizes the entropy of the input vector $\mathbf{x_G}$, linearly transformed $\mathbf{u}=\mathbf{W}\mathbf{x_G}$ and sigmoidally compressed $y=g(\mathbf{u})$. Then $\mathbf{W}$ performs component separation whilst the nonlinearity $g(.)$ provides the necessary HOS information, $g(\mathbf{u}_i)=(1+exp(-\mathbf{u}_i))^{-1}$. This gives an update rule $\hat{\mathbf{u}}_i = 1 - 2\mathbf{u}_i$. *Infomax* is able to decompose signals into independent components with sub and super-Gaussian distributions. The original learning rule for super-Gaussian distributions is

$$\Delta\mathbf{W} \propto \left[\mathbf{I} - \tanh(\mathbf{u})\mathbf{u}^T - \mathbf{u}\mathbf{u}^T\right]\mathbf{W}\ , \qquad 4\text{-}26$$

where **I** is the identity matrix, and **u** are the estimated sources. The extended learning rule (*Ext-Infomax*) [91], for sub-Gaussian distributions is

$$\Delta \mathbf{W} \propto \left[\mathbf{I} - \mathbf{\Lambda} \tanh(\mathbf{u}) \mathbf{u}^{\mathrm{T}} - \mathbf{u}\mathbf{u}^{\mathrm{T}} \right] \mathbf{W} . \qquad 4\text{-}27$$

The algorithm switches between two learning rules: one for sub-Gaussian and one for super-Gaussian sources. $\mathbf{\Lambda}$ is a diagonal matrix which includes the switching criterion between the two learning rules

$$\mathbf{\Lambda}_{ii} = \begin{cases} 1 \text{ super - Gaussian} \\ -1 \text{ sub-Gaussian} \end{cases} . \qquad 4\text{-}28$$

The estimated sources are computed as

$$\hat{\mathbf{s}} = \mathbf{W}^{-1} \mathbf{y} . \qquad 4\text{-}29$$

4.3.3 Temporal Decorrelation Source Separation ICA (TDSEP-ICA)

The standard algorithm of *FastICA* has been extended by Ziehe and Müller, *Temporal Decorrelation Source Separation ICA* (*TDSEP-ICA*) [135] includes the temporal structures of signals such as the EEG (this algorithm contains diagonalization as used in *JADE* [26]). The use of HOS is substituted by the use of several time-delayed second-order correlation matrices for source separation. *JADE* and *TDSEP-ICA* determinate the mixing matrix based on a joint approximate diagonalization of symmetric matrices; the principal difference between these two algorithms is that *JADE* maximizes the kurtosis of the signals whilst *TDSEP-ICA* minimizes temporal cross correlation between the signals. Instead of using *JADE* in this assessment, *TDSEP-ICA* was included, since this algorithm was used before on biomedical signals and more reliable estimates were obtained, than using *JADE* [94].

TDSEP-ICA could be summarized as follows: firstly, Ziehe and Müller [135] define the following cost function that measure the correlation between the signals $\boldsymbol{x}(t)$

$$R_{ij} = \sum_{i \neq j} \left\langle x_i(t) x_j(t) \right\rangle^2 + \sum_{k=1}^{N} \sum_{i \neq j} \left\langle x_i(t) x_j(t + \tau_k) \right\rangle^2 , \qquad 4\text{-}30$$

where ⟨.⟩ denotes a time average. After whitening, the first term in the cost function becomes zero; this equation imposes decorrelation over time. After that, they propose an alternative technique for the joint diagonalization using a rotation [94]. In the rotation step, the cost function can be minimized by approximate simultaneous diagonalization of several correlation matrices through several elementary JACOBI rotations [25], this to obtain the rotation matrix **Q**.

The *TDSEP-ICA* algorithm computes those matrices relying only on SOS and diagonalizes the covariance matrices $\mathbf{R}_0 = E\left\{\boldsymbol{x}(t)\,\boldsymbol{x}(t)^{\mathrm{T}}\right\}$ for a time lag $\tau = 0$ and at the same time diagonalizes the covariance matrix for a given delay $\mathbf{R}_\tau = E\left\{\boldsymbol{x}(t)\,\boldsymbol{x}(t-\tau)^{\mathrm{T}}\right\}$. The source covariance matrix $\mathbf{R}_\tau^{\mathbf{s}}$ is diagonal for all time lags $\tau = 0, 1, 2\ldots, N\text{-}1$

$$\mathbf{R}_\tau^{\mathbf{s}} = \mathbf{W}\mathbf{R}_\tau^{\mathbf{x}}\mathbf{W}^{\mathrm{T}}, \qquad 4\text{-}31$$

where $\mathbf{R}_\tau^{\mathbf{x}}$ is the signal covariance matrix. This algorithm determines the mixing matrix based on a joint approximate digitalization of symmetric matrices. Finally, using the whitening matrix **M** and the rotation matrix **Q**, an estimate of the mixing matrix can be calculated as $\hat{\mathbf{A}} = \mathbf{M}^{-1}\mathbf{Q}$; the estimations are given by $\hat{\mathbf{s}} = \hat{\mathbf{A}}^{-1}\mathbf{x}$. An advantage of *TDSEP-ICA* over other ICA algorithms is that it can separate signals whose distributions are Gaussian.

4.4 Summary

Common statistical concepts used in BSS and ICA were explained in this chapter. The general concepts and assumptions used in ICA, as well as the particular theory of three ICA algorithms (*FastICA*, *Infomax* and *TDSEP-ICA*) were described. Part of the aim of this research was to determine which of the algorithms described in this chapter is more convenient to recover the auditory response by isolating the CI artifact from the dataset used here. The results of these comparisons are included in the next chapter. Furthermore, the criteria to select the optimal parameters for each one of the algorithms are explained too.

Chapter 5.

ICA parameter selection for robust AEP component estimates

AEP recordings have been used to evaluate the performance of ICA algorithms in the literature. Different authors [78, 79, 129] have demonstrated that this procedure can remove the typical EEG artifacts i.e. blinking, muscle noise, line noise etc; the CI artifact included. However, there are few studies about the selection of the optimal parameters for estimating the AEP components, to reliably recover both the auditory response and the specific artifact generated by the normal functioning of a CI.

In this part of the research the optimal parameters of three ICA algorithms, *FastICA*, *Infomax* and *TDSEP-ICA* for robust AEP component estimating were determined (the theory behind of each algorithm was explained in Section 4.3). A total of 35 EEG recordings, from normal hearing children (20 recordings) and children with CIs (15 recordings), were used in this part of the research. This chapter is divided into two sections, Section 5.1 includes both the procedures and criteria used for the selection of the parameters of those ICA algorithms. Section 5.2 shows the waveforms and topographic maps of the most robust ICs recovered by *FastICA*, *Infomax* and *TDSEP-ICA*.

All the results shown in this and the following chapters correspond to auditory stimuli of 1000 Hz at 70 dB_{HL} for normal children and 80 dB_{HL} for children with CIs. The analysis was repeated over many different numbers of epochs, from the original number (150 epochs) to 50. Results analyzed over 75 epochs and using an ICA

algorithm with spatial constraints were reported in James and Castañeda-Villa [73]; results with 50 epochs are shown in the rest of this document.

5.1 Selection of optimal ICA algorithm parameters

Many authors have proposed diverse methods to validate each of their ICA algorithms [64;65;79;91;94]; either analyzing algorithmic stability or reducing the variability of the estimated components. The procedures proposed by the authors, of each one of the algorithms used in this research, were applied to select the model parameters more convenient for robust AEP and CI artifact estimation.

This section is focused on examining the differences between the estimates of the AEP and the CI artifact, obtained first by *FastICA* using three non-linear functions, which this algorithm uses to measure the negentropy of the sources, as well as two orthogonalization approaches (*symmetric* and *deflationary*). In the case of *Infomax* the estimates recovered by the standard *Infomax* and *Ext-Infomax* are compared using the kurtosis values and the pdfs of the estimated components. Finally, the effect of different time delays on the AEP component estimates using *TDSEP-ICA* was evaluated in this section too.

5.1.1 FastICA non-linearity function and orthogonalization approach selection

Himberg *et al* proposed a procedure, known as ICASSO [64;65], to investigate the algorithmic and statistical reliability of the ICs recovered by *FastICA*, by running this algorithm many times for three different initial conditions:

1. Random initial conditions (to evaluate the algorithmic reliability),
2. The same initial condition but the data are bootstrapped every time (to evaluate the statistical reliability),
3. Random initial conditions and the data are bootstrapped every time (see section 4.1), to evaluate both the algorithmic and the statistical reliability.

The estimated components are clustered according to their mutual similarities (the criterion applied by the authors is agglomerative clustering with average-linkage) and visualized as a 2-D plot; finally, the cluster quality (stability) index, I_q (see

Equation 5.1), is calculated to evaluate the robustness of the estimated clusters. A measurement of the similarity between the estimates is the absolute value of their mutual correlation coefficients r_{ij}, $i,j=1, 2,...,K$; the final similarity matrix has the elements Δ_{ij} defined by $\Delta_{ij}=| r_{ij} |$

$$I_q\left(C_{m_{int}}\right)=\frac{1}{\left|C_{m_{int}}\right|^2}\sum_{i,j\in C_{m_{int}}}\Delta_{ij}-\frac{1}{\left|C_{m_{int}}\right|\left|C_{m_{ext}}\right|}\sum_{i\in C_{m_{int}}}\sum_{j\in C_{m_{ext}}}\Delta_{ij}\ . \qquad 5\text{-}1$$

If C_m denotes the set of indices of all the estimates, $C_{m_{int}}$ the set of indices that belong in the m-th cluster and $\left|C_{m_{int}}\right|$ the size of the m-th cluster, then I_q is computed as the difference between the average intra-cluster similarities and the average extra-cluster similarities; $C_{m_{ext}}$ is the set of indices that do not belong to the m-th cluster.

The cluster quality index gives a rank of the corresponding IC clusters estimated. The ideal value of I_q is 1; the smaller the value, the less stable, compact and isolated, the estimated cluster is. In the best case of dataset dimensions 19, the estimates are concentrated into 19 compact and close to orthogonal clusters.

To determine the best parameters of *FastICA* to estimate the AEP components from the dataset recordings used in the research, ICASSO was run using the initial condition (3) mentioned before, in that manner both the algorithmic and statistical reliability of *FastICA* were assessed. The two orthogonalization approaches proposed by this algorithm, *deflationary* and *symmetric* were compared too. In the *deflationary* condition, the ICs are found one at time; whilst in the *symmetric* approach all the ICs are estimated at the same time. In addition, the three non-linear functions mentioned in section 4.3.1 for *FastICA* were compared.

Table 5.1 summarizes the six different test conditions assessed for *FastICA*, used in both EEG recordings from normal hearing children and children with CIs. For each condition ICASSO run *FastICA* 10 times (with a maximal number of iterations equal to 100) and the number of estimate clusters is equal to the data dimension, 19. ICASSO returns a plot of the quality index I_q for each estimate cluster, with the

clusters ranked according with the index values. As mentioned before, the ideal case is when the I_q values to all the estimate clusters are close to 1.

Table 5.1 The estimated components using six different test conditions for *FastICA* where compared in this research. The non-linear functions *G* (see Equations 4.22-4.24) are used to measure the *negentropy* of the sources. In the *deflationary* approach, the sources are estimated one at time and in the *symmetric* approach, all estimates are calculated at the same time.

Condition	Function	Approach
C1	$G_1(y)$	*Deflationary*
C2	$G_2(y)$	*Deflationary*
C3	$G_3(y)$	*Deflationary*
C4	$G_1(y)$	*Symmetric*
C5	$G_2(y)$	*Symmetric*
C6	$G_3(y)$	*Symmetric*

The criteria to select the optimal parameters, non-linear function and orthogonalization approximation, for *FastICA* are:

1. The test condition for the maximum number of estimate clusters with I_q values between 0.9 and 1.
2. Identify the largest number of estimates with physical or physiological meaning (AEP, CI artifact and/or noise) ranked first according to the I_q index. The ICs were identified using both the waveform and the topographic maps of the ICs at the centre of the estimated clusters.
3. The largest numbers of clusters with more than one estimate (the ideal would be 19).

Table 5.2 and Table 5.3 (recordings from normal hearing children and children with CIs, respectively) include the number of estimate clusters for each of the test conditions in Table 5.1, with I_q index values higher than 0.9, for the total dataset. The red numbers indicate the condition (for each recording), which satisfied the three criteria for the *FastICA* parameters selection above listed. When ICASSO was unable to complete the procedure, because *FastICA* did not converge in 100 iterations after 6 attempts, the cells are empty.

Table 5.2 Number of estimate clusters with I_q index between 0.9 and 1 (recordings from normal hearing children) for the six conditions listed in Table 5.1. Red numbers indicate the test condition, which satisfied the three criteria used to select the *FastICA* parameters.

Recording	C1	C2	C3	C4	C5	C6
ad	9	10	8	**12**	11	6
al	7	7	3	**12**	7	4
an	**11**	3	0	10	5	4
ax	10	**12**	7	9	10	5
bf	7	8	7	**18**	8	5
cc	7	6	6	4	**9**	4
dt	10	7	9	**15**	13	1
edg	**10**	6	5	**10**	4	2
fc	5	12	9	**19**	9	7
iv	7	11	3	**12**	4	4
jg	12	**19**	3	-	13	8
kc	3	3	2	**6**	1	1
mar2	0	2	1	**10**	2	2
mp	4	4	4	**13**	3	3
nan	18	0	6	**19**	18	7
st	4	4	2	**17**	3	2
of	13	5	-	**19**	5	6
pf	7	11	3	**12**	4	4
ug	7	6	10	**16**	10	6
xal	10	8	2	**11**	8	6

Table 5.3 Number of estimate clusters with I_q index higher than 0.9 (recordings from children with CIs). Red numbers indicate the test condition that satisfied the three criteria used for selecting the *FastICA* parameters.

Recording	C1	C2	C3	C4	C5	C6
S1-St1	**15**	6	6	11	7	2
S1-St2	8	7	5	**14**	10	2
S1-St3	8	6	3	**13**	3	2
S2-St1	7	7	5	**7**	7	4
S2-St2	8	9	7	**10**	7	8
S3-St1	3	1	3	4	**5**	2
S3-St2	6	9	2	**15**	6	4
S3-St3	9	8	**15**	12	9	5
S4-St1	9	8	2	**14**	10	3
S4-St2	**16**	7	6	14	16	5
S5-St1	8	**14**	9	10	8	12
S5-St2	6	8	4	**16**	8	7
S5-St3	6	12	5	**10**	6	5
S6-St1	13	5	4	**18**	7	2
S7-St1	7	-	3	**14**	4	3

In general, the performance of condition 4 is better than any other condition (in normal hearing children). This condition achieved 19 estimated clusters in three different recordings (***fc***, ***nan*** and ***of*** see Table 5.2) with I_q index values higher than 0.9 in two recordings. In 14 of 20 recordings from normal hearing children analyzed, the highest number of stable and isolated estimated clusters were obtained using the non-linear function $G_1(y)$; moreover, reliable estimates were achieved using this function together with a *symmetric* orthogonalization approach (test condition 4, Table 5.1). A *deflationary* orthogonalization approach achieved zero estimated clusters with stability indexes between 0.9 and 1 in three recordings (see ***an***, ***mar2*** and ***nan*** in Table 5.2).

In 10 of 15 recordings from children with CIs, the highest number of robust and isolated estimated clusters were obtained using the non-linear function $G_1(y)$; as in the case of normal hearing children, more reliable estimates were achieved using

this function simultaneously with a *symmetric* approach (test condition 4). In two recordings, S5-St1 and S5-St3 (see Table 5.3), more stable estimated clusters were achieved by condition 2 (non-linear function $G_2(y)$ and a *deflationary* approach), but it was not possible to recognize the AEP in those clusters. This condition also achieved the highest number of clusters with only one estimate.

In the following figures selected I_q stability index graphs are shown, in order to illustrate the performance of the conditions tested in this section. In the case of normal hearing children some graphs obtained with condition C4 are shown; this condition achieved the highest number of clusters with I_q index values between 0.9 and 1. In the case of children with CIs, I_q index graphs were selected in order to illustrate the comparison between the conditions with the best and the worst performance (condition 4 and 2, respectively), in terms of robust and isolated estimated clusters in most of the recordings analysed.

Figure 5.1 shows the stability I_q index for the 19 estimated clusters using *FastICA* with the non-linear function $G_1(y)$ and a *symmetric* orthogonalization approach (Table 5.1, test condition 4) in four normal hearing children; this condition achieves the most compact and isolated estimated clusters than any other condition, for these recordings. In recording I: subject ***fc***, 14 y.o., the 19 estimated clusters have I_q index values between 0.9 and 1. Cluster 2 is related to a noisy electrode whilst cluster 9 corresponds to the AEP. In recording II: subject ***bf***, 6 y.o., only one of the estimated clusters has I_q value lower than 0.9 (cluster 19); cluster 4 is linked to the auditory response and cluster 14 correspond to a noisy electrode. In recording III: subject ***mar2***, 10 y.o., 10 estimated clusters have I_q index values between 0.9 and 1; two of those clusters are related to the AEP (cluster 1 and 5). Finally, in recording IV: subject ***mp***, 11 y.o., 13 estimated clusters have I_q values higher than 0.9; clusters 8 and 10 are related to the AEP.

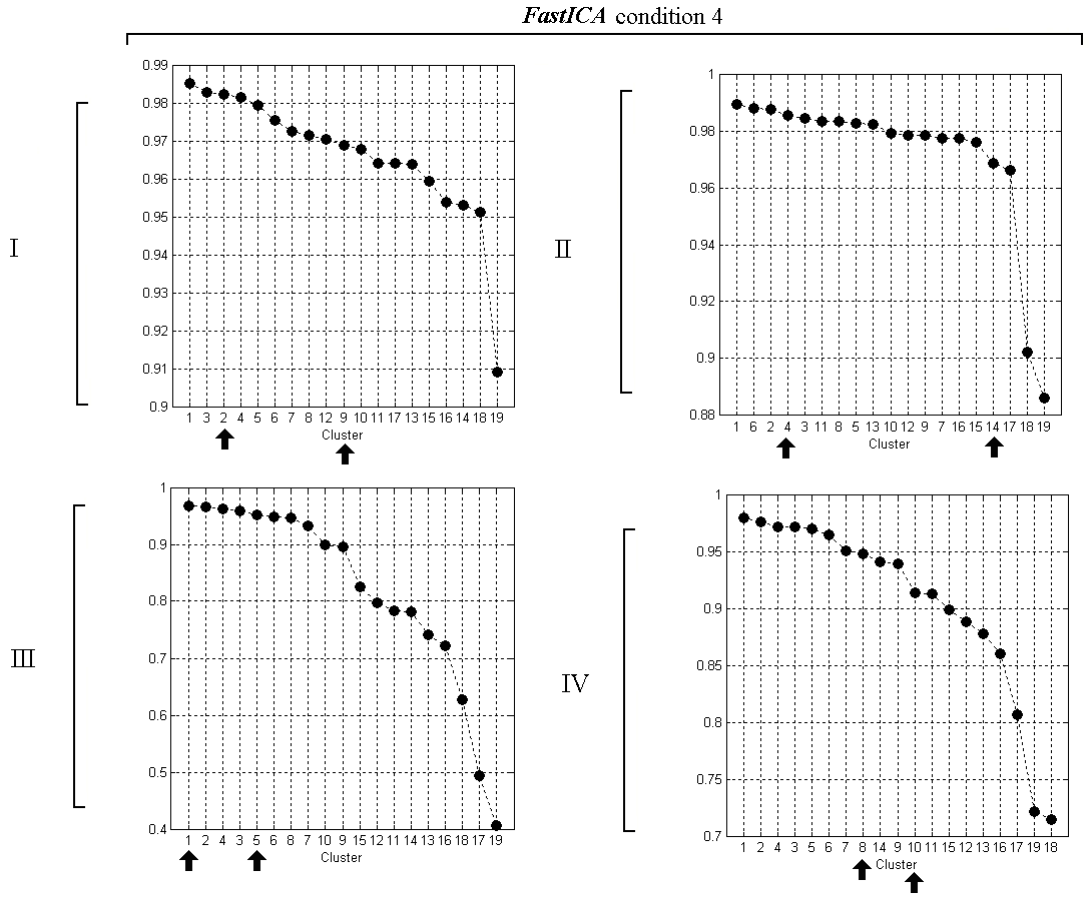

Figure 5.1 Stability index (I_q) for 19 estimates clusters recovered by *FastICA* using test condition 4 (recordings from normal hearing children, I: ***fc***, II: ***bf***, III: ***mar2*** and IV: ***mp***); this condition achieves the most robust clusters as well as reliable estimates of the conditions tested; arrows indicate the estimate clusters related to the AEP and noise.

In recordings from normal hearing children, condition 4 achieved stable and isolated estimated clusters, with ICs associated with the AEPs ranked first (according with I_q index value), in most of these recordings.

Figure 5.2 shows a comparison between the I_q indexes for the test conditions 2 and 4 (see Table 5.1) for four different recordings (children with CIs). Row I: recording S1-St1, in the test condition 2 only 7 clusters have more than one estimate (ICASSO cannot calculate the I_q indexes for clusters 1-12); it was not possible to recognize neither the AEP nor the CI artifact in any of these estimated clusters. Although test condition 4 does not have the largest number of estimated clusters with I_q values between 1 and 0.9, it is the condition where a clear AEP can be recognized (clusters 3 and 7) as well as which has a better estimate of the background noise, cluster 11. Row II: recording S1-St2, for the test condition 2, only 8 estimated clusters have more than one estimate each and none of those clusters are related to either the

AEP or the CI artifact. Condition 4 has the most robust clusters with I_q between 0.9 and 1; the clusters ranked first (cluster 1 and 3) correspond to noisy electrodes whilst cluster 16 (with a I_q index value lower than 0.9) is associated with the AEP. Row III: recording S3-St2, for condition 2 the I_q index was calculated for only five clusters (the rest of the clusters, 1 to 14 have only one estimate each); cluster 16 is related to the CI artifact; neither the AEP nor the background noise were recovered in these clusters. In this recording the highest number of clusters with I_q indexes more than 0.9 were obtained using condition 4, clusters 6 and 17 are related to the CI artifact; the AEP cannot be recovered clearly with any of the conditions. Row IV: recording S5-St3, the performance of *FastICA* for all the conditions was similar, although condition 2 has the highest number of clusters with I_q between 0.9 and 1 (14 clusters), it is also the condition with more clusters with only one estimate each (cluster 1 to 5). In this recording, test condition 4 estimates the most robust clusters for the components associated with the CI artifacts (cluster 1 and 4); although it was not possible to recover a clear cluster related to the AEP.

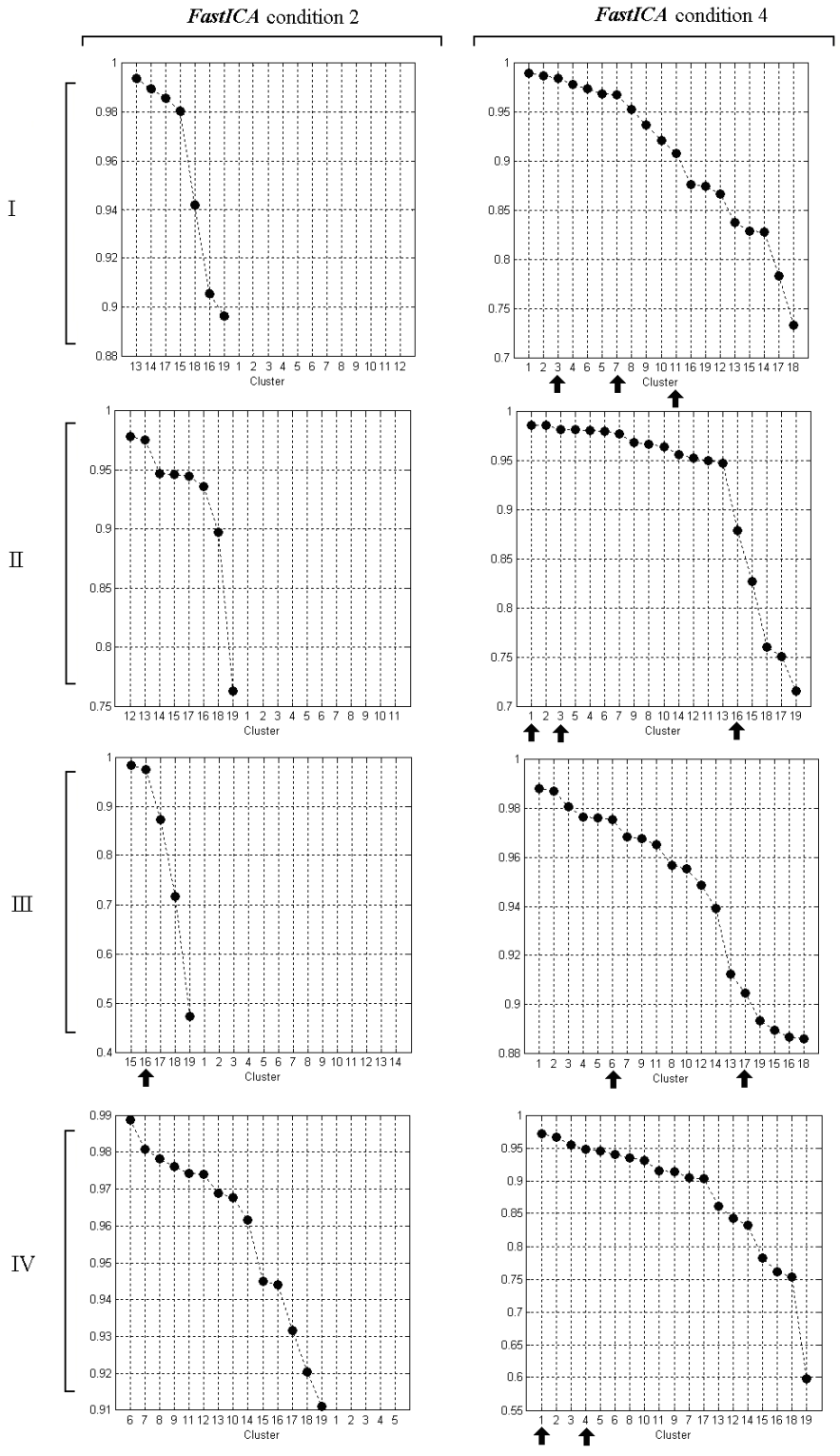

Figure 5.2 Comparison between test conditions 2 and 4 in four different recordings I: S1-St1, II: S1-St2, III: S3-St2 and IV: S5-St3 (recordings from children with CI, at different times after implantation). Test condition 4 achieved the most robust clusters as well as the most reliable estimates; arrows indicate the clusters related to the AEP, CI artifact and noise.

In the majority of recordings from children with CIs, test condition 4 recovered the most robust and isolated estimate clusters. The estimated clusters

ranked first were associated with the CI artifact and the background noise but not necessarili with the AEP.

For *FastICA* the highest values of the I_q index, in other world the most stable clusters, were obtained using the non-linear function $G_1(y)$ together with a *symmetric* orthogonalization approach. The estimate clusters ranked first (the highest I_q indexes values) were different for each recording, generally they were related to the AEP in normal hearing children and with the CI artifact in children with CIs. In 10 of the 13 recordings analysed from children with CIs, the number of clusters with a stability index between 0.9 and 1 was greater using test condition 4 than any other condition.

5.1.2 Infomax vs. Ext-Infomax

Infomax is another of the most popular ICA algorithms used to remove artifacts from EEG recordings [77;79;80;91]. It has also been used to remove the CI artifact from EEG recordings contaminated for that artifact [39;52]. Nevertheless, there is no a comparative analysis between the original *Infomax* and the *Ext-Infomax*, in order to determine the convenience of using one or other method in these recordings contaminated by the CI artifact.

The purpose of this section is to compare and contrast the ICs recovered by *Infomax* and *Ext-Infomax* such that to determine which algorithm achieves the most robust estimates for the AEPs, CI artifact and background noise. Two assumptions are considered for the sources:

a) There are no sub-Gaussian sources, thus *Infomax* is enough to recover the signals
b) It is necessary to apply the *Ext-Infomax* algorithm since the measures include mixed sub- and super-Gaussian sources.

In order to compare the estimated components recovered using *Infomax* and *Ext-Infomax*, the kurtosis values and the pdf of the estimates were used; along with if it was possible to associate the waveform of the estimates with the components of

interest, *i.e.* AEP, CI artifacts, and noise. Tables 5.4 and 5.5 include a comparison between the kurtosis values of ICs related to the AEP and noise (in normal hearing children) and with AEP, CI artifact and noise (in CI users) using *Infomax* and *Ext-Infomax*.

In the recordings S1-St1 and S1-St2 (Table 5.5) the electrode lying over the CI were not connected during the test. In the case of the recordings S2-St1, S2-St2, S5-St1 and S5-St3 the AEP was not recognised in any of the ICs calculated by *Infomax* and *Ext-Infomax*. The algorithms did not converge using the recording S7-St1. Appendix B includes the pdf histograms for the ICs related to the AEP, CI artifact and noise for all the dataset.

Table 5.4 Comparison between the kurtosis values for the ICs related to one component of the AEP and noise in recordings from normal hearing children, the estimates were recovered using *Infomax* and *Ext-Infomax*.

	Infomax		*Ext-infomax*	
Recording	AEP	Noise	AEP	Noise
ad	1.09	0.99	0.99	0.90
al	0.99	1.09	0.90	0.99
an	0.87	1.10	0.87	4.27
ax	0.83	8.37	1.42	8.07
bf	4.51	2.85	4.00	4.00
cc	2.16	0.47	2.13	0.48
dt	4.45	3.89	4.84	3.94
ed	1.49	2.54	1.63	2.56
fc	1.52	0.31	2.81	0.38
iv	27.93	7.53	27.14	7.30
jg	5.11	5.79	5.15	5.92
kc	0.93	4.50	0.87	3.90
mar2	5.12	2.04	5.11	1.99
mp	1.15	4.86	1.27	4.82
nan	2.91	20.47	3.73	20.25
of	4.31	0.13	4.37	0.11
pf	7.37	4.53	9.50	3.59
st	1.13	2.87	0.79	2.63
ug	4.01	23.32	3.92	23.27
xal	3.44	9.27	3.44	9.06

Table 5.5 Comparison between the kurtosis values for the ICs related to one component of the AEP, the CIs artifact and noise in recordings from children with CIs, the estimates were recovered using *Infomax* and *Ext-Infomax*. In the case of the empty cells the ICs were not identified in any of the estimates.

	Infomax			*Ext-Infomax*		
Recording	AEP	CI art	Noise	AEP	CI art	Noise
S1-St1	9.55	-	0.96	8.80	-	-0.85
S1-St2	3.41	-	0.88	3.46	-	-1.25
S1-St3	1.61	-	0.05	1.68	-	-0.87
S2-St1	-	2.36	12.88	-	2.32	12.83
S2-St2	-	2.59	-0.15	-	2.61	-0.64
S3-St1	1.26	1.88	-	1.41	1.81	-
S3-St2	4.68	6.18	-	4.64	6.19	-
S3-St3	5.33	3.47	0.38	5.38	3.48	-1.34
S4-St1	4.77	28.15	-	4.46	28.22	-
S4-St2	7.88	-	1.79	7.88	-	1.87
S5-St1	-	10.71	0.72	-	10.98	-0.54
S5-St2	5.69	3.93	-	5.61	3.84	-
S5-St3	-	7.97	0.19	-	7.85	-1.35
S6-St1	7.40	78.81	-	8.10	256.52	-
S7-St1	-	-	-	-	-	-

Figure 5.3 shows the pdfs and the kurtosis values for selected estimate components using *Ext-Infomax* in four normal hearing children (there were not considerable differences between the estimated components using the standard *Infomax* and *Ext-Infomax*, see appendix B). Estimated components related to the AEP and noisy electrodes were the principal ICs recovered for these algorithms. The kurtosis values of the AEP estimates were positive in all the recordings analysed.

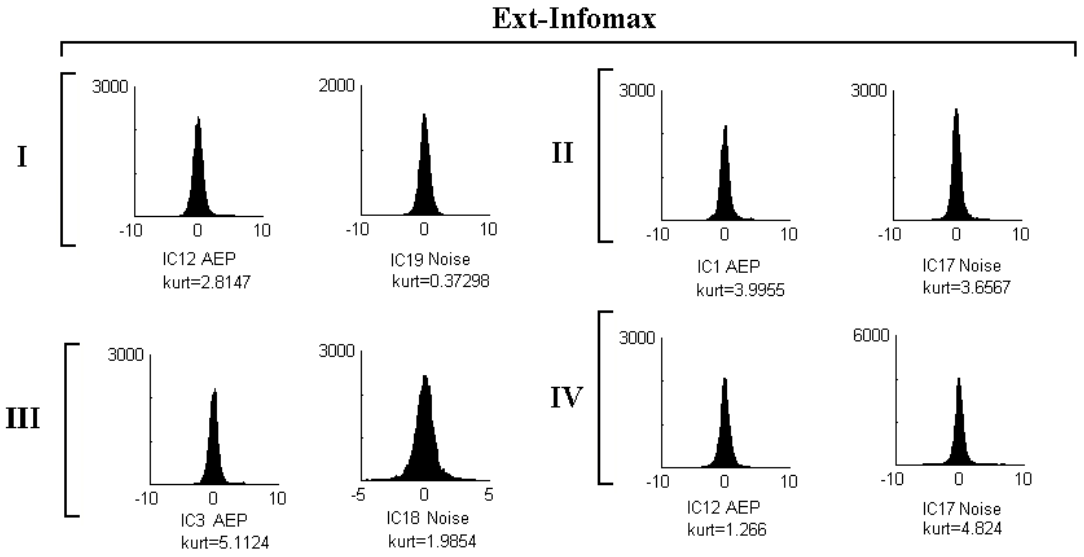

Figure 5.3 Probability distributions and kurtosis values for selected estimates recovered using *Ext-Infomax* (recordings from normal hearing children, I: ***fc***, II: ***bf***, III: ***mar2*** and IV: ***mp***). The AEP and noise were the principal ICs recovered by this algorithm.

There were no considerable differences between the AEP component estimates, in recordings from normal hearing children, using *Infomax* and *Ext-Infomax*. The kurtosis values of the ICs related to the AEP were positive, as expected (Jung *et al* [78] used the original *Infomax* to estimate super-Gaussian components with positive kurtosis, such as the AEP). At least two ICs can be clearly associated with the AEP and background noise in all the recordings from normal hearing children.

Figure 5.4 shows the pdfs and kurtosis values for selected estimates for four different recordings (children with CIs), using *Infomax* and *Ext-Infomax*. In Row I: recording S1-St1, the estimates associated with the AEP (*Infomax*: IC16 and *Ext-Infomax*: IC17) are essentially the same for both algorithms, although some differences can be observed in both the probability distribution histograms and kurtosis values of the noise estimate (IC6 in both algorithms). In row II: recording S1-St2, the difference between the estimates related to the AEPs are small using *Infomax* (IC16) and *Ext-Infomax* (IC10); the principal differences are in the noise estimates from electrodes with high impedance (IC6 and IC1), the pdf shape had modifications and the kurtosis value changed from positive (close to zero) to negative. In row III: recording S3-St2, the estimated components of the CI artifact are similar using *Infomax* (IC8) and *Ext-Infomax* (IC7), with a small difference in the pdf histograms

and kurtosis values. The estimates of the AEP (IC5 and IC6, *Infomax* and *Ext-Infomax* respectively) are almost the same too, although it is not clear in both ICs, the CI artifact still being mixed with the auditory response. In row IV: recording S5-St3, the principal difference between both algorithms is the estimates of the background noise (IC3); it was not possible to identify a clear AEP neither with *Infomax* nor with *Ext-Infomax*.

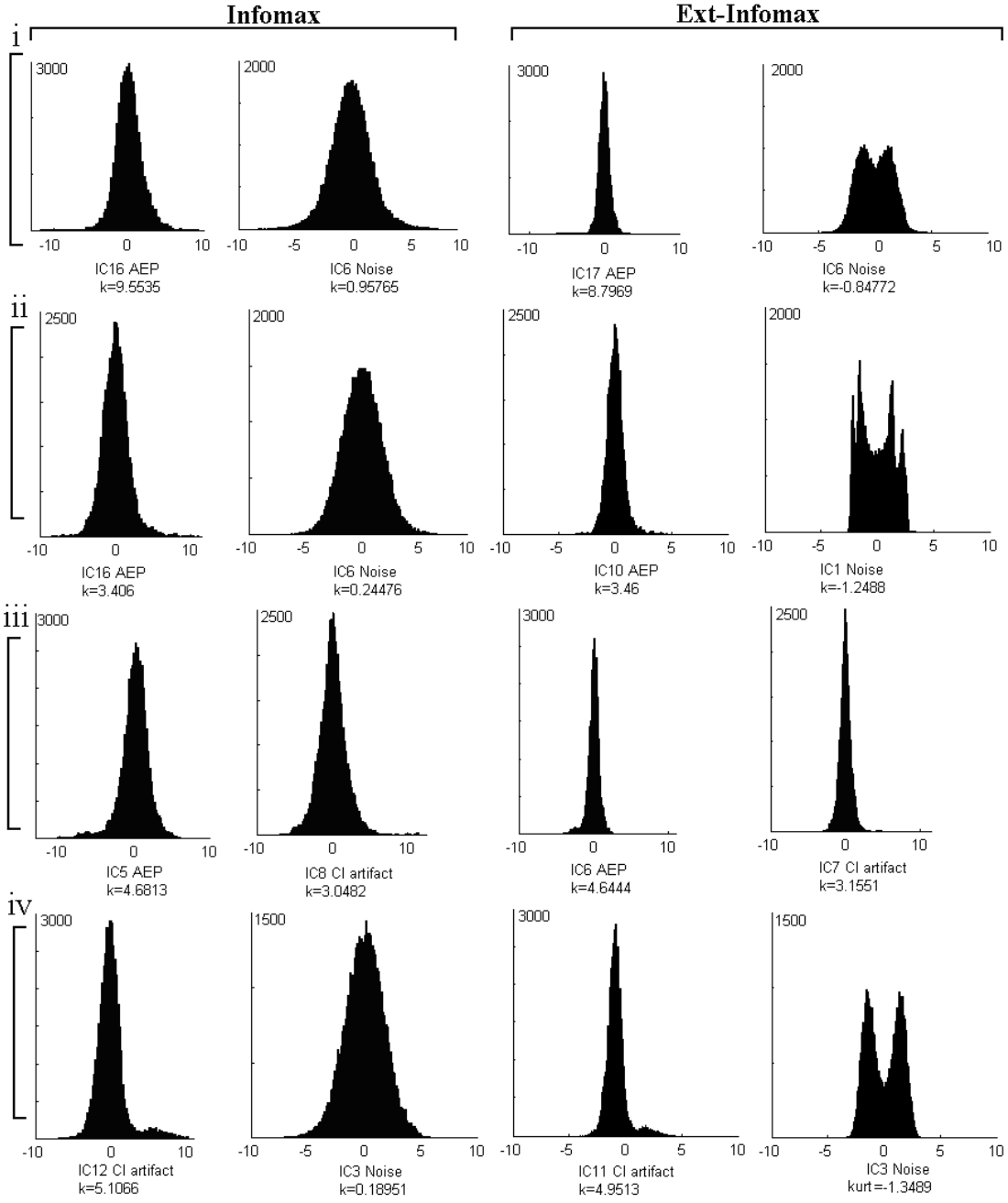

Figure 5.4 Comparison between the pdfs and kurtosis values for selected estimates (using *Infomax* and *Ext-Infomax*) for four different recordings from children with CIs (I: S1-St1, II: S1-St2, III: S3-St2 and IV: S5-St3); the principal difference between those algorithms is the noise estimates.

In recordings from children with CIs, the kurtosis values of the estimates in both original *Infomax* and *Ext-Infomax* for the AEPs and CI artifact are similar; the values for the estimates of the AEPs are positive, as expected. The kurtosis values of the CI artifact estimate depend on the part of the artifact recovered (the transient at the beginning and/or end of the artifact or the stimuli pulses). The principal differences between *Infomax* and *Ext-Infomax* are in the noise estimate components; *Ext-Infomax* is more appropriate to estimate sources with pdfs close to Gaussian distributions.

Based on the kurtosis values, *Ext-Infomax* was finally selected since the noise recovered is better than in the original *Infomax*, which result in an easier identification of the estimates related to the AEPs, however, in 5 of the 13 recordings from children with CIs analyzed using *Ext-Infomax* the AEPs cannot be associated with any of the estimate components. This algorithm has been used to remove the CI artifact from AEP recordings for other authors before; this allows comparing the results of this research with those of these authors.

5.1.3 TDSEP-ICA time delay selection

TDSEP-ICA is based on several time delayed (τ) correlation matrices; the τ parameter must be chosen to take advantage of the temporal structure of the signals. Meinecke *et al* [94] propose the use of resampling methods to assess the reliability of *TDSEP-ICA* and the variance of the estimates as a measure of the separation error. They suggest using this information for selecting the parameters in their algorithm, such as, the time delay value. The procedure used by Meinecke to do that can be summarized as follows:

1. Estimate the mixing matrix $\hat{\mathbf{A}}$ and calculate the ICs as $\hat{\boldsymbol{s}}(t)=\hat{\mathbf{A}}^{-1}\mathbf{x}(t)$,
2. Produce *N*, surrogate datasets *B* from $\hat{\boldsymbol{s}}(t)$ and whiten these datasets. In order to avoid destroying the temporal structure of the signals, when the dataset are surrogated, Meinecke *et al.* calculate the resampled time delayed correlation matrices as

$$\hat{R}_{ij}(\tau)=\frac{1}{2L}\sum a_t\left[x_i(t)x_j(t-\tau)+x_i(t-\tau)x_j(t)\right], \qquad 5\text{-}2$$

where the length of the time series is *L*, the bootstrap resampling defines a series with $\sum a_t = L$.

3. For each of the surrogate datasets produce a set of rotation matrices **Q** (which is approximated by a sequence of rotations) and calculate the variance of rotation parameters angles ($\boldsymbol{\alpha}$), each component α_{ij} of $\boldsymbol{\alpha}$ is the angle of rotation in the *i-j* plane.
4. Calculate each one of the elements of the separability matrix **S** (see Equation 4.19) in the rotation parameters angles as

$$S_{ij} = \sqrt{\frac{1}{B}\sum_{b=1}^{B}\left(\hat{\alpha}_{ij}^{*b}\right)^2}, \qquad 5\text{-}3$$

and identify the different one or high-dimensional subspaces according to the block structure of **S**; a low value corresponds to a good separation. The separability matrix measures how unstable the estimate is with respect to the rotation in the *i-j* plane.

To identify the different one or high-dimensional independent subspaces in the separability matrix, the notion of Multidimensional Independent Components (MICA) introduced by Cardoso [23] could be used. MICA is a generalization of ICA. Instead of the multiplicative model of ICA, where the principal assumption is that all the sources are mutually independent (see Equation 4.4), Cardoso reformulates the ICA model as an additive model (see Equation 4.6), where the measured signal is a sum of *n* one-dimensional independent sources. Instead of that assumption, Cardoso considers that the sources form *k* higher dimensional independent components; there is a set of components that fulfill Equation 4.3, subsequently. In other words, Cardoso proposes that after run an ICA algorithm to obtain the one-dimensional estimated independent subspaces, determine which estimations actually are independent and which should be grouped together as parts of a high-dimensional independent subspace because they are parts of the same component.

To determinate the best time delay parameter for the dataset of this research, τ for *TDSEP-ICA* was varied from 1 to 20 in steps of 5. It was selected such that τ had the lowest separability matrix values, and a clear block structure in the matrix where the AEPs, CI artifact and background noise could be recognized and also associated with one- or high-dimensional ICs. Appendix C includes the separability matrixes for different time values for the complete dataset of this research (the diagonal of the separability matrix was fixed to zero in all the cases).

Figure 5.5 shows the separability matrixes for four different recordings from normal hearing children; the most stable estimate components were obtained using a τ=0, 1, 2, ..., 20. In recording I, subject ***fc***, the two-dimensional independent subspace IC2-IC3 is associated with the AEP, the noise produced by a electrode with high impedance was recovered in a one-dimensional IC, IC18. In recording II, subject ***bf***, again a two-dimensional subspace IC9-IC10 is associated with the AEP and a one-dimensional IC is related to noise (IC1). A clear one-dimensional estimate IC1 linked to the AEP was recovered in recording III (subject ***mar2***); in addition IC9 and IC11 are related to the auditory response. In recording IV, subject ***mp***, two one-dimensional ICs can be recognized in the block structure of the separability matrix, one related to a noisy electrode (IC1) and another to the AEP (IC5).

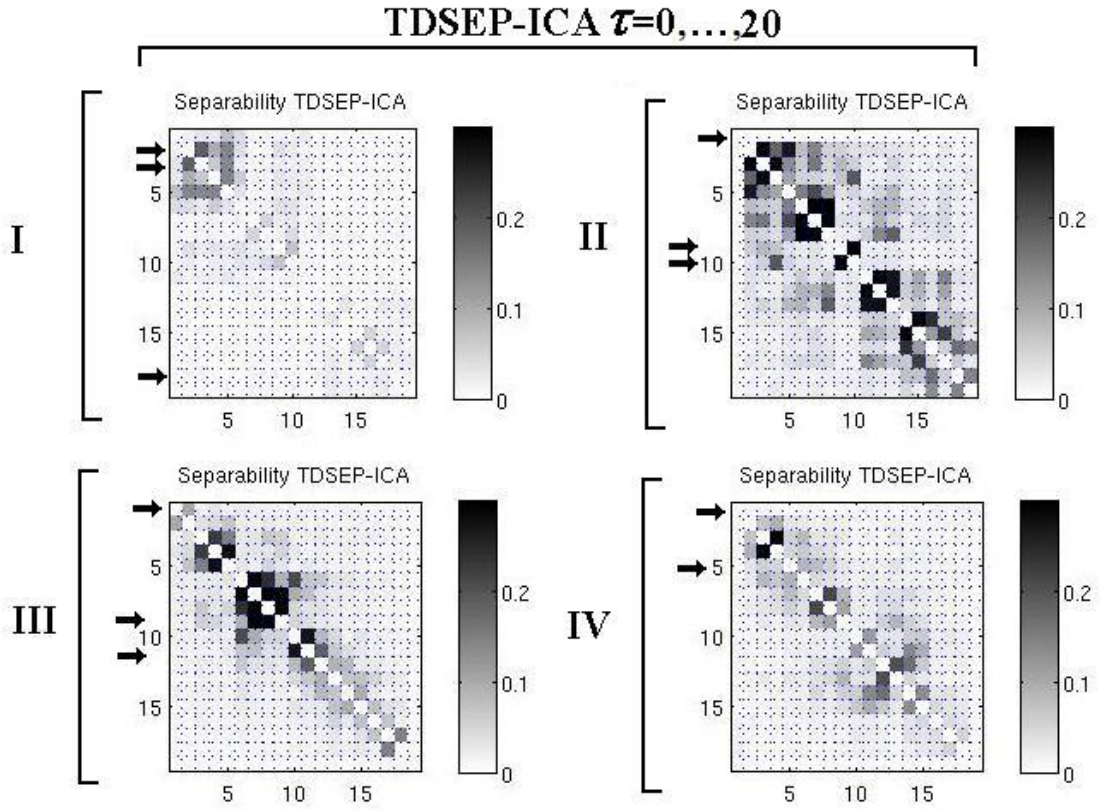

Figure 5.5 Separability matrix for four different normal hearing children using *TDSEP-ICA* (I: ***fc***, II: ***bf***, III: ***mar2*** and IV: ***mp***), the most stable estimates components were obtained with τ=0, 1,2,...,20; arrows indicate ICs related to the AEP and noise.

In recordings from normal hearing children, the separability matrix values decrease in agreement with the increase of the time delay. For τ=0,…,1 *TDSEP-ICA* only identifies one-dimensional ICs always related to noise. Once the time delay is increased, the block structure of the separability matrix is clearer until τ=0, 1, 2, ..., 20 where one-dimensional ICs can be related to the AEP and noise in most of the normal hearing children recordings.

Figure 5.6 shows a comparison between the separability matrix using a time delay τ=0,…,1 and τ=0, 1, 2, ..., 20 for four different recordings (children with CIs). The comparison between *TDSEP-ICA* using a time delay from 0 to 1 and from 0 to 20 for recording S1-St1 is shown in row I, the separability values for the noise estimates are similar between both conditions (τ=0,…1, IC1-IC2 and τ=0, 1, 2, …, 20, IC18-IC19) whilst the AEP estimated separability values are smaller for τ=0, 1, 2, ..., 20 (IC2) than τ=0,…,1 (IC12). The values of the *separability* matrix for recording S1-St2

are markedly lower using a time delay from 0 to 20 (row II). For τ=0,…,1 the estimate related to the AEP is IC8 and IC1 to τ=0, 1, 2, ..., 20; the estimates for the background noise are IC1-IC2 and IC18-IC19, respectively. For recording S3-St2 in row III, using a time delay from 0 to 1 only the CI artifact can be recovered clearly (IC 1, 2 and 3 one-dimensional ICs) whilst using a τ=0, 1, 2, ..., 20, more components are related to the CI artifact (IC16 to IC19) and some components can be associated with the AEP (IC7 and IC9). Row IV, recording S5-St3, *TDSEP-ICA* with τ=0,…,1, IC1 and IC18-IC19 are related to noise and IC2 to the CI artifact. In *TDSEP-ICA* τ=0, 1, 2, ..., 20, IC5, IC8 and IC18 are related to the CI artifact, whilst IC15 is linked to the AEP; although the CI artifact still being mixed with IC15 (neither *FastICA* nor *Ext-Infomax* recovered the AEP in this recording).

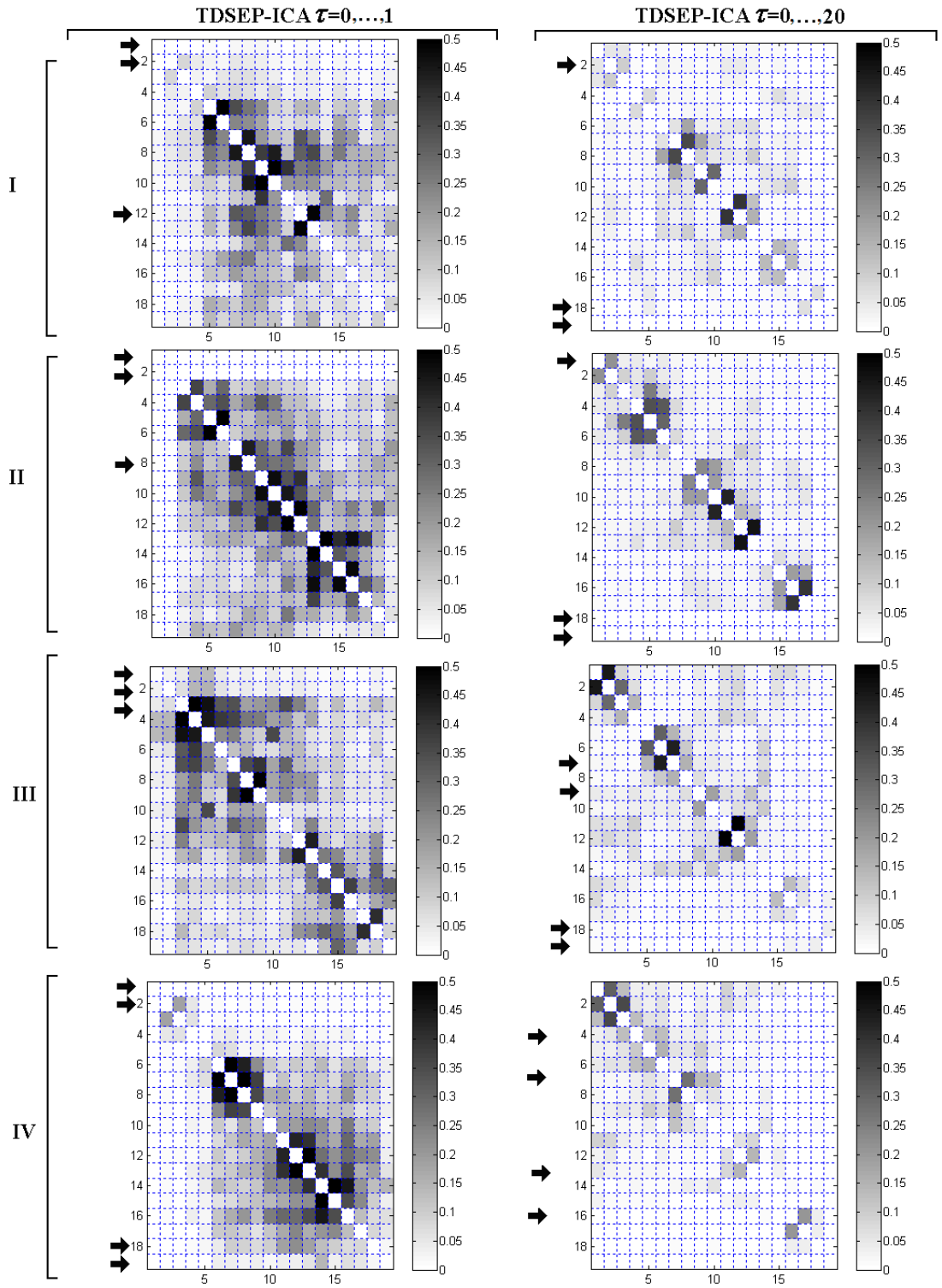

Figure 5.6 Comparison between the separability matrixes with two different time delays using *TDSEP-ICA*, column 1 τ=0,…,1 and column 2 τ=0,1,2,...,20, for four different recordings I: S1-St1, II: S1-St2, III: S3-St2 and IV: S5-St3. In general the separability matrix values were the lowest with τ=0, 1, 2, ..., 20; in most of the recordings one-dimensional ICs can be associated with the AEP, CI artifact and noise using this time delay.

Clearer block structures were identified using *TDSEP-ICA* with τ=0,1,2,...,20 than with τ=0…1, in recordings from children with CIs. Resulting in a notable separation between the ICs related to the CI artifact and noise and the AEP estimates.

The time delay with separability matrixes with one-dimensional ICs related to the AEP and the CI artifact was selected. For *TDSEP-ICA*, the lowest values for the separability matrix were obtained using τ =0, 1, 2, ..., 20 in normal hearing children, also in children with CIs. At this time delay, it was possible to identify a one-dimensional IC related to the AEP and another to the CI artifact [27]. In general, the separability matrix values are lower when the time delay is higher; some tests were performed varying the time delay with values higher than 20 (see Appendix E) but the ICs recovered do not have significant differences.

5.2 Waveform and topographic maps of robust AEP component estimates

This section includes the waveforms and topographic maps of the estimates components with physical and physiological meaning identified in the previous section, after the selection of the optimal parameters for robust AEP component estimates using *FastICA*, *Ext-Infomax* and *TDSEP-ICA*.

5.2.1 FastICA

Figure 5.7 shows the IC waveforms, in the centre of the estimate clusters, and the topographic maps of those components. Recordings from normal hearing children, using *FastICA* with test condition 4 (this condition achieves the most compact and robust estimate clusters); it was possible to recover the AEP in all these recordings. In recording I, subject ***fc***, the background noise remains in the AEP, IC9. In recording II, subject ***bf***, it was possible to indentify a clean AEP, IC4, although the corresponding topographic map is not well defined. Clear AEP components and topographic maps were recovered in recordings III and IV (subjects ***mar2*** and ***mp***, respectively).

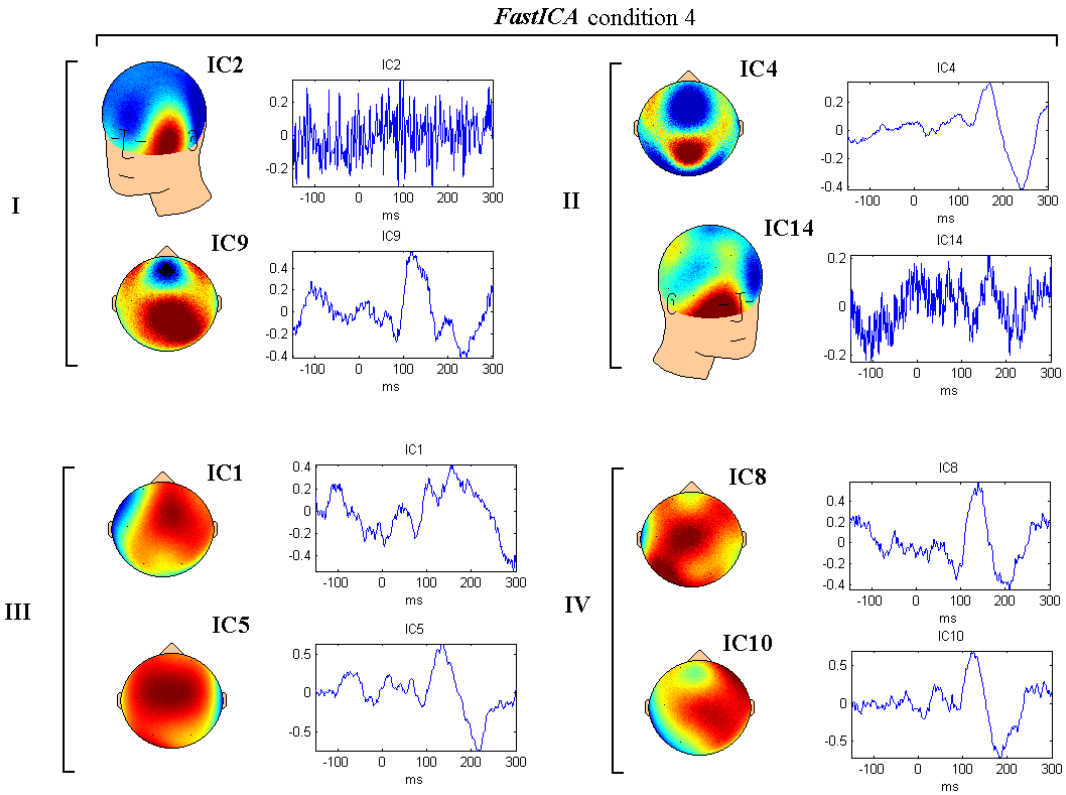

Figure 5.7 Topographic maps and waveforms of selected estimates using *FastICA symmetric* orthogonalization and non-linear function $G_1(y)$, for four normal hearing children (I: ***fc***, II: ***bf***, III: ***mar2*** and IV: ***mp***). The waveforms correspond to the IC in the centre of the estimates clusters; Figure 5.1 complements this figure.

Figure 5.8 shows the waveforms and topographic maps of selected estimate components, after determining the optimal parameters for *FastICA* for recordings from children with CIs (I: S1-St1, II: S1-St2, III: S3-St2 and IV: S5-St3). As for the case of normal hearing children, test condition 4 achieved the most compact and isolated estimated components (see Figure 5.2). However, it was not possible to recover the AEP in all the recordings (see recording III and IV, in this figure). The waveforms correspond to the estimates in the centre of the clusters; clear topographic maps were obtained for the CI artifact ICs (III: IC6 and IC17 and IV: IC1 and IC4) and noise ICs (I: IC11 and II: IC1).

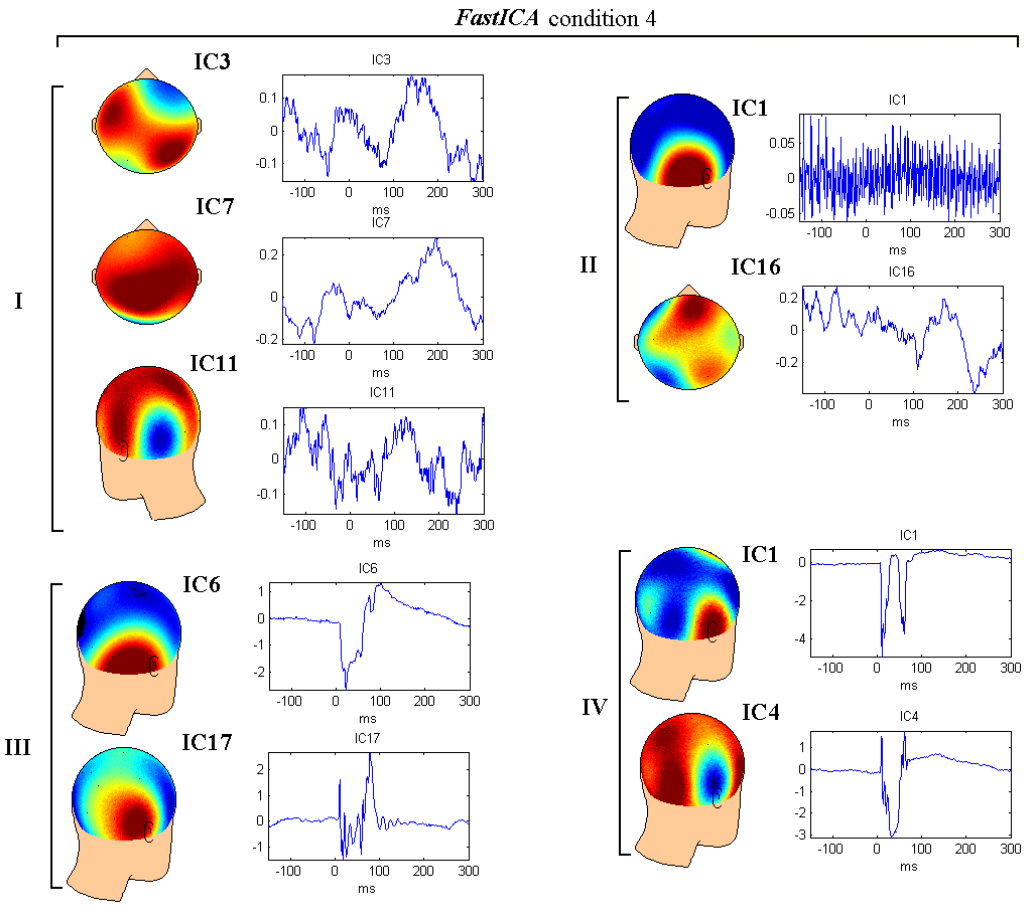

Figure 5.8 Topographic maps and waveforms of selected ICs using *FastICA* with *symmetric* orthogonalization approach and the non-linear function $G_1(y)$ for four different recordings from children with CIs (I: S1-St1, II: S1-St2, III: S3-St2 and IV: S5-St3); Figure 5.1 complements this figure.

5.2.2 Ext-Infomax

Figure 5.9 shows the topographic maps and waveforms of selected estimates using *Ext-Infomax* for four recordings from normal hearing children (see Figure 5.6 for complementary information). The principal ICs recovered using this algorithm were the AEP and noise. Although *Ext-Infomax* is recommended to decompose noisy recordings, it was not possible to recover the AEP without background noise in recordings I, III and IV.

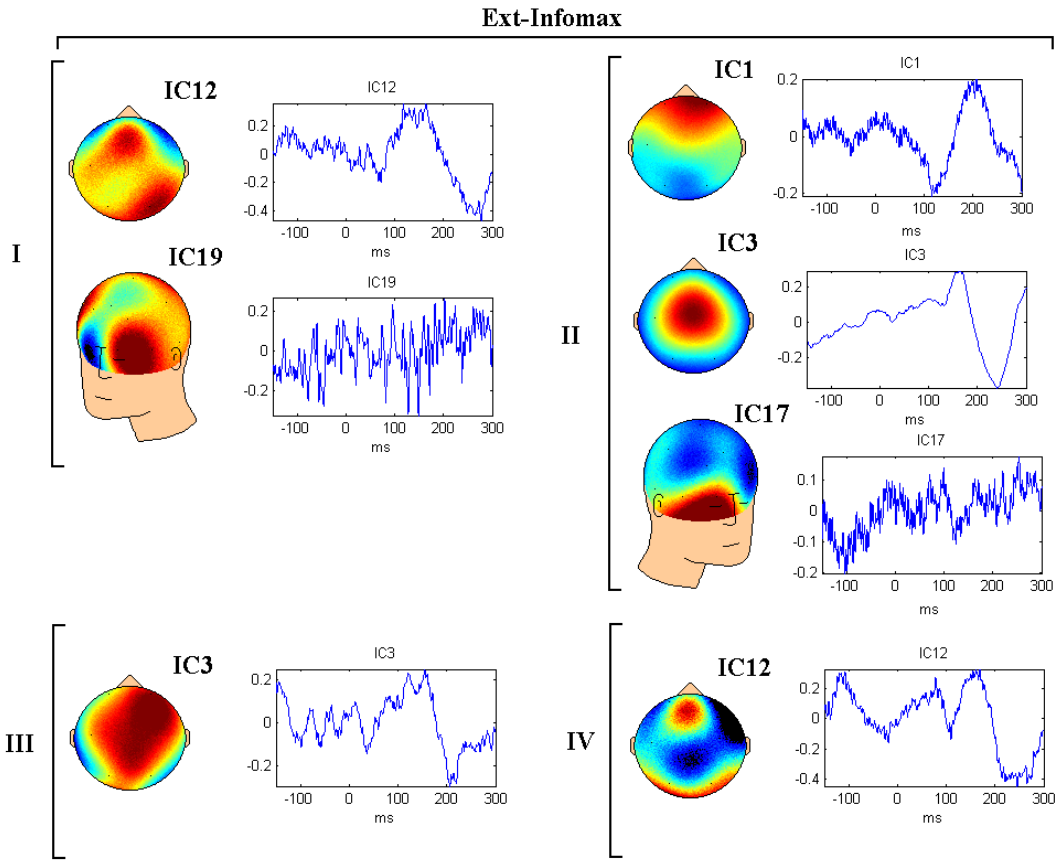

Figure 5.9 Topographic maps and waveforms of selected estimates using *Ext-Infomax* in four recordings from normal hearing (I: ***fc***, II: ***bf***, III: ***mar2*** and IV: ***mp***). The AEP (I: IC12, II: IC1 and IC3, III: IC3 and IV: IC12) together with noisy electrodes (I: IC9 and II: IC17) were the principal ICs recovered for this algorithm.

Figure 5.10 shows the waveforms and topographic maps of selected ICs using *Ext-Infomax* in recordings from children with CIs (I: S1-St1, II: S1-St2, III: S3-St2 and IV: S5-St3). In recordings I and II, is possible to recognize the AEP in IC17 and IC10, respectively. Clear components linked to the CI artifact were recovered from recording III (IC7 and IC9) and from recording IV (IC7 and IC11). The component related to the AEP is not clear in recording III, some of the artifact still being mixed in the auditory response (IC6). In recording IV, none of the estimated components show clear auditory response morphology.

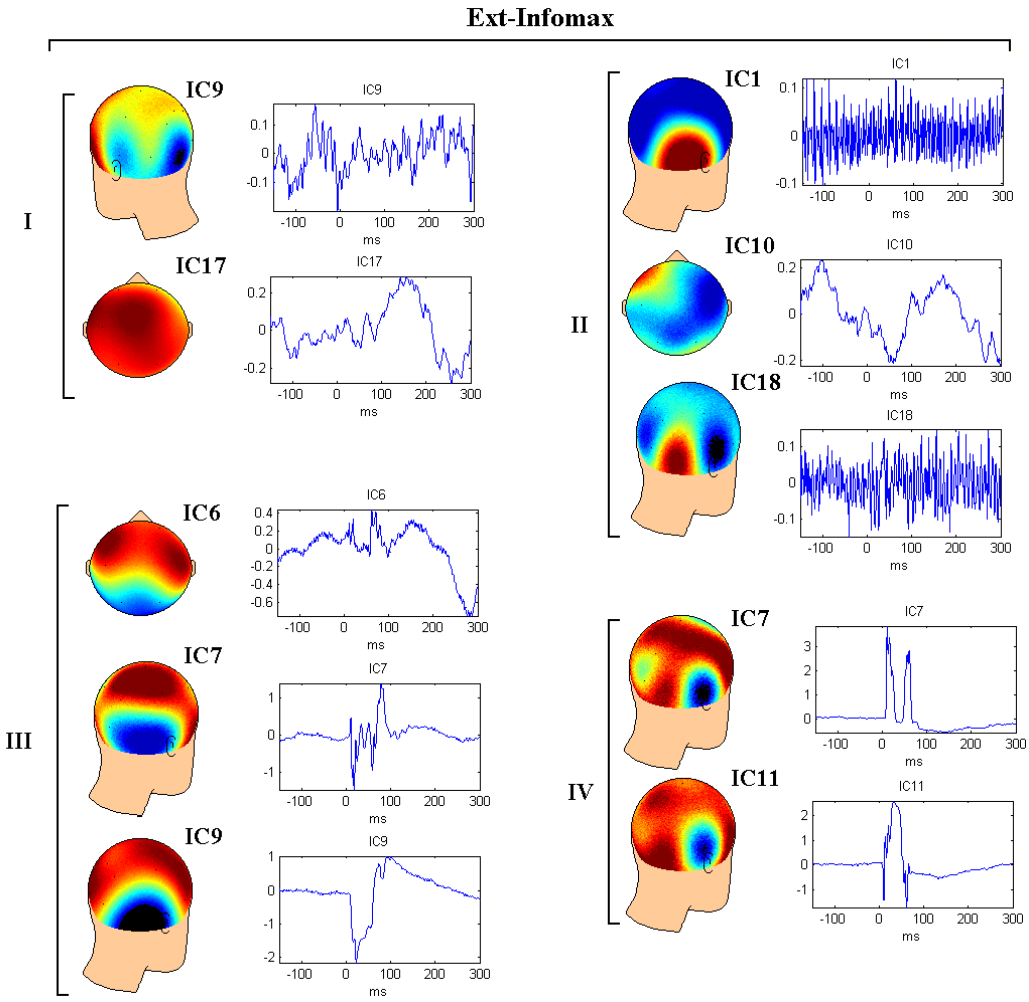

Figure 5.10 Waveforms and topographic maps of selected ICs recovered using *Ext-Infomax* in four different recordings from children with CIs (I: S1-St1, II: S1-St2, III: S3-St2 and IV: S5-St3). The AEP can be recognized in recordings I: C17, II: IC10 and III: IC6, although the CI artifact still being mixed in IC6. *Ext-Infomax* could not recover the AEP in recording IV.

5.2.3 TDSEP-ICA

Figure 5.11 shows the ICs indicated with arrows in Figure 5.5 using *TDSEP-ICA* with τ=0,1,2,...,20. I: The two-dimensional structures IC2-IC3 of the separability matrix have a clear physiological meaning (it can be associated with the AEPs) whilst IC18 correspond to a one-dimensional IC related to a noisy electrode. II: The one-dimensional estimate IC1 is associated with a noisy electrode and the two-dimensional structure IC9-IC10 is linked to the AEP. III: The AEP was recovered in a one-dimensional component IC1 and in a high-dimensional independent subspace; IC9 and IC11 are part of that subspace. Finally, two one-dimensional ICs were recovered in recording IV, IC1 and IC5 are associated with noise and the AEP, respectively. Clear topographic maps of the ICs of interest were obtained.

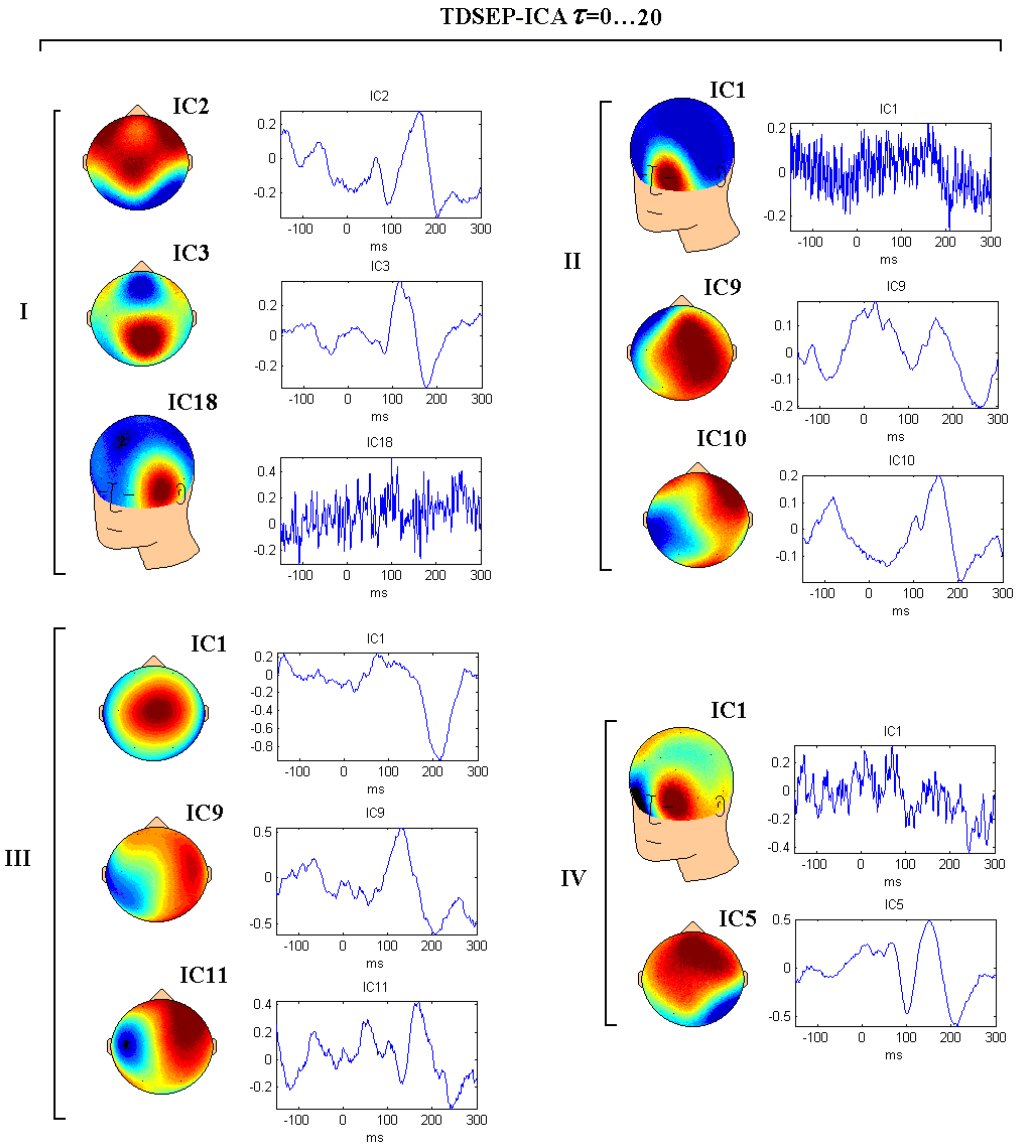

Figure 5.11 Topographic maps and waveforms of the estimate components indicated with arrows in Figure 5.5, using *TDSEP-ICA* with τ=0, 1, 2, ..., 20 (recordings from normal hearing child, I: ***fc***, II: ***bf***, III: ***mar2*** and IV: ***mp***), this condition recovers the most stable ICs related to the AEP.

Figure 5.12 shows selected ICs recovered using *TDSEP-ICA* with τ=0,1,2,...,20 (see Figure 5.6 for complementary information) for four different recordings from children with CIs (I: S1-St1, II: S1-St2, III: S3-St2 and IV: S5-St3). The block structure of the separability matrices show diverse one-dimensional ICs, for example in recording I, IC2 and IC18 are related to the AEP and a noisy electrode, respectively. In recording II, it was possible to identify two one-dimensional ICs related to contiguous noisy electrodes IC18-IC19, and IC1 related to the AEP. In recording III, IC7 is linked to the AEP (this component is part of a high dimensional subspace). The one-dimensional component IC9 is related to the AEP whilst IC18 and

IC19 (one-dimensional ICs) are related to the CI artifact. Finally, in recording IV, three one-dimensional ICs have physical or physiological meaning, IC5 and IC18 related to the CI artifact, and IC15 related to the AEP (the CI artifact still being mixed in this IC); another component of the CI artifact was recovered in a high dimensional subspace (IC8 is part of this subspace). Clear topographic maps of the ICs selected were obtained.

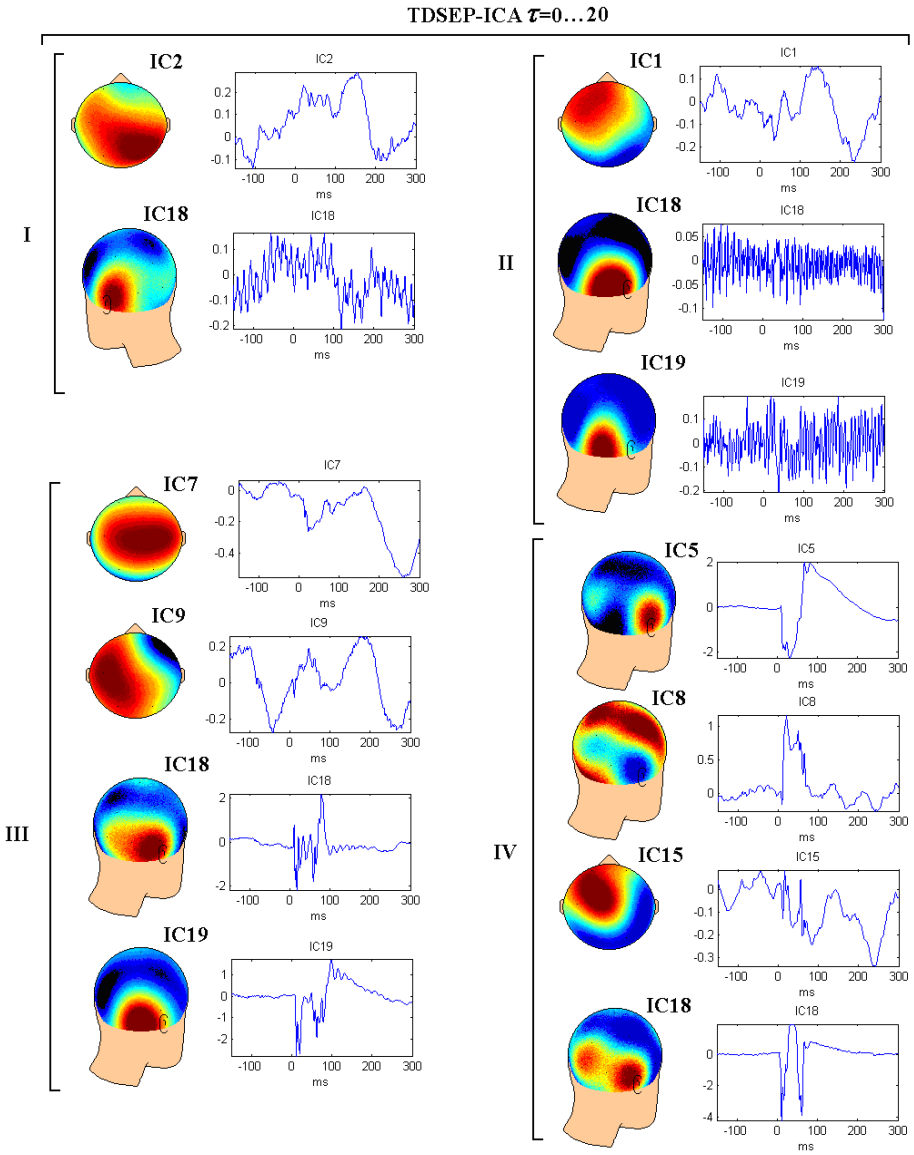

Figure 5.12 Topographic maps and waveforms of the ICs indicated with arrows in Figure 5.6 (using *TDSEP-ICA* with τ=0,1,2,...,20, recordings from children with CIs, I: S1-St1, II: S1-St2, III: S3-St2 and IV: S5-St3), the most stable estimate components correspond to the AEP, the CI artifact and noisy electrodes.

Of all the ICA algorithms, the most widely used to remove artifacts from biomedical signal is *FastICA* [71]. However, in the case of EEG analysis, algorithms that include the temporal structure of this signal are better suited to extract meaningful

estimations; this is the case of the dataset of this research where *TDSEP-ICA* take advantage of time coherence of the CI artifact onset time.

5.3 Summary

The optimal parameters to recover both the AEP (in normal hearing and children with CI), as well as the CI artifact (in recordings from children with CIs) for the three ICA algorithms assessed in Section 5.1 are: a) *FastICA* with a *symmetric* orthogonal approach and the non-linear function $G_1(y)=y^3$ (Table 5.1, test condition 4). b) *Ext-Infomax* instead of *Infomax*, and c) *TDSEP-ICA* with time delay τ=0,1,2,...,20.

FastICA, test condition 4, achieved the highest number of clusters with I_q index values between 0.9 and 1 (in 9 of the total recordings analysed in children implanted); the robustness of clusters and reliability of the estimates were better than any other test condition. Most of the times, those clusters are related to the CI artifact components and noise, but are not necessarily related to the AEP.

The principal differences between the estimated components using *Infomax* and *Ext-Infomax* were in the background noise; the kurtosis values of the estimates change from positive (close to zero) to negative; the pdf histograms have different shapes for the AEP, CI artifact and noise using *Ext-Infomax*.

TDSEP-ICA, with τ=0,1,2,...,20 achieved the lowest separability matrix values and the structure of the matrix is the clearest over all the time delays evaluated. One-dimensional ICs are related to the CI artifact and noise whilst one- or high-dimensional ICs are associated with the AEP, depending on the symmetry of the auditory response. In most of the children implanted, the response is lateralized, opposite to the CI.

The three algorithms recover at least two components for the CI artifact; one related to the transient at the beginning and/or the end of the artifact and another to the stimuli pulses. When the recording *SNR* is poor, only *TDSEP-ICA* with time delays from 0 to 20 recovered the AEP in recordings from children with CIs.

If the objective is to apply ICA to reduce the CI artifact both *FastICA* and *Ext-Infomax* are more than enough to do that. However, to also recover the AEP in EEG recordings contaminated by the CI artifact, *TDSEP-ICA* is better positioned to carry this out, because the assumption of this algorithm (temporal structure of the signal and the spatial uncorrelation between the auditory response and the CI artifact) best place it to do so. *TDSEP-ICA* relies only on simple lagged second-order correlations, which is estimated robustly, compared with the HOS methods that are generally less robust because the difficulty of the calculations. Additionally some authors have demonstrated that may be hard to estimate robust ICs if some temporal overlap is present in the sources [128; 129; 135]; which could occur in the dataset used in this research.

Once the optimal parameters for robust AEP component estimates for *FastICA*, *Ext-Infomax* and *TDSEP-ICA* have been selected, it is important to asses the performance and variability of the ICs recovered by the three ICA algorithms. The procedure proposed by Meinecke, summarized in section 5.1.3, was used to compare the algorithms (under the same condition). In the following chapter, the results of this comparison are shown.

Chapter 6.

Assessment of the performance and variability of ICA algorithms applied to AEP estimation

The performance and variability of three ICA algorithms (*FastICA, Ext-Infomax* and *TDSEP-ICA*), whose optimal parameters for robust AEP component estimates were determined in the previous chapter, are now assessed in this chapter. In section 6.1, the procedure suggested by Meinecke *et al*. (see section 5.1.3) which utilizes the block structure of the separability matrix (**S**) to evaluate the stability of the estimate components, is used to evaluate the performance of the ICA algorithms. In section 6.2, the Signal to Interference Ratio index [55] is used to measure the quality of the estimates recovered for each algorithm. Finally, in Section 6.3, the variability of the algorithms is measured, after repeating the estimate several times.

6.1 Reliability of AEP component estimates

Meinecke *et al.* proposed to use the separability matrix, **S,** of the ICs (see Equation 5.3) not only to select the parameters of *TDSEP-ICA* but also as a means of choosing between different algorithms that rely on different assumptions about the dataset and their criteria to measure independence. This matrix was used here to evaluate the reliability of three ICA algorithms, after selection of the optimal parameters for each one as described in the previous chapter.

To evaluate the reliability of the ICs recovered for the three algorithms (under the same conditions), the estimates were each repeated 10 times (N=10) using each of

the ICA algorithms; the number of ICs was set at equal to the dataset dimension, 19. The separability matrices, for the three algorithms were calculated for all the ICs and their block structures were compared. Three considerations were taken into account to compare the separability matrixes: 1) the values of the elements of **S** (low values correspond to a good separation). 2) The structure of **S**, the possibility to identify clear one-, two- or high-dimensional ICs. 3) The possibility of recognizing ICs with physical or physiological meaning (AEP, CI artifact and noise) in the one- and two-dimensional ICs. Appendix D includes a comparison between the separability matrixes, for the ICA algorithms mentioned, for the complete dataset of this research.

Figure 6.1 shows a comparison between the separability matrixes using *FastICA*, *Ext-Infomax* and *TDSEP-ICA*, in recordings from four normal hearing children. Row I: recording ***fc***, only *TDSEP-ICA* recovers the recording noise (background noise and noisy electrodes) in one-dimensional ICs (IC10-1C19), resulting in clearer estimates of the AEP (one-dimensional estimate, IC9, and two-dimensional estimates, IC2 and IC3) than *FastICA* and *Ext-Infomax*. In the second recording, row II: subject ***bf***, the three algorithms recover the noise generated by a noisy electrode, but only *FastICA* and *TDSEP-ICA* identify a one-dimensional IC with this noise (IC17 and IC1 respectively); *Ext-Infomax* recovers this noise in different ICs (IC6, IC9 and IC17). Clear ICs can be related to the AEP using the three algorithms (*FastICA*: IC2, *Ext-Infomax*: IC18 and *TDSEP-ICA*: IC17). One two-dimensional IC can be identified in each algorithm (*FastICA*: IC3-IC4, *Ext-Infomax*: IC5-IC6 and *TDSEP-ICA*: IC9-IC10), the two-dimensional ICs of *FastICA* and *Ext-Infomax* correspond to noisy AEPs, whilst the two-dimensional IC of *TDSEP-ICA* is related to two clear components of the AEP. In recording III: subject ***mar2***, both *FastICA* and *TDSEP-ICA* recovered the AEP in one-dimensional ICs (IC1s for both algorithms). The three algorithms indentified two-dimensional ICs (*FastICA*: IC8-IC9, *Ext-Infomax*: IC4-IC5 and *TDSEP-ICA*: IC6-IC7), but only the two-dimensional ICs recovered by *FastICA* had a clear physiological meaning (components of the AEP). Finally, in recording IV, subject ***mp***, it is possible to recognize the AEP using the three ICA algorithms, all with low separability matrix values (*FastICA*: IC14, *Ext-Infomax*: IC14 and *TDSEP-ICA*: IC5), but only *TDSEP-ICA* recovered clear one-dimensional ICs related to noise: IC1, IC18 and IC19.

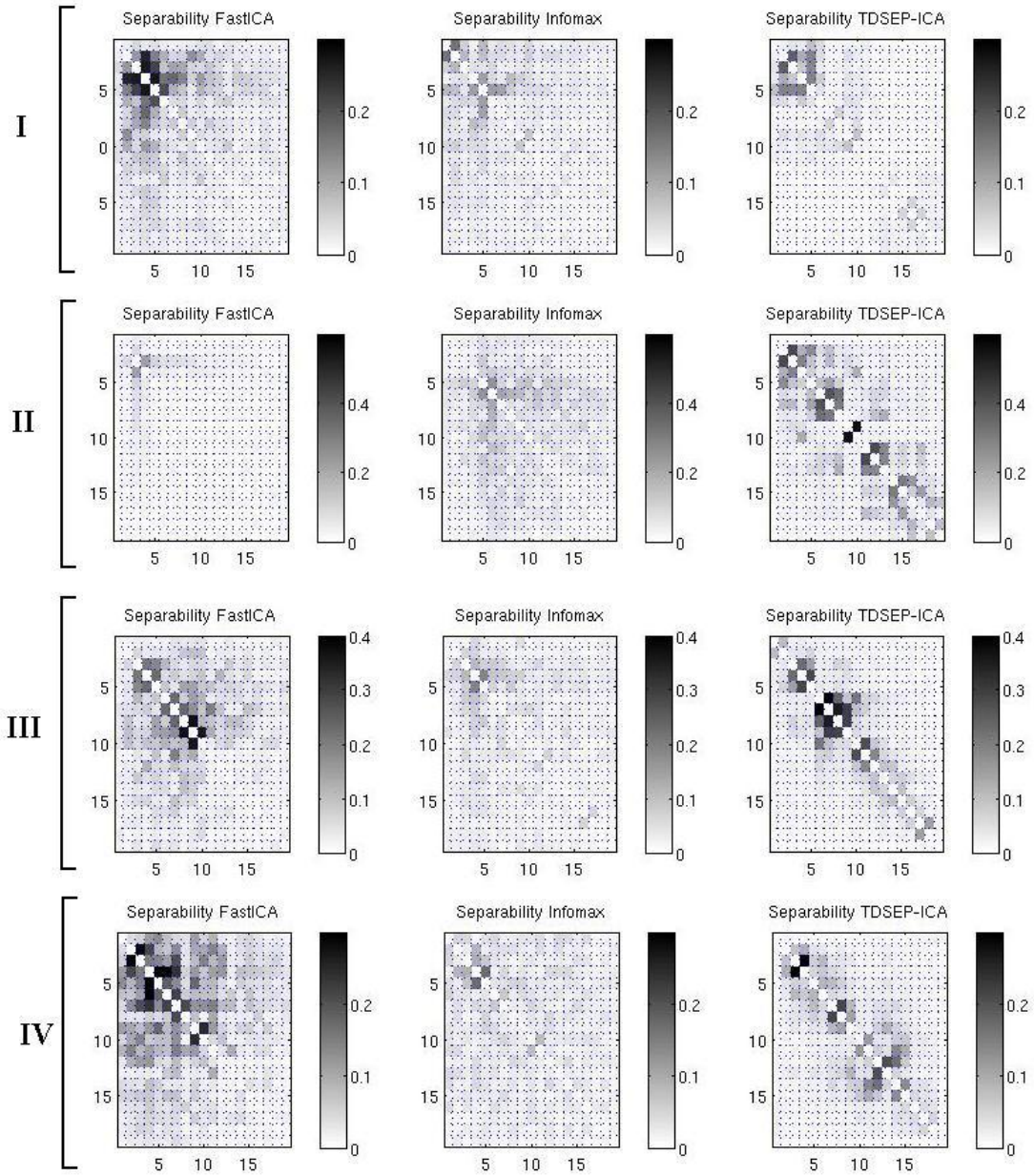

Figure 6.1 A comparison between the separability matrices using *FastICA*, *Infomax* and *Ext-Infomax*, for four different recordings (all normal hearing children, I: ***fc***, II: ***bf***, III: ***mar2*** and IV: ***mp***), *TDSEP-ICA* (column 3) is the algorithm with clearer block structure, in each case one and two-dimensional ICs are related to the AEP and background noise.

Although in most of the recordings from normal hearing children the separability values of **S** in both *FastICA* and *Ext-Infomax* are lower than the values of *TDSEP-ICA*, the block structure of this matrix is the clearest (see section 5.1.3); one-dimensional ICs related to the AEP and noise were identified in all the recordings.

Figure 6.2 show the separability matrices, **S**, for four different recordings from children with CIs, using *FastICA*, *Ext-Infomax* and *TDSEP-ICA*. In recording I:

subject S1-St1, all the algorithms recover the background noise (*FastICA*: IC3 and IC7, *Ext-Infomax*: IC18 and *TDSEP-ICA*: IC18 and IC19) but only *TDSEP-ICA* identified a clear one-dimensional IC for this noise (IC19); with respect to the AEP, *TDSEP-ICA* is the only algorithm which identified a one-dimensional ICs related to the auditory response (IC2). In recording II: subject S1-St2, two nearby electrodes had high impedance, although the three algorithms recover this noise, only *FastICA* and *TDSEP-ICA* estimated it into one-dimensional ICs (*FastICA*: IC14 and IC16 and *TDSEP-ICA*: IC18 and IC19), the ICs for the noisy electrodes for *Ext-Infomax* were IC1 and IC14 (only IC1 shows a clear one-dimensional structure). *FastICA* indentified a one-dimensional IC for the AEP (IC11); *TDSEP-ICA* recovered the auditory response in a two-dimensional space (IC11-IC12), additional to the IC1. The AEP is not clear in any of the ICs estimated by *Ext-Infomax*. In recording III, subject S3-St2, all the one-dimensional ICs recovered by *FastICA* correspond to components of the CI artifact (it was not possible to identify the AEP in the rest of the ICs). Although it is possible to identify some elements of the CI artifact in the ICs recovered by *Ext-Infomax*, the lack of a clear block structure in **S**, implies low reliable estimates. *TDSEP-ICA* shows the clearest **S** structure with a two-dimensional subspace (IC6-IC7) related to the AEP and three one-dimensional ICs (IC9: AEP and IC18 & IC19: CI artifact). Finally, in recording IV, subject S5-St3, all the algorithms recover a noisy signal (*FastICA*: IC16, *Ext-Infomax*: IC19 and *TDSEP-ICA*: IC19). The reliability of the estimates related to the CI artifact is similar for the three algorithms (*FastICA*: IC16, IC17 and IC8, *Ext-Infomax*: IC16, IC17 and IC18 and *TDSEP-ICA*: IC5, IC8 and IC18). Only *TDSEP-ICA* indentified a one-dimensional IC for the auditory response (IC15).

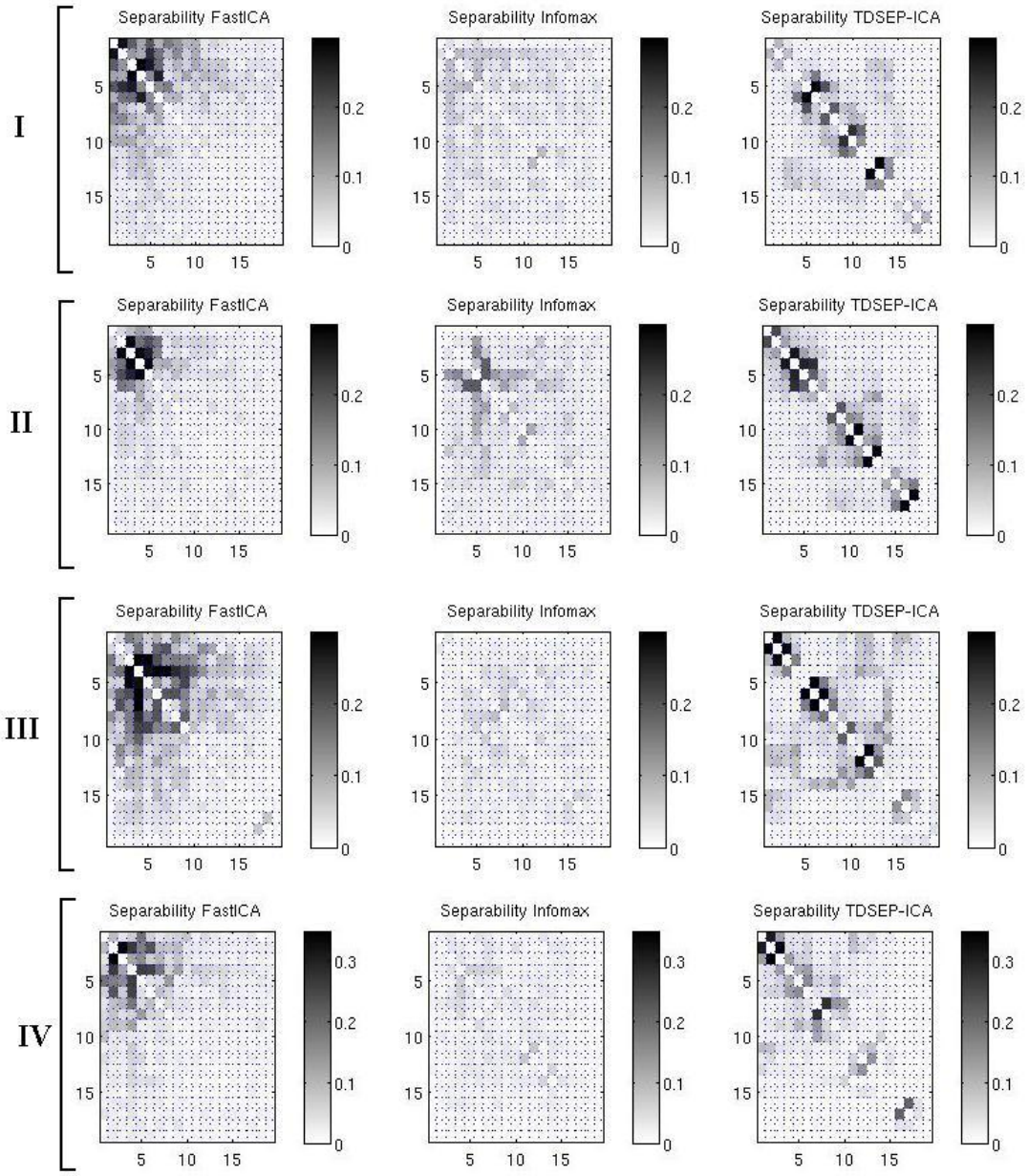

Figure 6.2 A comparison between the separability matrices using three ICA algorithms from four different recordings (children with CIs**,** I: S1-St1, II: S1-St2, III: S3-St2 and IV: S5-St3), *FastICA* (1st column) indentifies the AEP in high-dimensional ICs in all the recordings, *Ext-Infomax* (middle column) does not show a clear block structure; clear one- and two-dimensional ICs were recovered by *TDSEP-ICA* for the AEP, CI artifact and noise (3rd column).

Figure 6.3 shows a comparison between the separability matrix for the three ICA algorithms for both normal children and children with CIs (using the optimal parameters determined in the previous chapter for each algorithm). Although *Ext-Infomax* has the lowest separability values, it is not possible to identify a clear block structure in **S**. Neither *FastICA* nor *Ext-Infomax* recovers a clear estimate of the AEP

in these recordings from children with CIs. From the block structure of the separability matrix, it appears that *Ext-Infomax* recovered the less stable ICs in both normal hearing children and children with CIs.

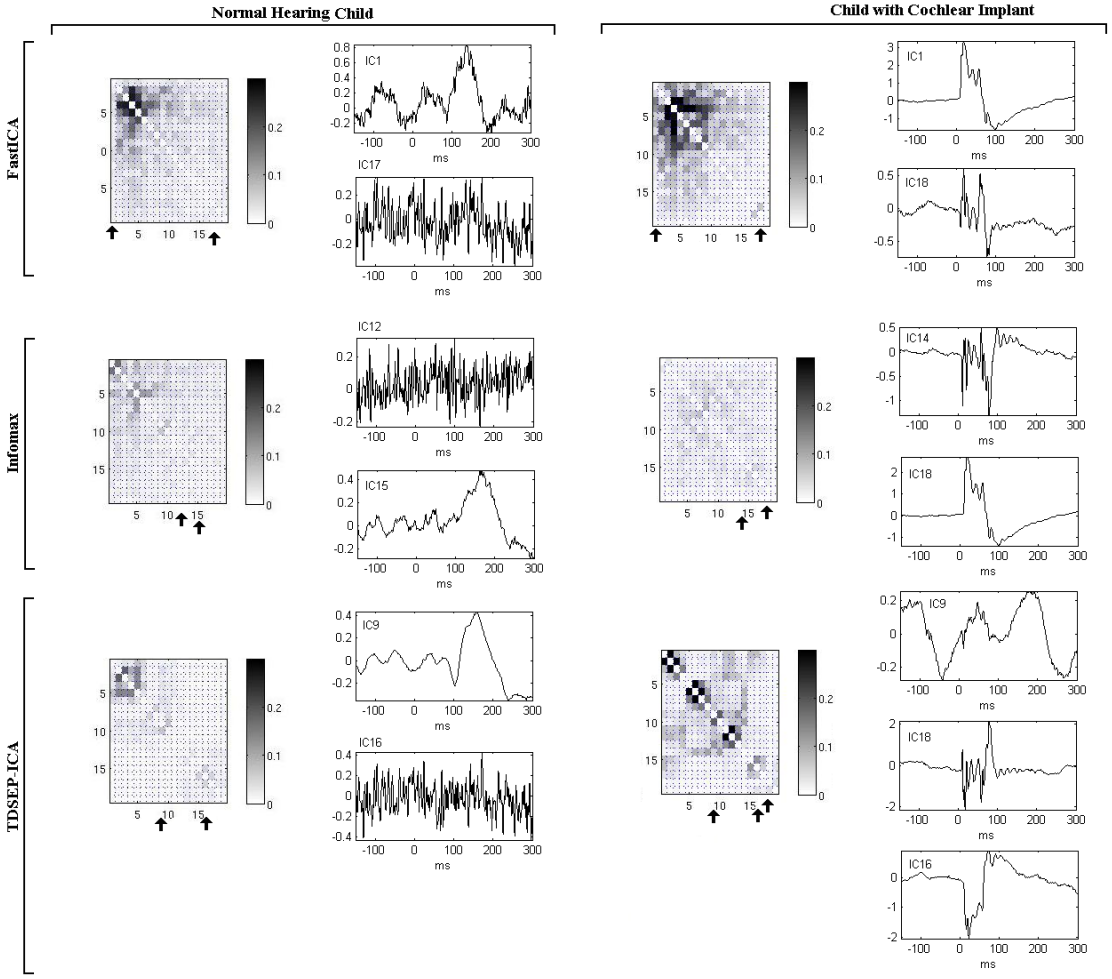

Figure 6.3 A comparison between the separability matrices for all the ICs estimated by three ICA algorithms (recordings from a normal hearing child, ***fc***, and child with CI, S3-St2), the arrows indicate the ICs with physical or physiological meaning. In normal hearing children, it is possible to recognize the AEP and background noise with all the algorithms (although those estimates are not one-dimensional ICs using *FastICA* and *Ext-Infomax*); whilst in children with CIs only *TDSEP-ICA* recovers the auditory response in one-dimensional IC.

Ext-Infomax does not show a clear block structure in recordings from normal hearing children, this algorithm cannot recover the background noise as well as *FastICA* and *TDSEP-ICA*. In general, *FastICA* recovers more stable ICs than *Ext-Infomax*, in both recordings from normal hearing children and children with CIs, but it was not always possible to identify clear one- or two-dimensional ICs associated with the AEP in some of the separability matrixes achieved using this algorithm. *TDSEP-ICA* is able to find more one-dimensional ICs than any other of the ICA algorithm

compared in this research. Most of the time, these one-dimensional ICs have a clear physiological (AEP) or physical meaning (CI artifact and noise).

The resampling approach used in this section to compare *FastICA*, *Ext-Infomax* and *TDSEP-ICA* showed that *TDSEP-ICA* is the most suitable algorithm for recovering stable ICs related to the AEP as well as the CI artifact in the dataset recordings used in this research.

Up to this point, the comparison between the three ICA algorithms has been using principally qualitative parameters, mainly the waveforms and topographic maps to relate ICs with physiological events, and the block structure of the separability matrix to establish the quality of the separation. In the following section, a quantitative parameter is used to assess the performance and the variability of the ICs recovered by *FastICA*, *Ext-Infomax* and *TDSEP-ICA* on real, physiological data.

6.2 The performance of the ICA algorithms

The performance of the ICA algorithms can be evaluated by different procedures

1) An inspection of the plots of the estimate,
2) Using an index such as *SNR*, or
3) Calculating the interference between the estimated sources.

The different methods to evaluate the performance of the algorithms depend on the data that are available, in other words, if the true mixing matrix (**W)** is known or not. In the case of synthetic data, the performance of an ICA algorithm can be measured using for example the Amari Index, *Am*, (see Equation 6.1) which is an assessment of the interference of source *n* on measurement *m* [9]; a perfect separation E_1 results in an index of zero; this method has been used by different authors [97;135] to compare diverse ICA algorithms for EEG components estimates and to analyze the quality of the separation in a hybrid mixture of acoustic signals (for example, speech and music) and synthetic sources.

$$\boldsymbol{Am} = \sum_{i=1}^{n}\left(\sum_{j=1}^{n}\frac{|p_{ij}|}{\max_k |p_{ik}|}-1\right)+\sum_{i=1}^{n}\left(\sum_{j=1}^{n}\frac{|p_{ij}|}{\max_k |p_{kj}|}-1\right), \qquad 6\text{-}1$$

where $\mathbf{P}=(p_{ij})=(\mathbf{WA})$; $\mathbf{P}$ is a permutation matrix.

In the case of real data and when the mixing matrix is unknown, there are different indexes to measure the performance of the estimate of ICA, the *Signal to Interference Ratio* (*SIR*) [55] is the index most frequently used, and is defined as follows

$$SIR = \frac{\left|\langle \hat{s}_i, s_i \rangle\right|^2}{\|\hat{s}_i\|^2 \|s_i\|^2 - \left|\langle \hat{s}_i, s_i \rangle\right|^2}, \qquad 6\text{-}2$$

where $\hat{s}_i$ represents the estimated sources, and s_i the real sources (*reference signal*); here the inner product is a measurement of the distance between two signals. When the estimated source is orthogonal to the true source, *SIR* is equal to zero; but if the estimated source is equal to a gain factor g of the true source, $\hat{s}_i = gs_i$, *SIR* is infinite. Higher values of *SIR* indicate a better estimate quality.

The reference signals: to assess the quality of the estimates of both the AEP and CI artifact, it was necessary to generate an accurate reference signal for both cases. AEP reference signals, for four age ranges, were obtained by averaging the auditory response of the normal hearing children in each control dataset group (see Table 3.1). The AEP references signals (target 1 to target 4 in Figure 6.4) correspond to the response at electrode site Cz, that are known to display the maximum amplitude for P_1 peak. The reference signal for the CI artifact was achieved by averaging the electrodes closest to the CI (around the temporal area) from five children with CI.

Figure 6.4 Average AEP waveforms for four groups of normal hearing children for different age range (see Table 3.1), target 1 to 4, and CI artifact signal used as reference signals in Equation 6.2.

Using Equation 6.2, the *SIR* index values for the 19 estimates recovered by each of the ICA algorithms, were calculated. The reference signal was changed from target 1 to target 4 in both recordings from normal hearing children and children with CIs; additionally the *SIR* values with the CI artifact as reference was calculated in children with CIs. The purpose of this test was to determine which algorithm achieved the highest values of *SIR*, to determine better quality estimates.

In order to establish the minimal *SIR* index values permitted for the AEP a first test was carried out, the *SIR* values for all the ICs recovered for the three algorithms were calculated using the four AEP reference signals (see Figure 6.4), but in the recordings from children without stimulation (where no one IC estimated is related with the AEP). The average *SIR* index values for the AEP in recordings from 20 normal hearing children without stimulation were $SIR_{FastICA}$=0.61, $SIR_{Ext\text{-}Infomax}$=0.61 and $SIR_{TDSEP\text{-}ICA}$=0.76; the average for the three algorithms was $SIR_{average}$=0.66±0.08.

In a similar fashion, the reference signal of the CI artifact was used to calculate the *SIR* index of the ICs recovered by the three algorithms in normal hearing children (where of course no one IC estimated is related with this artifact). The *SIR* index values for the CI artifact in 22 recordings from normal hearing children were $SIR_{FastICA}$=0.55, $SIR_{Ext\text{-}Infomax}$=0.53 and $SIR_{TDSEP\text{-}ICA}$=0.46; the average for the three algorithms was $SIR_{average}$=0.51±0.05.

With these results, it was established that recordings from both normal hearing children and children with CIs with the AEP *SIR* index values close to or less than **0.66** were discarded. In the same manner, if the *SIR* values of the CI artifact were close to or less than **0.51** in recordings from children with CIs the recordings were not taken into account for further analysis. Appendix F includes tables with the entire *SIR* index values for both normal hearing children and children with CIs, using the AEP and the CI artifact as reference signals.

Figure 6.5 shows the highest *SIR* index values calculated (using *FastICA*, *Ext-Infomax* and *TDSEP-ICA*) for two normal hearing children. (a) In recording ***xal***, 4 y.o

the highest values, for the three algorithms, were obtained using target 2 as reference signal. (b) For the normal hearing child ***mp***, 11 y.o., the highest values were obtained with target 4; the results of both subjects are in accordance with the age group of each child. The waveforms of the ICs with the maximal *SIR* values for each algorithm are shown at the right hand side of each one of the *SIR* histograms.

(a) (b)

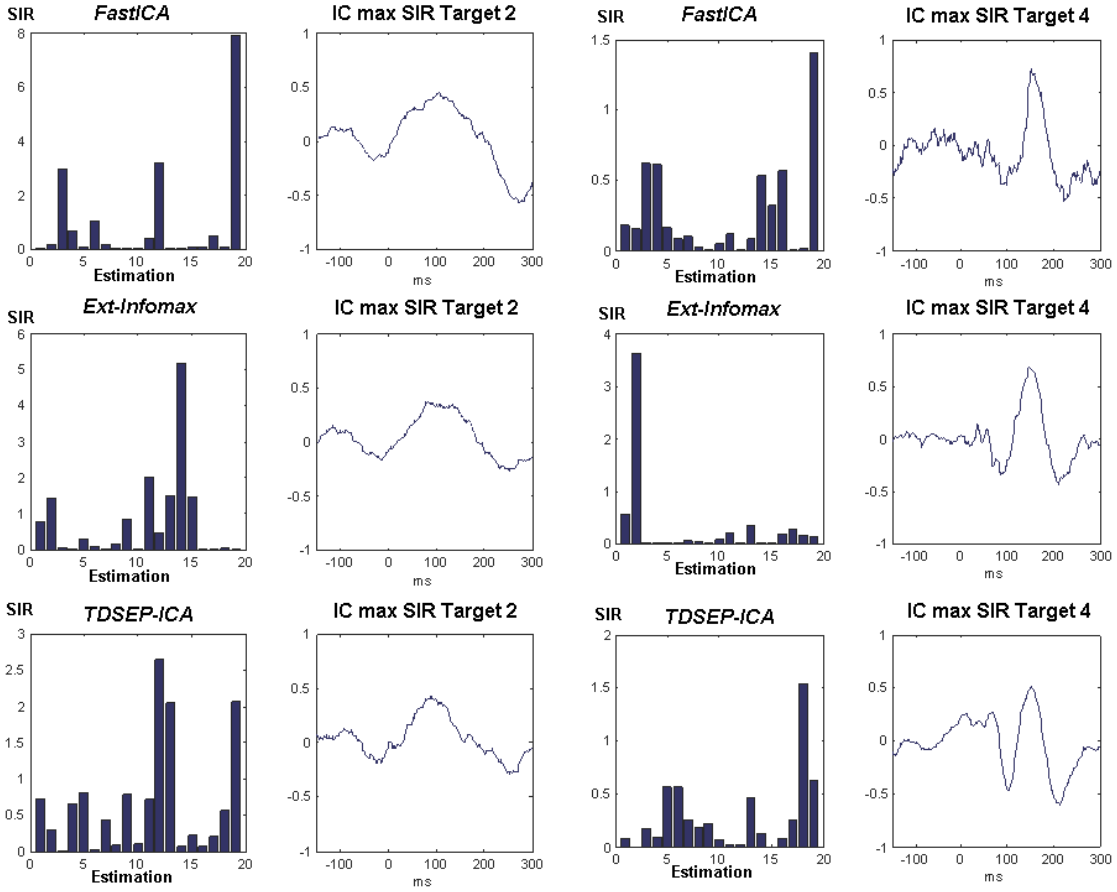

Figure 6.5 *SIR* index values for 19 estimates using *FastICA*, *Ext-Infomax* and *TDSEP-ICA* for two different normal hearing children (a) ***xal***, 4 y.o and (b) ***mp***, 11 y.o. The waveforms of the ICs with the maximum *SIR* value are shown at the right hand side of each of the histograms.

In general, in recordings from normal hearing children the three ICA algorithms, achieved the highest *SIR* values when the AEP target was in accordance with their age range; the waveform of the ICs with maximal *SIR* values corresponded to the auditory response in all the recordings.

Figure 6.6 shows the *SIR* index value histograms for the 19 estimates of the three ICA algorithms (*FastICA*, *Ext-Infomax* and *TDSEP-ICA*) for the recording from

one child with CI (S6-St1, 2.5 years using her CI); in this recording the highest *SIR* values for the three algorithms were calculated using the AEP target 2 as reference signal (see Figure 6.6(a)). In 6.6(b) the *SIR* values for the three algorithms, with the CI artifact signal as reference, are plotted. At the right hand side of each *SIR* index histogram the waveform of the estimates with the maximum *SIR* values are shown. Resulting estimates were compared by visualizing, *TDSEP-ICA* recovers the clearest ICs related to the AEP; almost with no CI artifact present; the *SIR* index values for these estimates were the highest compared with the other algorithms. *Ext-Infomax* achieved the highest CI artifact *SIR* values in this recording.

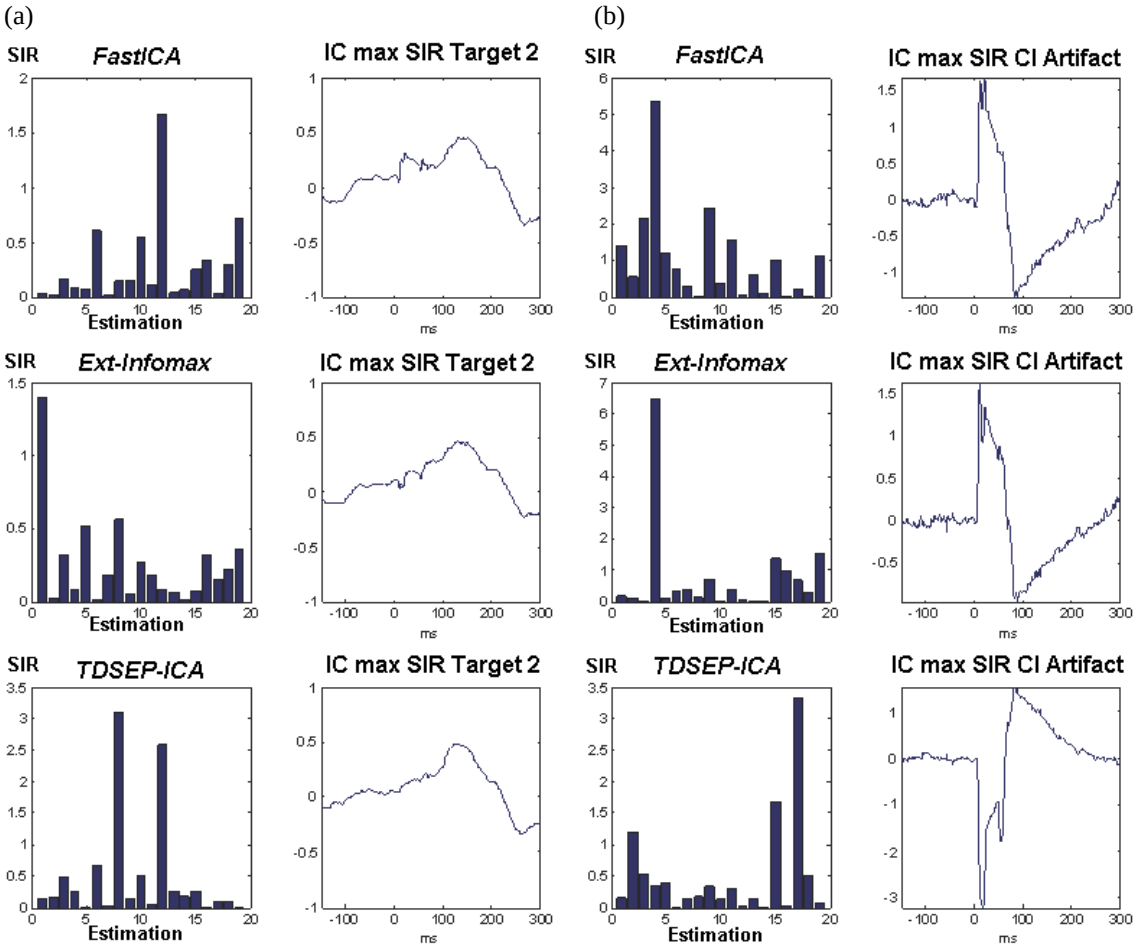

Figure 6.6 *SIR* index value histograms (19 estimates) of the three ICA algorithms and the waveforms of the estimates with the maximal *SIR* values for a child with CI, recording S6-St1 (2.5 years after implantation). (a) Target 2 and (b) CI artifact as reference signals.

Figure 6.7 shows the *SIR* index histograms for the 19 estimates of three ICA algorithms (*FastICA*, *Ext-Infomax* and *TDSEP-ICA*) for the recording from one child with CI (S5-St2, approximately 2.5 years after implantation); (a) the highest *SIR* values were obtained using the AEP target 2 as reference signal. In (b) the *SIR* values

for the three algorithms, with the CI artifact signal as reference, are plotted. At the right hand side of each *SIR* index histogram the waveforms of the estimates with the maximum *SIR* values are shown. Both *FastICA* and *Ext-Infomax* recover the AEP but the CI artifact still being mixed in the components. Visual inspection suggests that *TDSEP-ICA* recovers the clearest IC related to the auditory response and its *SIR* index value is the highest compared with the other algorithms. In this recording, the CI artifact *SIR* index value for *Ext-Infomax* and *TDSEP-ICA* are similar and higher than the values for *FastICA*.

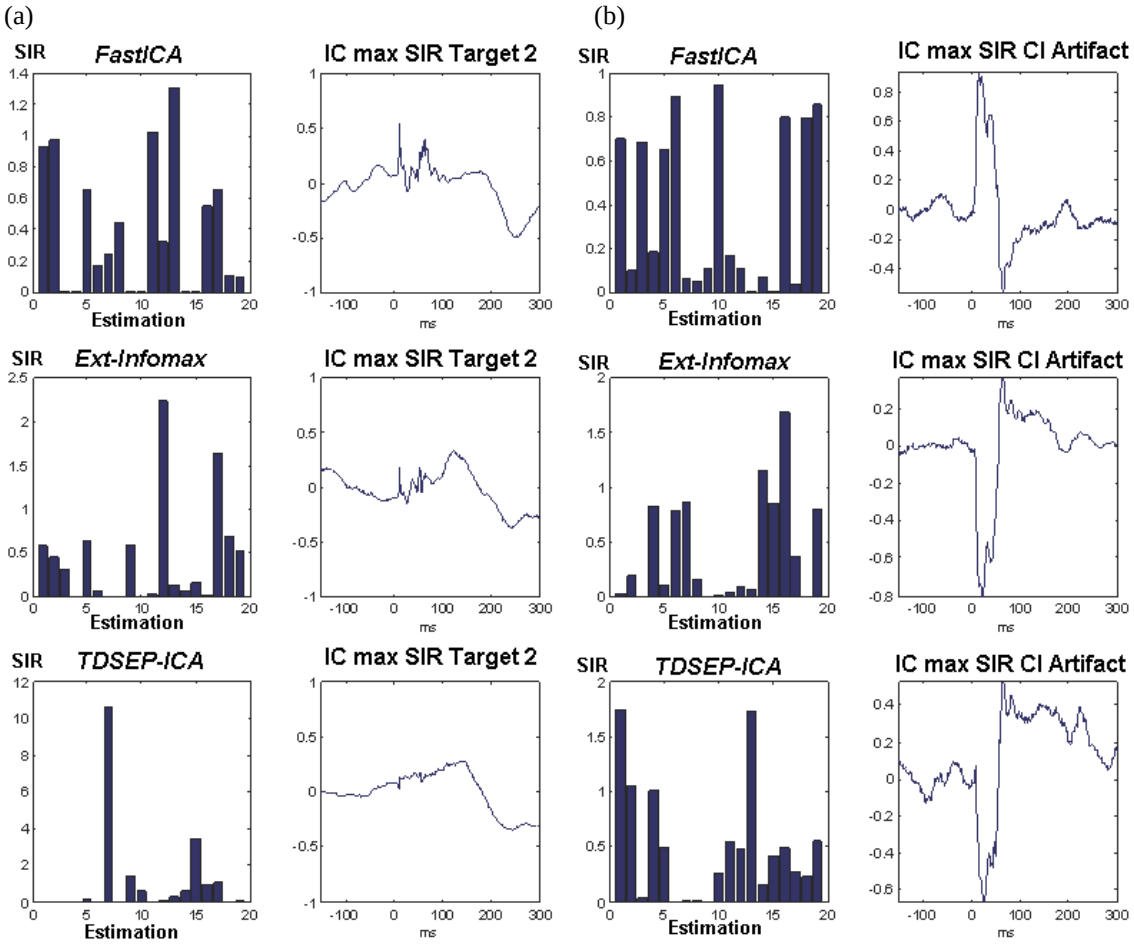

Figure 6.7 *SIR* index value histograms (19 estimates) of three ICA algorithms and the waveforms of the estimates with the maximum *SIR* value (child with CI, recording S5-St2). (a) Using the AEP target 2 as reference signal and (b) the CI artifact signal as reference.

Table 6.1 includes the average of the *SIR* index values for each of the three ICA algorithms for the AEP in recordings from normal hearing children (SIR_{AEP_NH}). The AEP *SIR* index values for children with CIs (SIR_{AEP_CI}) and the *SIR* index value for the CI artifact (SIR_{CI}) are included in this table also.

Table 6.1 The average of the *SIR* index values for the AEP in recordings from normal hearing children for each of the ICA algorithms.

	FastICA	*Ext-Infomax*	*TDSEP-ICA*
SIR_{AEP_NH}	2.87±1.30	2.04±1.02	2.43±1.35
SIR_{AEP_CI}	1.95±0.76	1.86±0.51	2.40±1.20
SIR_{CI}	3.49±2.13	3.21±1.88	3.27±1.79

In recordings from normal hearing children, the AEP *SIR* index values are somewhat higher using *FastICA*; *Ext-Infomax* achieved the lowest values. The three algorithms achieved the highest index values using the reference signal in accordance with the age range for each child.

In recordings from children with CIs, the maximal values of AEP *SIR* index (for the three algorithms) were achieved using target 1 (in children with less than 2.5 year using their CIs) and with target 2 (in children with more than 2.5 year using their CIs). Although the dataset includes children with more than 5 years post-implantation, it was not expected to have maximal *SIR* index values using target 3 and 4. This is because the maturation of the auditory system in those children is different to normal hearing children, the waveform of the AEP remains dominated by the peak P_1 as in the first years in normal hearing children (see section 2.5). In these recordings, *FastICA* achieved the highest *SIR* index values for the CI artifact and *TDSEP-ICA* achieved the next best index values for the AEP.

6.3 Variability of the AEP estimates

It is important to know the variability of the AEP component estimates because one of the objectives of this research is to objectively select the AEP estimated components in children with CIs. To evaluate the variability of the estimates, 20 repetitions were realized in the calculation of the ICs for the three ICA algorithms already mentioned. The *SIR* index was calculated, using a convenient signal reference, for each of the 20 repetition for all the estimates; the histograms of the maximal *SIR* indexes for the three algorithms are shown in this section.

Figure 6.8 shows the histograms of the maximal *SIR* indices for four different recordings from children with CIs (I: S3-St1, II: S5-St1, III: S4-St1 and IV: S4-St2), calculated for the estimates of both (a) the CI artifact and (b) the AEP. In all the cases, *FastICA* shows a larger spread of the *SIR* values than *Ext-Infomax* and *TDSEP-ICA*. In most of the recordings, *TDSEP-ICA* shows the higher values of the AEP *SIR* index. The range of values of the *SIR* index for the estimation of the CI artifact, using *FastICA* and *Ext-Infomax*, are similar in all the recordings shown in this figure. The ranges of values of the *SIR* index for the estimation of the AEP for the three algorithms are similar in recordings I and IV; in recordings II and III *TDSEP-ICA* shows the higher values of the AEP *SIR* index.

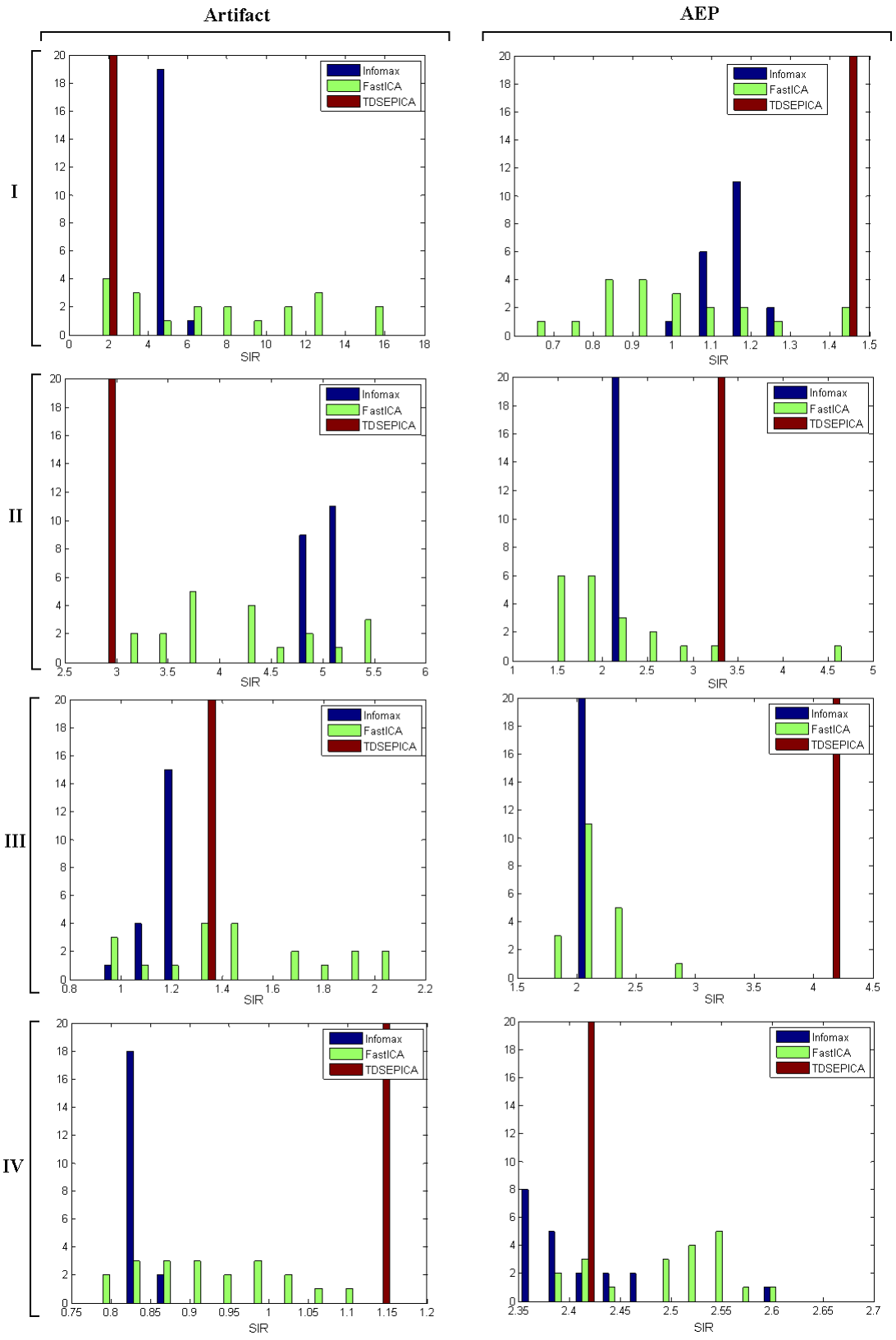

Figure 6.8 Comparison between, *Ext-Infomax*, *FastICA*, and *TDSEP-ICA* for (a) CI artifact separation and (b) AEP separation in 20 IC estimates (recordings I: S3-St1, II: S5-St1, III: S4-St1 and IV: S4-St2). Both *Ext-Infomax* and *FastICA* show a larger spread of values of the *SIR* than *TDSEP-ICA*.

With these results, it is possible to conclude that *TDSEP-ICA* is the algorithm with the smallest variability in the estimate of the ICs; this algorithm is the one that best estimates the AEPs *as well as* the artifact. Both *FastICA* and *Ext-Infomax* recover efficiently the components related to the CI artifact; however, only *TDSEP-ICA* successfully recovers the AEPs in all the subjects with CIs. In conclusion, the performance of the *TDSEP-ICA* algorithm is better and more optimal for the dataset analyzed in this research.

6.4 Summary

Although *FastICA* and *Infomax* are maybe the most popular ICA algorithms used to estimate the components of the AEP in normal hearing subjects, here it was found that the algorithm with the more stable IC estimates is *TDSEP-ICA* with τ=0, 1, 2, ..., 20. In normal hearing children, although *TDSEP-ICA* does not have the lowest separability matrix values, the block structure of this matrix is always clearer than *FastICA* and *Ext-Infomax*. One-dimensional ICs can be related with both the AEP and noise.

In children with CIs, *FastICA* and *Ext-Infomax* have problems in recovering a clear AEP (without the CI artifact), especially when the recordings have low *SNR*. *TDSEP-ICA* recovers the AEP in one- or two-dimensional ICs. All the algorithms estimate the CI artifact reasonable well, although only *TDSEP-ICA* recovers it in one-dimensional ICs. *TDSEP-ICA* is the algorithm with the best separation of noise in these recordings.

The average value of the AEP *SIR* index is higher with *FastICA* than with *Ext-Infomax* and TDSEP-ICA than in recordings from normal hearing children. In children with CIs, *TDSEP-ICA* is the algorithm with the highest AEP *SIR* index values whilst *FastICA* is the algorithm with the highest CI *SIR* index.

It can be seen that using the *SIR* index, the variability of the estimation of three ICA algorithms, *Infomax*, *FastICA* and *TDSEP-ICA*, can be estimated. In both recordings, from normal hearing children and children with CIs; *TDSEP-ICA* is the

algorithm with the smallest variability in the AEP component estimates. This permits to conclude that *TDSEP-ICA* has the most robust and efficient estimate of the AEPs and this is to be expected over shorter window sizes and for a technique that makes use of the inherent information available in the time-series itself.

On the other hand, standard implementation of the ICA algorithm results in the number of ICs being equal to or less than the number of measurements, although it is generally the case that some of the components do not have a physiological significance; for this reason it is fundamental to know the number of sources to be estimated. It is convenient to have an objective method to select the ICs with physiological meaning.

In the next chapter, a procedure to select objectively ICs with physiological and physical meaning, using the concepts of *Mutual Information* and *clustering* is described.

Chapter 7.
Selection of Independent Components using Mutual Information and Clustering

A crucial part of applying ICA to any neurophysiological data is the selection of *relevant* ICs; in other words, to decide which ICs have neurophysiological meaning (in our case the auditory response). Standard ICA implementation supposes a square mixing matrix; this results in as many ICs as EEG channels (19 in our case). Responses to repetitive stimuli are the most important signals here; so the ICs of interest should be repetitive and time-locked with the stimuli. In this chapter a novel procedure for the selection of ICs using MI and *cluster analysis* is presented (an introduction of MI is included in Section 4.1).

Section 7.1 explains the basic theory of *Cluster Analysis* including the basic terminology used in *hierarchical clustering*, used in the procedure proposed in this chapter. Section 7.2 includes the description of this procedure to identify robust ICs associated with the AEP and the CI artifact, using MI combined with cluster analysis theory. This procedure is a modification of the method implemented by Kraskov *et al* [86]. The authors utilize MI between the ICs as a similarity measure and recursively using the grouping property of the MI, they cluster the output of ICA of biomedical signals. Section 7.3 shows the results of *hierarchical agglomerative clustering* of the ICs recovered by *TDSEP-ICA* from children with CIs. The *dendrograms* produced by the agglomeration of the ICs are showed together with the most robust clusters in four different recordings.

7.1 Cluster Analysis

Cluster Analysis divides a collection of inputs or objects into a smaller number of clusters; a cluster is a collection of objects which are similar or related between themselves and are dissimilar or unrelated to the objects belonging to other clusters; the aim of cluster analysis is to determine the intrinsic grouping in a set of unlabeled objects (data). The concept of clustering is referred to an entire group of clusters; ideally all the clusters are well separated from each other, in other words the distance between two different clusters is larger than the distance between any two objects within a cluster.

One of the most important applications of clustering is in biology, specifically in taxonomy and hierarchical classification, where objects are classified according to their characteristics in species, classes or families; the concept of hierarchical refers to organising the objects into a "tree". Clustering has been used in biology for example to group genes which have similar functions [46;86].

There are different similarity criteria to merge the collection of objects, a criterion of similarity could be the distance between the objects [46]. Data to be clustered can be presented by a data matrix or by a dissimilarity matrix **D** with d_{ij} elements, d_{ij} is the dissimilarity between the *i*-th and *j*-th objects. The set of objects belonging to a cluster satisfy a minimum of three conditions:

1. The dissimilarity between objects *i* and *j* is positive $d_{ij} \geq 0$.
2. The dissimilarity is equal to zero if the object is the same $d_{ii}=0$.
3. The dissimilarity is symmetric $d_{ij}=d_{ji}$.

In some applications it is more convenient to consider the similarity Δ_{ij}, between the *i*-th and *j*-th objects instead of the dissimilarity; the dissimilarity must satisfy the conditions listed before.

In general there are different types of clustering, the three principal types are: *hierarchical*, *partitional*, and *constructive* clustering [46]. Hierarchical clustering methods are more commonly used, and this is the method used in this research. In

hierarchical clustering, the data are fused or partitioned in a series of steps. Hierarchical clustering using *agglomerative* methods consists in fusing *n* objects into groups where the last group contains all the objects at each step; in the agglomerative method, the most similar pair of objects is clustered. A *divisive* method consists in separating a number of objects into groups where every group contains only one individual; at the beginning of the divisive clustering there is one cluster containing all the data, at each step of the clustering an existing cluster is divided into two [83].

The two-dimensional diagram that illustrates the fusion or division made during the hierarchical clustering is called a *dendrogram* (see Figure 7.1). The dendrogram or rooted tree diagram is a mathematical and pictorial representation of the complete clustering procedure. The *height*, *h*, in this tree represents the distance at which each fusion is made and the *nodes* (labelled from A to E) in the diagram represent clusters; for each pair of objects (*i*, *j*), the smaller the value of h_{ij} the more similar objects *i* and *j* are. This diagram displays the order in which the clusters were fusioned. Each of the terminal nodes represents one of the objects clustered (numbered from 1 to 6); the arrangement of *nodes* and *heights* is the topology of the tree. The node E is called the root of the tree and is the cluster which includes all the objects.

The dendrogram in Figure 7.1 is a binary dendrogram, it has *n*-1 internal nodes and each internal node has two nodes lying below it in the tree; all the dendrograms included in this chapter are binary. Since there are 2^{n-1} different ways of representing each binary dendrogram, the left-right ordering of the edges leading down from each internal node can be interchanged.

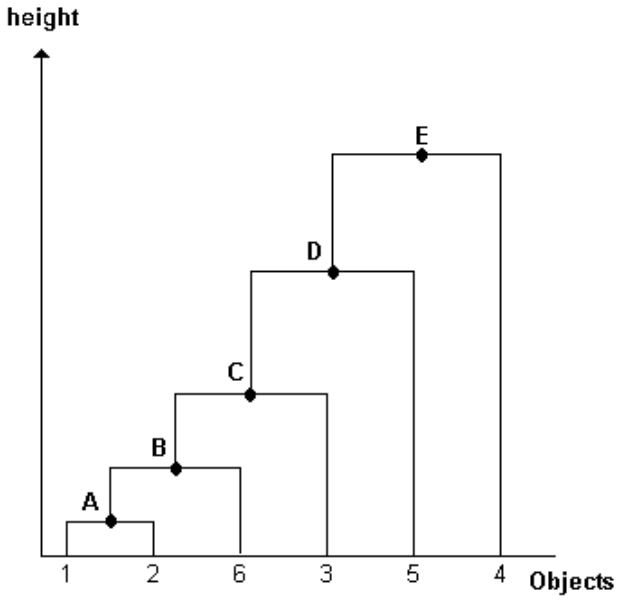

Figure 7.1 A dendrogram or rooted tree diagram, objects clustered are numbered from 1 to 6 and nodes are labelled from A to E, height is the distance at which cluster is made.

Different measures have been proposed to calculate the proximities between the data, typically measured by dissimilarities or the inter-objects distances [46]. Given a $m \times n$ data matrix **X**, the m entries of **X** are $1 \times n$ row vectors x_1, x_2,..., x_m, the commonly used distances measures between the vector x_i and x_j are defined as follows:

- Euclidean distance, $d_{ij} = \sqrt{\sum_{k=1}^{n} (x_{ik} - x_{jk})^2}$
- City Block metric, $d_{ij} = \sum_{j=1}^{n} \left| x_{ik} - x_{jk} \right|$
- Minkowski metric, $d_{ij} = \left\{ \sum_{k=1}^{n} \left| x_{ik} - x_{jk} \right|^p \right\}^{\frac{1}{p}}$.

  For the special case of p = 1, the Minkowski metric gives the City Block metric, and for the special case of p= 2, the Minkowski metric gives the Euclidean distance.

The most commonly used distance measure is the Euclidean distance; this can be interpreted as physical distance between two points in the Euclidean space.

There are three basic *agglomerative* methods used in hierarchical clustering to measure the inter-cluster similarity [65], all methods use generally a proximity matrix as input:

1) Single linkage clustering, also known as the nearest neighbour technique, defines the distance between groups as that of the closet pair of individuals.

2) Complete linking clustering or furthest neighbour is the opposite of single linkage and defines distance between groups as that of the most distant pair of individuals.

3) Group average clustering defines distance between groups as the average of the distances between all pairs of individuals.

Once the clustering procedure has been completed, the number of clusters must be decided by properly dividing of the dendrogram. There are two principal criteria to divide this hierarchical tree, by finding the natural divisions in the original data or by specifying an arbitrary number of clusters. In agglomerative clustering the number of cluster is performed by cutting the dendrogram at a particular height. The *inconsistency coefficient* can be use to identify the cutoff or height of comparison in the dendrogram [120]; each link between nodes in the hierarchical clustering is compared with adjacent links two levels below it. Another criterion is to determine the number the elements in each cluster according with the number the objects grouped [83].

The criterion used in this research, to cut off the dendrogram, in order to find the number of clusters in each "tree" was the 70% of the maximum height between clusters [83]. This criterion was considered more convenient than any other of the criteria mentioned since those involve make a subjective decision about the number of clusters or the number of elements in each cluster.

The objective of applying clustering to ICA is, for example, when the reliability of an ICA algorithm is assessed, that repeating the estimates several times in order to identify robust ICs. Himberg and Hyvarinen [64;65] propose to use

clustering to identify common components between estimates calculated by running *FastICA* many times. After performing ICA, it could be important to identify equivalent components across subjects, this is another application of clustering of ICs [40]. Stögbauer proposes to use clustering of mutually independent components to identify one- or multi-dimensional components [121].

The agglomerative method used in this research was single linkage clustering and the criterion of similarity measure was the Euclidean distance of the MI between the ICs calculated by *TDSEP-ICA*; when the Euclidean distance is used to measure similarities between values with different scales is convenient to normalize them (mean zero and standard deviation one). Authors in the literature who have used hierarchical clustering to group the ICs calculated by ICA include Himberg *et al* 2003 [65] and Krashov *et al* 2005 [86].

7.2 Objective estimation selection in ICA of AEPs

Standard implementation of the ICA algorithm results in the number of ICs being equal to or less than the number of measurements, although it is generally the case that some of the components do not have a physiological significance; for this reason it is fundamental to know the number of sources to be estimated. There are different methods that could be used to select the ICs with physiological meaning, such as by visual inspection of the topographies of the estimated sources or, say, based on a threshold imposed on the variance of the ICs.

Krashov *et al* [86] propose to use MI as a similarity measure for hierarchical clustering of the ICs computed by ICA from the ECG of pregnant women; MI values between variables satisfies the conditions to cluster objects (positive, symmetric and equal to zero only if the variable are the same or the variables are independent). The procedure proposed by the authors can be summarized as:

1. Calculate the MI matrix between the ICs.

2. Merge the closest two clusters *i* and *j*; the distance between clusters is computed by $d_{ij} = 1 - \frac{I(i, j)}{H(i, j)}$, where *I* is the MI and *H* is the entropy between the clusters.
3. Create a new cluster by combining *i* and *j*, using the joint MI.
4. Update the MI matrix between the new clusters using the grouping property of MI, where the mutual information of two clusters is conditioned on a third, $I(i, j, k) = I(i, j) + I((i, j), k)$.
5. Repeat steps 1-4 until only one cluster remains.

At the end of the procedure the authors indentify two big clusters related to different sources. Additionally, the authors use the MI to identify the one- and multidimensional independent components (see section 5.1.3) and to measure the reliability of ICA estimates [121].

This method was slightly modified in this research, in order to objectively select the ICs associated with the AEPs, from ongoing EEG recorded from children with CIs, as well as to identify the ICs related to the CI artifact. The procedure introduced here to objectively select ICs has two steps (see Figure 7.2 and Figure 7.3), the first to reduce the number of estimates to compute and the second to cluster the most robust estimates [28]. The procedure can be summarized as follows:

Step 1) Reduction of number of electrodes: Most of the ICA algorithms use PCA to estimate the number of ICs to be found; however, when PCA was applied in a pre-processing step in the dataset, the first principal components are related only to the CI artifact in most of the recordings. This reduction in dimension may eliminate the principal components associated with the auditory response (especially in recordings with large CI artifact).

If we consider that more channels of measurements generally imply more complex calculations, reducing the number of channels included in the estimation might help reduce the complexity. An alternative could be to randomly select a subset of *m* channels, from all the channels. In this way, the number of channels to be

analyzed would be gradually (and pseudo-randomly) reduced *e*. *g*. to 3, whilst making sure that in each selection, channels representative of all the areas of the brain are included.

The pseudo-random reduction of electrodes used in this procedure is graphically explained in Figure 7.2. The electrode labels were arranged in a 5 × 5 matrix (**elemat**, shown in matrix 7.1), in accordance with their position on the scalp (see Figure 3.1, the electrode distribution according to the standard international 10-20 system). For example, the first two rows correspond to the frontal electrodes (row 1: FP1 and FP2 and row 2: F7, F3, FZ, F4, F8), and so on until the fifth row where the occipital electrodes where located. The elements of this matrix without electrodes were filled in with zeros (**elemat**$_{11}$, **elemat**$_{13}$, **elemat**$_{15}$, **elemat**$_{51}$, **elemat**$_{53}$, and **elemat**$_{55}$). From **elemat**$_{11}$ until the last element of this matrix, **elemat**$_{55}$, arrays with alternate nonzero electrodes and size equal to number of channel to process (6 in this example) were selected from this matrix (see Figure 7.2(a)). In order to have more combinations of electrodes arrays, the rows and columns of **elemat** where circularly shifted several times and the selection of electrodes repeated.

$$\mathbf{elemat} = \begin{pmatrix} 0 & \mathbf{FP1} & 0 & \mathbf{FP2} & 0 \\ \mathbf{F7} & \mathbf{F3} & \mathbf{FZ} & \mathbf{F4} & \mathbf{F8} \\ \mathbf{T3} & \mathbf{C3} & \mathbf{CZ} & \mathbf{C4} & \mathbf{T4} \\ \mathbf{T5} & \mathbf{P3} & \mathbf{PZ} & \mathbf{P4} & \mathbf{T6} \\ 0 & \mathbf{O1} & 0 & \mathbf{O2} & 0 \end{pmatrix} \qquad 7\text{-}1$$

Using *TDSEP-ICA* with a time delay τ=0,1,2,...,20, the ICs for each subset of electrodes obtained pseudo-randomly in the reduction of electrodes, were calculated (see Figure 7.2(b)). In the recording S6-St1 is possible to recognize clear ICs related to the AEP and the CI artifact in the subset shown.

The MI between the ICs in each subset is calculated and used as a similarity measure to the cluster analysis. Using the residual MI between the ICs, the estimate with the minimal dependency with the rest of the estimations is selected in each subset, to do that, instead of the clustering procedure proposed by Krashov *et al* and listed in above paragraphs, the dendrogram construction was reformulated by finding

the Euclidean distance between the elements of the MI matrix [56]; the proximity of the ICs is defined as the minimum distance (maximum of the MI). Figure 7.2(c) shows the dendrograms obtained with this procedure and the ICs selected in specific subsets. The minimally dependent IC in subset 1 corresponds to the AEP, whilst it corresponds to artifacts in subsets 4 and *n*.

Step 2) Clustering estimates: The ICs selected in the preceding step are grouped using the Euclidean distance as measure of similarity; the hierarchical agglomerative dendrogram for these ICs is shown in figure 7.3(a). The final number of clusters is determined selecting an appropriate level in the dendrogram; the 70% of the maximum distance (height) between clusters. Only the clusters with more than one estimate were considered as robust clusters (clusters 2, 5 and 6 in this example, figure 7.3(b)). The trace in red is the average of the estimation in each cluster.

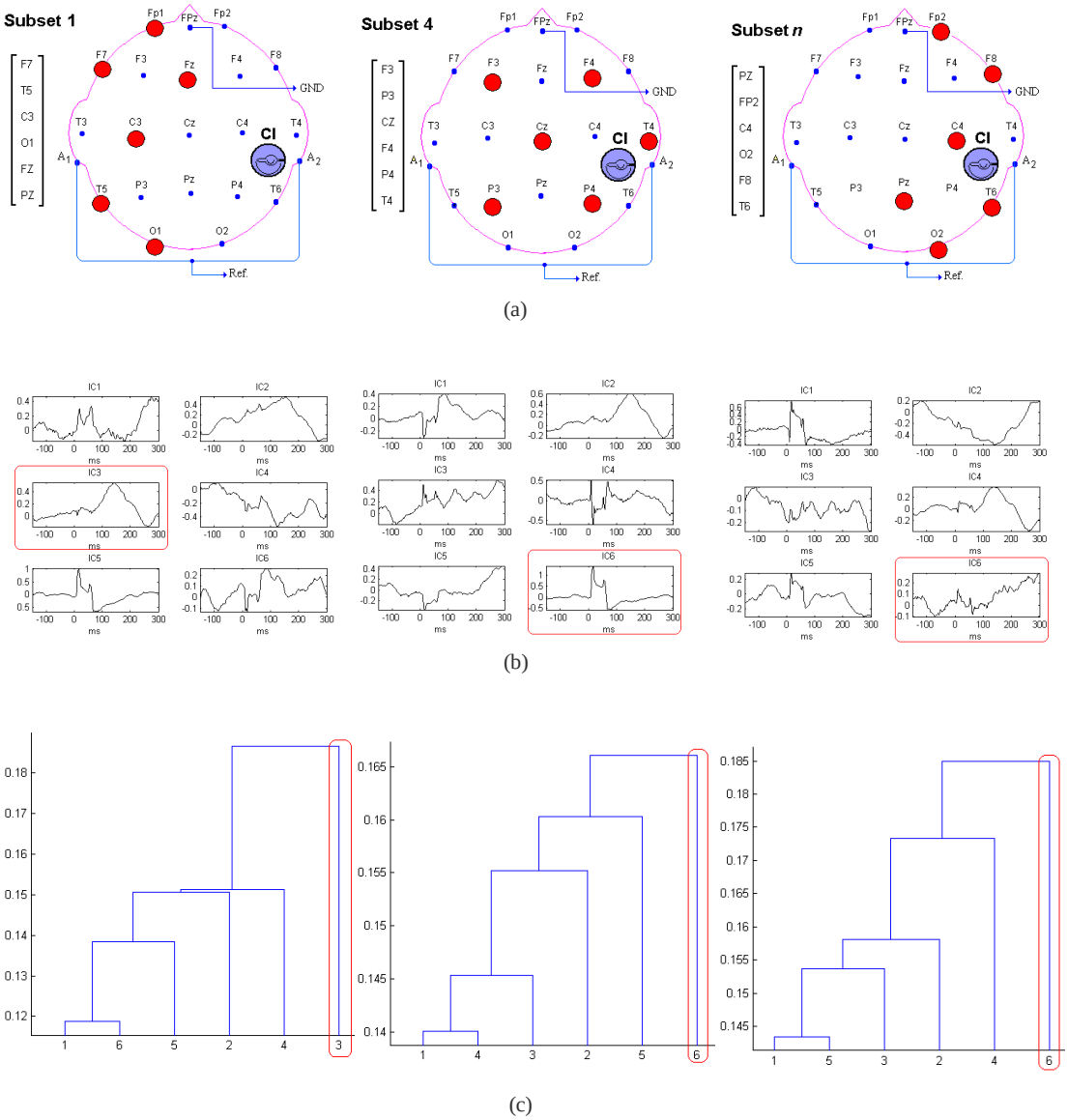

Figure 7.2 Outline of the electrodes reduction in the procedure to objectively identification of consistent ICs through MI and clustering (recording S6-St1). (a) For each electrode subsets, 6 electrodes selected pseudo-randomly, (b) the ICs were calculated using *TDSEP-ICA*. (c) These ICs were grouped using the residual MI between them; the IC last merged was selected in each subset (IC4 for subset 1, IC6 for subsets 4 and *n*).

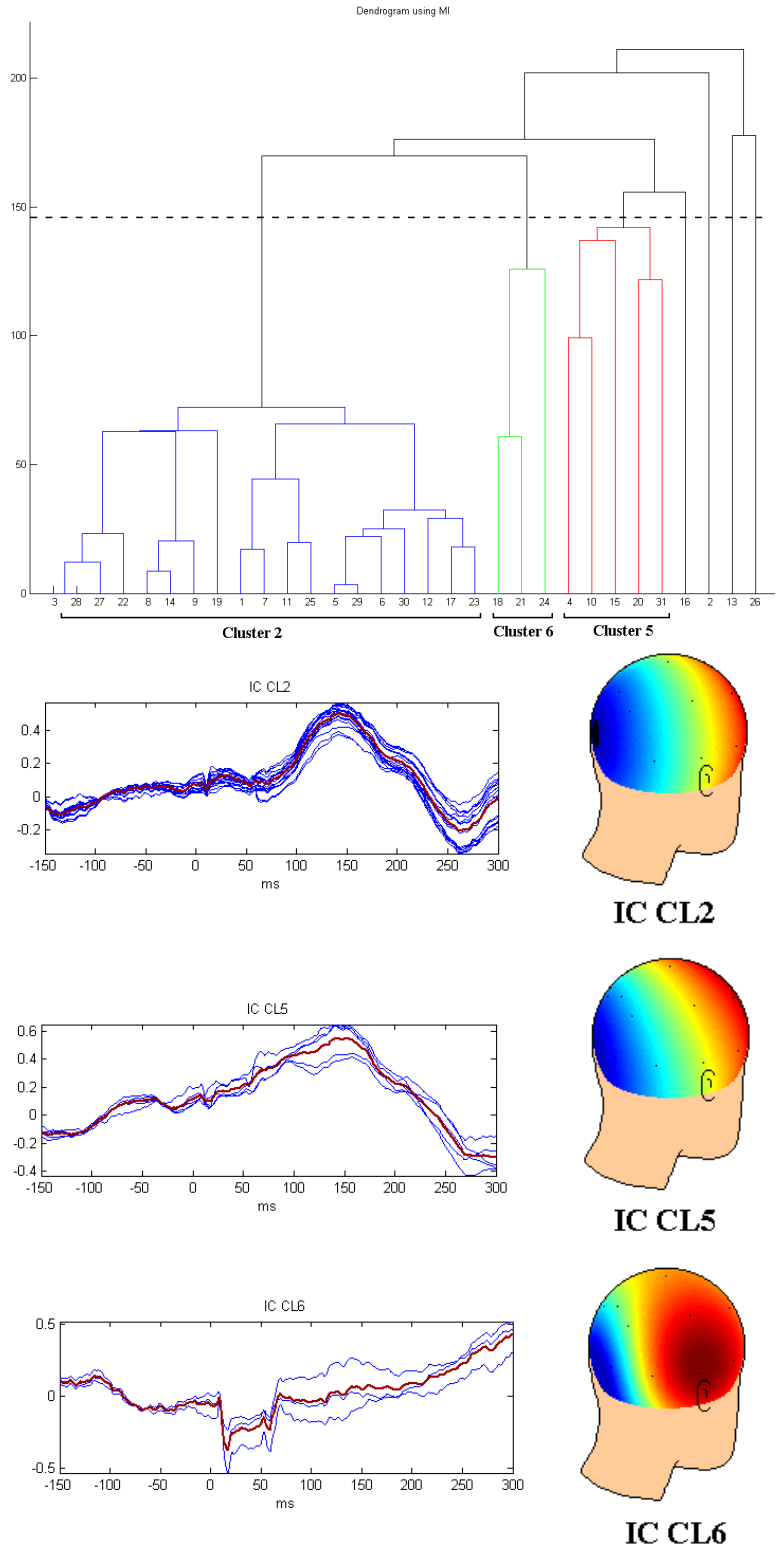

Figure 7.3 All of the ICs selected in the previous step (see figure 7.2) were clustered using the Euclidean distance as a similarity measure. The hierarchical agglomerative dendrogram (top) was cutoff at 70% of the maximum distance between ICs. Three robust clusters can be seen in this example (botton), CL2 and CL5 related to the AEP (with a frontal distribution) and CL6 associated with the CI artifact (recording S6-St1**,** CI in the right side).

7.3 Hierarchical agglomerative clustering results

The procedure described before was carried out in 7 recordings from children with CIs. Recordings S1-St2 and S4-St2 were excluded from the analysis because the electrodes around the CI were not connected during the AEP recording. Since the objective is to recognise the most robust ICs related to both the AEP and the CI artifact, the identification of the CI artifact was expected to be more difficult in those recordings; additionally the comparison between results could not be viable.

Figure 7.4 shows the dendrogram and the most robust estimates for recording S5-St1 **(**CI user at 8 m after implantation); in this case each subset of channels analysed includes 6 electrodes. The final number of clusters, using the criteria of 70% of the maximum dendrogram height is 5. Three robust clusters (with more than one IC) were observed in this recording. Using the spatial projection of the average IC (trace in red) for each robust cluster the estimates were identified; two clusters are related to the AEP: CL3 and CL5 and one cluster with the CI artifact CL4. The topographic maps associated with the AEP have a distribution predominantly central whilst the distribution of the estimate related to the CI artifact is principally between electrodes T6 and O2 where the antenna of the CI is positioned.

Figure 7.5 shows the dendrogram and the most robust estimations for subject S3-St2, this child has been using his CI for 1 year; these results were obtained using 4 electrodes in each subset analysed; the maximum number of cluster using the criteria of 70% of the maxima height is 11, but only two clusters have more than one estimate each (robust clusters). The spatial projections of the average IC in CL10 show a central distribution which could be associated with the AEP whilst the principal activity in the topographic map of CL 9 is in the right hemisphere where the CI is located.

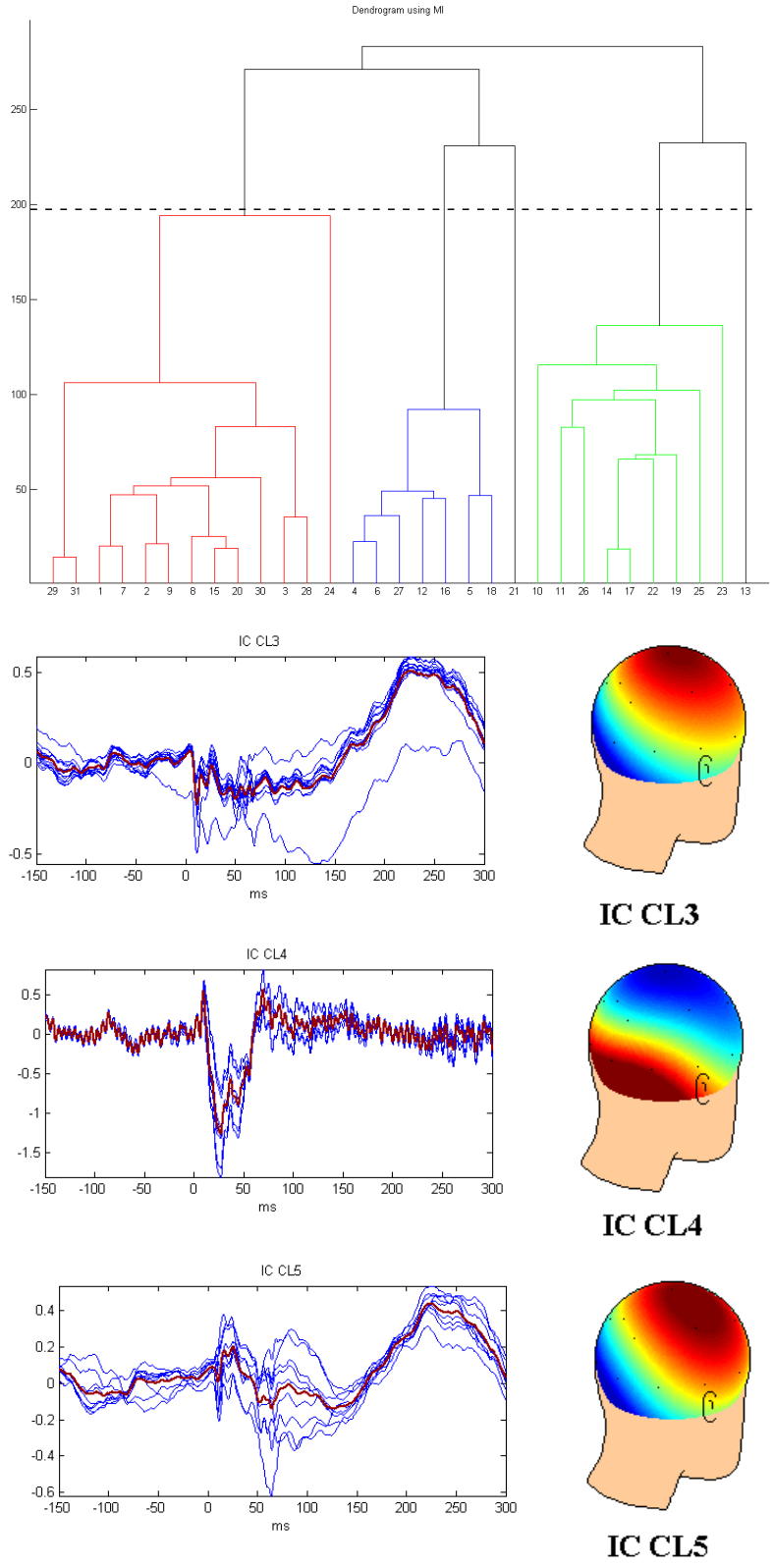

Figure 7.4 Dendrogram (top) and robust ICs and average spatial projections for child S5-St1 CI user (bottom), 8m after implantation; two clusters are related to the AEP CL3 and CL5 and one cluster is associated with the CI artifact (CL4).

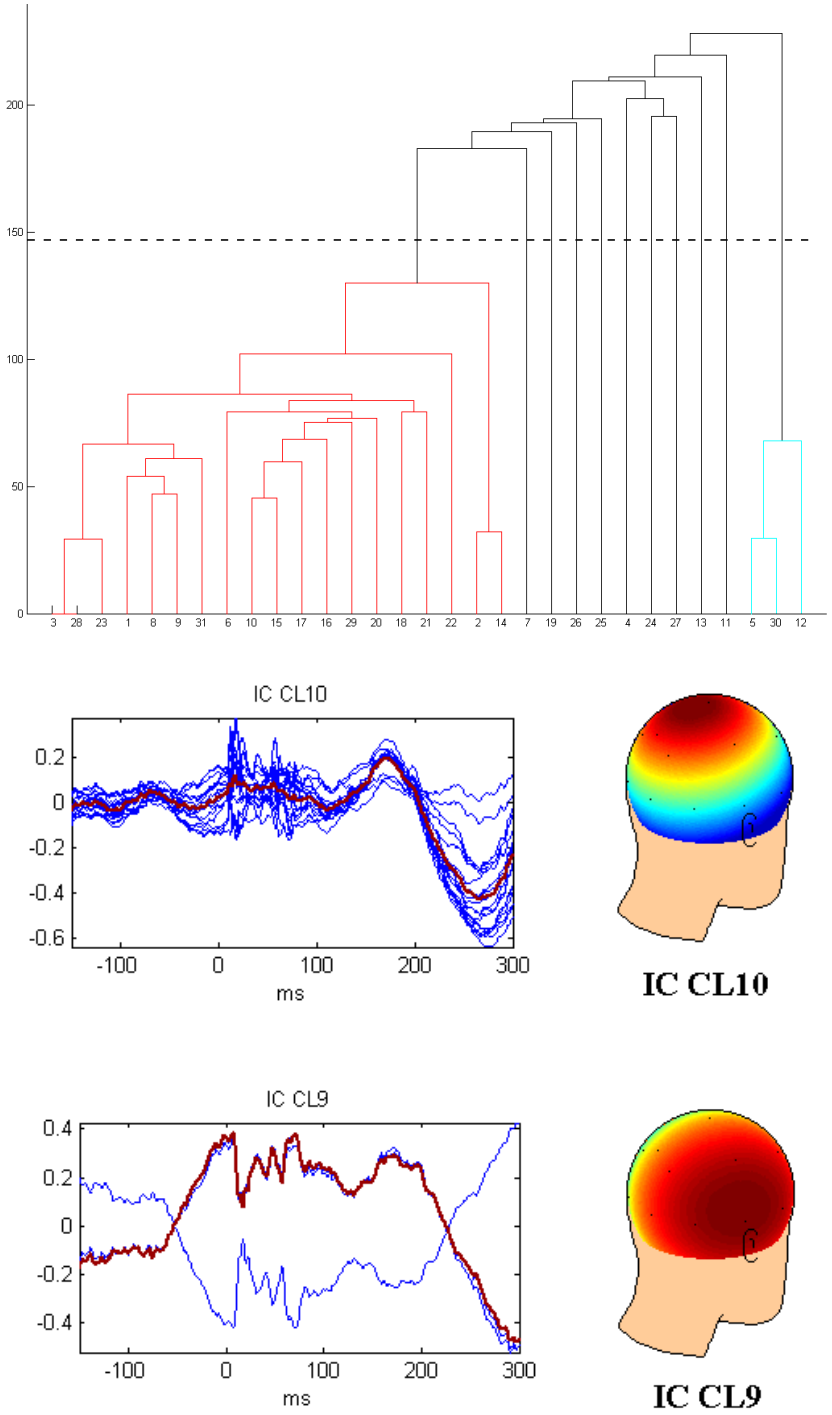

Figure 7.5 Dendrogram (top) and estimations clustering and topographic maps (bottom) for subject S3-St2 (subsets of 4 electrodes were analysed). The number of cluster using the 70% of the maximum distance between clusters is 2; one cluster is related to the AEP (CL10) and one with the CI artifact (CL9).

Figure 7.6 shows the hierarchical dendrogram robust cluster and spatial projections of the ICs for the same subject of figure 7.4 but 5 years and 5 months after implantation; the ICs in clusters CL1 and CL3 are two components of the AEP and cluster CL2 is noise electrodes around the CI; the trace in red is the average of the estimation. In this recording 5 electrodes for each subset were selected and the final the number of clusters was 3. The spatial projections of the average ICs related to the AEPs shown lateralised distribution opposite to the CI.

Figure 7.7 shows the hierarchical dendrogram and the most robust ICs recovered from recording S5-St2; subsets of 4 electrodes were analysed. The final number of clusters obtained using the 70% of the maximum distance between clusters was 3. The spatial projections of the average ICs in each cluster indicate that CL4 is related to the AEP with a frontal distribution lateralised opposite to the CI. CL5 could be another element of the AEP with a frontal distribution. Finally, the spatial projection of the average IC in CL6 shows activity around the electrodes where the CI is located; the noise could be generated by the CI itself.

Three robust clusters were recovered by the procedure proposed in this chapter in recording S4-St1 (see Figure 7.8); subsets of 9 electrodes were analysed. According with the spatial projections of the average ICs in each cluster it is possible to say that clusters CL2 and CL3 are related to the CI artifact whilst cluster CL4 is associated with the AEP with a posterior distribution.

Robust ICs related to the AEP and CI artifact were identified in recording S5-St3 (Figure 7.9); subset of 7 electrodes were analysed in this recording. Using the criteria of the 70% of the maximum distance between cluster, 4 clusters were recovered. Two clusters are related to artifacts; CL2 corresponds to the CI artifact and Cl6 with noisy electrodes (F4, F8 and C4). The spatial projections of the average ICs in CL3 shows activity opposite to the CI location but predominant parietal and frontal in CL7.

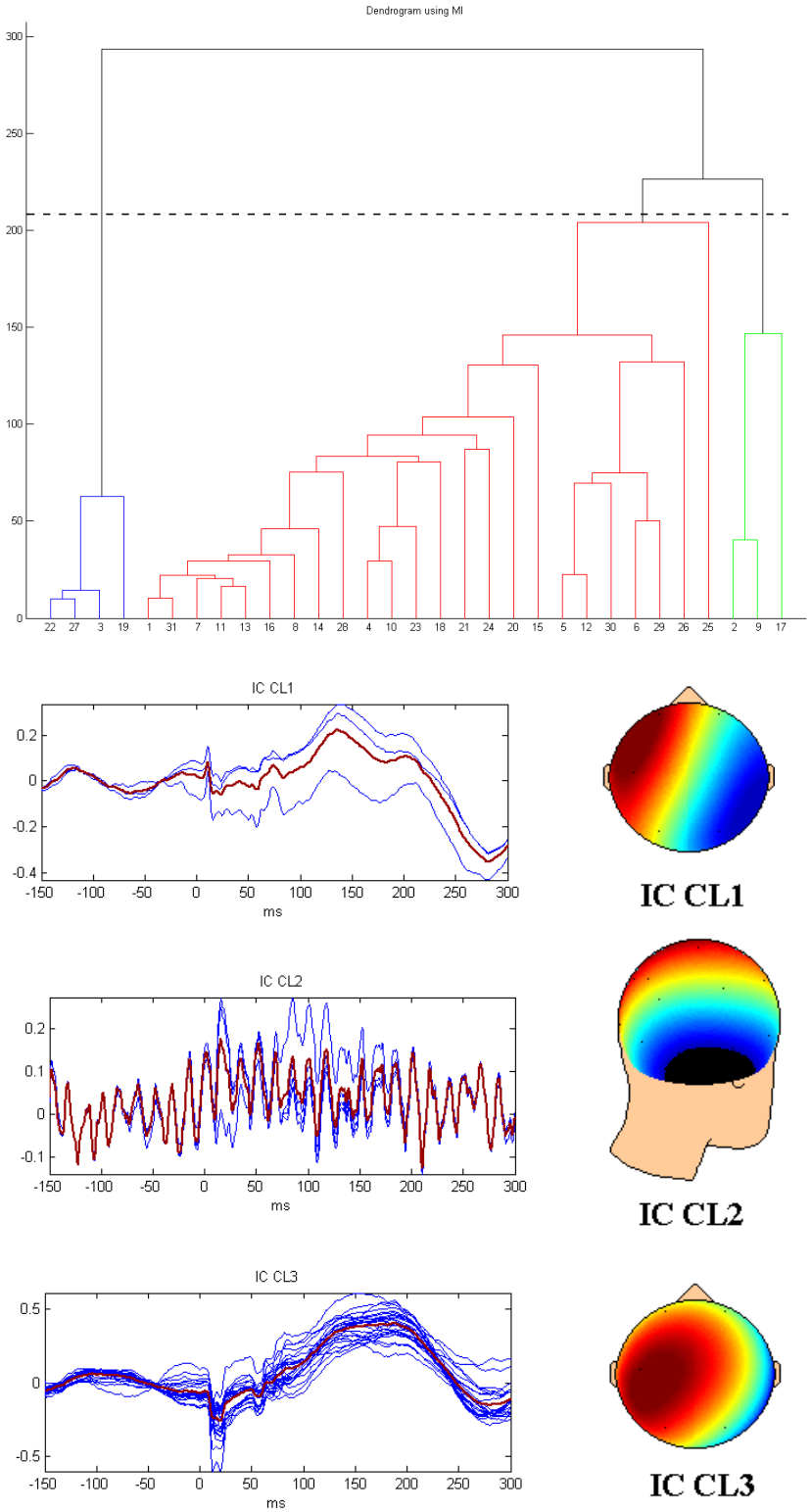

Figure 7.6 Dendrogram (top) and estimations clustering and topographic maps (bottom) for subject S3-St3 (child with CI, 5y 5m after implantation). The number of clusters using the 70% of the maximum distance between clusters is 3; two clusters are related to the AEP (CL1 and CL3) and one to noisy electrodes around the CI (CL2).

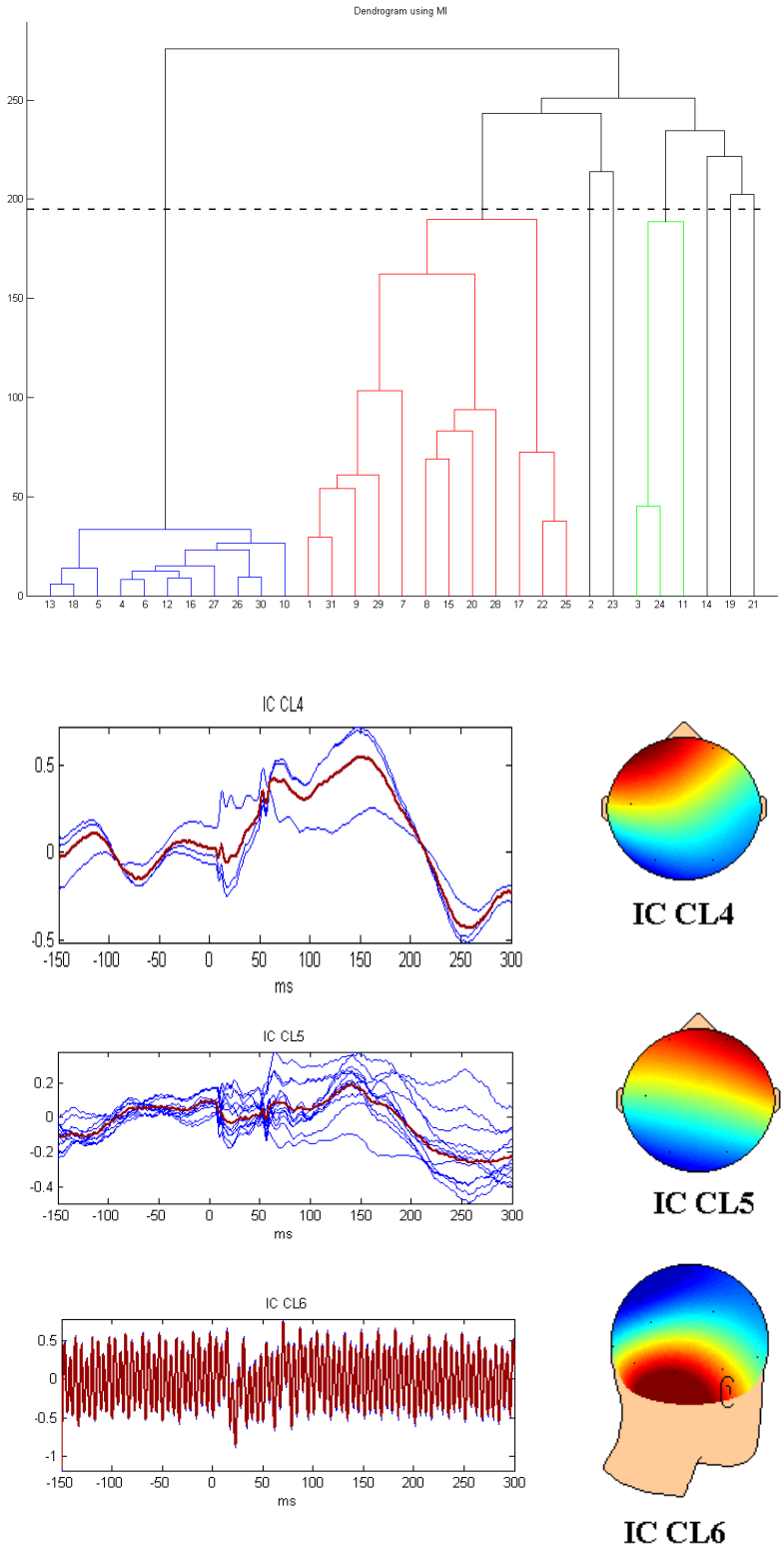

Figure 7.7 Dendrogram (top) and estimations clustering and topographic maps (bottom) for subject S5-St2 (subsets of 6 electrodes were analysed). The number of cluster using the 70% of the maximum distance between clusters is 3; two clusters are related to the AEP (CL4 and CL 5) and one with noise generated by the CI (CL6).

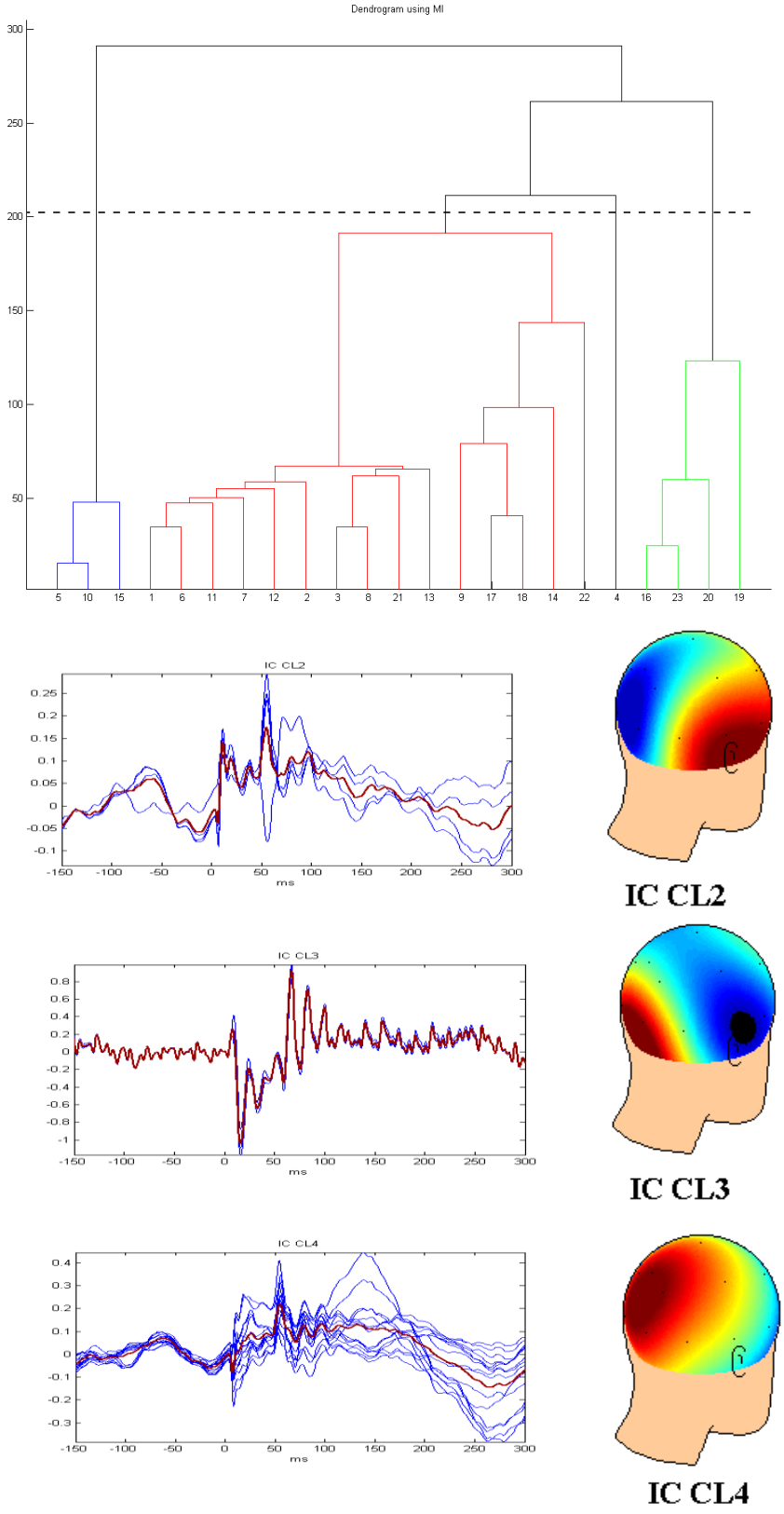

Figure 7.8 Dendrogram (top) and estimations clustering and topographic maps (bottom) for subject S4-St1 (subsets of 9 electrodes were analysed). The number of cluster using the 70% of the maximum distance between clusters is 3; two clusters are related to the CI artifact (CL2 and CL 3) and one with the AEP (CL4).

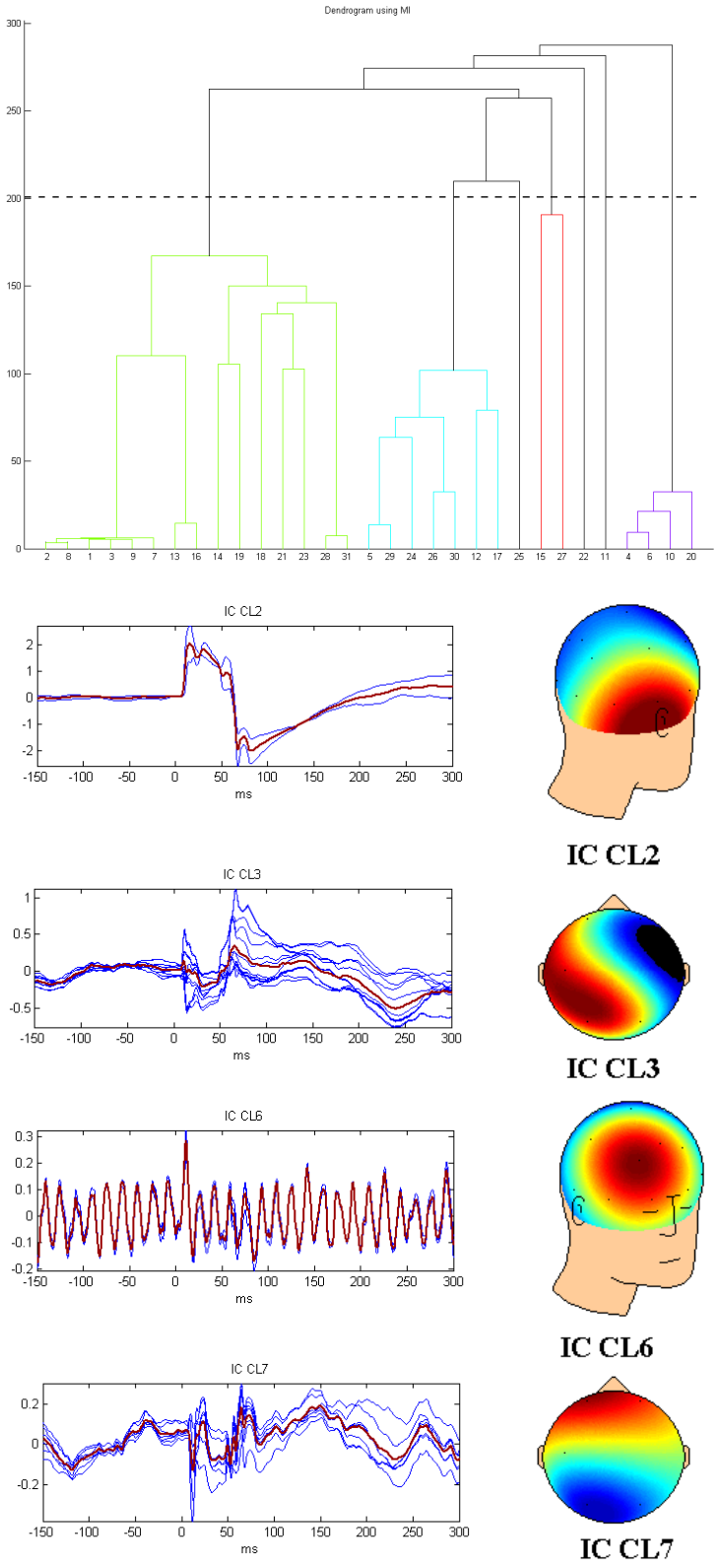

Figure 7.9 Dendrogram (top) and estimations clustering and topographic maps (bottom) for subject S5-St3 (subsets of 7 electrodes were analysed). The number of cluster using the 70% of the maximum distance between clusters is 4; two clusters are related to artifacts (CL2 and CL 6) and one or two possibly related to the AEP (CL3 and CL7).

The number of robust clusters indentified across subjects was diverse; in general one or two for the AEP (it could be related to the symmetry of the auditory response and the time after implantation). One or two related to the CI artifact and one related to another type of component (blinking, line noise or spontaneous EEG activity). In general, the AEP is more robust and is in accordance with the time of implantation (compare Figures 7.4 and 7.5). The advantage of the procedure proposed in this chapter over the methodology proposed by Krashov *et al* is that it is the less time consuming to run; approximately one octave of time to run the procedure proposed by those authors.

Since the CI artifact is located in a very specific area of the brain (right or left temporal lobe), the performance of *TDSEP-ICA* is better in recovering the AEP when distant electrodes to the CI were selected. The AEP and the CI artifact are spatially uncorrelated, this procedure emphasises this between both signals and better positions *TDSEP-ICA* to carry out the estimates.

Although the clustering of the estimations is correct visually, and the topographic maps of the average ICs in each robust cluster are close to the expected, it is necessary to compare different agglomerative methods as well as to determine the optimal number of clusters in each dendrogram. Furthermore, it is necessary to include criteria to determinate the number of clusters in accordance with the reduction of electrodes. For that, the *consistency* between links of the clusters could be used, for example. If the length of a link does not vary significantly from the length of neighbouring links, it means that the objects merged at that level of dendrogram have similar characteristics (there is consistency between the objects). Another option is use a *silhouette plot* which reflects the strength of a clustering to the nearest stable cluster, compared to the next best cluster [46].

Moreover, it is important to analyse the convenience of using a partitional clustering instead of hierarchical agglomerative clustering used in this chapter. Since the objective of this thesis was to propose a method to evaluate objectively the maturation of the auditory system of children with CI and not necessarily to develop a procedure to select the ICs with physical and physiological meaning after using ICA, it was decided do not use the procedure proposed in this chapter, as mentioned before

more work is needed to obtain reliable results that can be used in the analysis of sources of the AEPs.

Finally, it is possible to mention that this part of the research opens an alternative line of study to extend the use of cluster analysis applied to this type of dataset (AEP recordings with CI artifact).

7.4 Summary

A fundamental stage when applying ICA to neurophysiological data is the selection of relevant ICs. The standard implementation of ICA supposes a square mixing matrix; this results in as many ICs as EEG channels (19 in this case). Because of that it is important to have an objective procedure to select the relevant ICs consistently. The procedure for robust selection of ICs proposed in this chapter can be summarized in two steps:

1. The number of channels to be analysed using ICA was gradually and pseudo-randomly reduced from the original 19 to 3 (ensuring the inclusion of electrodes representative of all the areas of the brain), the best results were obtained using from 9 to 4 electrodes. The ICs with least dependence on the rest of the ICs was selected in each data subset; the parameter used to measure the dependence between the ICs is the MI.

2. The ICs selected in the preceding step are grouped using the Euclidian distance as a measure of similarity. Clusters with the most robust (stable across the different data subsets) ICs for each subject were then obtained.

The number of robust clusters obtained with the procedure proposed was from 2 to 4 depending on the number of electrodes selected at the beginning of the procedure. In general, the most robust ICs correspond to the AEP and the CI artifact. The principal advantage of the procedure proposed in this chapter over the Krashov *et al* procedure is the favourable computational cost. On the other hand, it is necessary to

include a systematic study about the optimal number of electrodes to select in order to obtain the most number of robust clusters with physical and physiological meaning.

The number of robust clusters and ICs in each cluster is different for each subject, which introduce more variables in the source analysis procedure; making the interpretation of the results for the assessment of children with CIs very difficult. Because of this, it was decided to not use the procedure proposed in this chapter in the source analysis of the AEPs.

At this point, the most optimal ICA algorithm (*TDSEP-ICA*) and its best parameters to remove the CI artifact of the dataset used in this research have been selected. In addition, a procedure to recover the most robust components in each recording has been explained. The AEPs recovered after removing the ICs associated with the CI artifact are now shown and discussed in Chapter 8; moreover the changes in the topographic maps of the ICs related to the auditory response are analyzed in order to establish their relative changes with respect to the time of use of the CI.

Chapter 8.
Assessment of the neurological maturation of children with CIs

The objective of this chapter is to show that *TDSEP-ICA* can be used not only to reduce the CI artifact of contaminated AEP recordings, which is fundamental to the next part of this research (to facilitate and increase the accuracy of the source analysis of the AEPs), but also demonstrates that it is possible to use the topographic maps (spatial projections) of the ICs associated with the auditory response to follow the auditory maturation of children with CIs.

In section 8.1, the ICs recovered by *TDSEP-ICA* related to the AEP in normal hearing and implanted children are shown, together with an analysis of changes in the P_1 peak latency in accordance with the age of normal subjects and with the time of implantation in child CI users. After that, the topographic maps of relevant ICs in children with CIs are shown. Section 8.2 includes an explanation of how the changes of the spatial projections of the ICs related to the AEP can be used to evaluate the maturation of the auditory system in children with CIs. Finally, section 8.3 includes some examples of de-noised AEP recordings which were used in the last part of this research.

All the results shown in this chapter correspond to 1000 Hz and 70 dB_{HL} sound stimuli and using *TDSEP-ICA* (τ=0,1,2,...,20) applied to the 19 EEG recordings with only 50 epochs; plots have arbitrary units for the amplitude of the ICs. Each one of the plots was labelled with the implanted subject number and the number of the study (see Table 3.2), whilst the plots for the normal children were labelled with a sequence of letters.

8.1 Identification of the AEP in normal hearing and implanted children using TDSEP-ICA

First, *TDSEP-ICA* was applied to ongoing EEG recordings from normal hearing children with number of ICs equal to number of channels (19). Figure 8.1 shows the ICs associated with the AEP in three different children for the groups listed in Table 3.1. In group 1, children from 3 to 4 years old, it is possible to identify a P_1 peak with latencies between 175 and 225 ms; in group 2 the latency of P_1 is between 140 and 170 ms. In group 3 the latency of this positive peak is around 100 ms. Finally, in group 4 instead of P_1, a negative peak around 100 ms is present in the response (similar to the adult auditory response morphology). The changes in the P_1 peak latency in children younger than 10 y.o. are as expected, the latency of the peak decrease as a function of age [109;132;133].

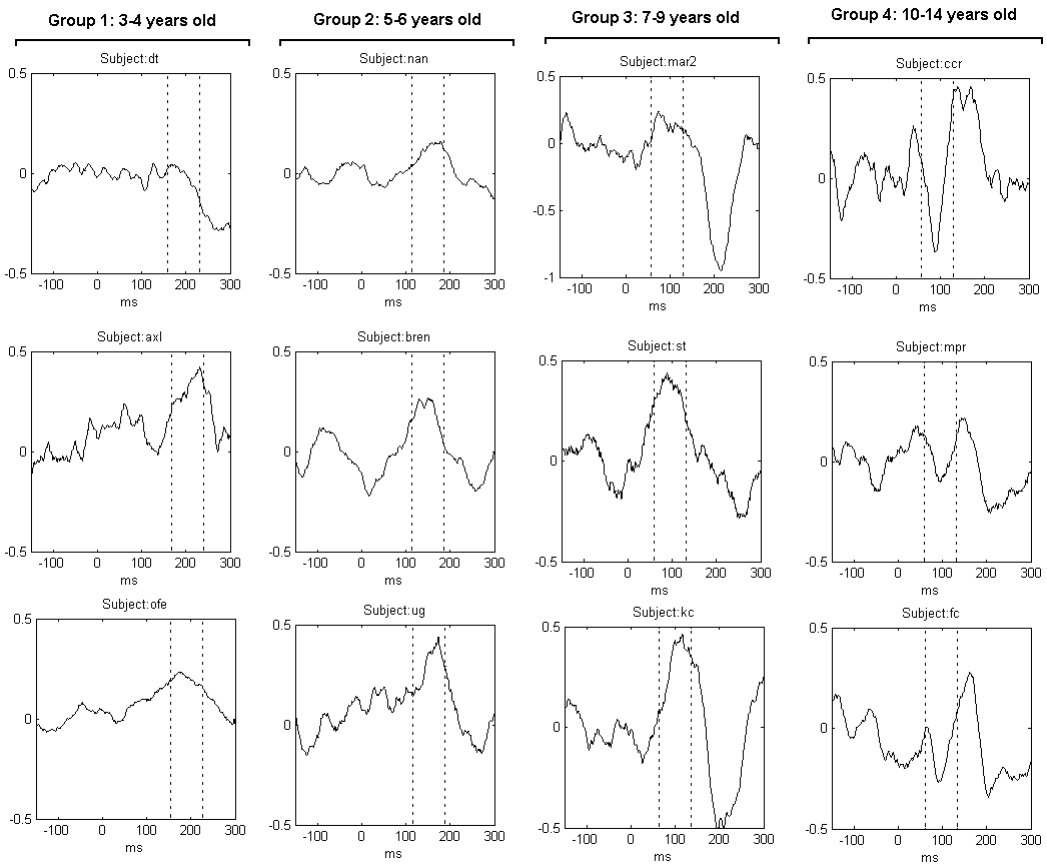

Figure 8.1 ICs related to the AEP in normal hearing children. For children less than 10 years old the components have a positive peak with difference latencies at different ages, whilst between 10 and 14 years old, it is possible to recognize a negative peak around 100 ms, instead of the positive peak.

Figure 8.2 shows the ICs related to the AEP in six implanted children at different times after implantation. Although the reduction of the CI artifact is not total, it is possible to recognize the P_1 peak in all of the recordings, the latency of this peak is variable from 130 to 200 ms across the recordings. A transversal comparison between the latencies of the P_1 is not possible since the number of recordings in each group is reduced. In a longitudinal comparison, the latency of P_1 peak is shorter in accordance with the time of use of the CI (length of time since implantation). Even though the latency of P_1 decreased, it remains prolonged compared with age-matched normal hearing children.

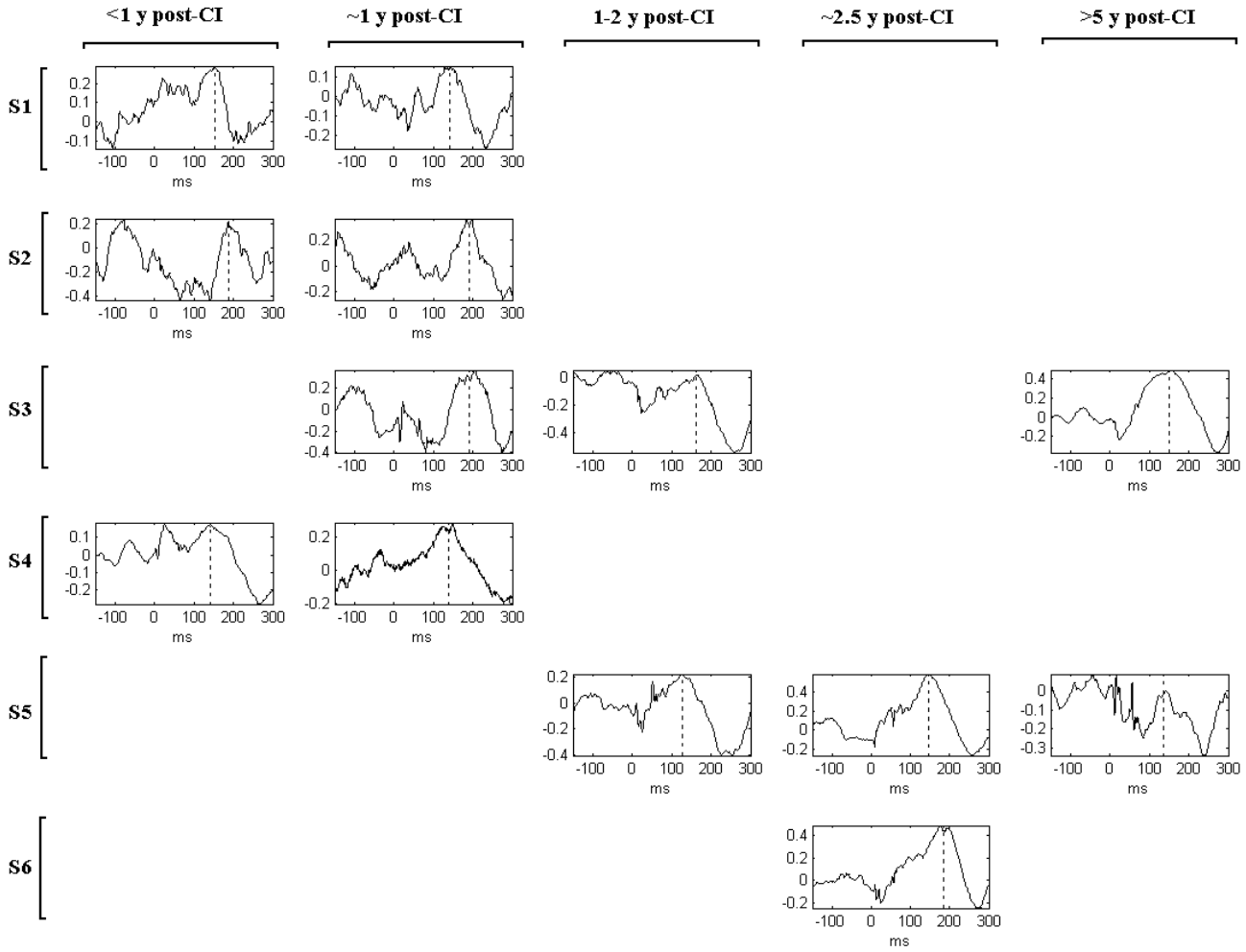

Figure 8.2 ICs related to the AEPs in six different child CI users, at different times after implantation. A positive peak between 130 and 200 ms can be identified in all the recordings.

The waveforms of the ICs related to the AEP in three different subjects, one normal hearing and two implanted children, are compared more closely in Figure 8.3; the latencies of P_1 and N_1 in ***kc***, normal hearing 7 y.o. child, are 109 and 210ms respectively. Subject S3-St3 has used his implant for 5 years and 5 months, P_1 (168.3ms) and N_1 (273ms) can be recognized in this subject. Both P_1 and N_1 were recognized in subject S6-St1 with latencies at 174 and 279ms respectively; this subject has used her implant for 2 year and 6 months. Although the IC waveforms of the implanted children are similar to the IC of the normal hearing child, the P_1-N_1 complex is presented in the three subjects, the latencies of this complex are prolonged in S3 and S6.

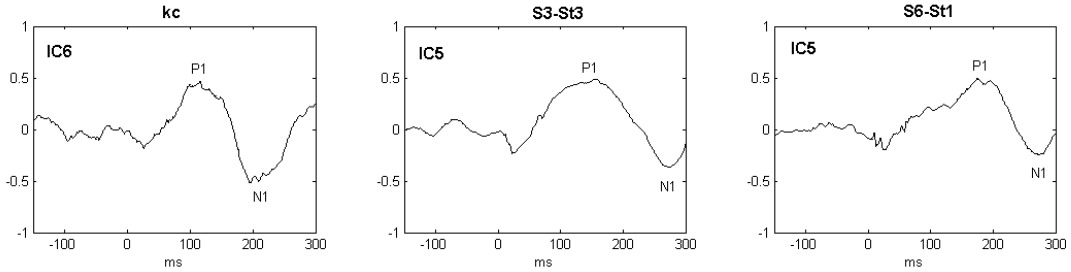

Figure 8.3 ICs associated with the AEP in three different subjects; (a) ***kc*** is a normal hearing child, 7 y.o. and (b) S3-St3 and (c) S6-St1 are two children with different times of implantation; subject S3 was implanted at 7 y.o. whilst subject S6 was implanted at 4 y.o.

In addition to the AEP ICs, several artifacts were identified during the analysis of the dataset; Figure 8.4 shows the waveform and spatial projections (views were selected for easier visualization of the ICs) of three of the most common ICs associated with artifacts in the subjects. The artifacts shown in this figure were observed in three different recordings; the ICs associated with the CI artifact (Figure 8.4(a)) have two distinguishing characteristics:

1. Waveform and duration, pulses with width ≤ 100 ms

2. Spatial projection centred over the CI site (temporal area). Others artifact identified were blinking (Figure 8.4(b)) and noisy electrodes (Figure 8.4(c)).

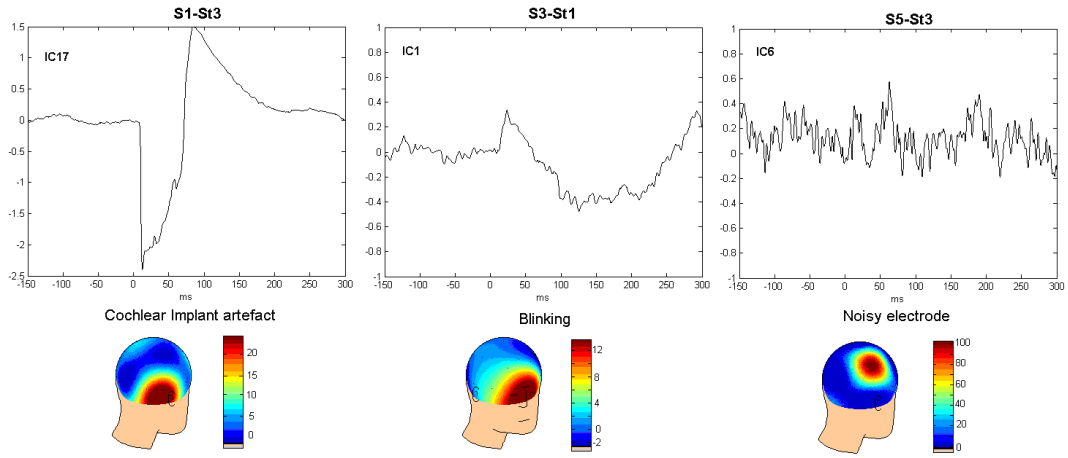

Figure 8.4 Waveforms (top) and spatial projections (bottom) of the most consistent ICs related to artifacts in all the subjects. (a) The IC of the CI artifact is a pulse with a width of 67 ms and spatial projection around T4 and T6 which corresponds to the localization of the CI in S1-St3, (b) the topography of this IC should be associated with blinking, (c) this IC is related to a noisy electrode (C4).

8.2 Assessment of the neurological maturation of children with CIs using TDSEP-ICA

Neurological maturation of the auditory cortex or cortical plasticity refers to structural and functional changes of neural properties which occur on different temporal and spatial scales; the temporal scale extends from seconds to a whole life and the spatial scale extends from the molecular level to changes on topographic (scalp) maps [85]. The changes in the morphology of the ICs offer us a way to evaluate the temporal aspect of the plasticity whilst the changes seen in the topographic maps give us the opportunity to follow the spatial aspect of maturation in children with CIs.

Figure 8.5 shows both the ICs and spatial projections related to the AEP in all the children implanted. Each row corresponds to different subjects whilst columns correspond to time after implantation. A closer analysis of the modification of the spatial projections in accordance with the time of implantation is shown in the rest of the figures in this chapter.

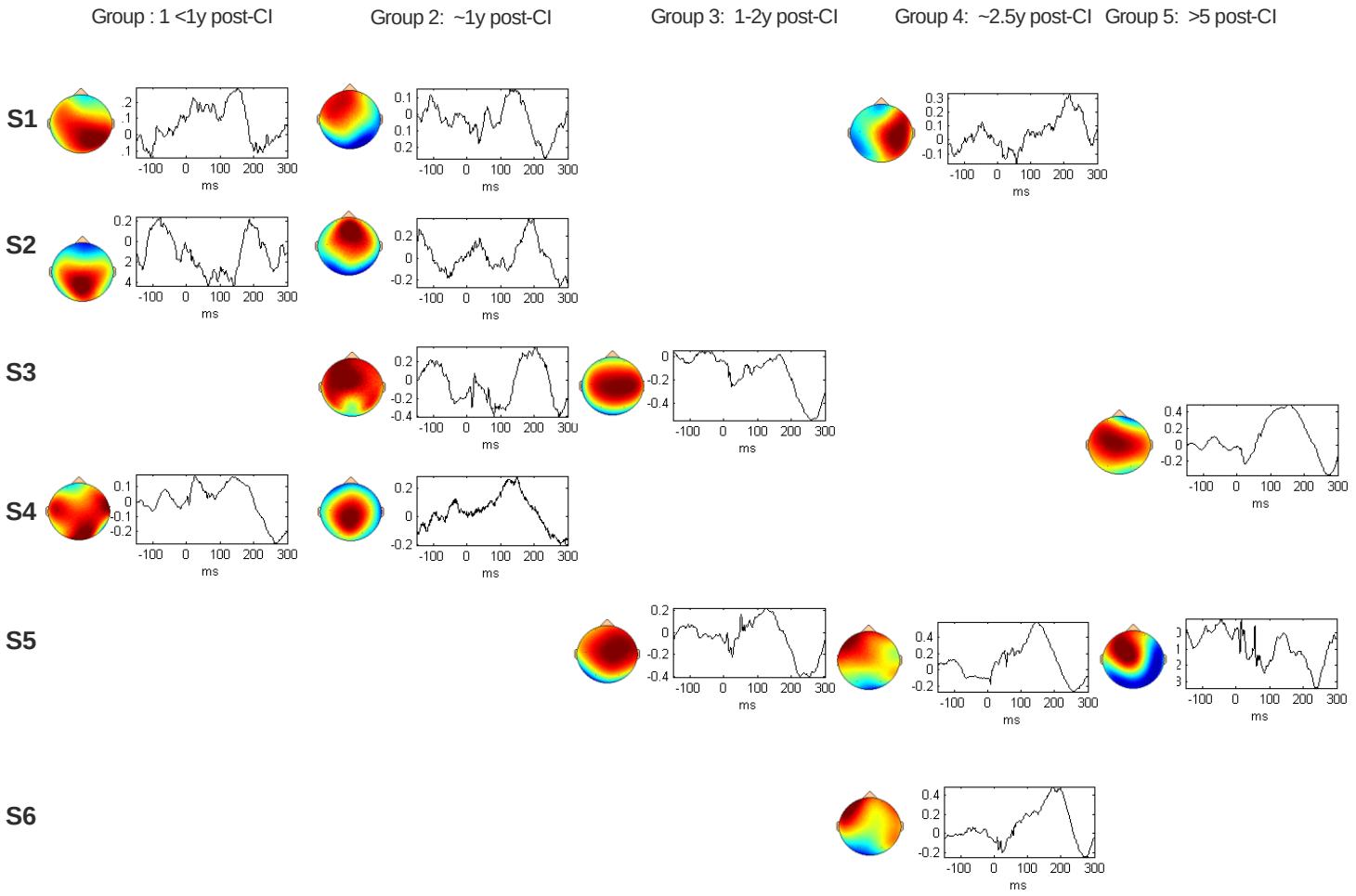

Figure 8.5 Waveforms and spatial projections of the ICs related to AEPs in all the subjects with CIs.

The changes in the IC waveforms associated with the AEP, as well as their spatial projection in the first year of implantation of three different subjects (S1, S2 and S4), are shown in Figure 8.6. In (a) the subjects have used their CIs for less than one year (5 months on average); (b) shows the recordings of the same subjects at one year after implantation. The changes in the latency of P_1 peak of the ICs associated with the AEP between both recordings varied among subjects, 16 ms in S1 and only 3 and 4 ms in S2 and S4, respectively. However, changes of the spatial projections are similar in the three subjects, from parietal to front-central at one year of using their implants.

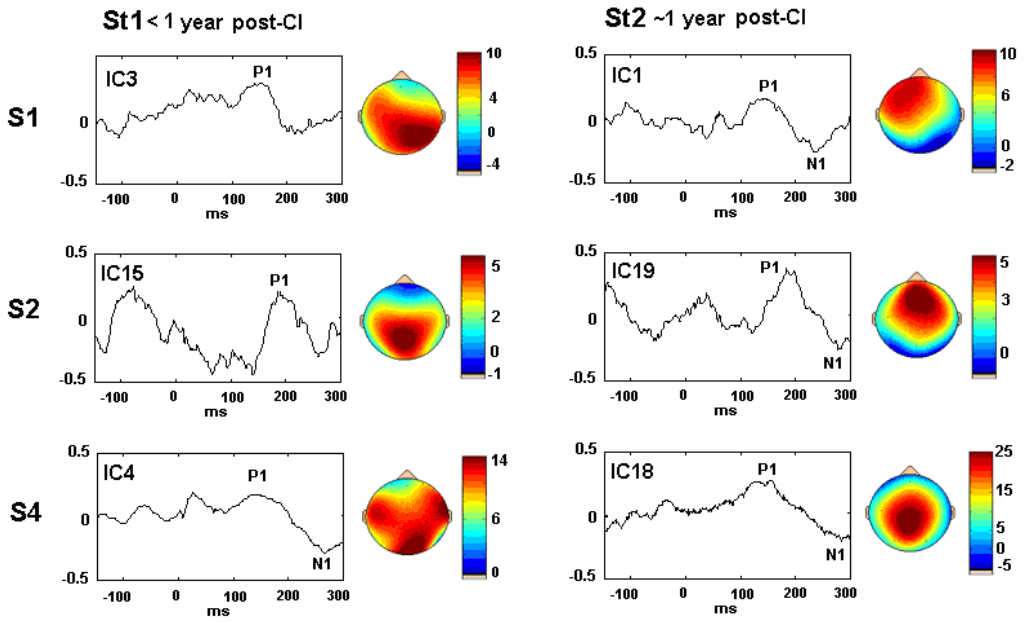

Figure 8.6 Changes in the IC waveforms and spatial projections of three different subjects (S1, S2 and S4) during the first year of use of their CIs; (a) St1: less than one year post-implantation and (b) St2: approximately one year post-implantation.

Figure 8.7 shows the changes in the topographic maps and waveforms of the ICs related to the AEP in two subjects at different times after implantation. In subject S3 the latency of P_1 changed from 165 ms to 160 ms whilst in subject S5 the latency changed from 156.3 to 143 ms; the spatial projections of these components changed from central (1-2 years post-CI) to fronto-central contra-lateral to the CI (>5 years post-CI). Both subjects have their CIs on the right side.

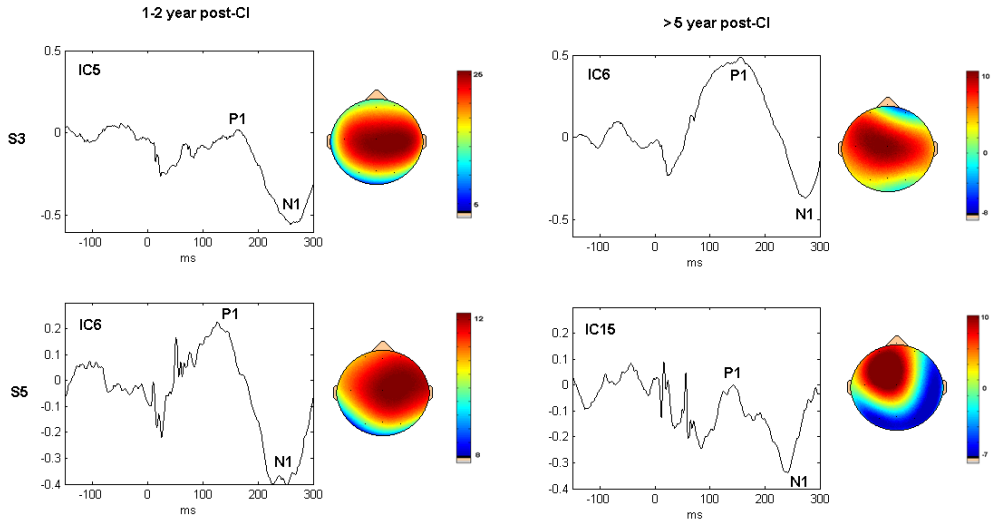

Figure 8.7 Changes in the IC waveforms and spatial projections of two different subjects (S3 and S5); (a) between one and two years post-implantation and (b) more than five years post-implantation.

Figure 8.8 shows the ICs related to the AEPs and their spatial projections of one subject (S5, implanted at 4 y.o. in the right side) at two different times of use of his CI (Study 1: 1 year and 9 months and Study 2: 2 years and 8 months post implantation), compared to a normal hearing child (***xal***, 4 y.o.). The latencies of P_1 and N_1 remain similar between study 1 and study 2, there is a difference of one year between these two recordings; however, the spatial projection of the ICs related to the auditory response changes from fronto-central almost symmetric to frontal lateralized in the left side. The topographic map in study 2 is very similar to that of a normal hearing child.

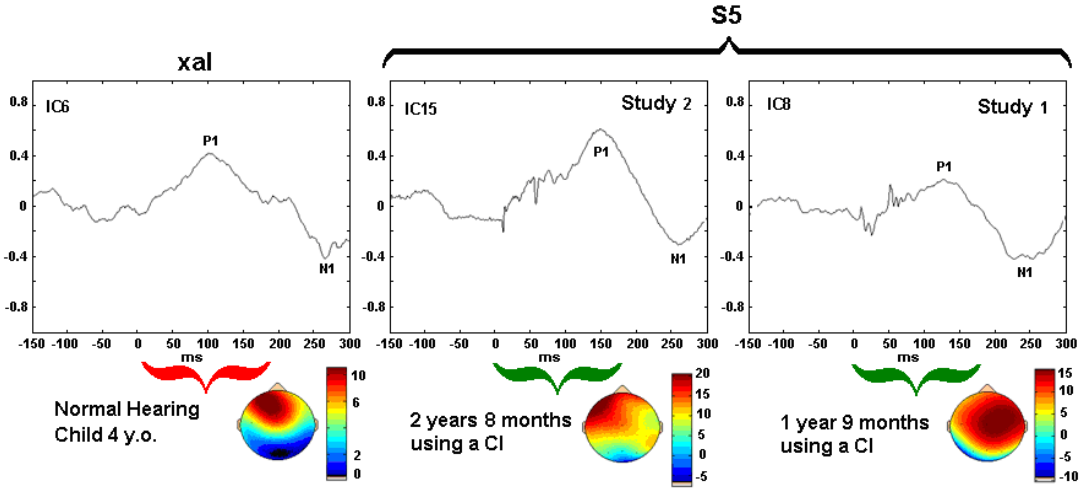

Figure 8.8 Changes in the ICs related to the AEP and their spatial projections of one subject (S5, implanted at 4 y.o. in the right side), at two different time of use of his implant, compared with a normal hearing child (*xal*, 4 y.o.).

Figure 8.9 shows the ICs associated with the AEPs and their spatial projections of one subject (S3, implant at 7 y.o. in the right side) at two different times of use of his CI (Study 1: 1 year and Study 2: 1 year 8 months post implantation), compared with a normal hearing child (***kc***, 7 y. o.). In study 1, only a P_1 peak is observed; the latency of P_1 shifted from 200ms in study 1 to 163 ms in study 2; moreover the spatial projection is more central and localized and is more similar to the topographic map of a normal child.

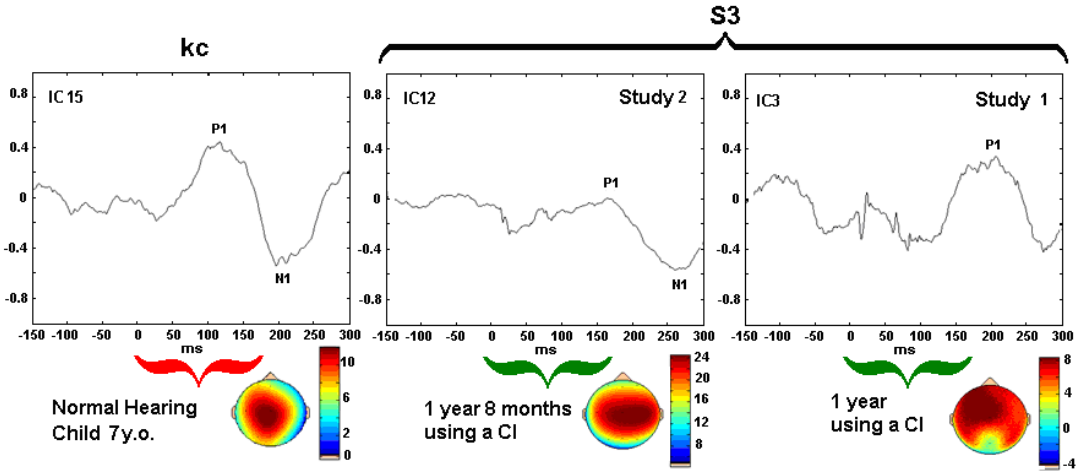

Figure 8.9 Changes in the IC of the AEP and its spatial projection of one subject at two different times of use of his CI (S3, implanted at 7 y.o. in the right side), compared with a normal hearing child (***kc***, 7 y. o.).

Figure 8.10 shows the ICs associated with the AEP and their spatial projection of three different subjects (S3, S5 and S6, implanted in the right side) with more than two years using their CIs (2 year 5 months on average); it is possible to identify both P_1 and N_1 peaks in all subjects. The latency of P_1 is 160.3, 148.3 and 174 ms respectively. The spatial projections have a fronto- to fronto-central distribution lateralized opposite to the CI.

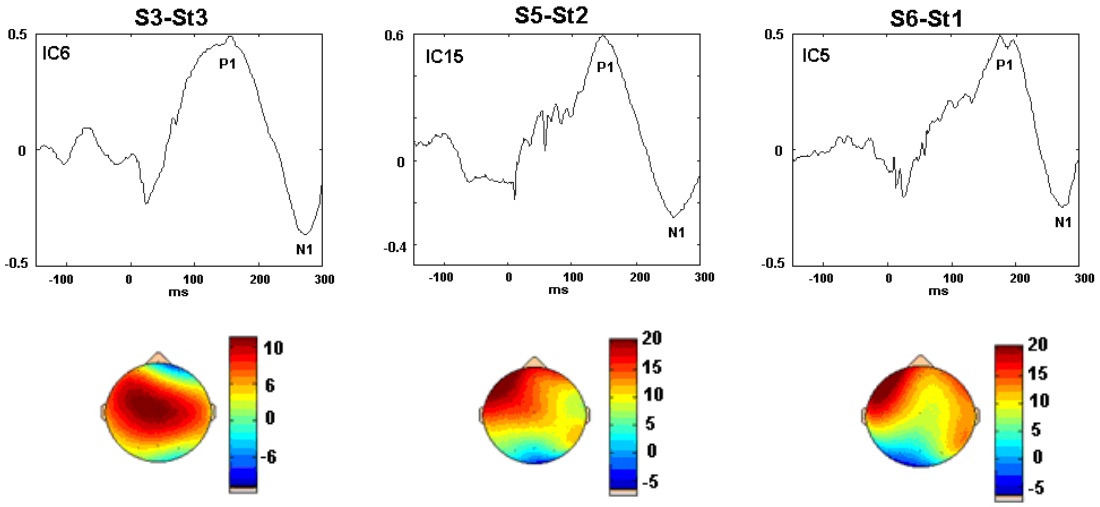

Figure 8.10 ICs associated with the AEPs and their spatial projection of three different subjects (S3 implanted at 7 y.o., S5 and S6 implanted at 4 y.o.) with more than two years using their CI (implanted in the right side); it is possible to identify both P_1 and N_1 peaks in all subjects. The spatial projections have a front to front-central distribution lateralized opposite to the CI.

The latencies of the P_1 peak in the ICs related to the AEP among subjects are diverse and it is not possible to identify the complex P_1-N_1 in all the subjects (S1-St1, S2-St1 and S3-St1). In general the latency of this positive peak is shorter as a function of the use of the CI. It is difficult to draw any conclusion about the auditory system maturation of these children using just this parameter. Nevertheless, the spatial projection of these ICs shows more consistent changes in accordance with the use of the CI, across all the subjects. Although it is necessary to increase the number of subjects and recordings, in order to have more reliable results, it is possible to say that subjects implanted younger present topographic maps more focussed in a specific area contra-lateral to the CI than children implanted at an older age (compare for example Figures 8.8 and 8.9).

In general, the spatial projections of the AEPs' ICs are spread out around the head with no focus in any specific area, although predominantly parietal when the children have used their CIs for less than one year. At one year after implantation the spatial projections are characterized by a central to fronto-central distribution. Finally, the spatial projections of the ICs have a distribution fronto- to fronto-central, contra-lateral to the CI implantation at more than two years post-implantation. The spatial projections of the ICs related to the AEP show similarities with normal hearing

children's spatial projections, which could be used for an objective assessment of the maturation of the auditory system in children with CIs.

8.3 De-noising the AEP

In this section the original signals and the de-noised signals after removing artifactual ICs, using *TDSEP-ICA* (τ=0,1,2,…,20), are shown. The columns of the mixing matrix corresponding to those components were made zero to generate the de-noised signal. Appendix G includes all the artifactual ICs identified in the recordings from children with CIs. The principal artifact recovered were those related to the CI artifact and noisy electrodes; additionally, both the original and the de-noised signal after removing those artifacts are shown in this appendix too. Some examples of those signals are shown in the following figures.

The original and de-noised signals (plots on red and black, respectively) for recording S2-St1 (female implanted in the left side) are shown in Figure 8.11. The ICs related to the CI artifact and noisy electrodes were removed from this recording. After removing those artifacts, it is possible to identify P_1 peak in the electrodes around the CI (T3 and T5).

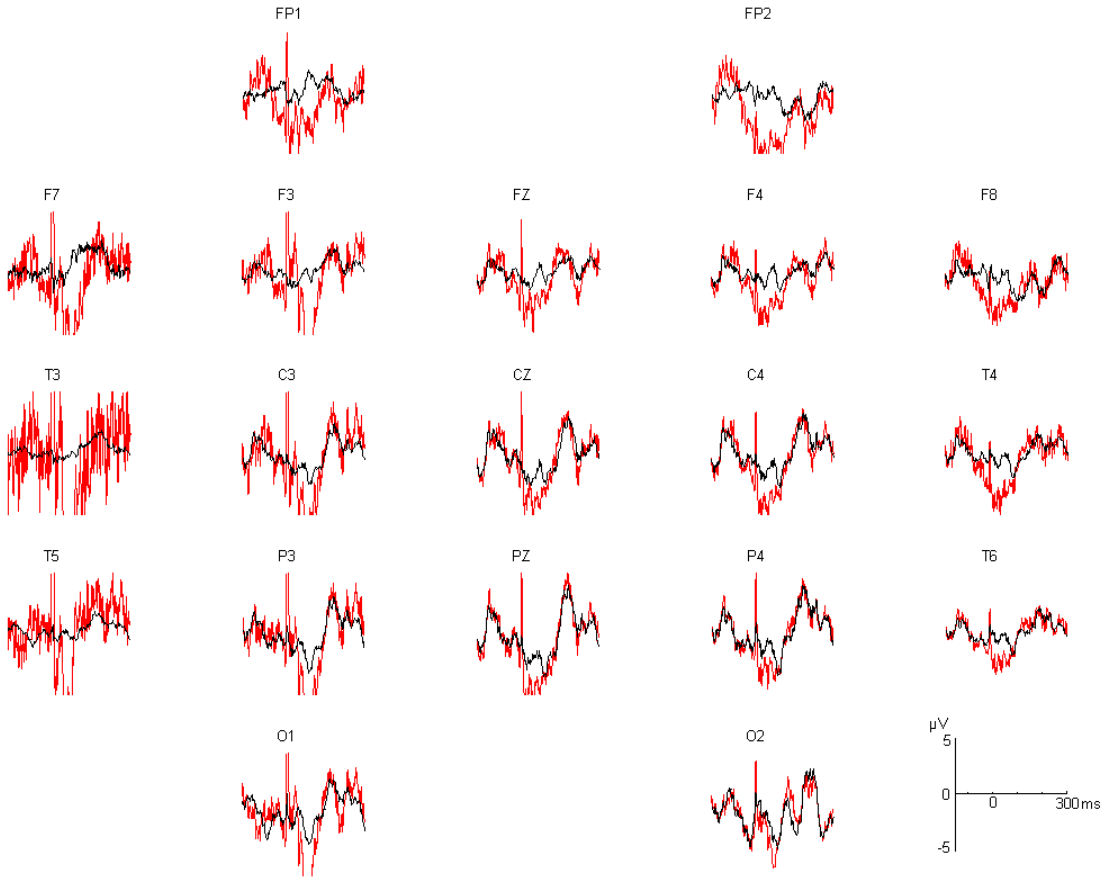

Figure 8.11 Comparison between the original (red) and de-noised signal (black) in recording S2-St1, the ICs related to the CI artifact and noisy electrodes were removed in this recording.

Figure 8.12 shows the original signals and their de-noised version (after removing the ICs associated with the CI artifact using *TDSEP-ICA*) for three different recordings. The reduction of the CI artifact is not total but it is now possible to identify the AEP in the electrodes that were contaminated by this artifact (T4 and T6 for these subjects). Subject S3-St1 is a child one year post implantation; it is possible to identify a positive peak at 166 ms. The complex P_1-N_1 was identified after de-noising in subject S3-St2 and S6-St1. For the case of subject S3-St2 who had used his CI for 1 year and 8 months at the time of this recording, the latency of P_1 is 171 ms and 276 ms for N_1. Subject S6-St1 had used her CI for 2 years and 5 months; the latency of P_1 is 174 ms and 279 ms for the negative peak.

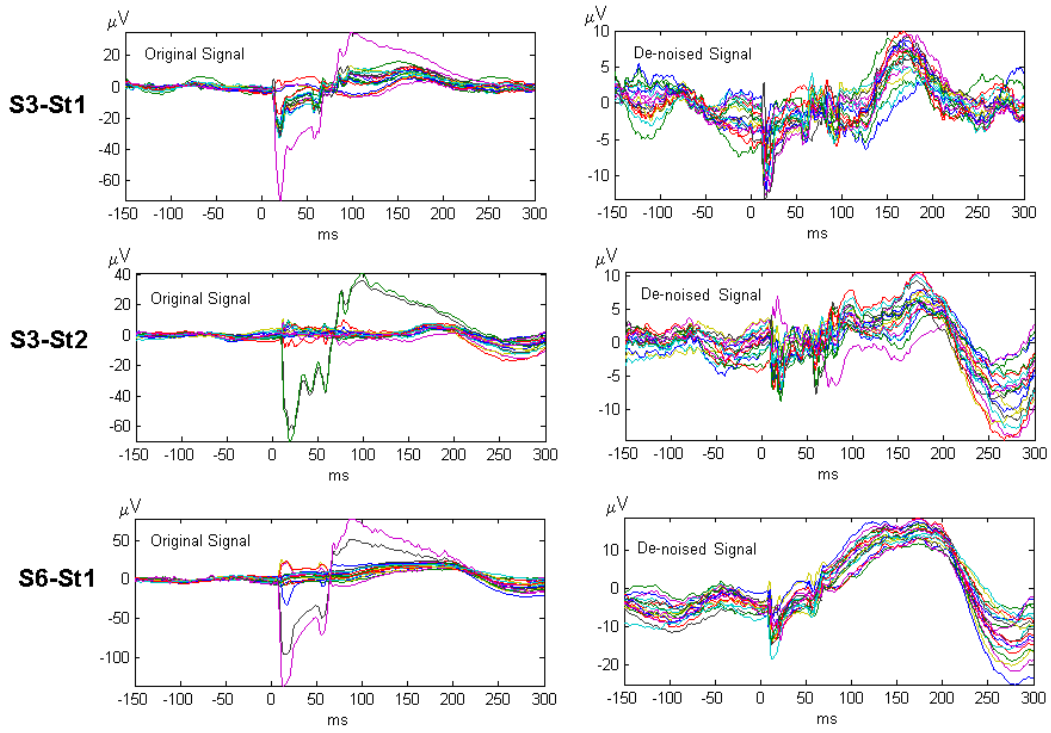

Figure 8.12 Butterfly plots of both the original signal (left column) and the signal after removing the ICs associated with the CI artifact (right column); both P_1 and N_1 were identified in subject S3-St2 and S6-St1 whilst only P_1 was detected in subject S3-St1.

8.4 Summary

This part of the research consisted of applying the ICA technique not only to reduce the CI artifact [39;52] but also to detect AEPs in ongoing multi-channel recordings. After that, using the spatial projection of the ICs associated with the AEPs, which provides a global representation of the response to the auditory stimulus, it was possible to follow the auditory system maturation of children with CIs in accordance with the time of use of their implants.

The topographic maps related to the AEP change from being spread out around the head with parietal predominance, to fronto-central localization contra-lateral to CI implantation. The spatial projections of the ICs related to the AEP show similarities with normal hearing children's spatial projections in accordance with the time of implantation, which could be used for a robust and objective assessment of the maturation of the auditory system in children with CIs. Furthermore, this method should be suitable to be implemented in practice in a clinic.

One advantage of ICA is that it can be applied directly to un-averaged EEG data with the possibility of reducing the number of epochs and hence the testing time. The results obtained using *TDSEP-ICA* with only 50 epochs show that it is feasible to reduce the time of the recording to one third of the original EEG recording time; this is particularly useful, since it is hard to obtain good results from children without sedation, over long experimental sessions.

Once all the artifacts have been removed, the *source analysis* for the P_1 peak of the AEPs of both normal hearing and children with CIs is carried out. In the following chapter a review of the most important concepts involved in source analysis theory are included; moreover the assumptions of the head model, type of dipoles and the mode to validate the source analysis results are mentioned in this chapter. Finally, the results of the source analysis of the AEPs to assess the performance of CI users are shown at the end of that chapter.

Chapter 9.

Source analysis of the AEP in children with CIs

The results shown so far exposed the changes in the topographic maps of the ICs associated with the AEPs in accordance with the use of CIs over time. It is interesting however, to follow the changes in neural sources in the form of *Equivalent Current Dipoles* (ECDs) of these potentials, at different times post implantation. This gives a basis for an objective technique to evaluate the maturation of child CI users. The aim is for this to be an objective procedure to assess the maturation of the auditory system of an implanted Child-CI as a complete system, viable for implementation in a practical clinic.

This chapter is organized as follows: Section 9.1 includes an introduction of source analysis theory, the assumptions behind the use of the ECDs considered in this theory, as well as an overview of some electromagnetic equations relevant to model the EEG in this way. Source analysis consists of solving the forward and the inverse problem, both these topics are described in Section 9.2. In Section 9.3 the parameters used in commercial software used here for the source analysis of AEPs are described. In Section 9.4, the description of an alternative procedure, which uses *TDSEP-ICA* in the pre-processing step of the source analysis of the AEPs, is detailed. In Section 9.5 results of the source analysis of the AEP P_1 peak, in both normal hearing children and children with CIs, are shown. Finally, in Section 9.6 source analysis of the P_1 peak for the assessment of CI users is explained.

9.1 Brain Source analysis

Using functional data (multi-channel EEG or MEG) and anatomical data, such as Magnetic Resonance Image (MRI) and Computer Tomography (CT), it is possible to obtain an estimate of the localization of the current sources generated by specific neurological events within the brain. Useful for example, for determining the location of epileptic focii and EPs which are generated within the cerebral cortex. This activity is the consequence of depolarisations or hyperpolarisations in concert, giving in result a dipolar current source generally orthogonally oriented to the cortical surface; the active regions in the cortex could be *focal* or *distributed* [37]. *Focal* source models are suitable for electrical activity within small areas of the brain whilst *distributed* sources models represent the activity with a grid containing hundreds of dipolar sources with fixed position and orientations. The first model is solved using single dipole fits, whilst the second model is computed by current density methods; these models are able to describe extended sources, estimating the time course for each one of the dipoles. The problem of recovering the current sources from superficial EEG recordings is that it is intrinsically ill-posed; it is impossible to uniquely determine the spatial configuration of neural activity based on EEG recording alone [115], no matter how many recording channels are used.

Source analysis consists of calculating the current sources and potential fields within the brain; for this, a model of the source and the head is assumed in order to calculate a solution of the inverse problem (nonlinear and intrinsically ill-posed) which is obtained (usually) by an iterative process. This iterative process consists of moving a ECD, whilst its amplitude and orientation are changing within the head model, to obtain the best fit between the EEG data (as measured at the scalp) and those produced by the source in the model. As already mentioned, there is no unique solution to this inverse problem since different internal source configurations can produce equal external electromagnetic fields; the quality of the solutions depends on the source and head models used. The most simplistic source model is a single dipole which is convenient if the distance between disparate dipoles is large or the dipoles are thought to have different temporal activities. There are different *volume conductor* head models used to solve the inverse problem; spherical models with 3, 4 or 5 shells and realistic head models calculated from MRI data. A spherical model is the most

simplistic volume conductor; this model contains concentric layers that represent the scalp, cerebrospinal fluid (CSF), skull, and brain, each one with different electrical conductivity [127]. The *Boundary Element Method* (BEM) is a realistic head model which approximates compartments of the head by triangular meshes with a limited (but large) number of nodes [47;48]. The solution of the inverse problem depends on the geometry and conductivities of the volume conductor selected.

Three principal prior assumptions in source analysis should be considered:

1) A small number of focal sources that can be modelled by ECDs to generate EP.
2) The localization, orientation and activity over time of each ECD are interactively determined by minimizing the difference between the predicted and the actual EP.
3) The electrical activity is generated by the pyramidal cells of the brain i.e. the sources of the recorded potentials are located in the cerebral cortex.

Maxwell's equations (Equations 9.1-9.4), which state the fundaments of electricity and magnetism, are used to compute the electrical field $\boldsymbol{E}$ and the magnetic field $\boldsymbol{B}$ generated by neural currents density $\boldsymbol{J}$; ε is the *permittivity* of the medium.

$$\nabla \cdot \boldsymbol{E} = \rho / \varepsilon, \qquad 9\text{-}1$$

$$\nabla \times \boldsymbol{E} = -\frac{\partial \boldsymbol{B}}{\partial t}\ , \qquad 9\text{-}2$$

$$\nabla \cdot \boldsymbol{B} = \boldsymbol{0}, \qquad 9\text{-}3$$

and

$$\nabla \times \boldsymbol{H} = \boldsymbol{J} + \frac{\partial \boldsymbol{D}}{\partial t}. \qquad 9\text{-}4$$

Equation 9.1 (Gauss' law for electricity) states that the electrical potential $\boldsymbol{E}$ is proportional to the charge density ρ, at the same time $\boldsymbol{E}$ is proportional to the time rate of change of magnetic field $\boldsymbol{B}$ (Equation 9.2, Faraday's law of induction). Equation 9.3 (Gauss' law for magnetism) state that the magnetic field, $\boldsymbol{B}$, has divergence equal to zero.

Equation 9.4 tell us that the magnetic fields (***H,*** due only to macroscopic currents) may be generated in two distinct way, by currents ***J*** or by a time varying electric field (the electric displacement ***D***); these relations are linear in conductive, dielectric and magnetic senses, that is

$$\boldsymbol{J} = \sigma \boldsymbol{E}\,, \tag{9-5}$$

$$\boldsymbol{D} = \varepsilon \boldsymbol{E}\,, \tag{9-6}$$

and

$$\boldsymbol{B} = \mu \boldsymbol{H}\,. \tag{9-7}$$

σ is the *electrical conductivity* of the medium, ε is the *permittivity* of the medium, and μ is the *permeability* of the magnetic material.

At the low frequencies of brain dynamics, the electric and magnetic fields are separate then the magnetic field may be calculated from the Biot-Savart law which describe the magnetic field generated by an electric current. This equation is a special case of Equation 9.4

$$\boldsymbol{H} = \frac{\boldsymbol{P} \times \mathbf{r}}{4\pi r^3}\,, \tag{9-8}$$

where ***H*** is the magnetic field, ***P*** is the current dipole moment, and **r** is the vector from the dipole to the field point; the direction of ***H*** is circular, enfolded around the dipole axis.

The conservation of free charges, the charge is neither created nor destroyed, follows from Equations 9.1 and 9.4 that is

$$\nabla \cdot J + \frac{\partial \rho}{\partial t} = 0\,. \tag{9-9}$$

The equations listed in this section constitute the basis to model the electrical activity into the brain. The current flow causes an electrical field and also a potential inside the human head which can be calculated using these equations.

9.2 Inverse and Forward problem

The inverse problem consists of calculating the localization and magnitudes of the ECD(s) within the brain using: a set of electric potentials from discrete sites on the scalp, the associated electrode position of those measurements, and both the geometry and conductivity of the different regions in the head. Each ECD source has six parameters, three which correspond to localization coordinates (x, y, z), two with the orientation (θ, φ) and one with the time-dependent source strength, (see Figure 9.1 [127]). In order to solve the inverse problem is necessary to solve the forward problem first where the strength, location and orientation of a source inside the head are known whilst the measurements on the outside of the head are unknown; in this case the problem has a unique solution.

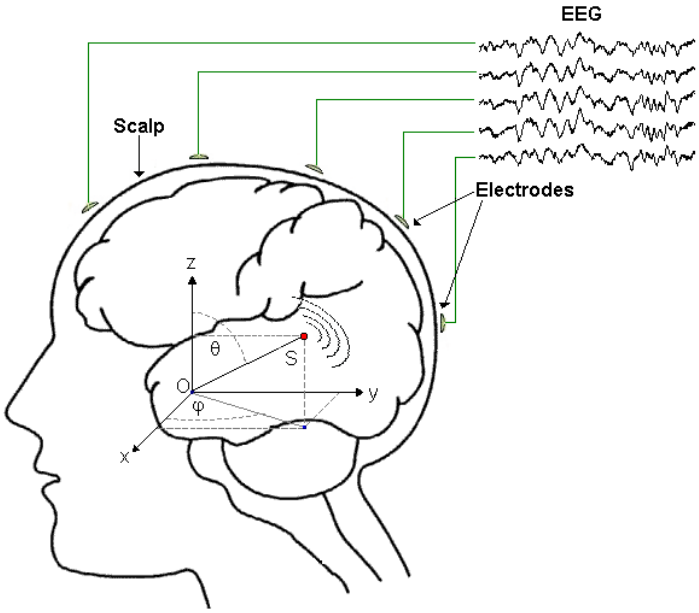

Figure 9.1 Each one of the ECDs, S, has six parameters, three which correspond to localization coordinates (x, y, z), two with the orientation (θ, φ) and one with the time-dependent source strength.

Constraints are needed to single out one solution to the inverse problem; once the source model (focal or distributed), the number of sources (symmetric in both hemispheres or not), as well as an anatomical constraint (specific area in the brain) must be included then the inverse problem can be solved. Information on sensor location is required to compute the solution too. Using landmarks positions (often the nasion, inion and pre-auricular points), the centre-of-gravity of these landmarks is then the most well defined location.

Basic equations for the forward problem

The EEG is the result of the intracellular currents generated by specific neurons in the grey matter (pyramidal neuron cells). Mathematical models in EEG include the so-called volume conductor models. The basic equations of these models relate current and potentials produced in the volume conductor. These currents can be modelled by the Poisson' equation, this equation is derived via Maxwell's equations (Equations 9.1-9.4). Poisson's equation follows directly from Ohm's law for an isotropic conductor (see Equation 9.5).

Equation 9.1 gives the relation between the electrical field and the charge density; additionally, the electrical field is related to the electrical potential, ***V***, by

$$\boldsymbol{E} = -\nabla \boldsymbol{V}. \qquad 9\text{-}10$$

The Poisson equation relates the electrical potential with the charge density

$$\nabla^2 \boldsymbol{V} = -\frac{\rho}{\varepsilon}, \qquad 9\text{-}11$$

in a charge free region of the space, this becomes Laplace's equation, which is appropriated for calculation of potentials at the membrane scale. Once the electric potential has been calculated, the electrical field is computed by the gradient of the potential, when the charge distribution has spherical symmetry, the Laplacian is used in polar coordinates.

The potential at any location in the head volume conductor due to brain sources can be expressed as

$$\boldsymbol{V}(\mathbf{r},t) = \iiint \boldsymbol{G}(\mathbf{r},\mathbf{r}')\,\boldsymbol{P}(\mathbf{r}',t)\,d\mathrm{V}(\mathbf{r}'), \qquad 9\text{-}12$$

where ***P*** (**r**, *t*) is the current dipole moment per unit volume at location **r** and time *t*. The Green's function ***G*** (**r**, **r**'), which includes all the volume conductor properties, weight the integral; when the electrical distance between the recording localization **r** and the source location **r**' is small, the ***G*** (**r**, **r**') is large.

The forward problem, which involves calculation of scalp potentials from known current sources, may be solved by Equation 9.12 for potentials $\boldsymbol{V}$ due to known source magnitudes and locations. The inverse problem consists of finding the locations and strengths of the current sources of Equation 9.12, from EEG recordings, with respect to some reference, in the scalp [100].

In order to solve the inverse problem, the brain volume is divided into N voxels of volume ΔV with a dipole moment $p_n(\mathbf{r}_n,t_i)=\boldsymbol{P}(\mathbf{r}_n,t_i)\,\Delta V$.
Then Equation 9.12 may be replaced by

$$\boldsymbol{V}_S\left(\mathbf{r}_k,t_i\right)=\sum_{n=1}^{N}\boldsymbol{G}_n\left(\mathbf{r}_k,\mathbf{r}_n\right)p_n\left(\mathbf{r}_n,t_i\right). \qquad 9\text{-}13$$

Equation 9.13 can be interpreted as: the surface potentials $\boldsymbol{V}_S$ are generated by dipole moments $p_n(\mathbf{r}_n,t_i)$ in voxels ΔV located at $\mathbf{r}_n$.

Then, the basic inverse problem in EEG is to experimentally estimate the potential distribution at the scalp surface $\boldsymbol{V}_S\,(\mathbf{r}_k,\,t_i)$ to invert Equation 9.12, that is, to solve this integral, for the function $\boldsymbol{P}(\mathbf{r},\,t)$ using a head volume conductor model to specify the function $\boldsymbol{G}(\mathbf{r},\,\mathbf{r}')$. As mentioned, the inverse problem is intrinsically ill-posed, there are a very large number of functions $\boldsymbol{P}(\mathbf{r},\,t)$ that will give up the same surface distribution $\boldsymbol{V}_S\,(\mathbf{r}_k,\,t_i)$; then, the inverse solution requires constraint given the non-uniqueness of the inverse problem.

9.3 Curry for source analysis

Curry [3], from *NeuroScan Lab*, is a software package which combines functional data and anatomical images, for determining electrical activity within the brain. *Curry* provides powerful techniques for accurately localizing the source of such activity; all of this in a research context. The following paragraphs summarize the procedure implemented in *Curry*, as well as the criteria to select the parameters used in the source analysis of the AEP, P_1 peak, in children with CIs as used in this research.

Data Pre-processing

Noise estimation: One of the most important parts in the pre-processing step of source analysis is determining the *SNR* of the data. *SNR* is fundamental in the regularization of the parameters (sensor weighting); correct noise estimation leads to correct regularization parameters. The weight of any sensor is inversely proportional to its noise. The *SNR* of each recording was calculated using the standard deviation of the pre-stimulus interval (150 ms). According to the *Curry*'s user Manual [38] this is appropriate for epoched files containing EP data.

Reference selection: A reference has to be selected before performing the source analysis. For EEG, the common average reference (CAR) is usually used; this reference is more appropriate for source analysis comparison than a single reference site [105].

Included in the pre-processing step is the baseline correction to remove the DC offset from the data and the selection of the number of epochs to be averaged. In both normal hearing children and children with CIs the number of epochs averaged was chosen to be 50.

Parameters

PCA and ICA Decomposition: Using PCA Curry reduces the number of variables in the dataset; PCA is used to pre-white the data and to find the number of valid components in the ICA step. ICA is applied to filter artifactual components before the source analysis.

The *Mean Global Field Power* (MGFP): is a measure that indicates the strength of the signal against the noise background. MGFP is commonly used to obtain a quick overview of the measured EEG time courses, since it collapses the information of all electrodes into a single trace. One can easily distinguish latency ranges with meaningful signal from noise or background activity periods, which is useful to identify the components of the EPs.

The MGFP is an average of the *common average re-referenced* data and is computed as follows: x_i is the measured data, i=1,2,...,m; where m is the number of electrodes for a given time point. The steps to calculate to MGFP are:

1. The *common average* C_{avg} is: $C_{avg} = \frac{1}{m}\sum x_i$.
2. The *re-referenced* measured data $R_i = x_i - C_{avg}$.
3. Finally, $MGFP = \left[\frac{1}{m}\sum_{i=1}^{m}\left(R_i \cdot R_i\right)\right]^2$

In other words, MGFP is an averaged measure for the signal power [116;117]; estimating the *SNR* from the MGFP together with the *residual standard deviations* percentage can tell us if the chosen source model is at least able to explain in part the data.

Source Analysis

Volume conductor head model: The head is a volume conductor which distorts the potential of the sources in the brain. The very complex shape of a human head with all its anatomical details is represented by a simplified model; in order to solve the inverse problem it is necessary to know its shape and electrical conductivities of the head model [95]. The human head parts such as the brain or the skull are represented by different compartments with each compartment being assigned an electrical conductivity; the shape of these compartments could be spherical, or could derive from anatomical data; the latter improves the accuracy of the solution of the forward problem.

Curry uses a concentric spherical volume conductor head models with one to four shells, values of their conductivities and relative radii are listed in Table 9.1; the spherical model assumes constant cranial curvature and constant scalp and skull thickness [35]. In a three shells spherical head model the inner sphere represents the brain, the middle shell represent the skull and the outer layer represent the scalp.

Table 9.1 Conductivities and relative radii for four concentric structures for a spherical head model (CSF: Cerebrospinal fluid) [100].

Structure	Conductivities [Ω^{-1}/m]	Relative Radii [%]
Brain	0.33	83.0
CSF	1.00	85.0
Skull	0.0042	93.0
Scalp	0.33	100.0

The real varying thickness and curvatures of the skull assumed by the spherical head model could vary the source analysis solution; the so-called realistic head models would be more accurate than spherical head models.

In each compartment of the standardized Boundary Element Method (BEM) model (realistic model), the electrical conductivity is modelled to be homogeneous, isotropic and ohmic [36;104]. This volume conductor head model is derived using an automated routine, from an average T1-weighted MRI dataset included in the software from Montreal Neurological Institute and Hospital [5]; 91 axial slices with 91×109 pixels and a voxel size of 2×2×2 mm^3. It is possible to choose between a low discretization with approximately 3000 nodes, medium with 4000 nodes, and high with approximately 5000 nodes.

The spherical shells head model is fast and numerically stable but BEM is superior in non-spherical parts of the head like temporal and frontal lobes and basal part of the head. Most of the volume conductor models for solving the inverse problem have less accuracy with deep dipoles [95]; in our case the dipoles for the AEP are cortical dipoles so the models mentioned before should be sufficient to recover these type of dipoles.

Dipole type: the dipoles types calculated by *Curry* are: Moving, Rotating, Regional and Fixed Coherent models. The moving dipole solution consists in dipole analysis in a serie of time points, the six ECD's parameters are determinated to minimize the deviation between measured and forward calculated data. The rotating dipole solution is an approach where the position of the dipole is fixed for all time points and its components (orientation and strength) can freely vary with time [131]. The regional

dipole is computed when three orthogonal main dipoles orientations are extracted from a rotating dipole, using PCA; their dipole strengths are calculated as a function of time. Finally, in the fixed coherent dipole solution both the location and the orientation are kept fixed for all time points and the dipole strength can vary with time; when more than one dipole is fitted, they have coherent loadings. For both moving and rotating dipole solutions, the optimum dipole is determined by an optimisation of the three location parameters. In the case of fixed dipole the optimum requires the simultaneous optimisation of the three location parameters as well as the two orientation parameters, for all time points [126;127].

Number of sources: the number of generators for the AEP N_1 peak in adults, which is equivalent to peak P_1 in children, can be as many as six [96], see Section 2.4. The number of dipoles that may fit the data is limited by the number of surface measurements (electrodes, m), in general $m=6d$ where d is the number of dipoles [40]; in our case $m=19$ then $d=3$. Additionally, the number of ECDs used in the literature for AEP source analysis is two -symmetric in both hemispheres [22;81;106;109;123]; source analysis using one and two symmetric ECDs has thus been compared in this research.

Electrode positions and landmarks: three landmarks (nasion, left and right preauricular points, determined using a 3-Dimensional digitizer [2]) were used; their centre-of-mass is near the centre of the head. When a spherical shell volume conductor is used the electrode position are fitted to the outermost shell and when a BEM model is used, the electrode are fitted to the outermost surface, which both cases represent the skin.

The PAN co-ordinate system (Pre-Auricular point and nasion) and landmarks are used to match the BEM with the electrode system. In the PAN system with direction of the axes R: right, A: anterior, S: superior, the *x* axis goes through auricular left and auricular right and point right, the *y* axis goes through the nasion and the *z* axis points up (see Figure 9.2). *Curry* introduces a global scaling factor in order to improve the match between the BEM model dimension and the electrodes. It is calculated from the average of the ratios of the nasion-origin distances and the left-right pre-auricular point distance [38].

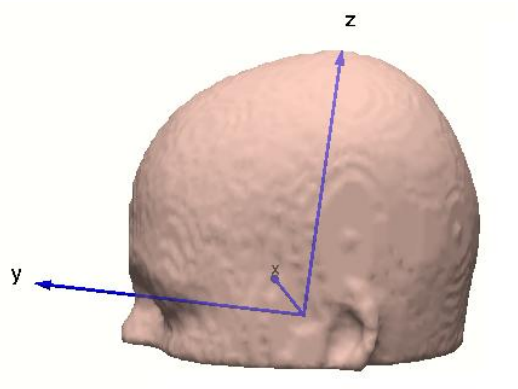

Figure 9.2 The PAN coordinates system with direction of axes *x*, *y*, *z*, as right, anterior, superior [32]. The positions of electrodes used in the source analysis were obtained by projecting the locations of the electrodes (relative to three points –nasion and two preauricular points) onto the external surface (skin).

Visualization of results

Anatomy of the human auditory cortex: a brain atlas with all the structures listed in the Talairach system is included in *Curry*; the Talairach coordinate system, developed by Talairach and Tournoux (1988) [66], identifies brain structures in the MRI data in terms of their anatomy or function. The *Curry* user can segment automatically any of the structures listed in the Talairach system or may click on a point in the MRI data to see in which structure of the brain the ECDs are localized. Using this *Curry* option both the location and Brodmann areas where the ECDs are situated were identified. ECDs were superimposed onto cortex segmentation from averaged MRI.

The Brodmann area is a map, proposed by Korbinian Brodmaan in 1909, of the organization of the cortical areas in humans (and any other species) [85]. Figure 9.3 shows the Broadmann areas of the temporal lobe: a) the primary auditory cortex includes areas 41 and 42; superior, middle and inferior temporal lobe are areas 22, 21 and 20, respectively. Brodmann area 38 is part of the middle temporal lobe whilst area 37 identifies the Fusiform gyrus. b) The medial temporal lobe includes the Amydala, Hippocampus, Parahipocampal gyrus (areas 27, 28, 34, 35 and 36).

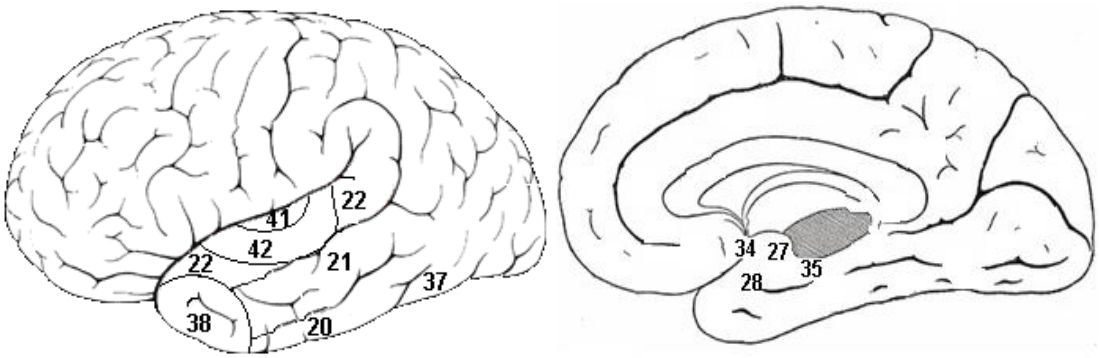

(a) (b)

Figure 9.3 Brodmann areas of the human temporal lobe (a) lateral surface of the brain and (b) medial temporal lobe.

Validation of the results

Two parameters were used to validate the source analysis results:

a) The *Residual standard deviation* (*Res. Dev.*). *Res. Dev.* is a parameter to validate the ECD location; it is a measure of how well the source model explains the measured data. The percentage of the *Res. Dev* suggest by *Curry* as a good fit parameter is less than 10%, dipole fit and is calculated as

$$\mathrm{Re}\,s.Dev = \left[\frac{\sum \left((R_i - F_i)(R_i - F_i) \right)}{\sum \left(R_i \cdot R_i \right)} \right]^{1/2}$$

Where F_i are the calculated signal in the source analysis procedure

b) The *confidence ellipsoid* (*CE*). *CE* is computed by slightly moving the coordinates (*x, y, z*) of the best-fit dipole by small increments, in the order of 1 mm, for each dipole independently. The confidence range of the individual ECDs can be estimated comparing the field variation and the noise level; confidence ellipsoids and the *SNR* of the measured data are inversely proportional [20;49]. *Curry* computes the confidence ellipsoids to visualize the localization accuracy; a SVD is used to determine the orientation and length of the confidence ellipsoids. The confidence ellipsoids are characterized by their axes and volumes, the size of the axes is inversely proportional to the *SNR* of the data whilst the confidence volume is inversely proportional to the third power of the data. The confidence ellipsoids can be used to determine the number of ECDs; superfluous dipoles have large confidence volumes.

9.4 Alternative source analysis procedure

In Chapter 6 the reliability of three popular ICA algorithms was assessed; this included the ICA algorithm used in *Curry* to remove the signal artifacts in the pre-processing step -*FastICA*. The principal conclusion in that chapter was *TDSEP-ICA* is better to recover the AEP and to remove the CI artifact than *FastICA* and *Ext-Infomax*. In this section, the source analysis of the AEPs of children with CIs using *TDSEP*-ICA and the algorithm implemented in *Curry* to remove artifact was compared.

Figure 9.4 shows a block diagram of the principal steps of the *Curry* procedure for source analysis of EPs. In order to assess the effect of using *TDSEP-ICA* instead of *FastICA* in the source analysis of AEP generators, the next procedure was followed in order to generate two sets of signals (*de-noised* and *original signals*). Using *TDSEP-ICA* the ICs associated with artifacts were identified, the columns of the mixing matrix corresponding to those components were made zero to generate the so-called *de-noised signal*; for this signal the artifact removal step of *Curry* was omitted. In the so-called *original signal*, each one of the steps of *Curry* was followed (see Figure 9.4). In the pre-processing step of *Curry* the ICs related to artifact were removed from the *original signals*, whilst all the ICs with *SNR*>1 were left in the *de-noised signal*. With both *original* and *de-noised signals* the generators of AEPs, normal hearing children and children with CIs, were calculated using the rest of the steps of the *Curry* procedure.

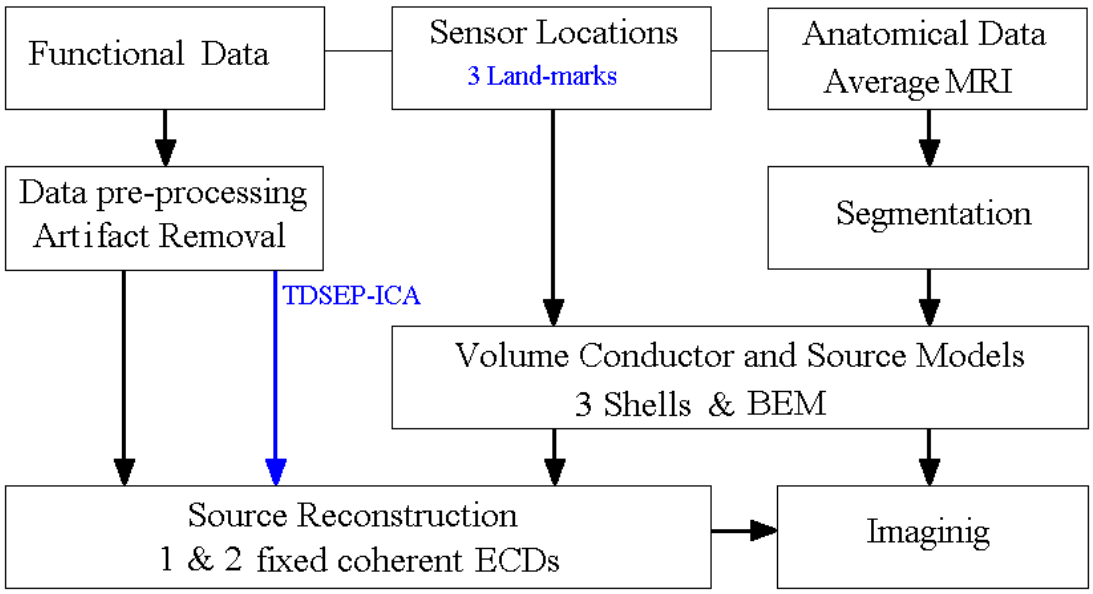

Figure 9.4 Outline of the *Curry* procedure for source analysis of EPs. The alternative method proposed in this research adds a step in the data pre-processing step where *TDSEP-ICA* was used to remove the CI artifact, instead of the ICA algorithm implemented by default in this software.

Two volume conductor models were used and compared in this research; the characteristics for each one are as follow:

a) Three concentric spherical head model. The conductivities of the three shells volume conductor head models were 0.33, 0.0042 and 0.33 [Ω^{-1}/m] brain, skull and scalp respectively [100].

b) BEM head model (average head model). It consists of three surfaces (skin 10 mm, outer skull 9 mm, and inner skull 7 mm) with 2710, 2578, and 3196 overall. The skin, skull, and brain comportments are triangulated using a mean triangle side length of 9 mm, 6.8 mm, and 5.1 mm; resulting in 1357, 1291 and 1600 nodes respectively [47;48].

Fixed coherent (i.e., only the strength of the dipole varies) sources were fitted in a window of approximately 10 ms before and after the AEP P_1 peak, which was identified using the MGFP. Three land-marks digitized at the moment of the test for each one of the subject were included in the source analysis procedure. The source analysis was carried out for four conditions:

C1: One ECD with a three shell spherical head model

C2: One ECD with a BEM head model

C3: Two symmetric ECDs with a three shells spherical head model

C4: Two symmetric ECDs with a BEM head model

In additional to the MGFP, the ICs related to the AEP in both normal children and children with CIs (see Figures 8.1 and 8.2) were used to identify the P_1 peak in the source analysis procedure.

9.5 Source analysis in normal hearing children and children with CI.

Figure 9.5 shows the ECDs (including their confidence ellipsoids), using the four conditions mentioned in the previous section, of four normal hearing children. ***kc*** is a female 7 y.o. child; condition C4 has the smallest confidence ellipsoid whilst condition C1 has the largest ellipsoids. The location of the ECDs is better using two dipoles and a BEM head model (less *Res. Dev*). In subject ***cc***, female 9 y.o., the location of the ECDs is in the expected brain area when the number of dipoles was increased from one to two and using a BEM head model. However, the confidence ellipsoids are largest in conditions C3 and C4. In subject ***ug***, male 10 y.o., all the conditions have a good dipole location but the increase of the number of dipoles produces larger confidence volumes; something similar happens in subject ***mp***, female 11 y.o.

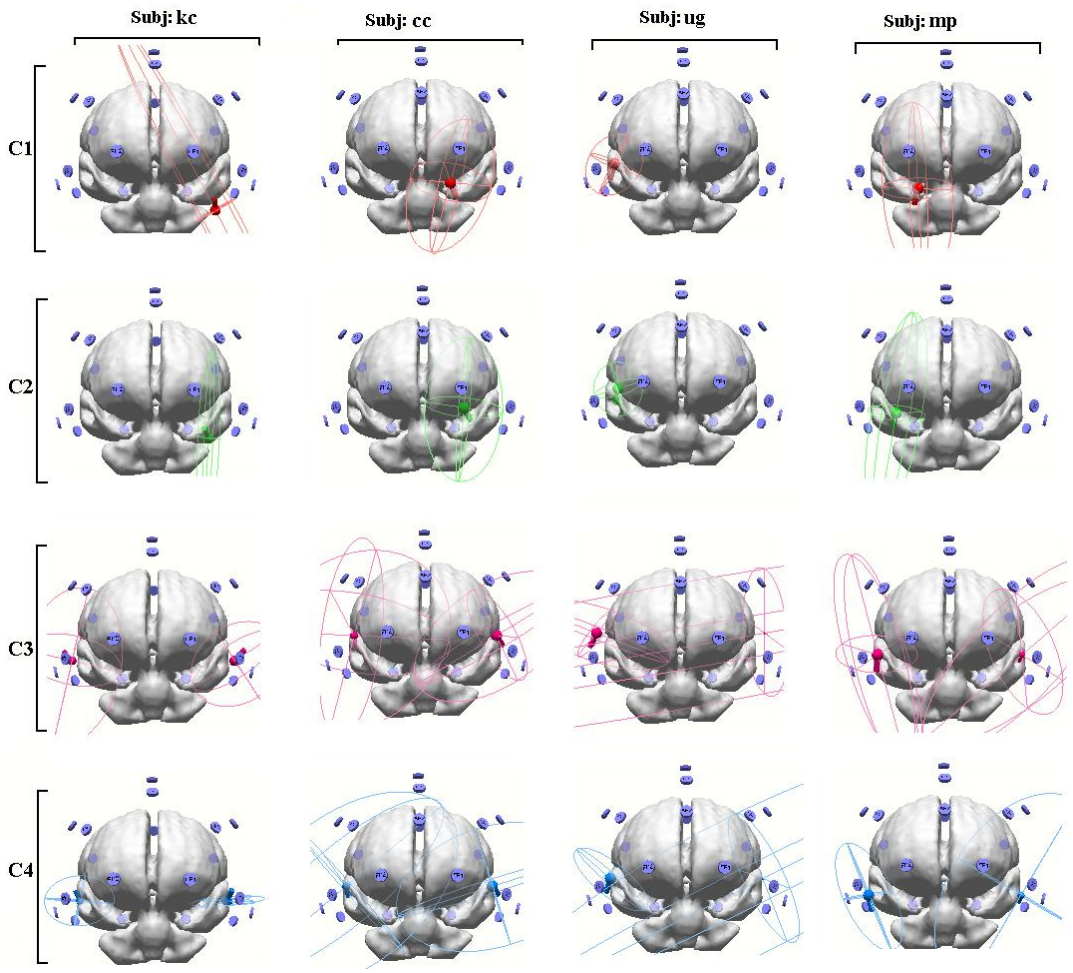

Figure 9.5 Source analyses for the P_1 peak of the AEP from four normal hearing subjects (***kc***, ***cc***, ***ug*** and ***mp***). ECDs were fitted using a fixed coherence model and superimposed onto cortex segmentation from averaged MRI. Every one of the rows corresponds to each one of the conditions used in the source analysis process.

Table 9.2 shows the *Res. Dev.* percentages, location and time of best fit for the ECDs in condition C4 for the four normal hearing children shown in Figure 9.5. The times of best fit of the ECDs for all the normal children were slightly different but close to the expected latency, 100 ms; the location of the dipoles was always in the temporal lobe; middle and superior temporal gyrus, and Brodmann areas 21 and 22.

Table 9.2 *Residual standard deviation*, localization and time of best fit for the ECDs in test condition C4 for four normal hearing children.

Subject	*Res. Dev.* [%]	Location	Brodmann	Time [ms]
kc	13.9	Superior Temp. Gyrus	22	100.5
cc	18.7	Superior Temp. Gyrus	22	97
ug	20.6	Superior Temp. Gyrus	22	104.5
mp	22.7	Middle Temp. Gyrus	21	100.5

Figure 9.6 shows the ECDs of the P_1 peak including their confidence ellipsoids of one subject at different times after implantation. Every one of the rows corresponds to each one of the conditions described in section 9.4. In all the *original signals* (pre-processed using *FastICA*) the confidence ellipsoids were larger than in the *de-noised signal* (pre-processed using *TDSEPICA*) except in conditions C3 and C4 in recording S5-St2, although the fitted dipoles are not in the expected area (temporal lobe). In the *original signals* the anatomical locations of the dipoles were diverse and were not in the expected zone, only in condition C2 in both recordings S5-St1 and S5-St2, the locations were acceptable (inferior and superior temporal gyrus, respectively). The anatomical localizations using the *de-noised signal* were next to or in the temporal lobe and the confidence ellipsoids were the smallest for condition test condition C2.

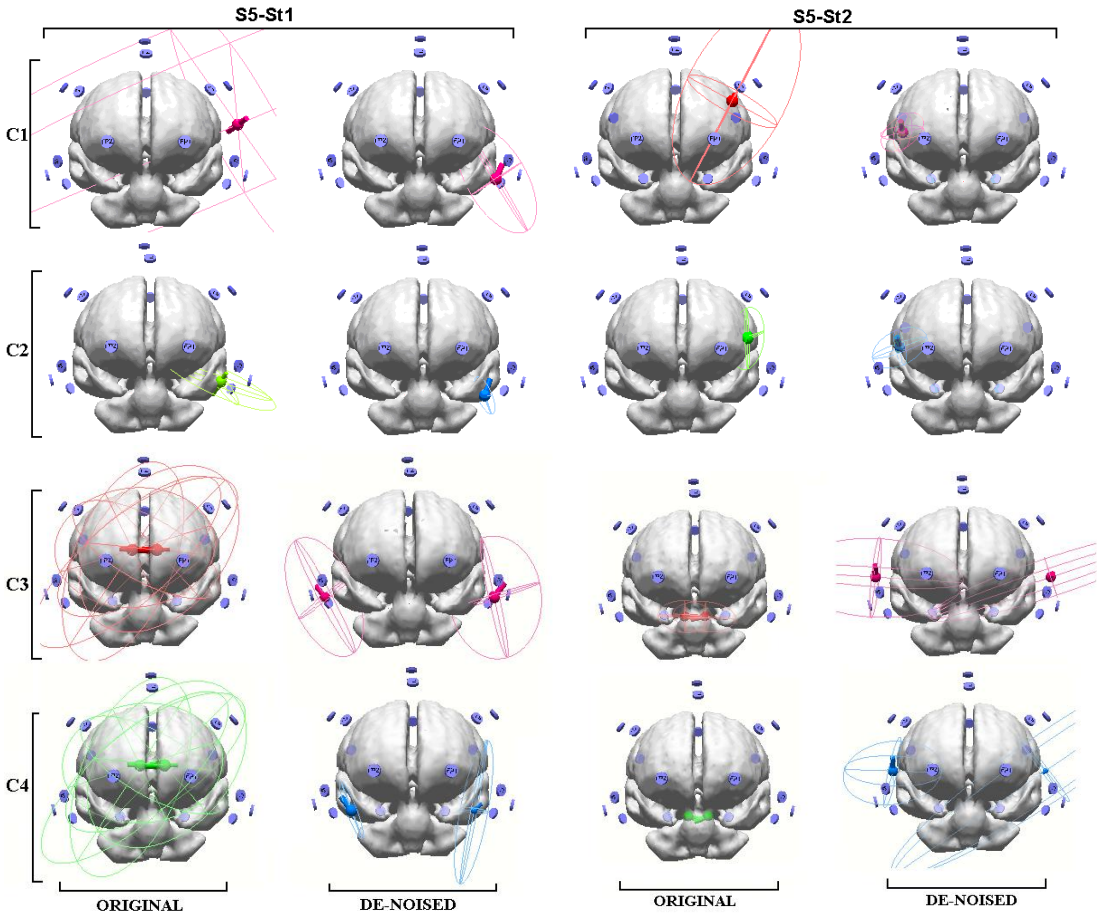

Figure 9.6 Source analyses for the P_1 peak of the AEP from two different recordings (S5-St1, 1y 9m after implantation and S5-St2, 2y 8m post-implant). ECDs were fitted using a fixed coherence model and superimposed onto cortex segmentation from averaged MRI. Every one of the rows corresponds to each one of the conditions used in the source analysis processes; the dipoles obtained with the *original* and *de-noised signals* are shown for comparison.

Res. Dev. dipole fit, of four different recording in the four conditions previously described, between the *original* and *de-noised signal*s are shown in Table 9.3. Lowest *Res. Dev.* was obtained in condition C4 for all the subjects except in one, S5-St3; the *SNR* in this recording is lower than in the rest of the recordings.

Table 9.3 *Res. Dev.* [%] of ECD fit of four different recordings in four conditions of source analysis; C: conditions, O: *original signal* and D: *De-noised signal*.

	S3-St1		S5-St1		S5-St2		S5-St3	
C	O	D	O	D	O	D	O	D
1	44.1	21.4	59.9	36.7	40.3	22.3	61	50.9
2	42	22.5	56.6	40.1	41.3	21.1	54.6	53.5
3	23	15.1	33.6	18.3	38.2	12.9	58.8	46.4
4	25.1	14.9	32.9	16.1	36.0	13.5	40.6	48

In general the confidence ellipsoids, in both normal hearing children and children with CIs, were smaller in the *de-noised* than in the *original signals*. The spatial filtering using *TDSEP-ICA* facilitated both the identification of the AEP P_1 peak in the MGFP as well as the source analysis process. The lowest *Res. Dev.* was obtained in the *de-noised signals* (using 2 symmetric ECDs with a BEM head model). Even though the *Res. Dev.* are not lower than 10% (the percentage recommended by *Curry*), the anatomical location of the dipoles from these signals were in the temporal lobe (superior, transverse, middle and inferior temporal gyrus).

In children with CIs the MGFPs of the *original signals* were dominated by the CI artifact with a maximum peak in the first 50 ms post-stimulus; after removing the ICs related to the CI using *TDSEP-ICA*, the maxima of MGFPs produced by the CI artifact decreased on average by 50%. The reduction of the CI artifact in the *de-noised signals* facilitated the source analysis procedure.

After comparing the four conditions mentioned before, in both normal hearing children and children with cochlear implants, the final parameters for the source analysis of the AEP were: two symmetric fixed coherent dipoles and BEM head models. Sources were fitted in a window of approximately 10 ms before and after the P_1 peak, this peak was identified using both the MGFP and ICs related to the auditory response recovered using *TDSEP-ICA* and shown in Chapter 8, Figure 8.1 and 8.2.

The locations of the fitted dipoles were determined using the Talairach coordinate system and the Brodmann areas included in *Curry*. The position of the electrodes was obtained from three landmarks digitised at the moment of the test and projecting it onto the external surface of the head model (skin). Finally, the ECDs were superimposed onto cortex segmentation (3mm thickness) from average MRI.

Figure 9.7 shows the ECDs locations for the AEP, P_1 peak, from normal hearing children grouped according to age (see Table 3.1). The locations of the dipoles are the superior temporal lobe in all the subjects except in Group 1. In this group, the ECDs are in the inferior temporal gyrus (Brodman area 20), contiguous to Brodmann area 38 (middle temporal gyrus).

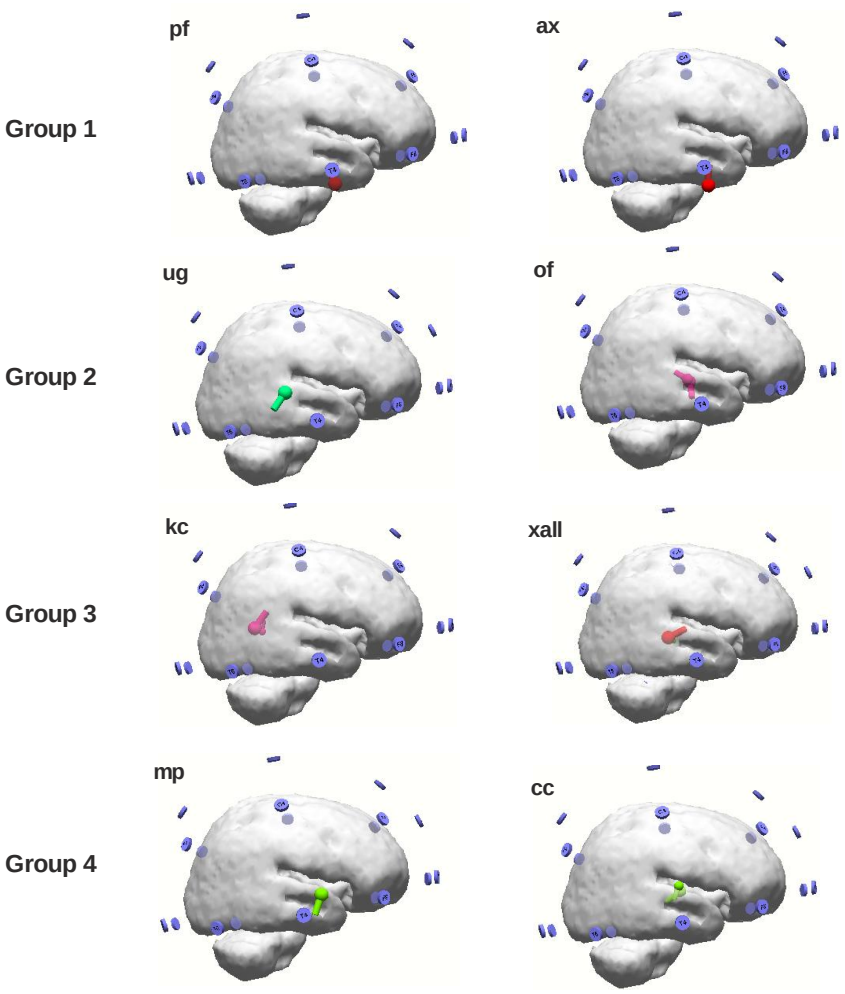

Figure 9.7 ECDs for the P_1 peak of the AEP from normal hearing children grouped in accordance with age. The locations of the dipoles in group 1 are the inferior temporal gyrus and the superior temporal gyrus to Group 2-4. Two symmetric fixed coherent dipoles and BEM head models were used in the source analysis process.

9.6 Source analysis of AEPs for the assessment of CI users

Figure 9.8 shows two symmetric fixed coherent ECDs (the position of the dipoles is fixed and only the strength of the dipole vary) for different subjects at different time after implantation. Sources were fitted in a window of approximately 10 ms before and after the AEP P_1 peak with a BEM head model, a standard 10-20 system was used to project the 19 electrodes position on the scalp surface of the head model. Subject are organized into four group (based on time after implantation); the confidence ellipsoids were not included for a better visualization of the ECDs. The location of the ECDs in the group at one year after implantation was the inferior lobe (Brodmann area 20). In the group between one and two years after implantation the ECDs are located at middle temporal lobe (Brodmann area 38). At 3 year and more

than 5 years post-implantation the locations of the ECDs were the superior temporal lobe (including the Brodmann areas 22, 41 and 42); contra-lateral to the CIs.

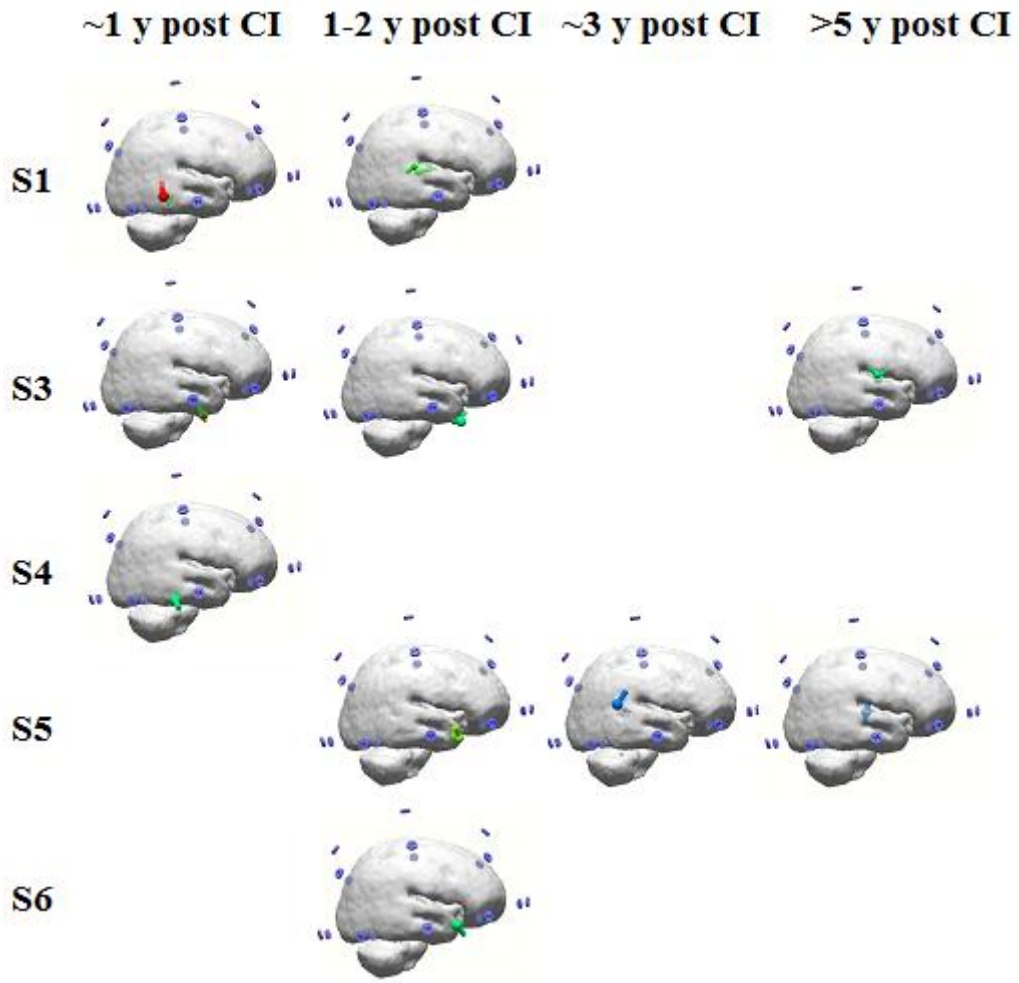

Figure 9.8 Changes in the ECDs locations for the P_1 peak of the AEP from different subjects at different time post-implantation. ECDs were fitted using a fixed coherence model and superimposed onto cortex segmentation from averaged MRI.

Although the AEPs for each child at less than one year after implantation (between 3 and 9 months after implantation) was recorded, it was not possible the find the ECDs of P_1 peak with low residual values and small confidence ellipsoids, in most of the cases; additionally, the anatomical locations of the dipoles were not necessarily in the temporal area.

Figure 9.9 shows the changes in the localization of the P_1 peak of the AEP in accordance with the time of implantation for three different subjects. ECDs were fitted using two symmetric fixed coherence dipoles and superimposed onto cortex segmentation from averaged MRI. The ECDs location changed from inferior or

middle temporal gyrus (Brodmann area 20 and 21) to superior temporal gyrus (Brodmann area 42).

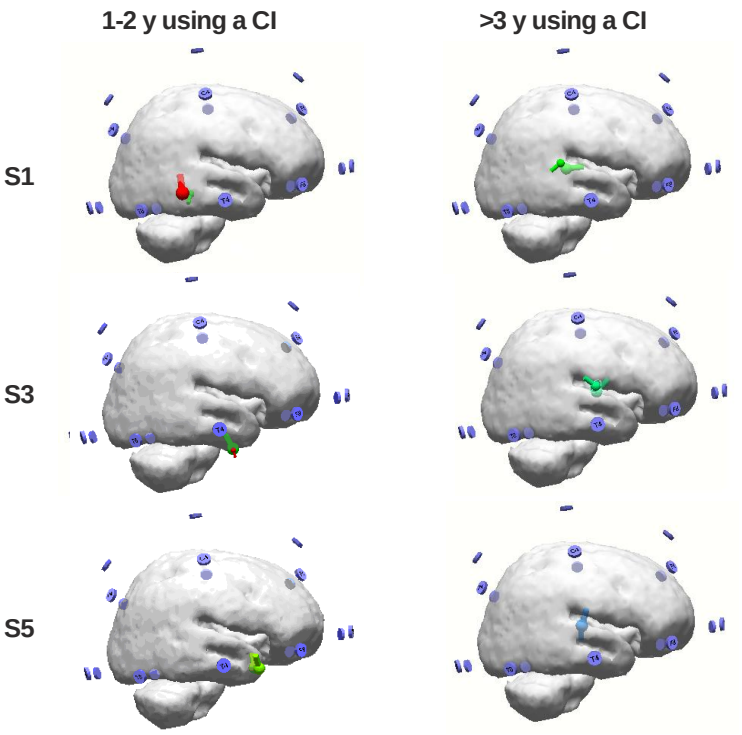

Figure 9.9 Changes in the location of the P_1 peak of the AEP from three subjects in accordance with the time of use of their CIs (between 1 and 2 year and more than 5 year after implantation). ECDs were fitted using two symmetric fixed coherence dipoles and BEM head model.

Figures 9.10 shows the global changes in the localization of the P_1 peak of the AEP in accordance with the time of implantation in subject S3; the ECD location changes from inferior temporal gyrus (Brodmann area 20) to middle temporal gyrus (Brodmann 38) and finally to the superior temporal gyrus (Brodmann area 22).

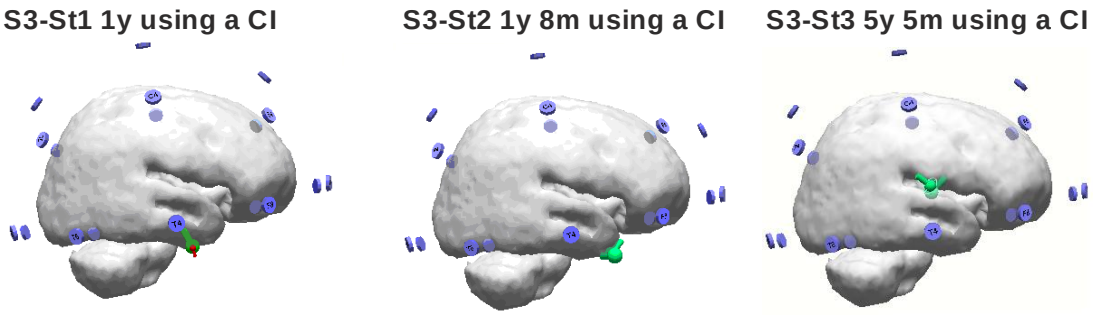

Figure 9.10 Changes in the location of the P_1 peak of the AEP from one subject in accordance with the time of use of his CI. ECDs were fitted using two symmetric fixed coherence dipoles and BEM head model; the ECDs were superimposed onto cortex segmentation from averaged MRI.

Figure 9.11 shows another example of the changes in the location of ECDs in a child after using his implant for more than 5 years. In this case, the position of the dipoles changed from the middle temporal to the superior temporal gyrus at 2 y and 8 m after implantation. At 5 years 1 month after implantation the position of the dipoles remains in the superior temporal gyrus (Brodmann area 41), but closer to the location of normal hearing children (see Figure 9.7)

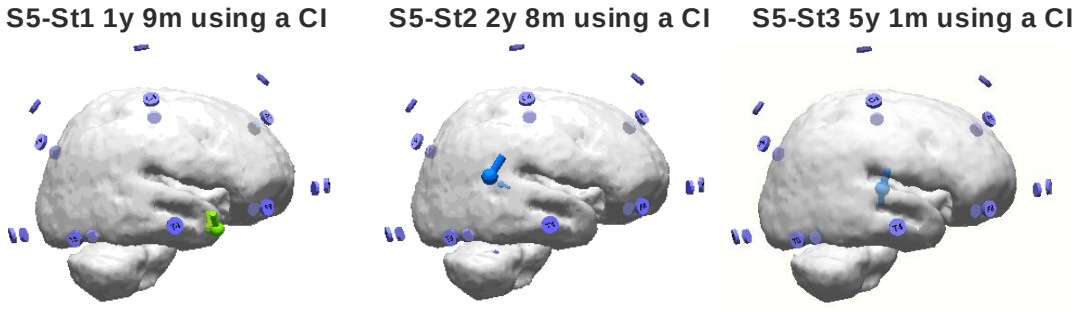

Figure 9.11 Changes in the ECDs location in accordance with the time of implantation, for subject S5. After 2y 8m after implantation, the positions of the fixed coherent dipoles are in the superior temporal gyrus.

In both normal hearing children and children with CIs, the BEM head model gets better localization (as expected because this head model best fit the temporal lobes and the base of the head), but not necessarily smaller ellipsoids according to the number of ECDs, this could be because of the low number of electrodes used in this dataset.

The lowest *Res. Dev.* value obtained in the *de-noised signals* is 13.4% for condition C4; even though the *Res. Dev.* is no lower than 10%, the anatomical location of these dipoles for the *de-noised signal* were in the temporal lobe (superior, middle and inferior temporal gyrus). One way to increase the accuracy of the source analysis is by increasing the number of electrodes, however increasing the number of electrodes increases the test time and the complexity of the analysis.

9.7 Summary

In this chapter the basic theory of source analysis and the parameters used in a commercial software package to determine the electrical activity in the brain, were included. The differences in the source analysis accuracy of the P_1 peak between a

temporal ICA (*TDSEP-ICA*) algorithm and a statistically based algorithm (*FastICA* – default ICA algorithm implemented in *Curry*) used for spatial filtering of EEG from children with CIs and normal hearing children are shown. The results of the ECDs of the P_1 peak for both normal hearing children and children with CIs were shown; in general source analysis was simplest after removing the CI artifact using *TDSEP-ICA* –as expected.

Moreover, the changes of the location of the dipoles in children with CIs, in accordance to the time of use of their implants, are shown at the end of this chapter. In the first period after implantation, the locations of the ECDs are principally in the inferior temporal lobe (Brodmann area 20); between 1 and 2 years after implantation the sources are located at the middle temporal gyrus (Brodmann area 21 and 38). From 3 year and more than 5 year after implantation the position is the superior temporal lobe (Brodmann areas 22, 41 and 42).

The number of electrodes used in these recordings is limited (19 electrodes plus 2 reference electrodes and 1 ground); the electrodes resolution does not permit us to determine in detail the changes in the tonotopy of the auditory cortex at different stimuli frequencies, but this was not the fundamental aim of this research [88]. The purpose is to determine the global changes in the ECD localization, in accordance with the time of implantation in order to implement an objective procedure to follow the maturation of the auditory system in those children that can be put into clinical practice.

Chapter 10.

Conclusions and future work

Since CI began to be used as an alternative procedure in rehabilitation of deaf people, it has been a challenge to understand how the brain processes the new information supplied by the CI. One question that needs to be answered is how the auditory system of CI subject matures in accordance with the time of use of the CI. Some authors have proposed to explain the central auditory system maturation, using multi-electrodes recordings of AEPs. Deaf children who have been deprived of sound for a period of time and then have been implanted make it possible to determine the effects of that deprivation on the maturation of the central auditory system, and, in general, children with CI present delayed auditory responses compared to normal hearing children of the same age.

Authors, who have researched the auditory system maturation in adult subjects with CIs following the development of AEP, reported the presence of a negative wave around 100 ms, N_1, after cochlear implantation. Instead of this peak observed since adolescence, the AEP for both normal hearing children and children with CI is dominated by a positive peak, P_1, around 100 ms; this peak could be delayed in children with CI, depending of diverse factors, for example the age of implantation. The latency of the P_1 wave of AEPs has been used as a biomarker of the development and plasticity of the central auditory system in children with a HA and/or CI receiver.

Some authors have used multi-channel AEP recordings to study the maturation of the auditory system; however, the amplitude and latency of the peaks of the potential change electrode-by-electrode, i.e change according to location. The analysis of brain (spatial) maps may be suitable in a longitudinal study; however in a transversal study it could be inappropriate because brain map patterns might be variables from subject to subject. Because of this some authors have chosen source

analysis, which includes the AEP information of all electrode localization, to describe the central auditory system maturation.

With all these arguments in mind, the objective of this research was to describe the auditory system maturation of children with CI, tracing the development of the components of the AEP by ICA and source analysis. However, there is an inconvenience when the AEP has been recording from CI patients, in the presence of the artifact associated with the stimulus; this artifact usually covers the AEP partially or totally. Because of this the first part of this research was to review the state-of-the-art in ICA and to evaluate the applicability of this technique to detect and to isolate the AEP and the CI artifact from ongoing multi-channel EEG in children with CI receivers. Three algorithms were tested and compared (*FastICA*, *Infomax* and *TDSEP-ICA*). The most adequate ICA algorithm, as well as its parameters, for this type of biomedical signal analysis in this research was identified. IC selection is a problem when ICA is applied to real data, so a new procedure to differentiate ICs with physiological and physical meaning, through MI and cluster analysis was implemented here. Although promising results were obtained with this procedure, it is necessary to include an assessment of the cluster formation as well as the criteria to determine the number of clusters in each subject before it can be used formally.

The maturation of the auditory system in children with CIs was evaluated using the modification of the topographic maps of the ICs related to the AEP, since the latencies of these ICs were variable; the data of implanted children were analysed in sub-groups based on time of implantation. After removing the CI artifact, it was possible to begin the localisation of the generators of the P_1 peak of the AEP. This was done using and average MRIs provided in commercial software for 3-D source localization and standard coordinates of the electrode position. It was necessary to decide both source type and spherical head model; also the expediency of using a realistic model. This research provides a basis for a practical, clinical procedure to assess the benefits of a CI following the changes of the modelled ECDs of the AEPs attributed to the length of time of use/implantation of the CI on the child.

Conclusions

In this research an important innovation in the analysis of brain signals through ICA of CI users was presented. ICA shows promise as a means of isolating AEPs in ongoing multi-channel EEG recordings contaminated by a CI artifact.

Although ICA is a statistical technique which requires sufficient data points to reliably calculate estimations, satisfactory results were obtained reducing the number of epochs from 150 to just 50 EEG epochs; the results obtained using only 50 epochs show that it is possible to reduce the time of the recording to one third of the original EEG recording time and still get superior results. This is particularly useful since it is hard to obtain good results from children over long experimental sessions without sedation. A short-time test, without participation of the subjects and low complexity off-line analysis is feasible to implement in routine audiological practice; the test would be particularly useful in young implanted children.

The *SIR* index was used to asses the variability of the estimations of three ICA algorithms, *FastICA*, *Infomax*, and *TDSEP-ICA*. Although *FastICA* and *Infomax* are maybe the most popular ICA algorithms used to reduce the artifact of the AEPs, the algorithm that is the least variable and that best estimates *both* the AEP and the CI artifact is *TDSEP-ICA*; *FastICA* and *Infomax* correctly identify the AEPs in normal hearing children recordings, but has problems when estimating the auditory response from children with CIs, especially when the artifact is extended onto most of the recording electrodes; this is especially useful to detect the presence of the auditory response in the electrodes around the CI (temporal area). All the algorithms estimate the CI artifact, although only *TDSEP-ICA* recovers it in a one-dimensional subspace; making identification easier. This demonstrates that this algorithm in recovers the most robust and efficient estimations of the AEPs; this is to be expected over shorter window sizes and for a technique that makes use of the inherent information available in the time-series itself. This condition better situates *TDSEP-ICA* as an algorithm for the implementation of an objective method for selection of ICs.

A procedure for the objective selection of the ICs associated with the AEPs and with the CI artifact was also introduced and implemented in this work; this

procedure uses the concept of MI, cluster analysis and the pseudo-random reduction of the number of recording electrode. The procedure proposed in this research identifies principally 3 robust clusters related to the AEPs, the CI artifact and noise. However, although the hierarchical clustering of the estimations is correct visually, it is still necessary to include an assessment of the cluster formation as well as the criteria to determine the correct number of clusters in accordance with the reduction of electrodes proposed in the procedure.

Due to the fact this method needs to be subjectively calibrated for each recording, it was decided not to use this for the source analysis of AEPs for the assessment of CI users; the main reason being that the possible differences in the method due to the subjectivity could modify the real expected variability in the source analysis for CI maturation and lead to erroneous conclusions being made. However, this part of the research was useful in order to obtain experience to identify first the ICs related to the auditory responses which were used to evaluate the maturation of children with CIs and the ICs associated with different artifacts which were subsequently removed from the recordings before the source analysis based on the P_1 peak in the AEPs.

Using the optimal parameters selected to *TDSEP-ICA* and applying this algorithm on the original number of electrodes, the relevant ICs in each recording from children with CIs were identify using the morphology and topographic maps (spatial projection) of the ICs. The latencies of the P_1 peak of the ICs recovered by *TDSEP-ICA* and related to the AEPs among subjects are diverse and it was not possible to identify the complex P_1-N_1 in all the subjects; in general the latency of this peak is shorter as a function of the use of the CI –although it is difficult to draw any conclusion on the auditory system maturation of these children using just this parameter. However, using the spatial projection of the ICs associated with the AEP (which provides a global representation of the response to the auditory stimulus at the scalp), it is possible to conclude the following about the auditory system maturation of children with CIs:

- The spatial projections of the AEPs' ICs come into being spread out around the head with no focus in any specific area, although predominantly parietal when the children have used their CIs for less than one year.
- At a year after implantation the spatial projections are characterized by a central to fronto-central distribution.
- Finally, the spatial projections of the ICs have a distribution front to fronto-central, contra-lateral to the CI implantation, after more than two years post-implantation; the spatial projections of the ICs related to the AEPs show similarities with normal hearing children's spatial projections, which could be used for an objective assessment of the maturation of the auditory system in children with CIs. This procedure could be performed routinely every few months, for instance after fitting the current levels of CI, to assess the benefits of this adjustment. Changes in the spatial projections could be correlated with the results obtained in other audiological tests such as the level of comprehension and production of speech in determining the overall performance of children implanted.

After removing the CI artifact, it was possible to begin the localisation of the generators of the P_1 peak in the AEPs; using fixed coherent ECDs and BEM head models implemented in commercial software (*Curry*, by *NeuroScan*). Spatial filtering, using *TDSEP-ICA* in the pre-processing step of source analysis, results in better ECD fits than when using *FastICA*, implemented in this software package. The alternative method for source analysis proposed in this research, facilitates the identification of the P_1 peak and the source analysis procedure.

At the moment, only 19 electrodes have been used (as the data was collected using a standard clinical paradigm) which does not have the highest accuracy in the source analysis, but it is enough for the proposes of this research as a proof-of-principle; one way to increase the accuracy of the source analysis is by increasing the number of electrodes, however increasing the number of electrodes increases the test time and the complexity of the analysis. It is important highlight that although the number of electrodes is higher the source analysis problem will still be ill-posed and will not give 100% accuracy. An alternative solution to increase the accuracy could

be to constrain the localization to a specific area (e.g. the temporal lobe) and to use the real position of the electrodes that were digitally acquired at test time.

The effect of using the position of the electrodes and the MRI for each patient in the source analysis of the AEP P_1 peak should be assessed in a further research. The coordinate axis used in the source analysis procedure is calculated in the MRI, using three or four anatomical landmarks and the electrode position information; the head coordinates have to be scaled to fit into the MRI coordinate system [90]. Realistic head model from the MRI of each subject as well as the location of every electrode on the scalp at the moment of the EEG recording could increase the precision of the coordinate axis calculation as well as the accuracy of the source analysis solution.

It is shown that it is plausible to follow the maturation of the auditory system in children with CIs using the location of the dipoles and the time of best ECD fit (this parameter is less variable inter-subject than the strength of the ECD); in general the position of the dipoles changed from the inferior temporal gyrus (Broadmann area 20), to the superior temporal gyrus (Brodmann area 41 and 42), in accordance with the time of use of the CIs; close to the normal hearing children location. The results of this research could be used as an objective technique for a general assessment of the performance of children with CIs. The maturation of the auditory system of these children could be evaluated using both the changes in the topographic maps of the ICs related with the AEP and the changes in the location of the ECD of the P_1 peak. A procedure to evaluate the fitting of CIs in young children could be derived from this research by observing the changes of the topographic maps in accordance with changes in the CI levels of current. Since the analysis of the database used in this research through *TDSEP-ICA* allowed the identification of ICs associated not only with the AEP and the CI artifact but also with noise generated by the implant, this procedure could be also extended to detect technical problems of the implants.

Future work

Currently, both ICA and source analysis have been completed in data for a stimulus of 1000 Hz and 70 dB_{HL}; future work would compare the results of these

techniques over different frequency tones and intensity levels. Some modifications of the current protocol could be pertinent, for example to reduce the sample rate of the EEG, to increase the number of electrodes to 32 or 64 but reducing the number of epochs recorded, since it was possible to obtain robust ICs related to the AEPs and the CI artifact with only 50 trials.

As mentioned before, in order to increase the accuracy of the source analysis, it is important to include the digitization position of the electrodes at the moment of the recording as well as the MRI for each one of the subjects. Source analysis solution requires the co-registration of functional with anatomical data; this co-registration is perform by the rotation, translation and scaling of three or four landmarks digitised in the EEG and/or MEG coordinate system [38]. The typical landmarks used are the nasion and the two pre-auricular notches; using those points a coordinate system whose origin is the centre of the head is defined [32].

Using stimuli centred at the frequency bands of the CIs, it could be feasible to establish the changes of the ECD locations in accordance with these stimuli frequencies, in order to develop a procedure to objectively fit the CIs to children. Additionally, this way of stimulation together with high-resolution EEG recordings could allow tracing the development of the tonotopic organization of the auditory cortex in children with CIs; in adults with CIs this tonotopic organization is similar to the tonotopy of normal hearing subjects [54]. Extending the type and complexity of stimuli (syllables, words and even sentences) to evaluate *cognitive* processes in children with CIs could be plausible. More over, a procedure to investigate how the brain of CI users proceses speech characteristics as pitch and intonation could be feasible. At this point a comparison between the ECD locations of the P_1 peak and even the N_1 peak and the improvement of language perception and development in children with CIs is necessary to globally evaluate the rehabilitation of these children [53].

Furthermore, it would be useful to establish if it is plausible to follow the maturation of the auditory system in children with CIs using simultaneous EEG and functional MRI (fMRI) and/or MEG-fMRI recordings, by means of the changes of the blood oxygenation level-depend (BOLD) contrast mechanism and the ECDs in

accordance with the time of use of this electronic device. Giraud *et al* [53] review different brain imaging techniques and discuss the viability of these techniques for studies in implant subjects; finally the authors suggest that fMRI is a promising system for examining CI users. Some authors have obtained functional images from CI users (their devices did not have electronics in the internal part of the implants) to study the electrically-evoked brain activity [90].

It is important to identify neuroimaging approaches which can be applied to ultimately improve diagnosis and rehabilitation of deaf people using Cortical Auditory Evoked Potentials; regarding maturation and plasticity of the auditory system and auditory cortex after cochlear implantation.

Appendices

Appendix A. AEP recordings: Normal hearing children and children with CIs

In this appendix the AEP recordings from normal hearing children and children with CIs are shown. Details about the recording parameters are included in Chapter 3. Information about the latency and amplitude of the most prominent peak in the AEPs in each normal hearing subject are included. In the case of children with CIs, information about the latency and amplitude of P_1 peak were included when it was possible to measure it.

Normal hearing children AEP recordings

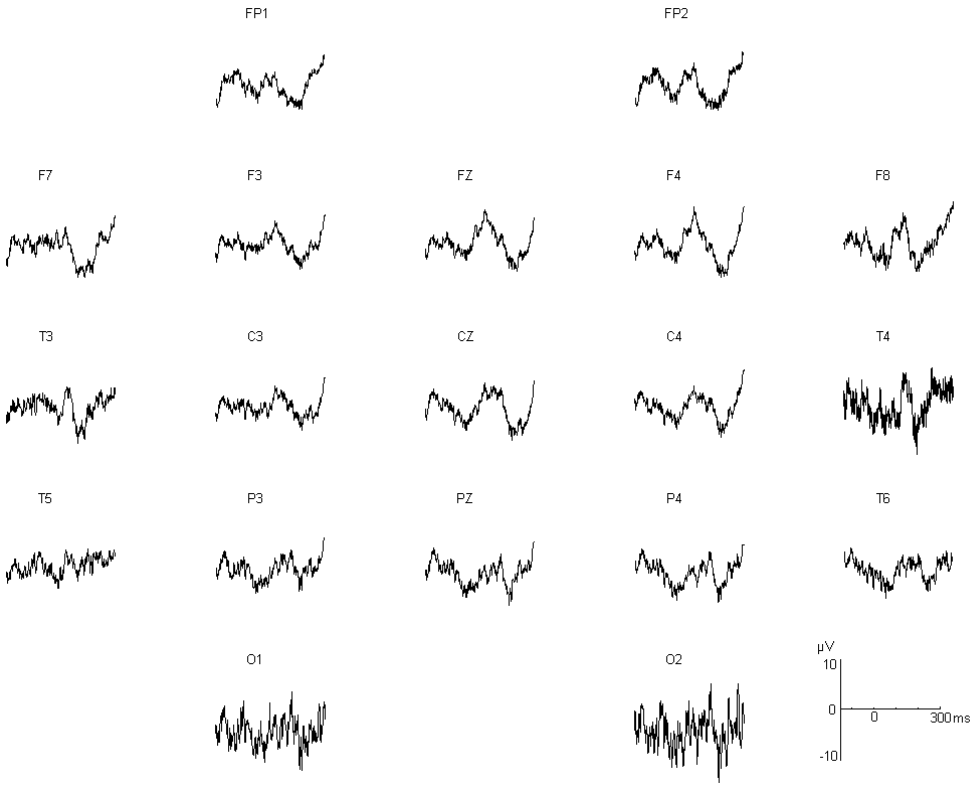

Figure A.1 Subject *ad* (female, 8 y.o) P_1 peak latency and amplitude at Cz electrode, 127.8 ms and 3.221 μV.

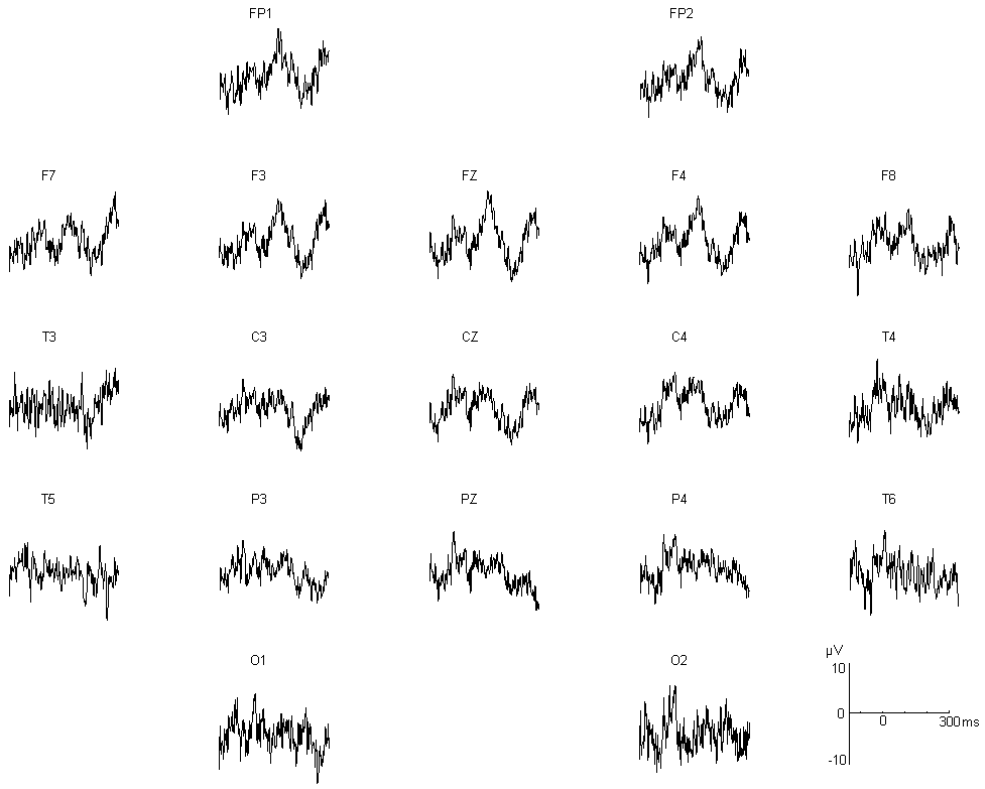

Figure A.2 Subject ***al*** (male, 3 y.o) P_1 peak latency and amplitude at Cz electrode, 102.8 ms and 9.264 μV.

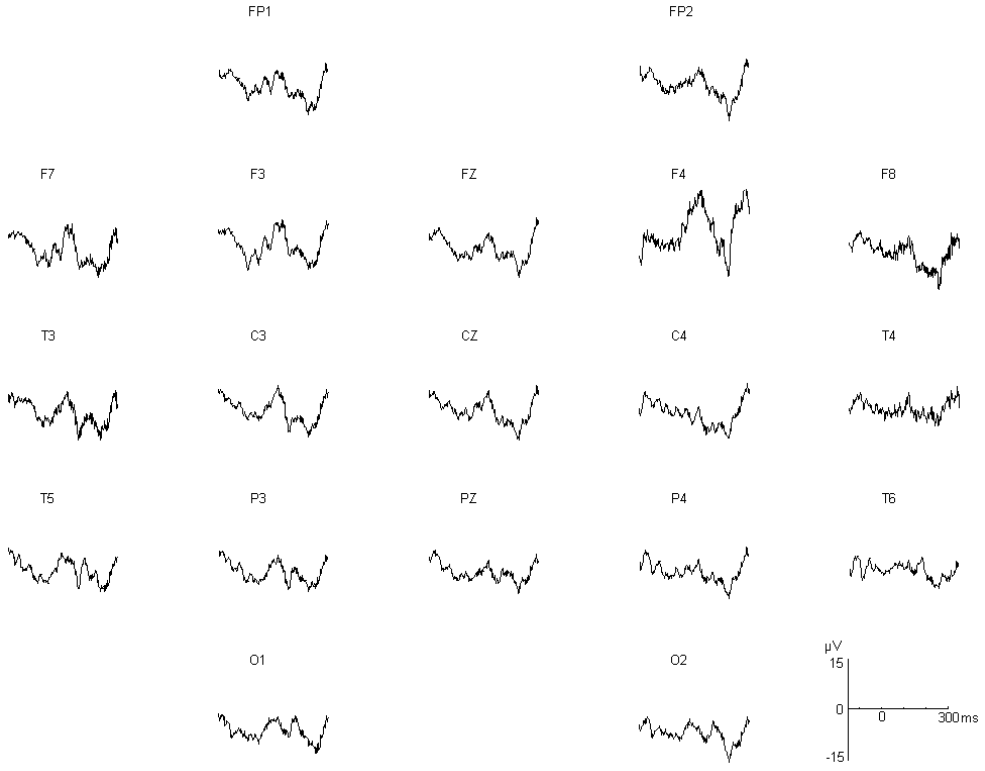

Figure A.3 Subject ***an*** (female, 5 y.o) P_1 peak latency and amplitude at Cz electrode, 95.27 ms and 3.394 μV.

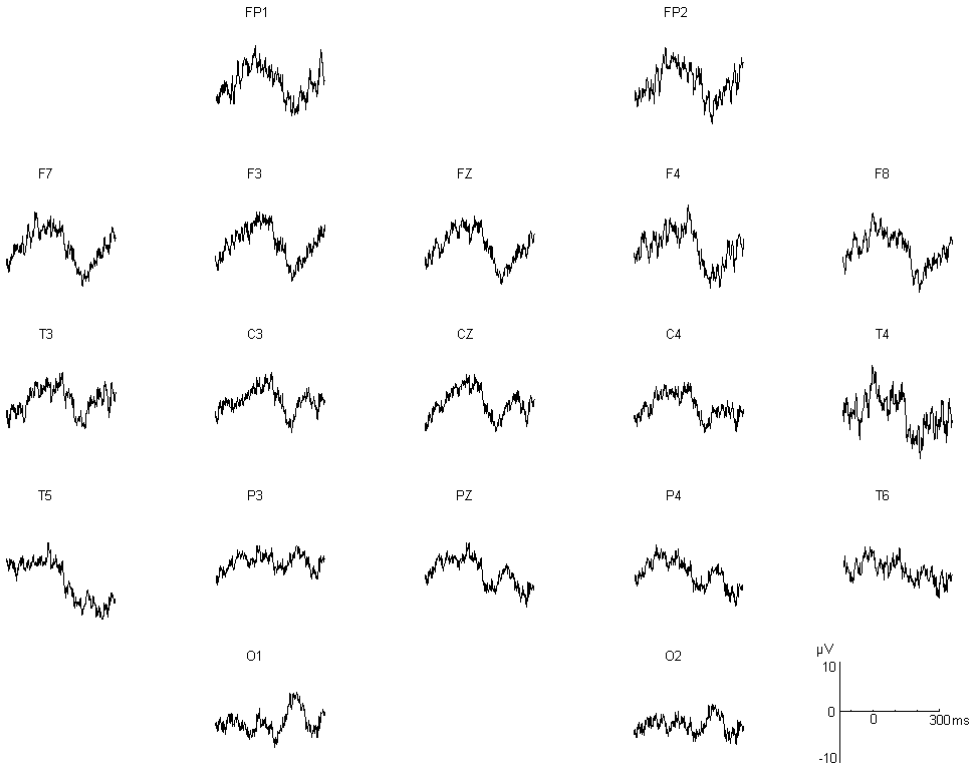

Figure A.4 Subject ***ax*** (male, 4 y.o) P_1 peak latency and amplitude at Cz electrode, 216 ms and 1.708 μV.

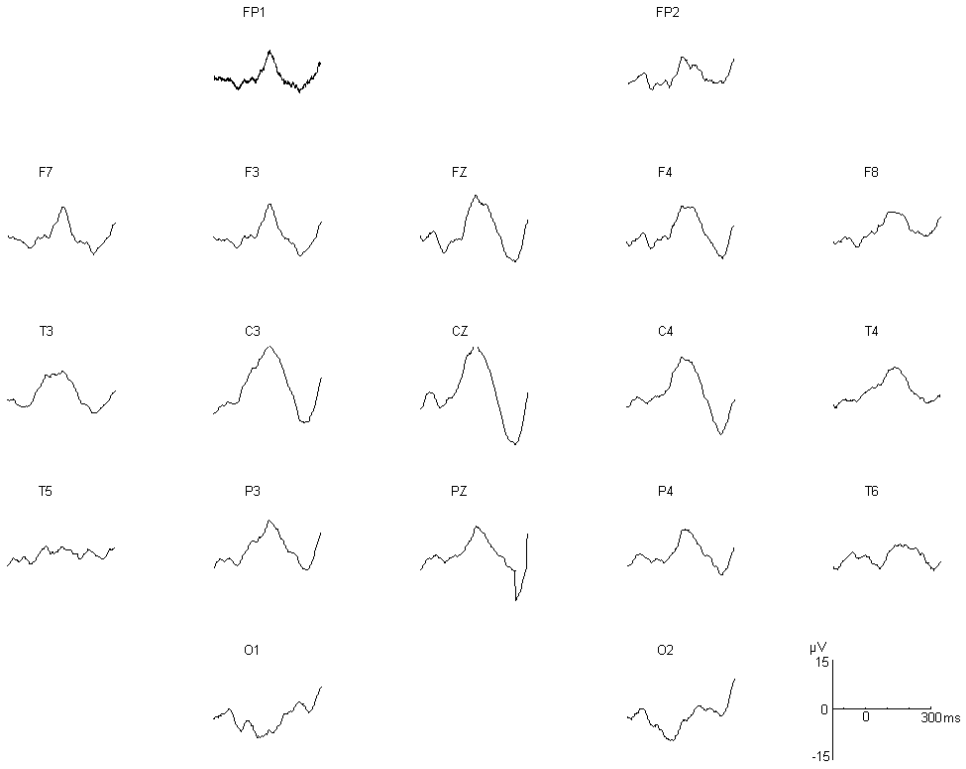

Figure A.5 Subject ***bf*** (female, 6 y.o) P_1 peak latency and amplitude at Cz electrode, 90 ms and 8.26 μV.

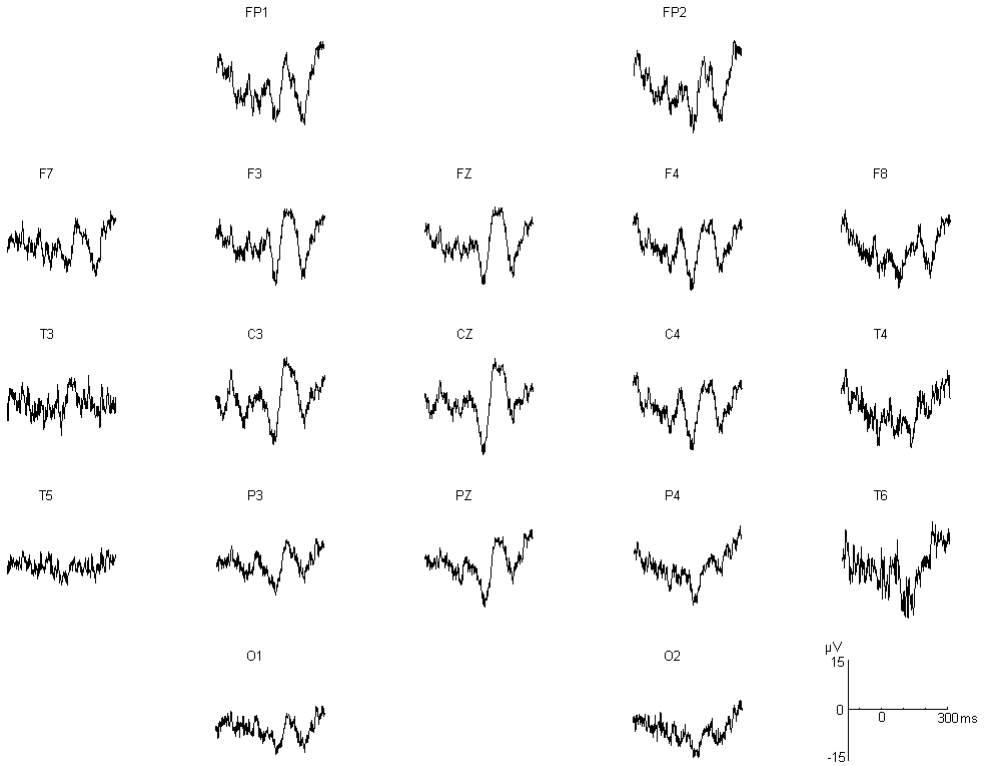

Figure A.6 Subject ***cc*** (female, 11 y.o) N_1 peak latency and amplitude at Cz electrode, 99.28 ms and -7.40 μV.

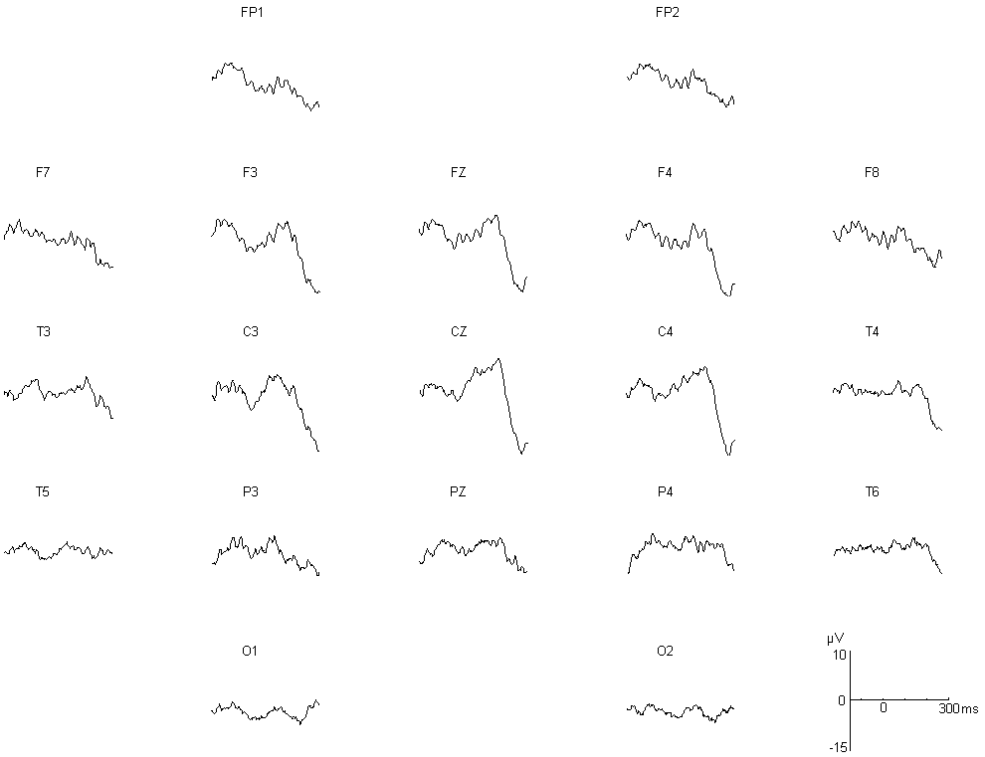

Figure A.7 Subject ***dt*** (female, 3 y.o) P_1 peak latency and amplitude at Cz electrode, 183.4 ms and 7.431 μV.

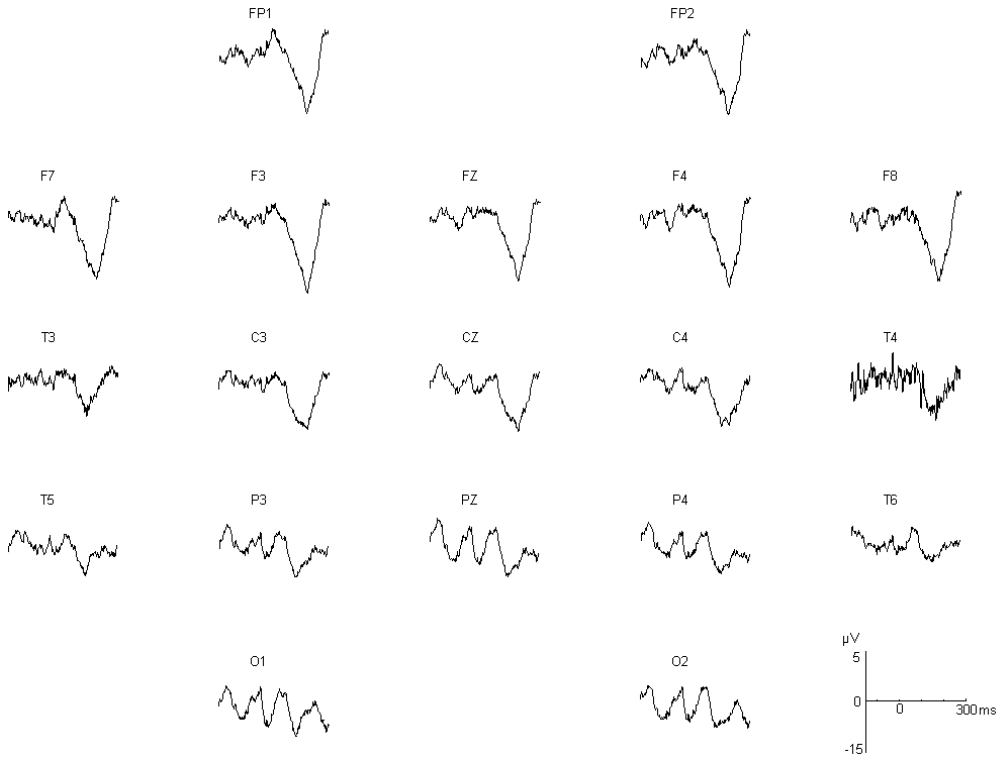

Figure A.8 Subject ***ed*** (male, 6 y.o) P_1 peak latency and amplitude at Cz electrode, 93.27ms and 3.03 μV.

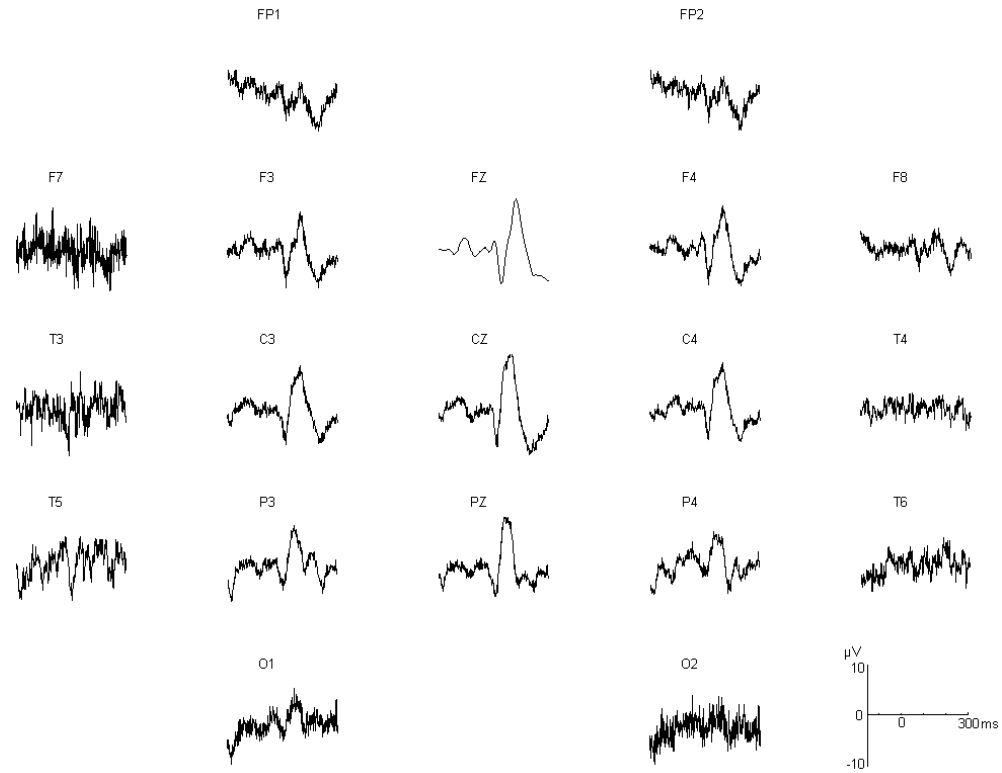

Figure A.9 Subject ***fc*** (female, 14 y.o) N_1 peak latency and latency at Cz electrode, 84.76 ms and -6.36 μV.

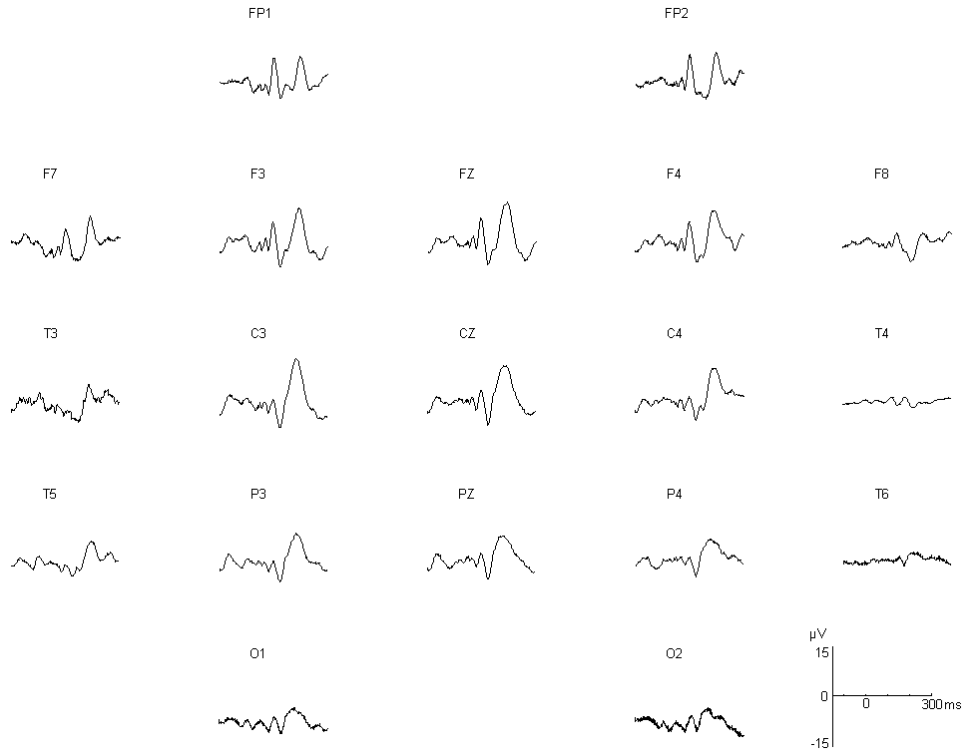

Figure A.10 Subject ***iv*** (male, 8 y.o) N_1 peak latency and latency at Cz electrode, 100.3 ms and 6.295 μV.

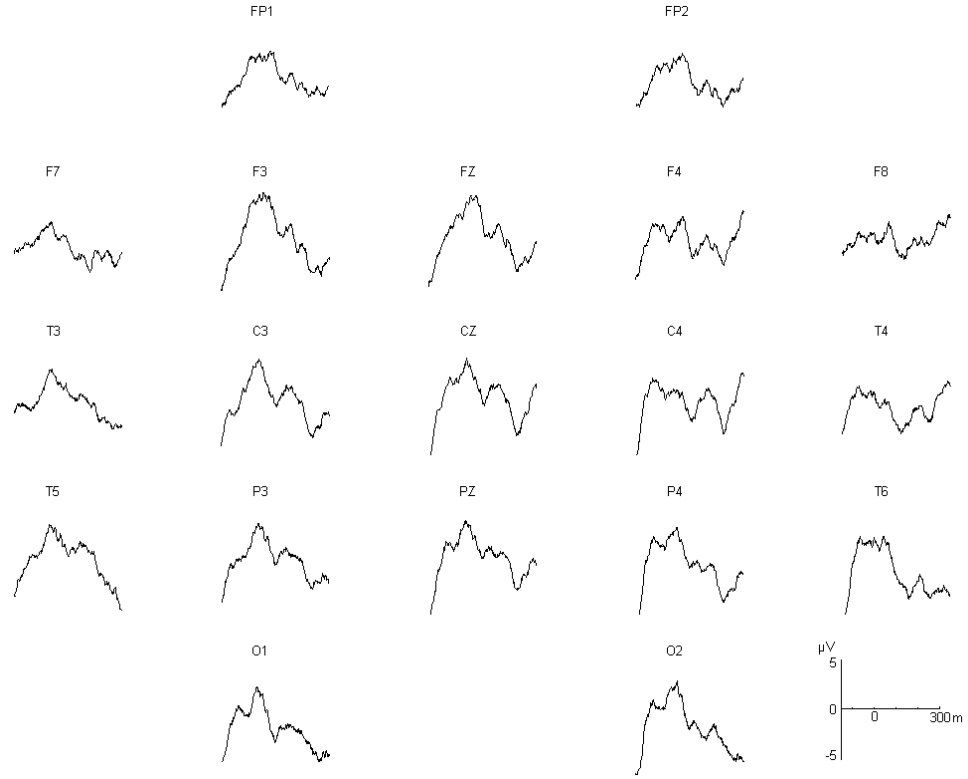

Figure A.11 Subject ***jg*** (male, 5 y.o) P_1 peak latency and amplitude at Cz electrode, 139.3 ms and 1.424 μV.

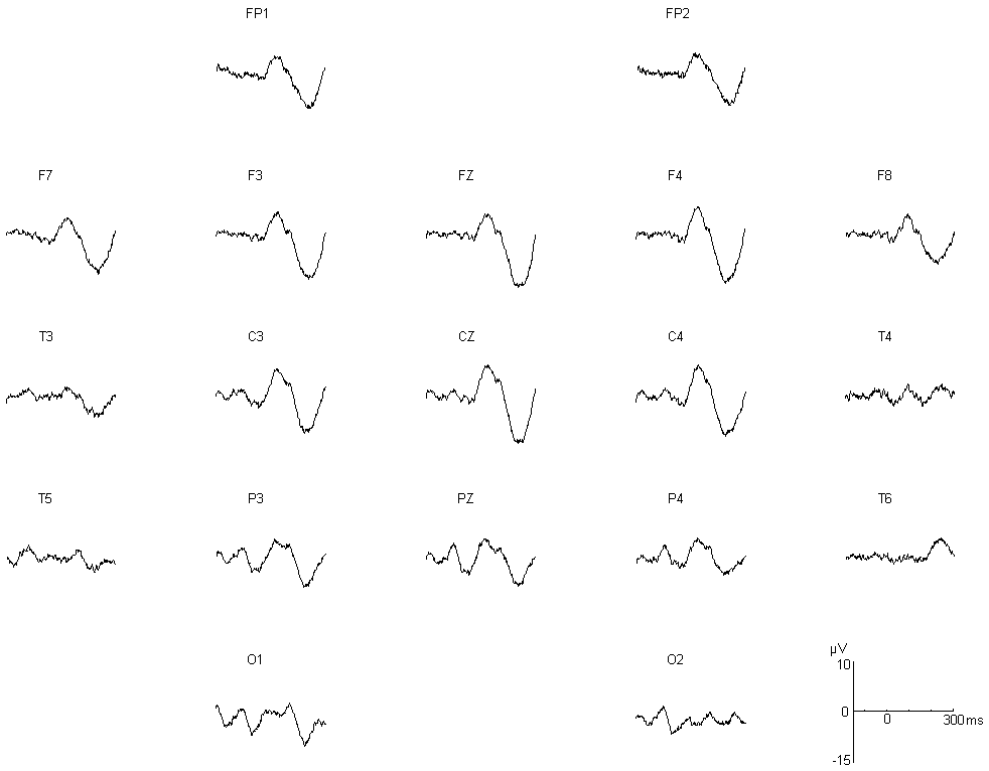

Figure A.12 Subject ***kc*** (female, 7 y.o) P_1 peak latency and amplitude at Cz electrode, 103.3 ms and 6.69 μV.

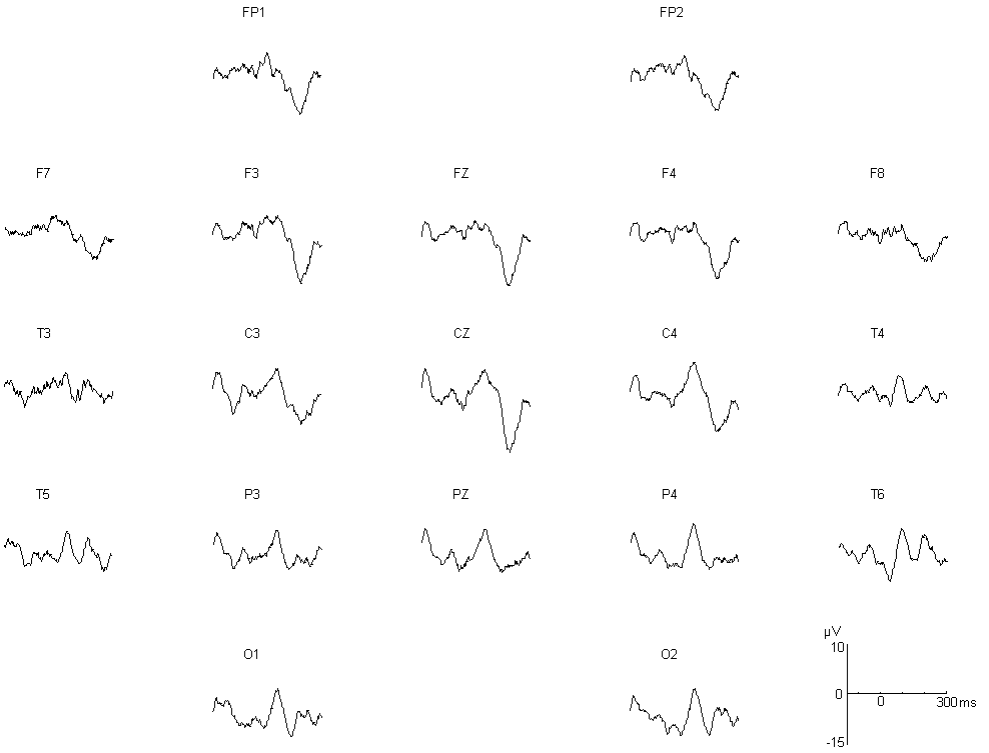

Figure A.13 Subject ***mar2*** (female, 10 y.o) P_1 peak latency and amplitude at Cz electrode, 121.3 ms and 10.46 μV.

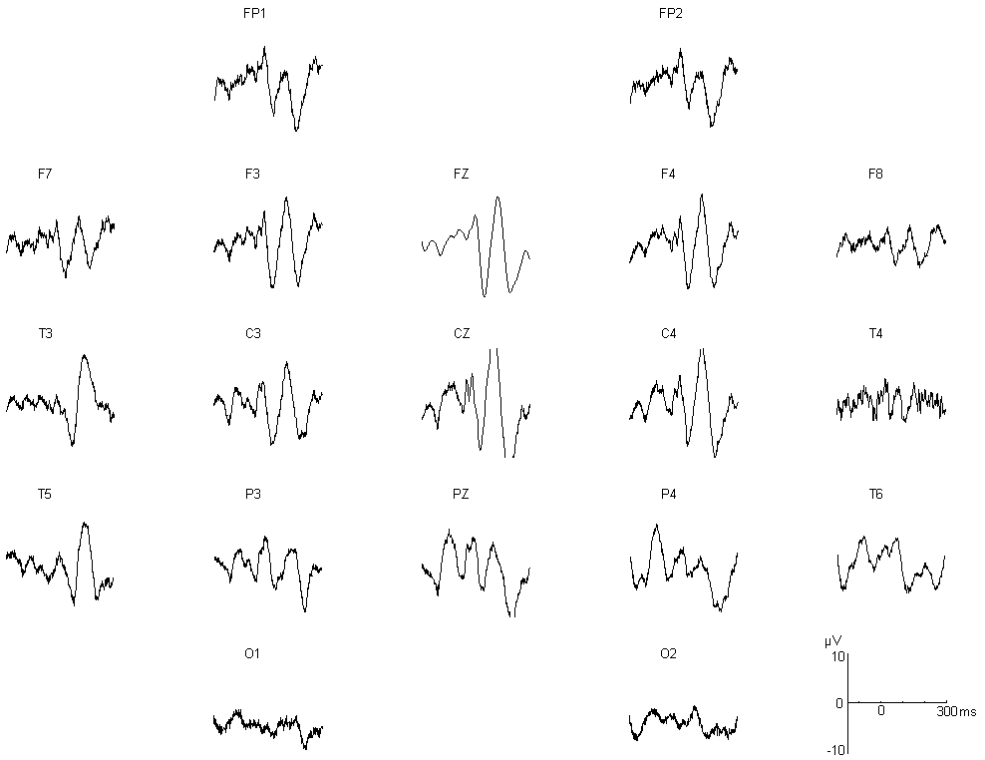

Figure A.14 Subject ***mp*** (female, 11 y.o) P_1 peak latency and amplitude at Cz electrode, 91.27 ms and -7.71 μV.

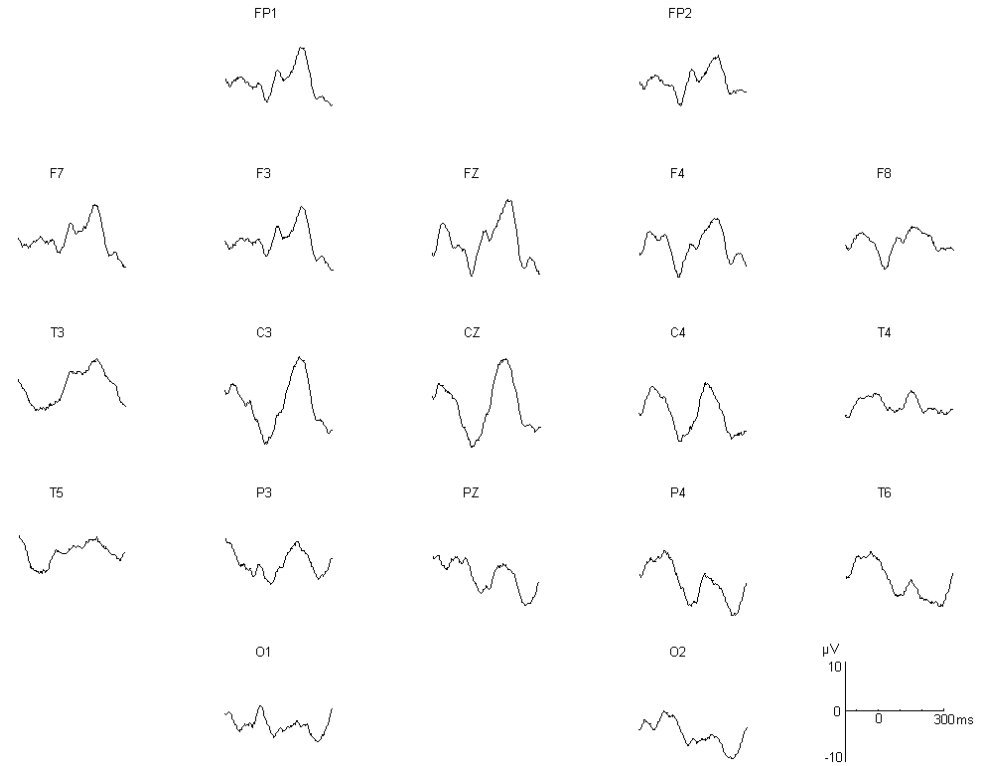

Figure A.15 Subject ***nan*** (female, 6 y.o) P_1 peak latency and amplitude at Cz electrode, 157.8 ms and 11.92 μV.

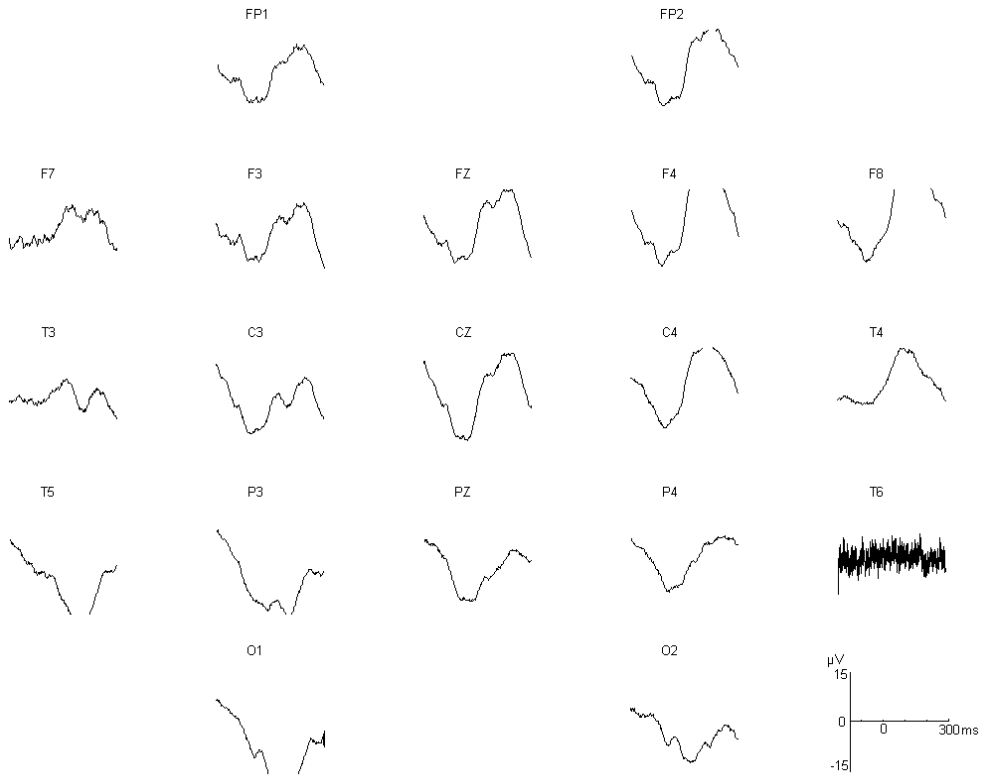

Figure A.16 Subject ***of*** (female, 7 y.o) P_1 peak latency and amplitude at Cz electrode, 178.9 ms and 16.61 μV.

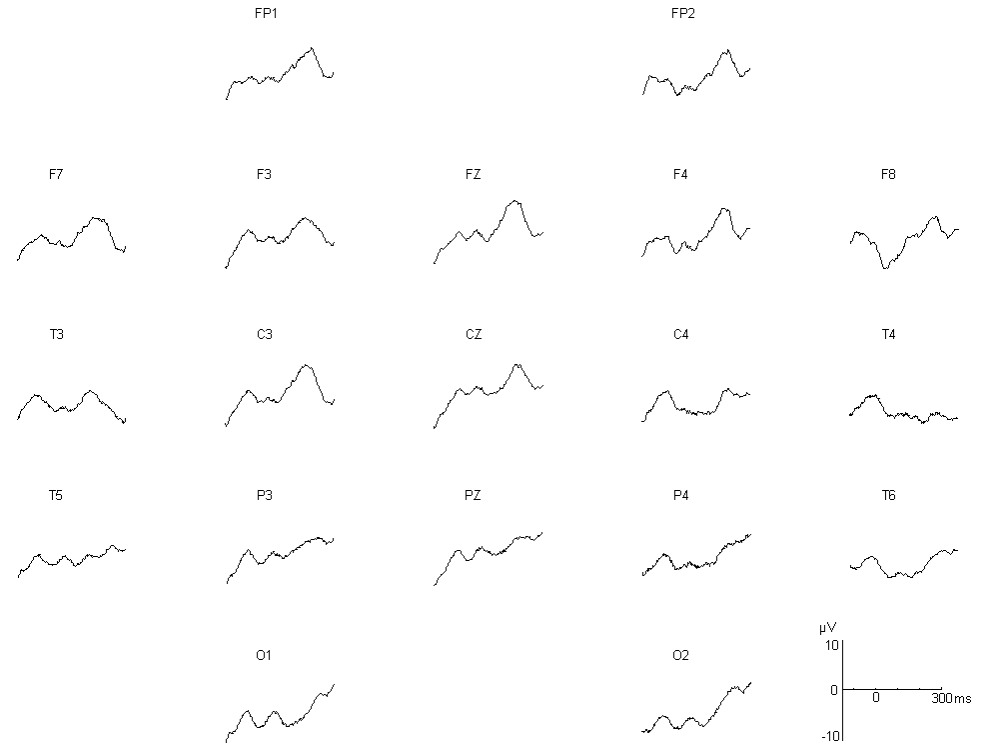

Figure A.17 Subject ***pf*** (female, 4 y.o) P_1 peak latency and amplitude at Cz electrode, 195.4 ms and 10.64 μV.

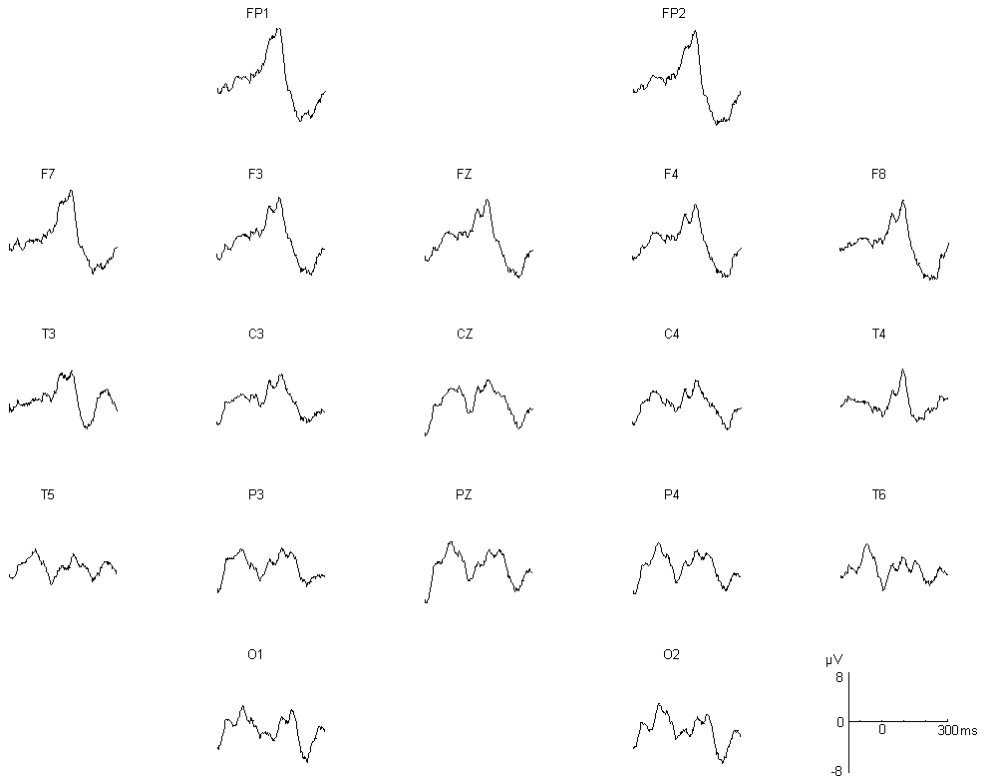

Figure A.18 Subject ***st*** (female, 7 y.o) P_1 peak latency and amplitude at Cz electrode, 111.3 ms and 3.427 µV

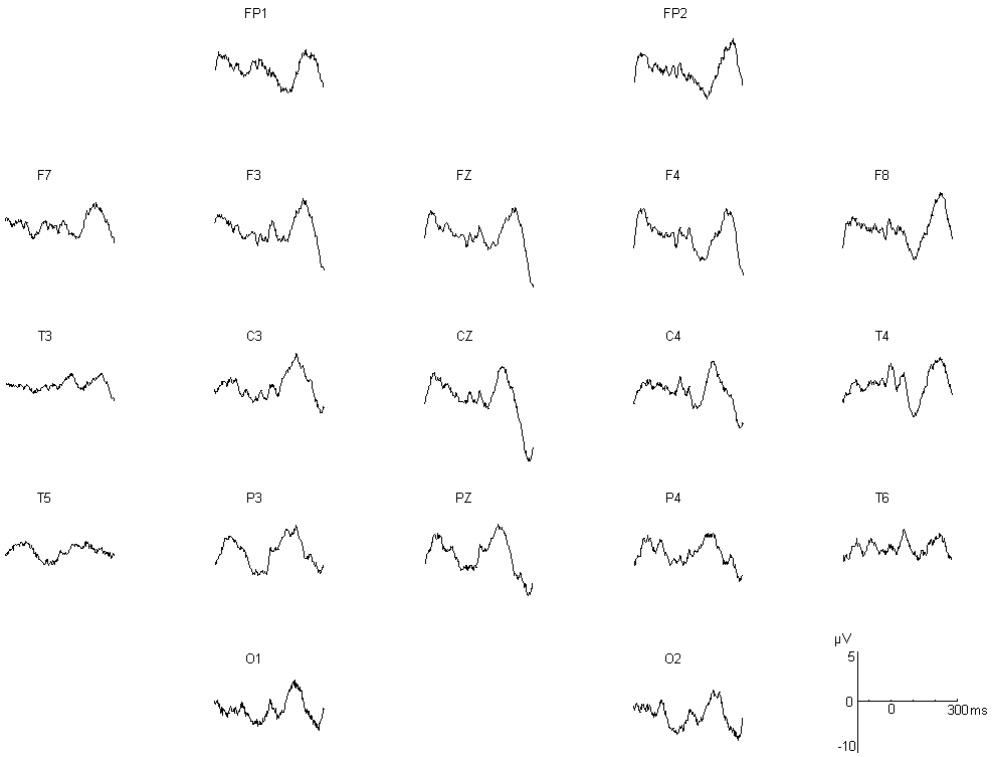

Figure A.19 Subject ***ug*** (male, 10 y.o) P_1 peak latency and amplitude at Cz electrode, 161.3 ms and 2.30 µV.

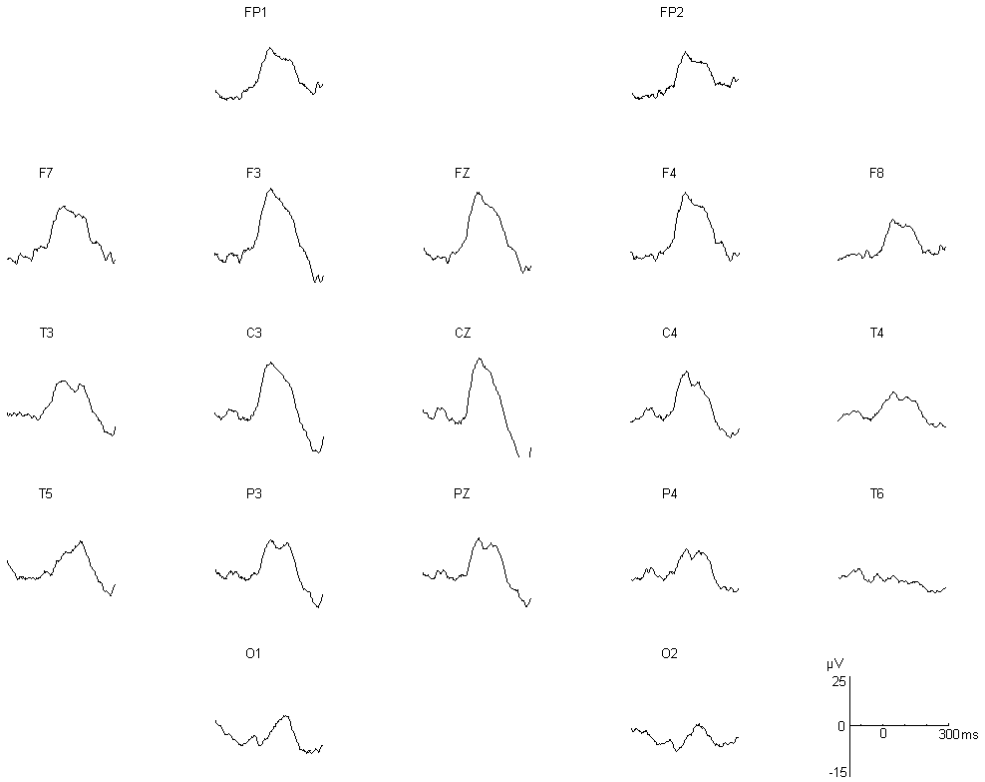

Figure A.20 Subject ***xal*** (female, 4 y.o) P_1 peak latency and amplitude at Cz electrode, 99.78 ms and 10.86 μV.

Children with CIs AEP recordings

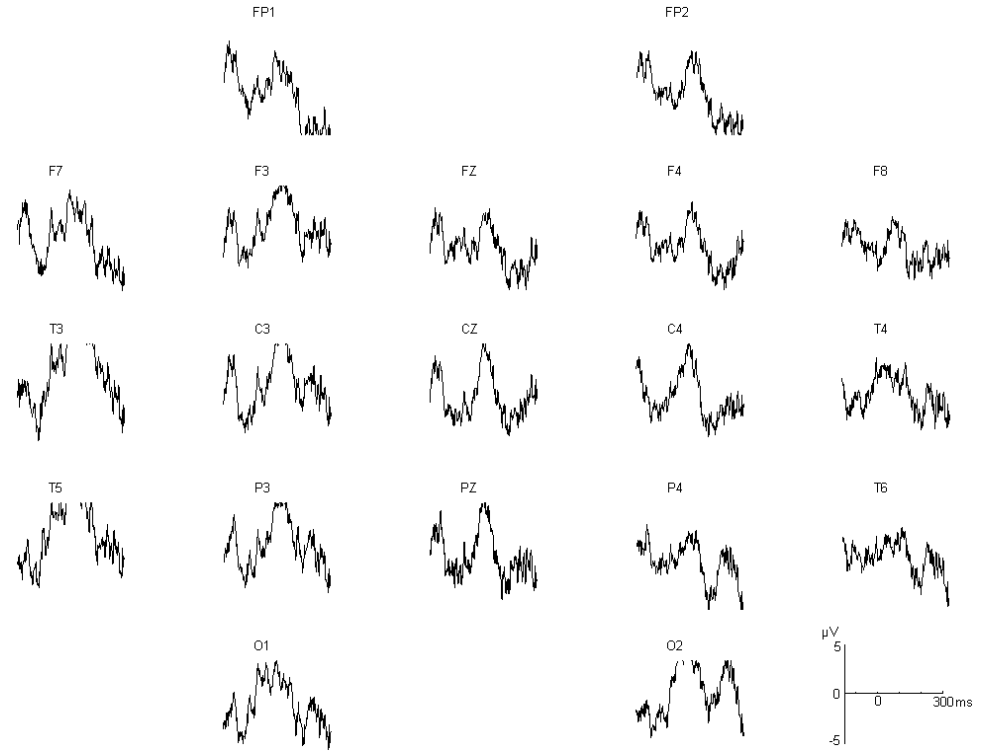

Figure A.21 Recording S1-St1, male 5 months after implantation. P_1 peak latency and amplitude at Cz electrode, 110 ms and 2.1 μV. (CI in the right side).

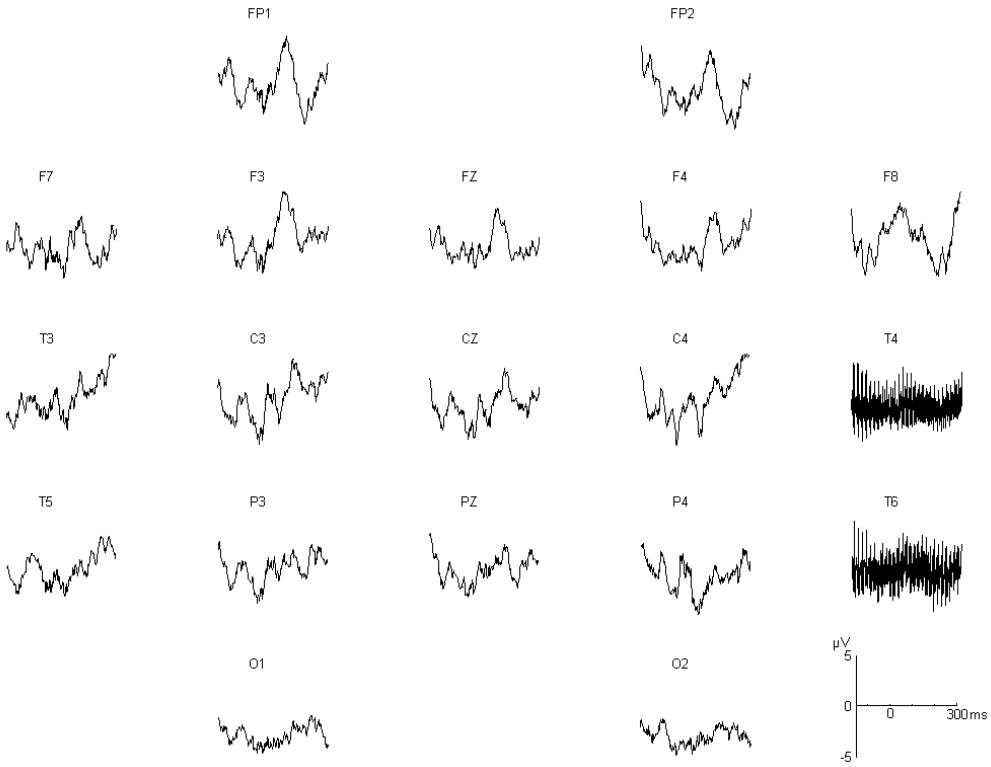

Figure A.22 Recording S1-St2, male 1 year after implantation. P_1 peak latency and amplitude at Cz electrode, 159.3 ms and 3.32 μV (neither T4 nor T6 was connected, CI in the right side).

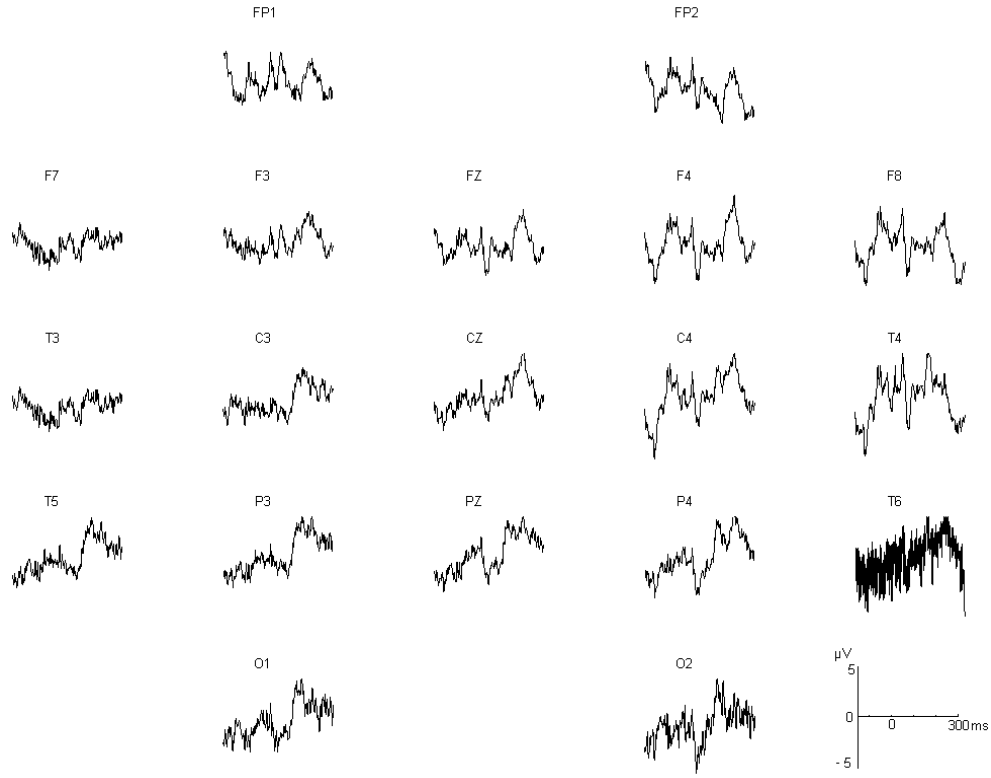

Figure A.23 Recording S1-St3, male 2 years 6 months after implantation. P_1 peak latency and amplitude at Cz electrode, 208.4 ms and 4.63 μV (CI in the right side).

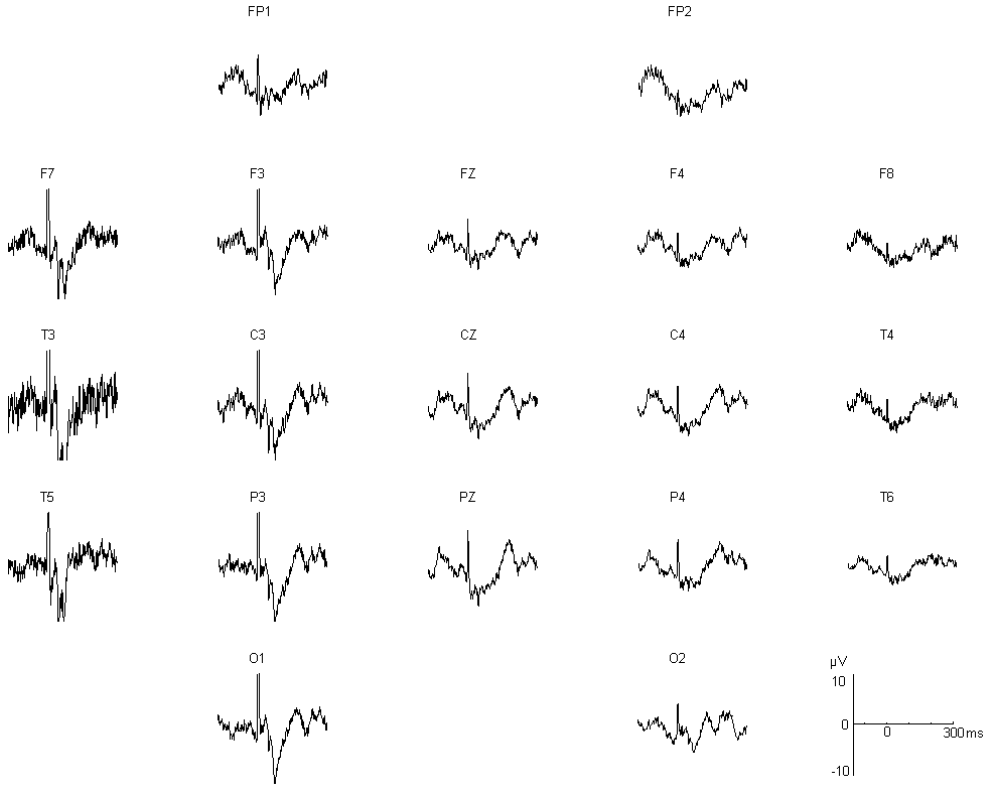

Figure A.24 Recording S2-St1, female 3 months after implantation. P_1 peak latency and amplitude at Cz electrode, 183.9 ms and 3.20 μV (CI in the left side).

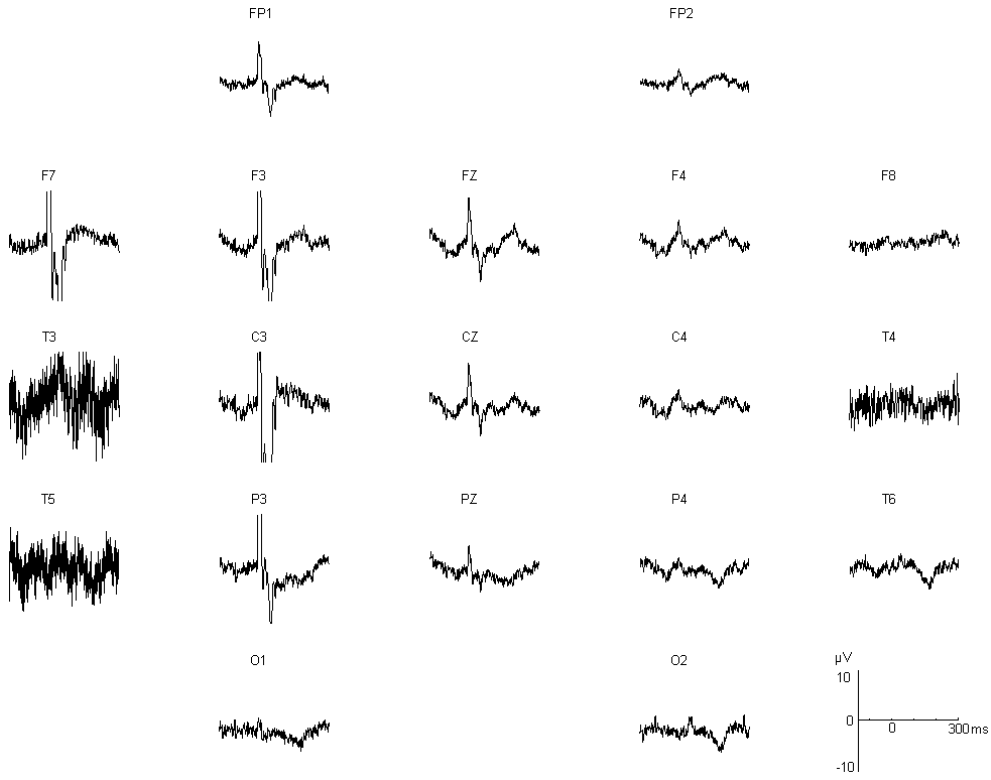

Figure A.25 Recording S2-St2, female 9 months after implantation. P_1 peak latency and amplitude at Cz electrode, 196.4 ms and 1.81 μV (CI in the left side).

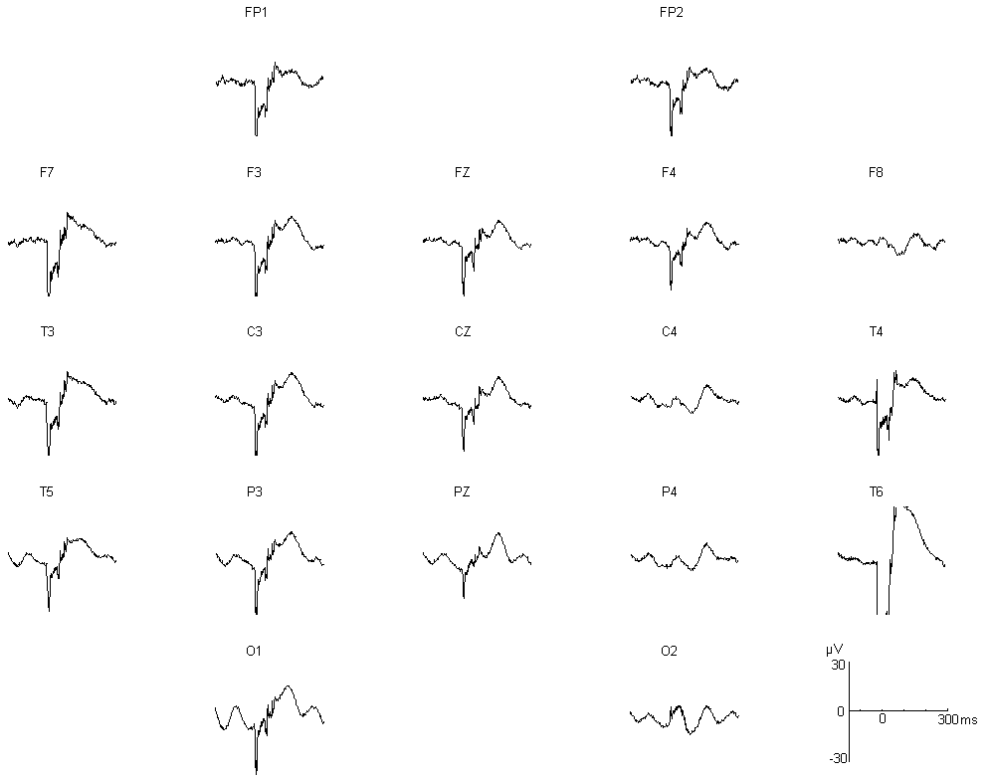

Figure A.26 Recording S3-St1, male 1 year after implantation. P_1 peak latency and amplitude at Cz electrode, 172.9 ms and 6.31 μV (CI in the right side).

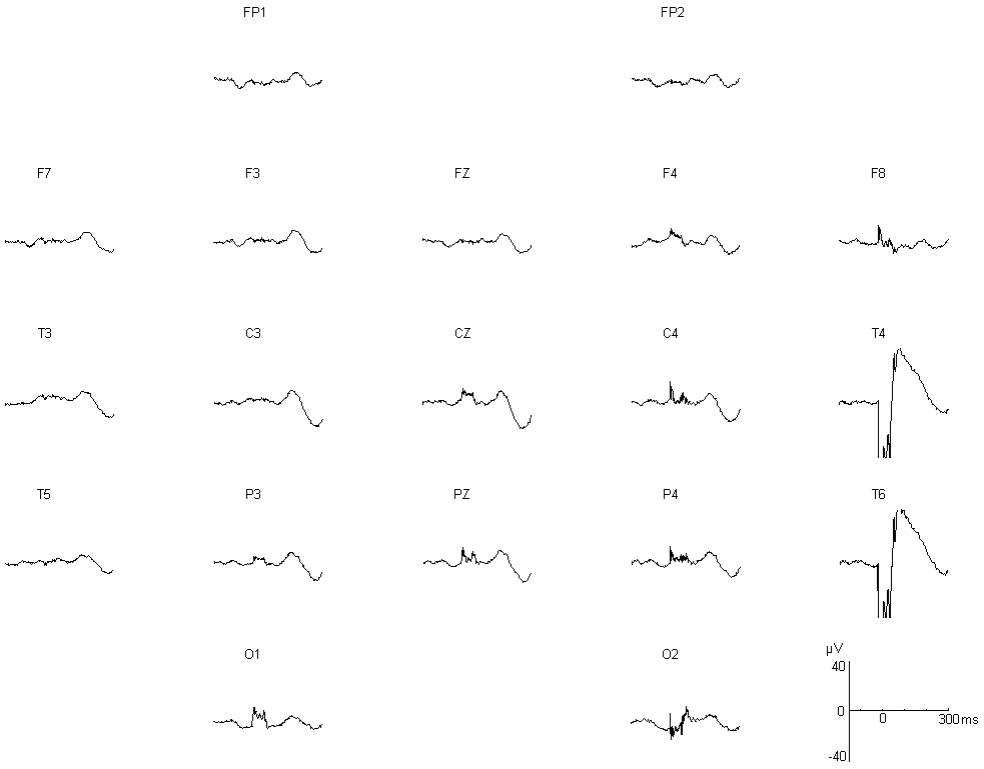

Figure A.27 Recording S3-St2, male 1 year and 8 months after implantation. P_1 peak latency and amplitude at Cz electrode, 173.9 ms and 9.649 μV (CI in the right side).

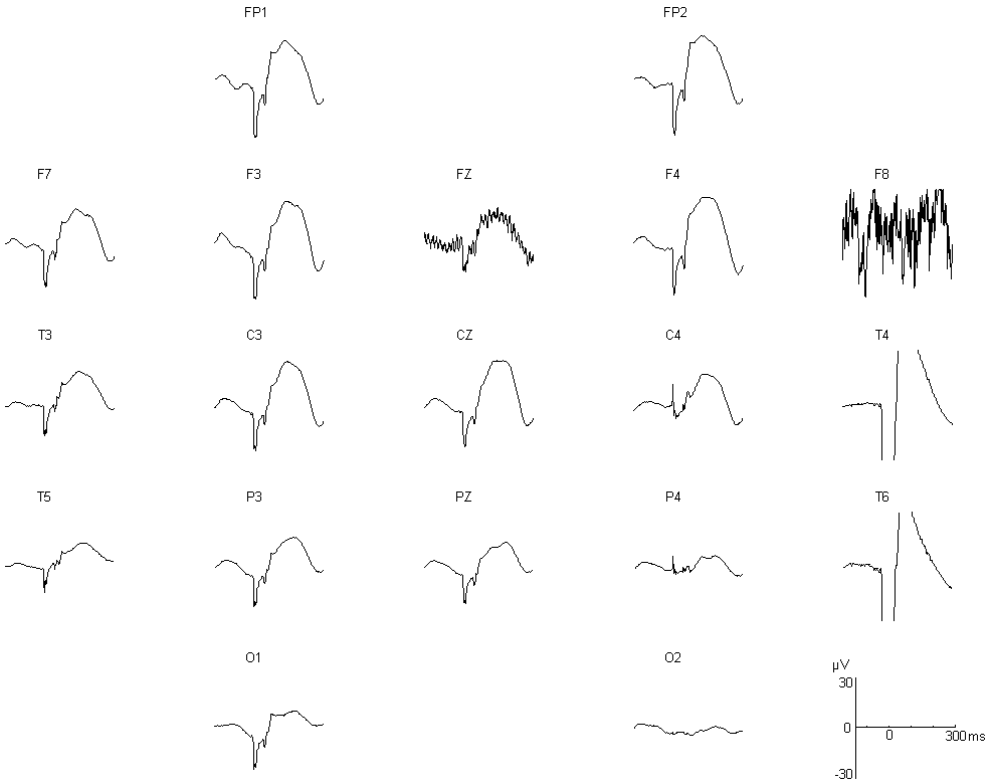

Figure A.28 Recording S3-St3, male 5 year and 5 months after implantation. P_1 peak latency and amplitude at Cz electrode, 146.8 ms and 16.49 µV (CI in the right side).

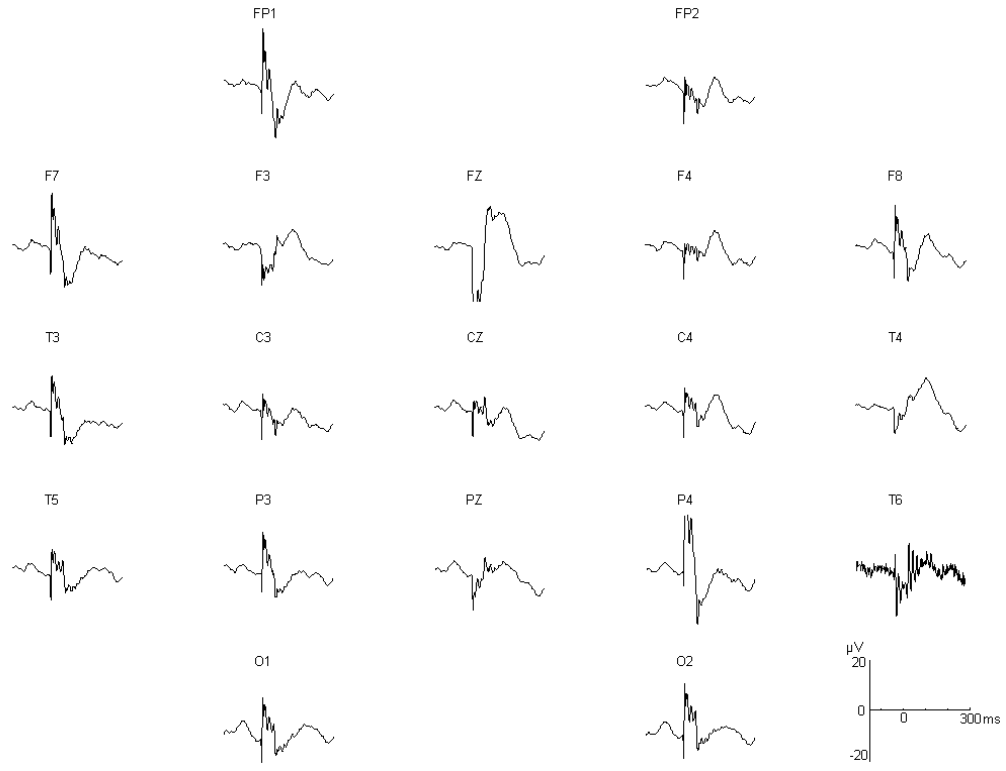

Figure A.29 Recording S4-St1, female 8 months after implantation. P_1 peak latency and amplitude at Cz electrode, 134.3 ms and 4.1 µV (the CI artifact is spread out around all the electrodes), CI in the right side.

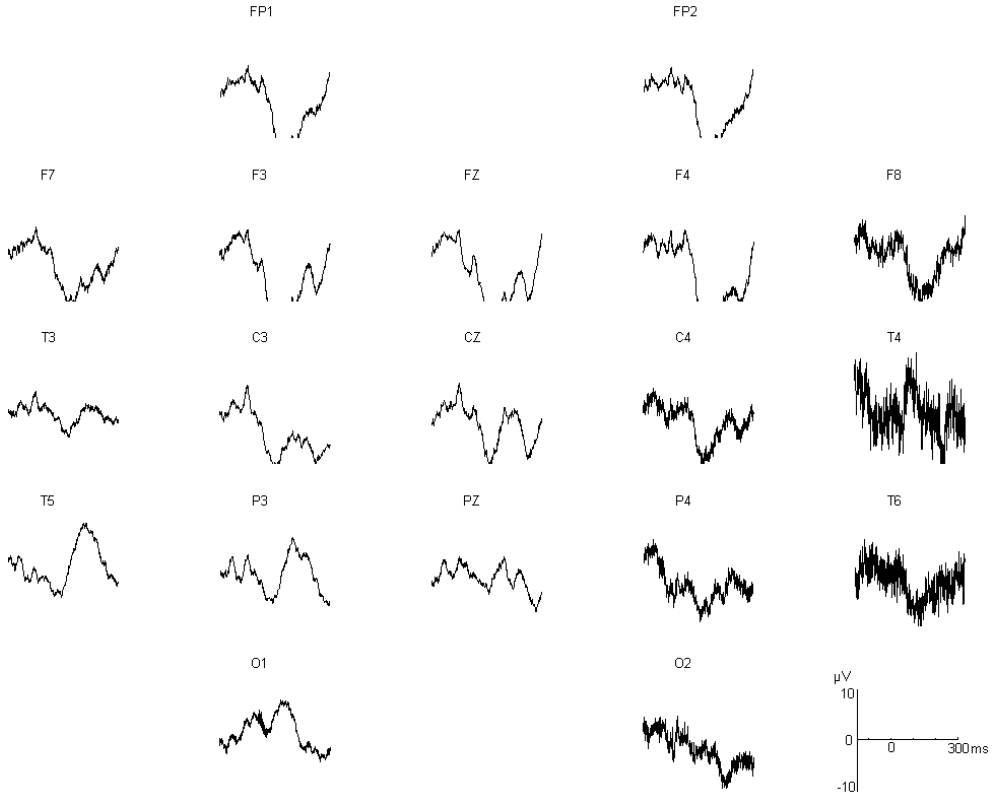

Figure A.30 Recording S4-St2, female 1 year and 1 month after implantation. P_1 peak latency and amplitude at Cz electrode, 185 ms and 4.3 μV (CI in the right side).

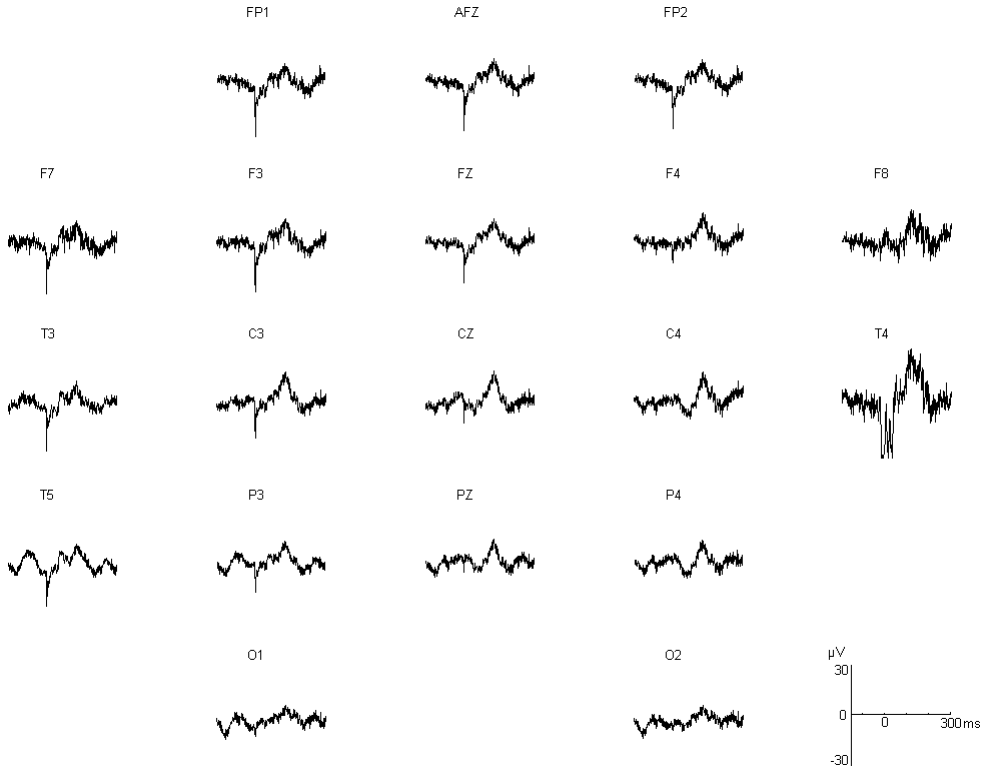

Figure A.31 Recording S4-St3, female 1 year and 6 months after implantation. P_1 peak latency and amplitude at Cz electrode, 135.8 ms and 9.92 μV. In this recording instead of electrode T6, the electrode AFz was used (CI in the right side).

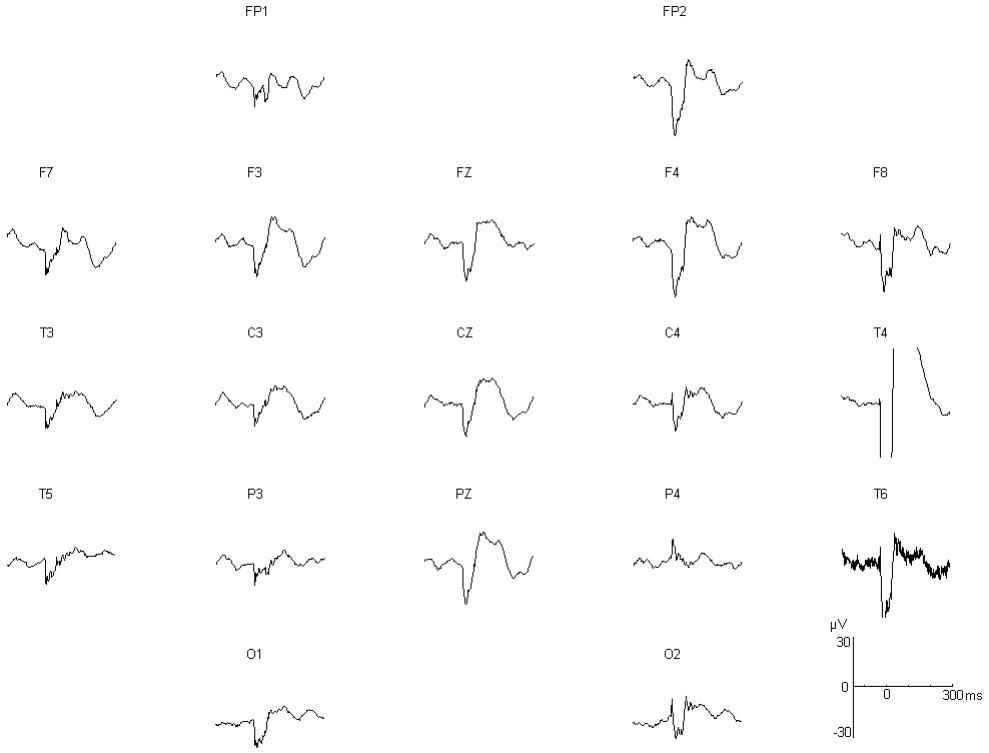

Figure A.32 Recording S5-St1, male 1 year and 9 months after implantation. P_1 peak latency and amplitude at Cz electrode, 124.3 ms and 13.44 μV (CI in the right side).

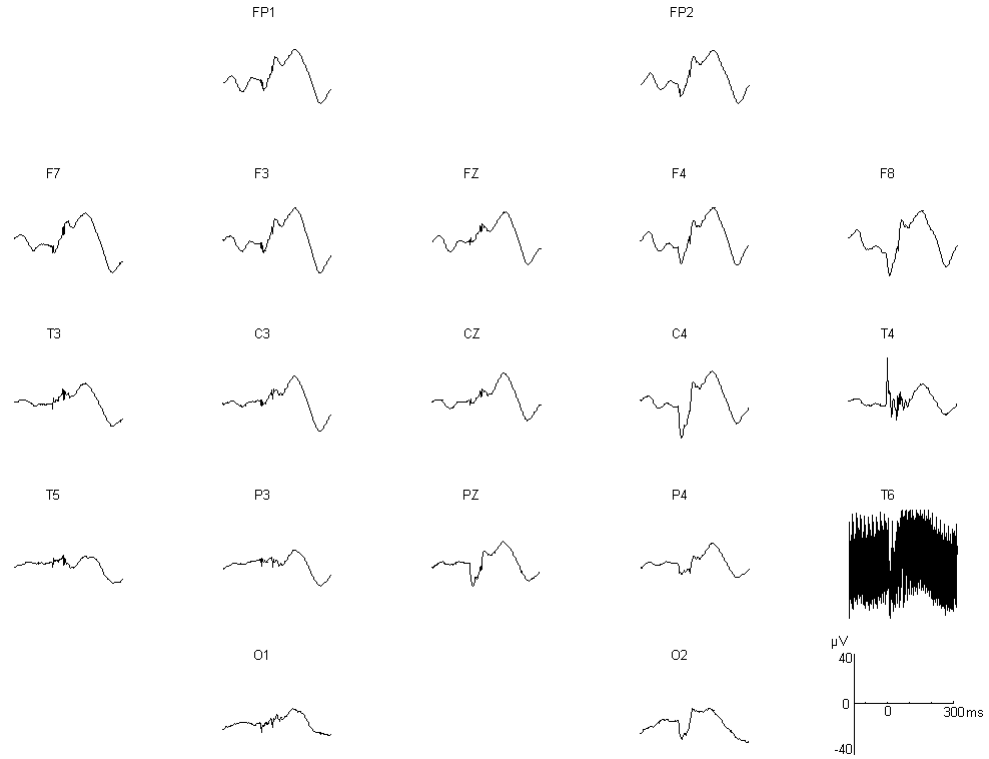

Figure A.33 Recording S5-St2, male 2 year and 8 months after implantation. P_1 peak latency and amplitude at Cz electrode, 150.8 ms and 21.79 μV (CI in the right side).

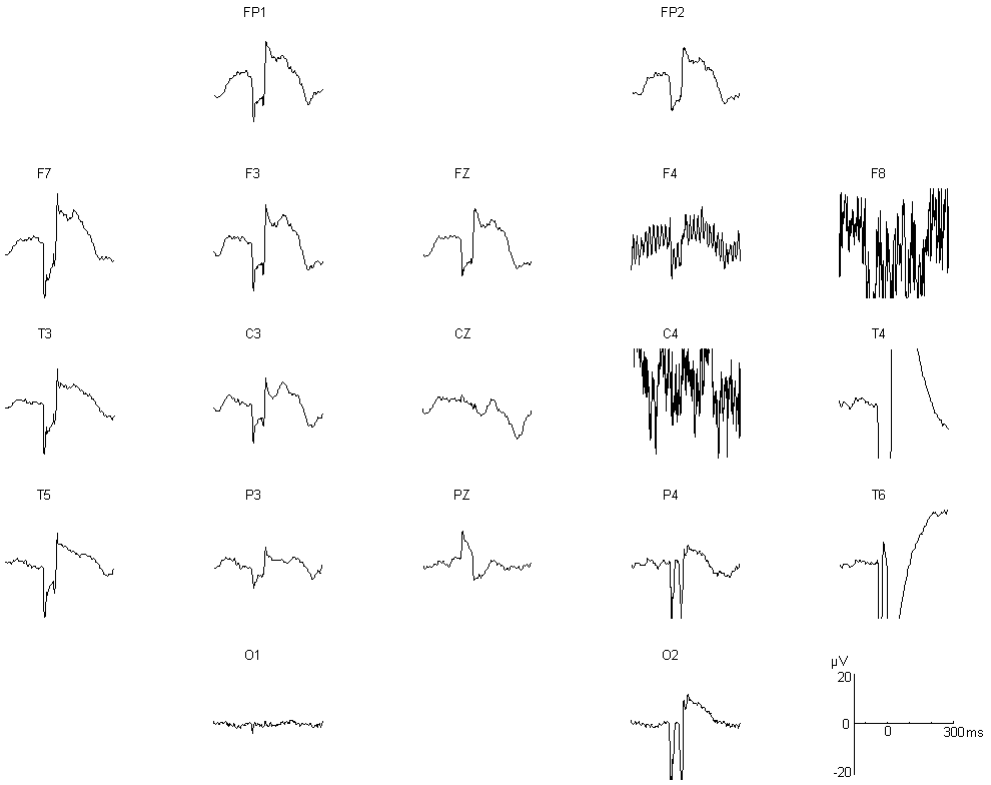

Figure A.34 Recording S5-St3, male 5 year and 1 month after implantation. P_1 peak latency and amplitude at Cz electrode, 131.3 ms and 7.28 μV (CI in the right side).

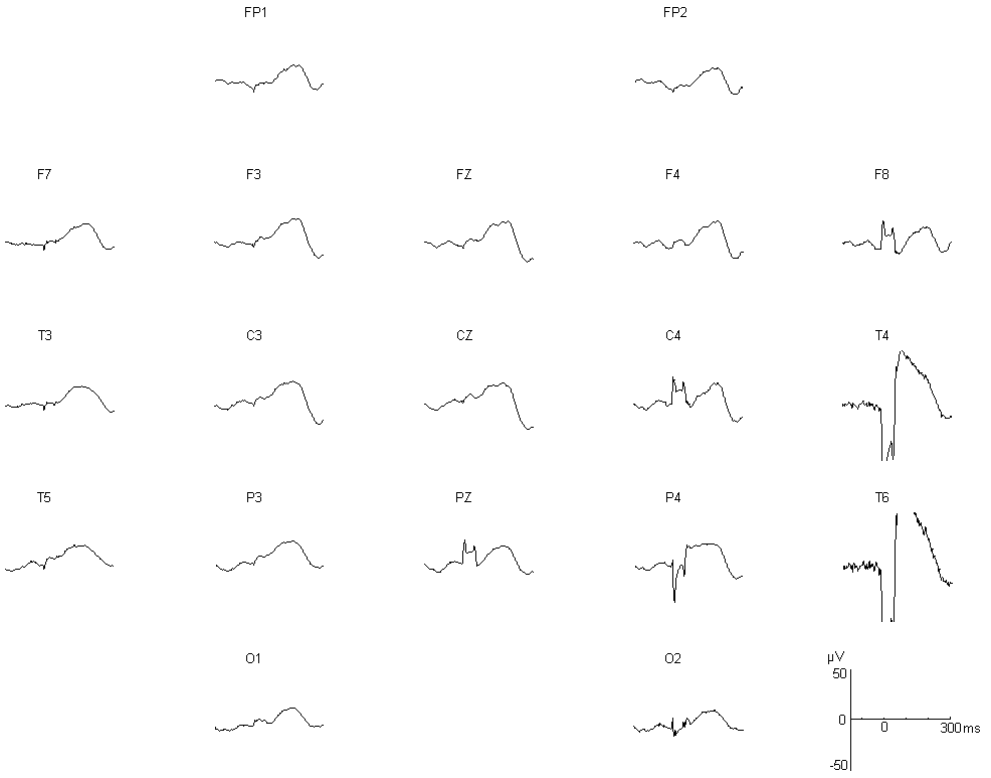

Figure A.35 Recording S6-St1, female 2 year and 5 months after implantation. P_1 peak latency and amplitude at Cz electrode, 173.9 ms and 16.54 μV (CI in the right side).

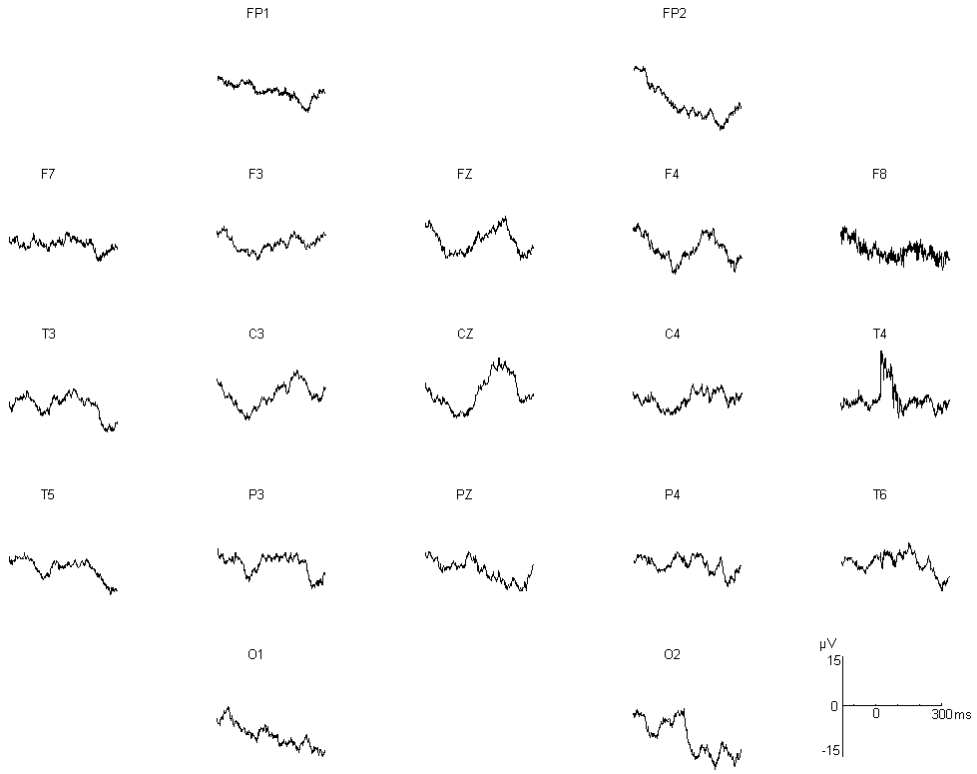

Figure A.36 Recording S7-St1, female 1 year and 8 months after implantation. P_1 peak latency and amplitude at Cz electrode, 164.3 ms and 10.78 μV (CI in the right side).

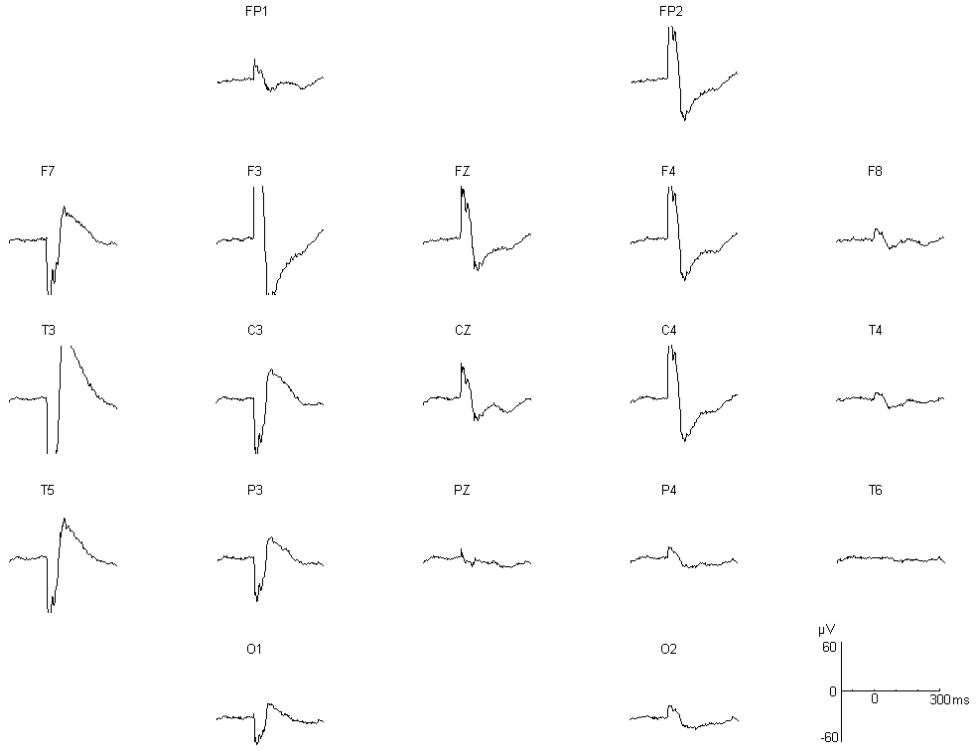

Figure A.37 Recording S9-St1, female 5 months after implantation. It is not possible to recognise the P_1 peak (CI in the left side).

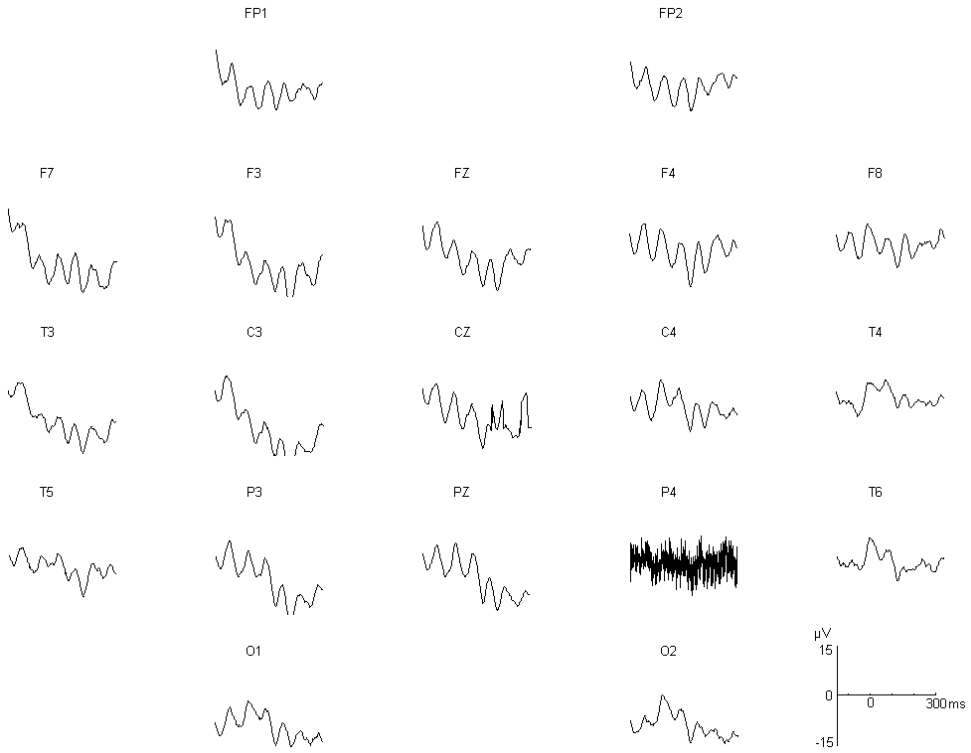

Figure A.38 Recording S10-St1, male 5 months after implantation. P_1 peak is not recognised (CI in the right side).

Appendix B. Comparison between the kurtosis values and pdf histograms using *Infomax* and *Ext-Infomax*.

Appendix B. Comparison between the kurtosis values and pdf histograms using *Infomax* and *Ext-Infomax*.

Normal hearing children

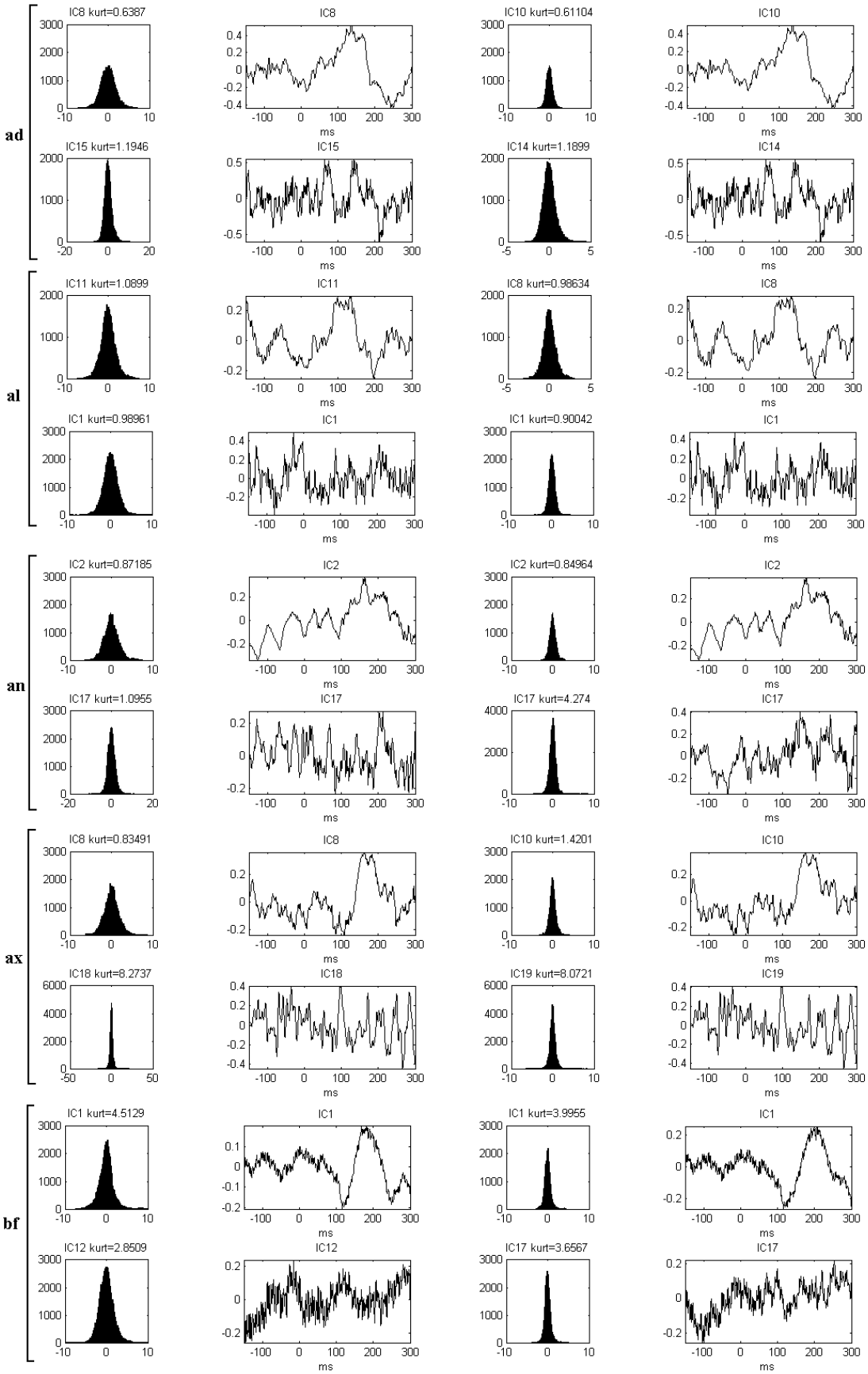

Appendix B. Comparison between the kurtosis values and pdf histograms using *Infomax* and *Ext-Infomax*.

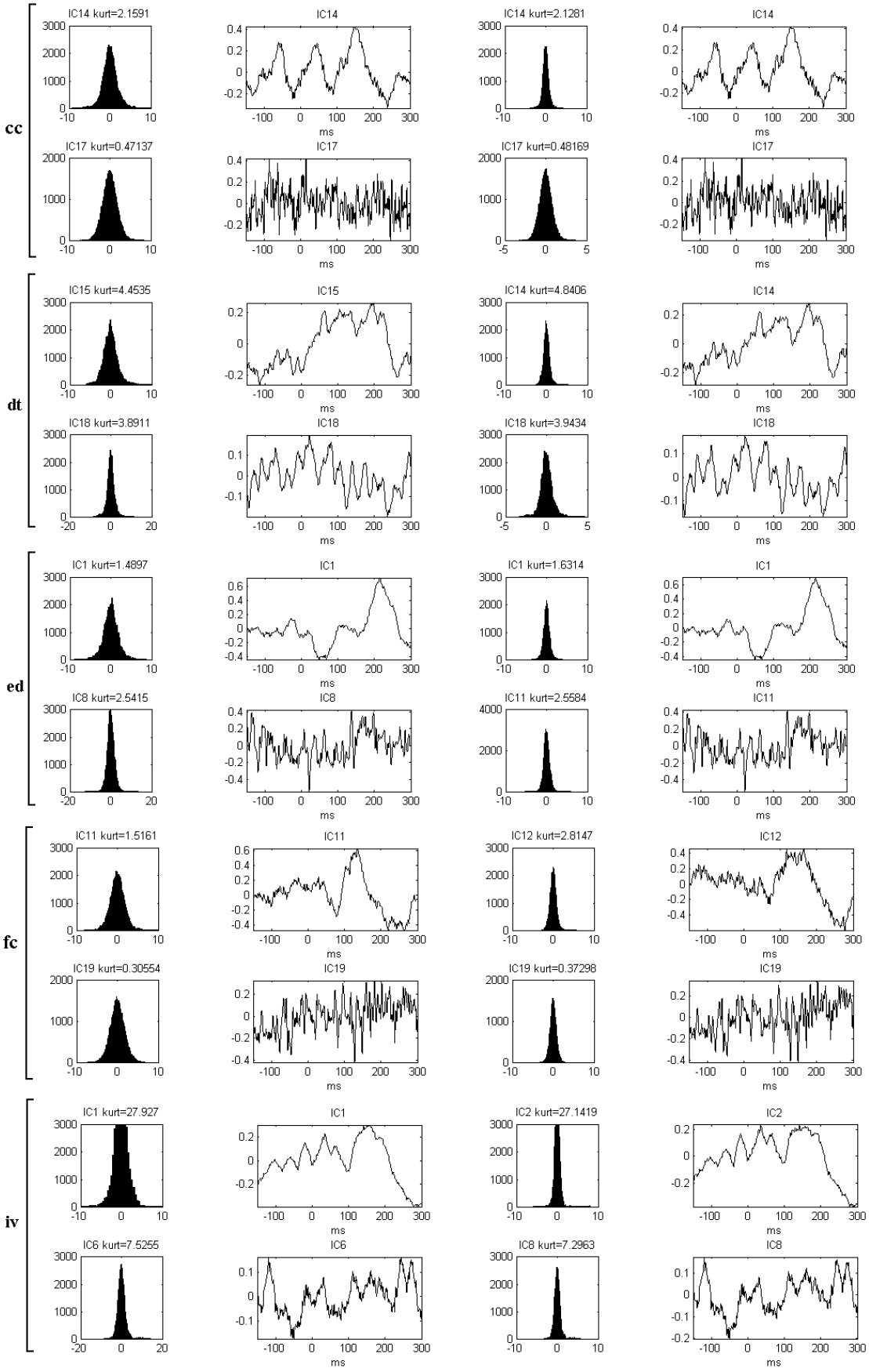

Appendix B. Comparison between the kurtosis values and pdf histograms using *Infomax* and *Ext-Infomax*.

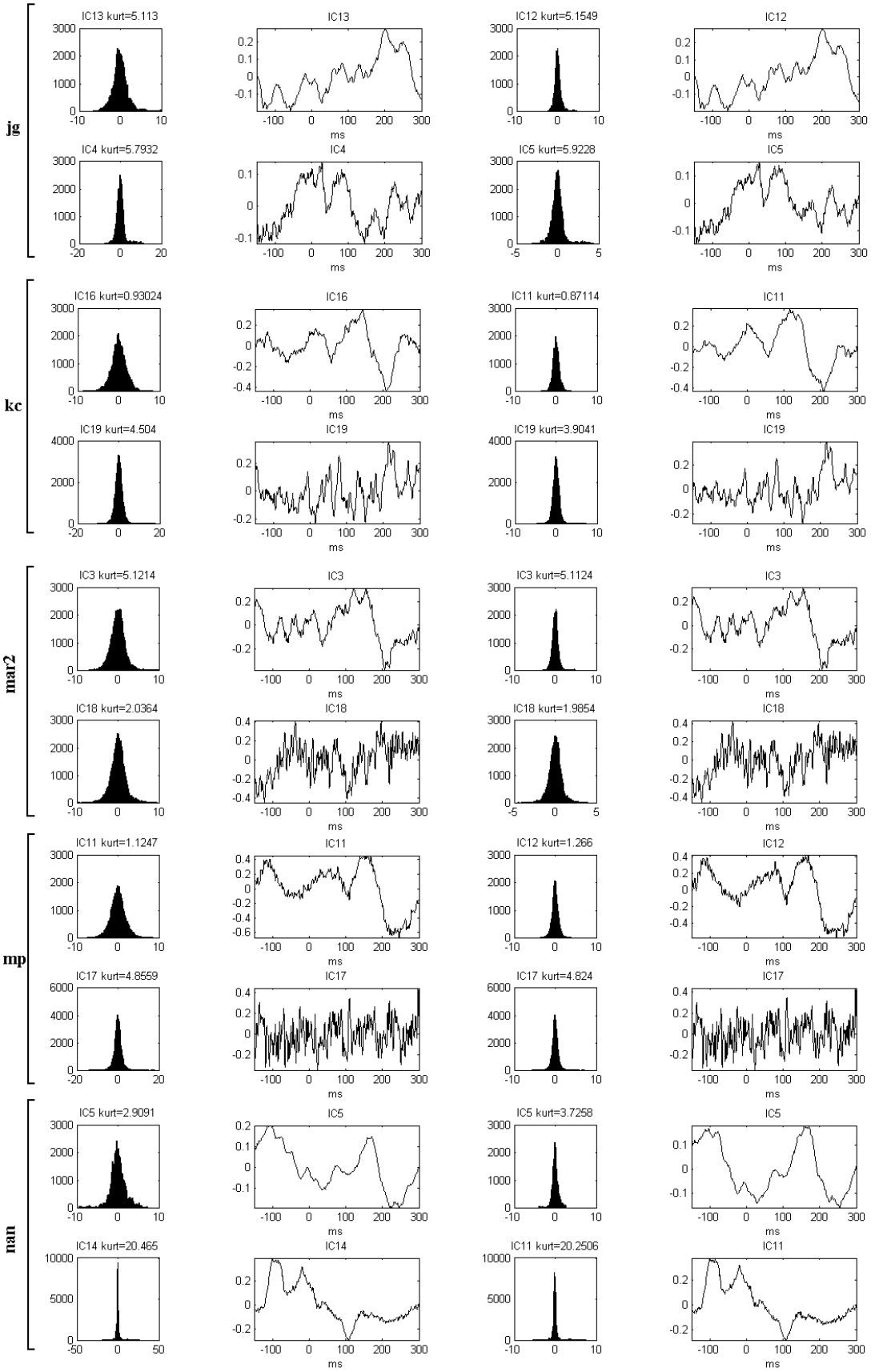

Appendix B. Comparison between the kurtosis values and pdf histograms using *Infomax* and *Ext-Infomax*.

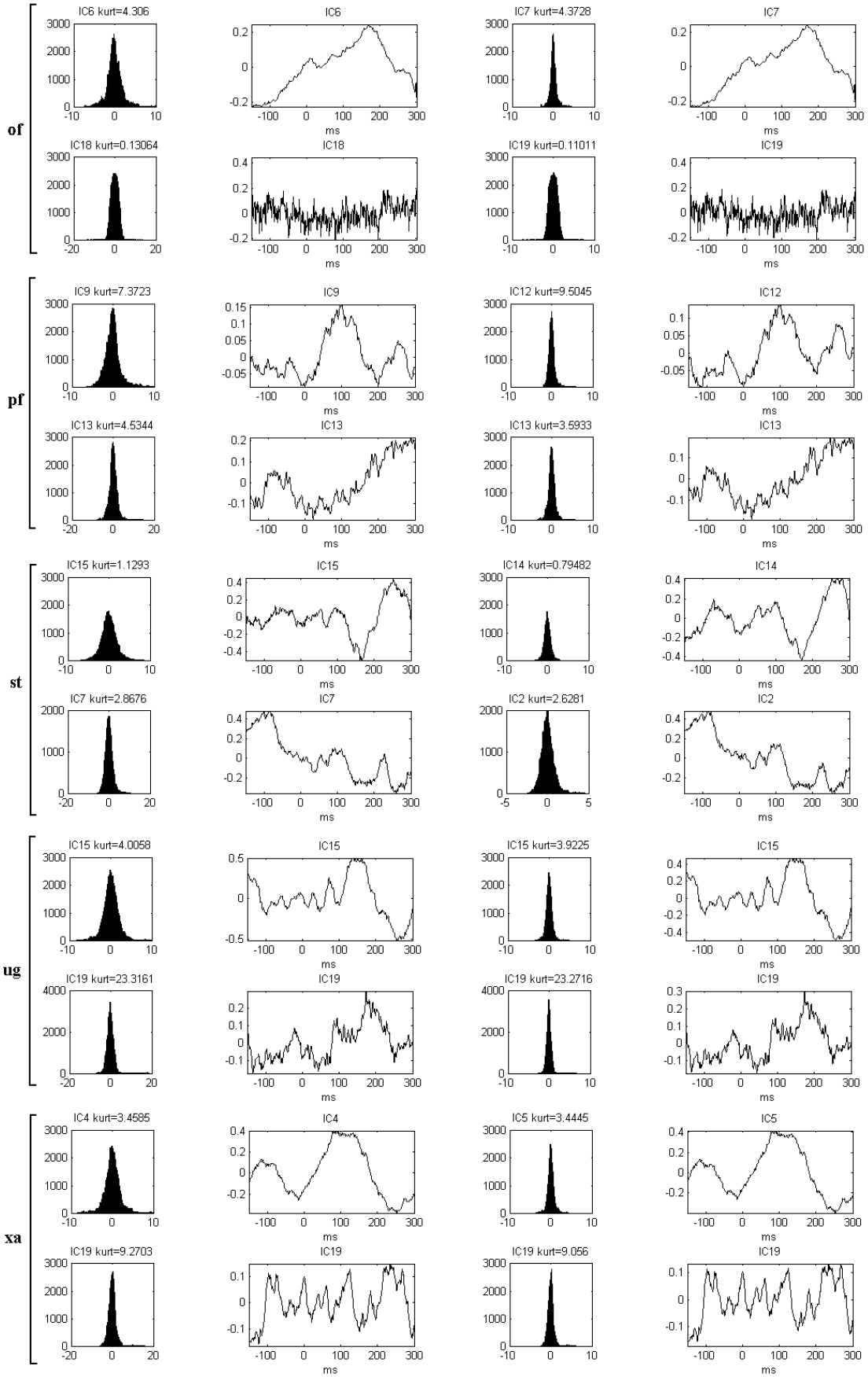

Children with CIs

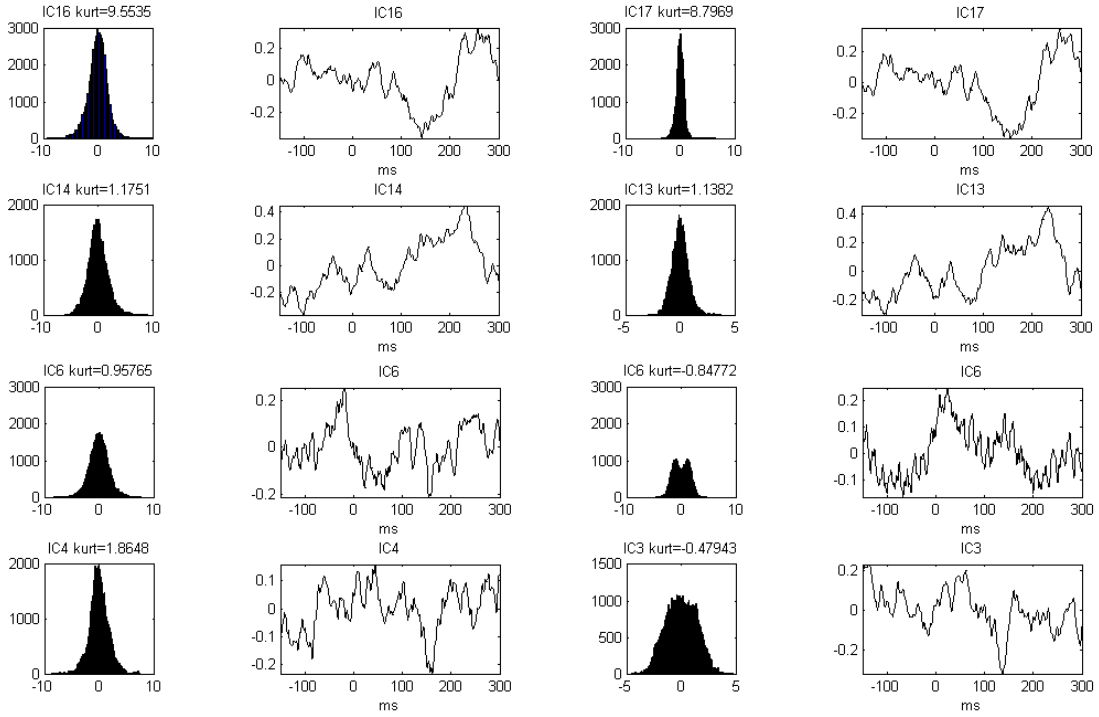

(a) (b)

Figure B.1 Comparison between the estimates related to the AEP (row 1-2) and the background noise (rows 3-4) using (a) *Infomax* and (b) *Ext-Infomax* for S1-St1; this subject has been using his CI for less than 1 year. The estimates associated with the AEP are essentially the same for both algorithms whilst some differences can be observed in both the histogram and kurtosis values of the back noise estimates.

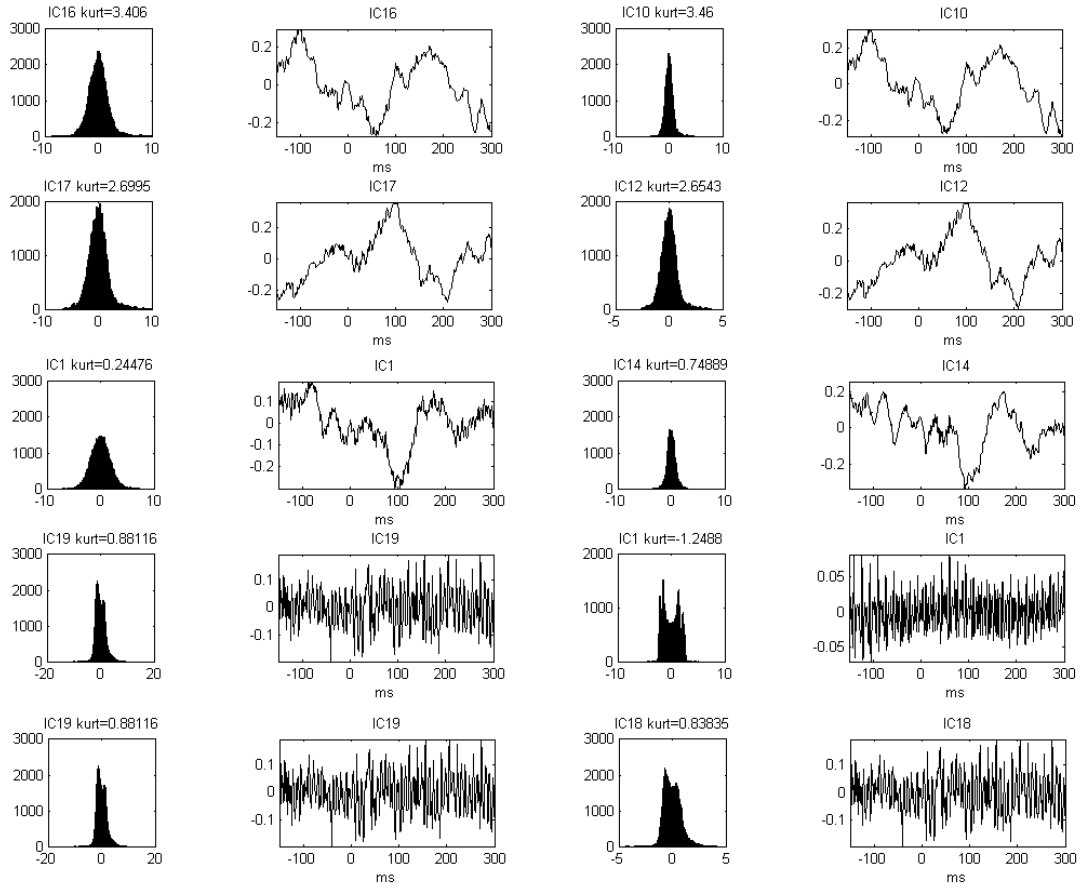

(a) (b)

Figure B.2 Comparison between the estimates using (a) *Infomax* and (b) *Ext-Infomax* for S1-St2; this subject has been using his CI for more than 1 year. The principal difference between the algorithms is in the background noise; *Infomax* recovers only one background noise estimate (IC19) while that *Ext-Infomax* recovers components with negative kurtosis and almost cero kurtosis IC1 and IC 18, respectively.

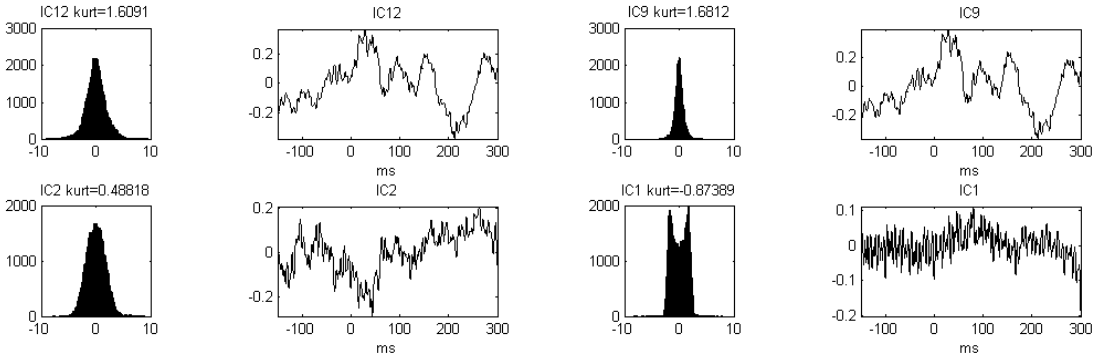

Figure B.3 Comparison between the estimates using (a) *Infomax* and (b) *Ext-Infomax* for S1-St3. The principal difference between the algorithms is in the background noise.

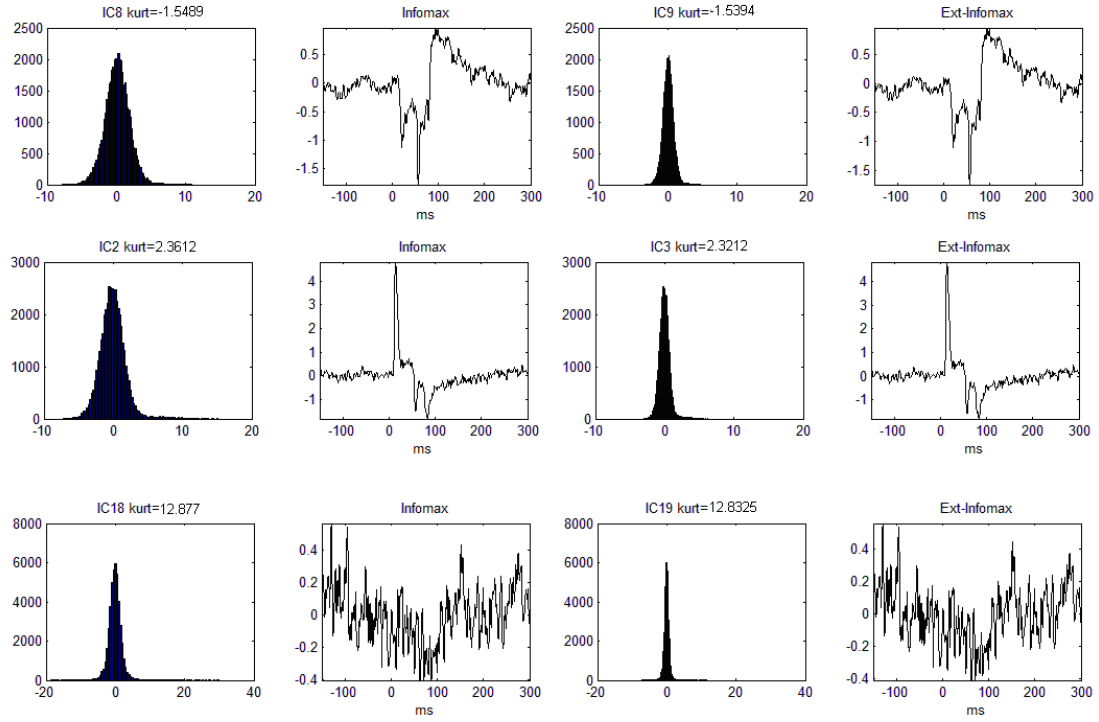

(a) (b)

Figure B.4 Comparison between the estimate of the CI artifact (rows 1 and 2) and the background noise (bottom row) using (a) *Infomax* and (b) *Ext-Infomax* for S2-St1; this subject has been using his CI for less than 1 years. There are not significant differences between the estimate between (a) and (b); neither *Infomax* nor *Ext-Infomax* recovered a clear AEP.

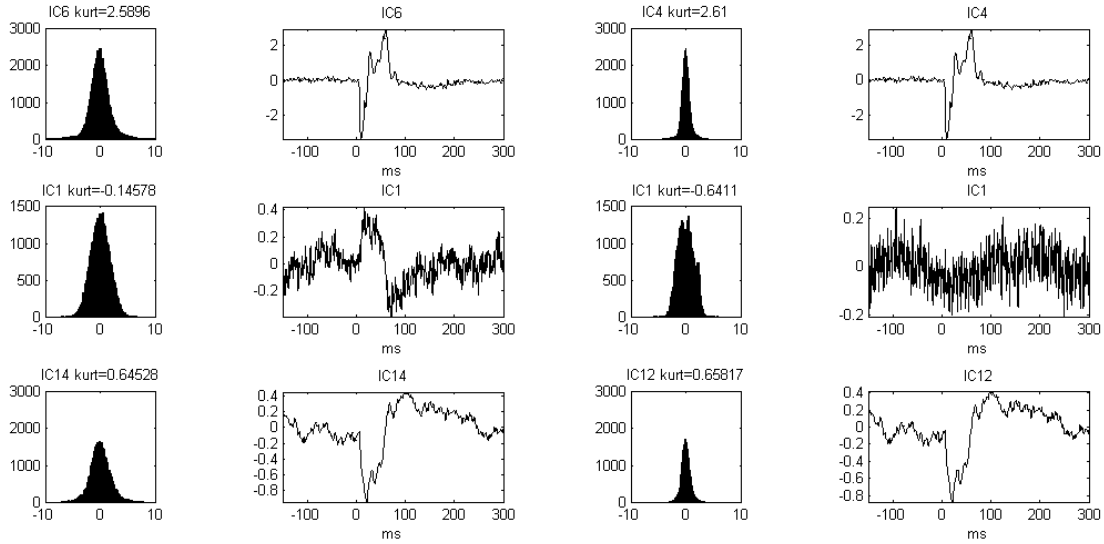

(a) (b)

Figure B.5 Comparison between the estimates recovered using (a) *Infomax* and (b) *Ext-Infomax* for S2-St2. There is not significant difference between both algorithms; it was no possible to identify a clear AEP.

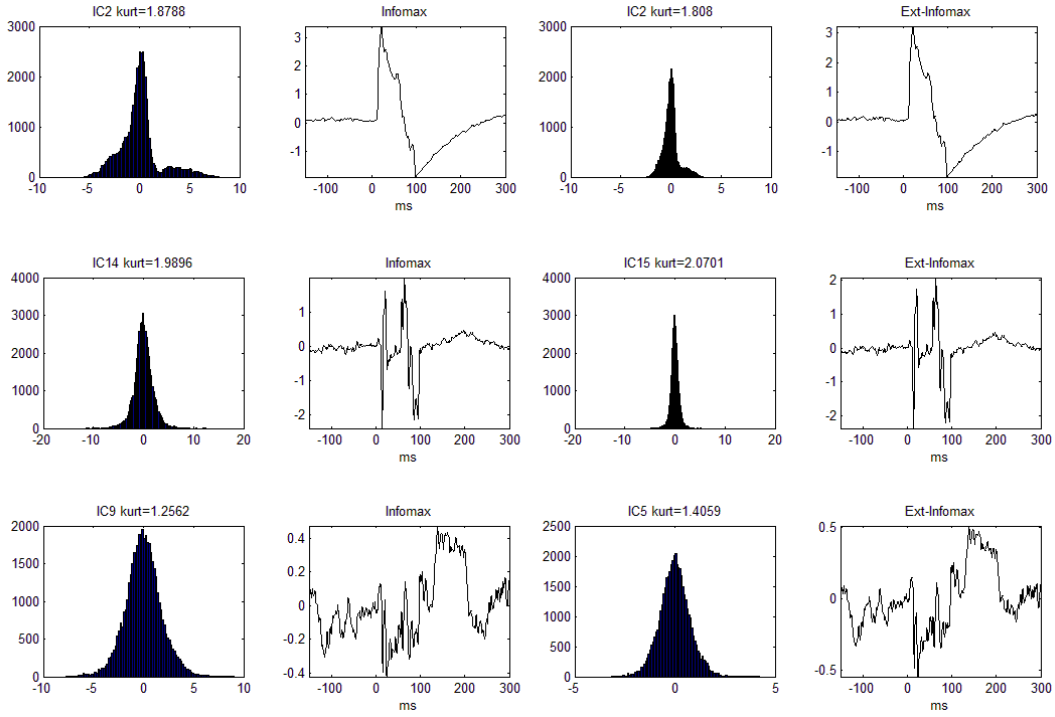

(a) (b)

Figure B.6 Comparison between the estimates recovered using (a) *Infomax* and (b) *Ext-Infomax* for S3-St1; this subject has been using his CI for one year. There is not significant difference between both algorithms; it was no possible to identify a clear AEP.

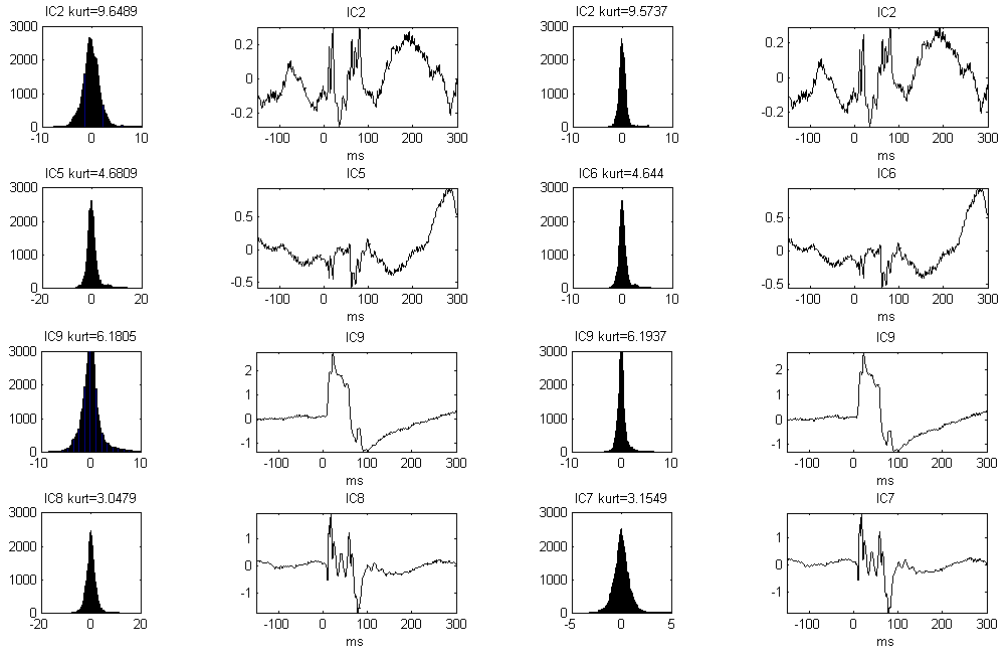

(a) (b)

Figure B.7 Comparison between the estimates using (a) *Infomax* and (b) *Ext-Infomax* for a subject (S3-St2) who has been using his CI for more than 1 year. The estimate of the AEP is not clear neither in (a) nor (b). In both cases the CI artifact still being in the auditory response (row 1-2). The estimates of the CI artifact are similar in both cases with a small difference in the histograms and kurtosis values.

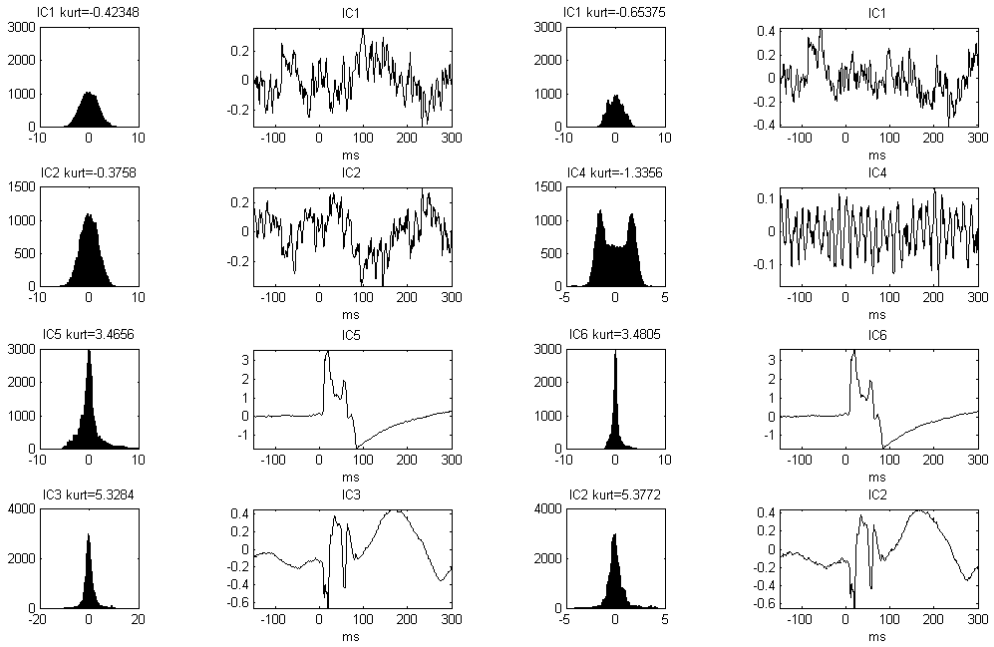

(a) (b)

Figure B.8 Comparison between the estimate of the background noise and the CI artifact (row 3) using (a) *Infomax* and (b) *Ext-Infomax* for S3-St3; this subject has been using his CI for more than 5 years. The principal difference between both algorithms is the estimate of the background noise; it was no possible to identify the AEP clearly, the CI artifact effect is significant in both *Infomax* and *Ext-Infomax*.

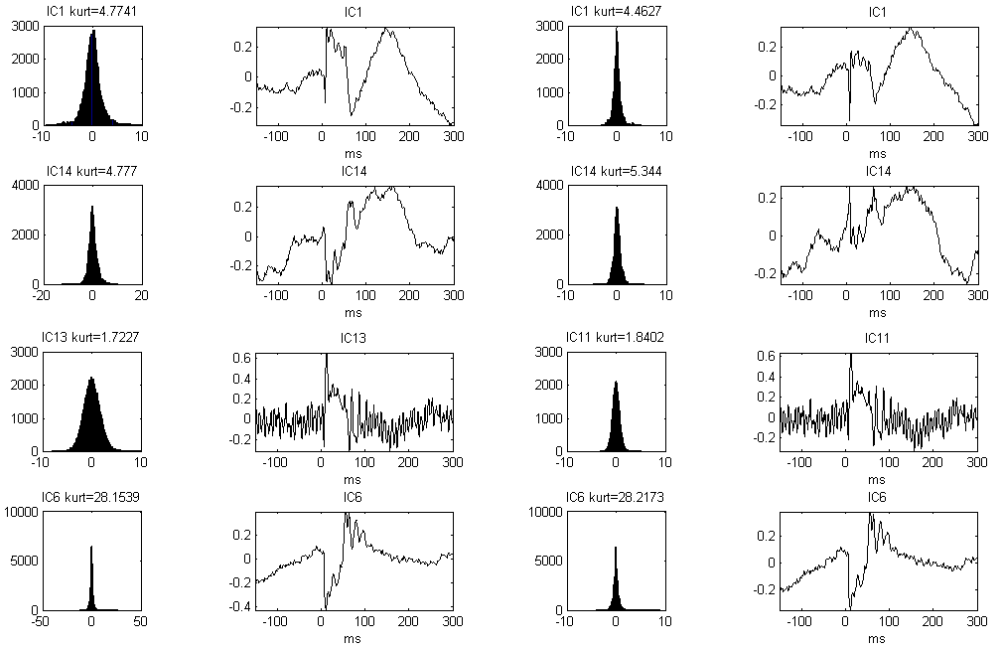

(a) (b)

Figure B.9 Comparison between (a) *Infomax* and (b) *Ext-Infomax* for subject S4-St1 (this child has been using her CI for less than one year). There are not significant differences between the estimates using those algorithms of the CI artifact and the background noise (rows 3 and 4, respectively). The AEPs estimates (rows 1 and 2) have components of the CI artifact.

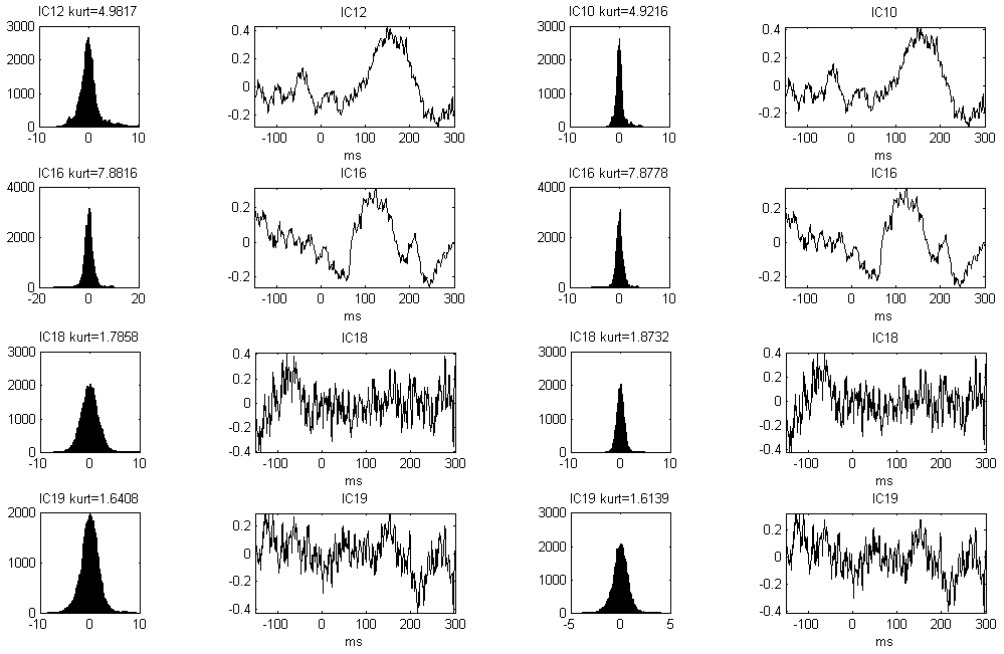

(a) (b)

Figure B.10 Comparison between the estimates using (a) *Infomax* and (b) *Ext-Infomax* for subject S4-St2 (this child has been using her CI for one year approximately). In this case the AEPs can be recognized in rows 1 and 2 although contaminated by the background noise.

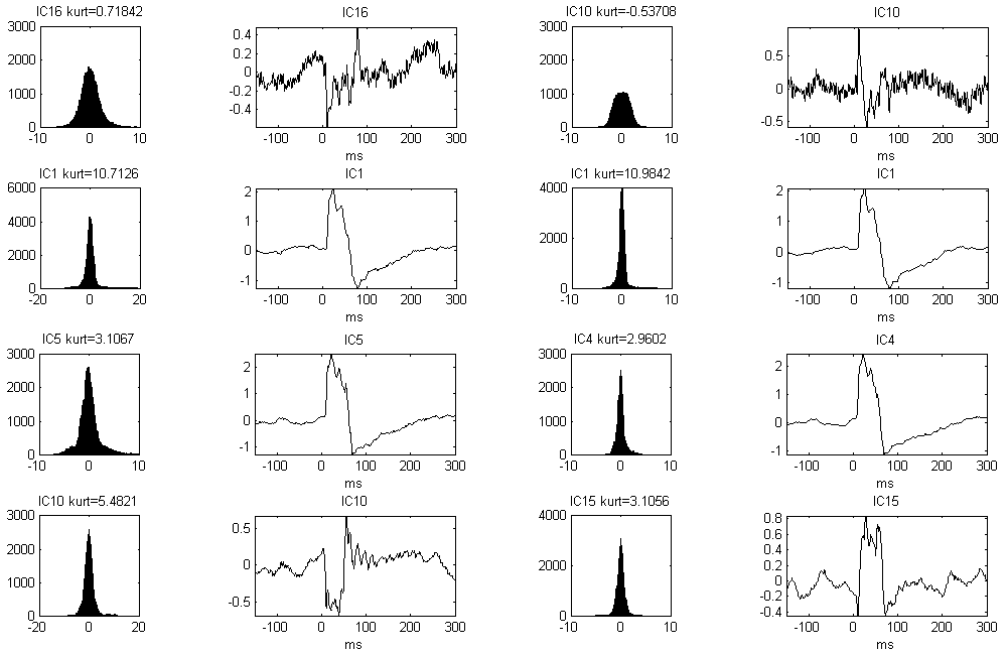

(a) (b)

Figure B.11 Comparison between the estimate of the background noise (top row) and the CI artifact using (a) *Infomax* and (b) *Ext-Infomax* for S5-St1; this subject has been using his CI for more than 1 years. There are not important differences between the estimates associated with the CI artifact between (a) and (b); neither *Infomax* nor *Ext-Infomax* separated a clear AEP.

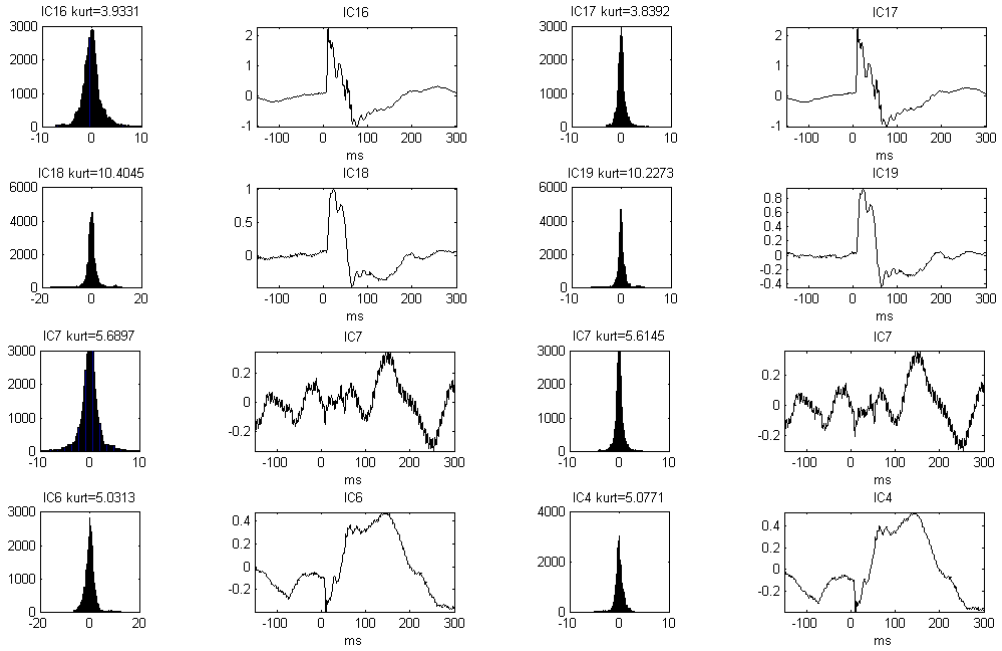

(a) (b)

Figure B.12 Estimates for S5-St2 (2.5 year after implantation); there are no difference neither in the histogram nor the kurtosis values between (a) *Infomax* and (b) *Ext-Infomax*. The AEPs can be recognised in the ICs of the rows 3 and 4 however the estimates are contaminated by the background noise or the CI artifact.

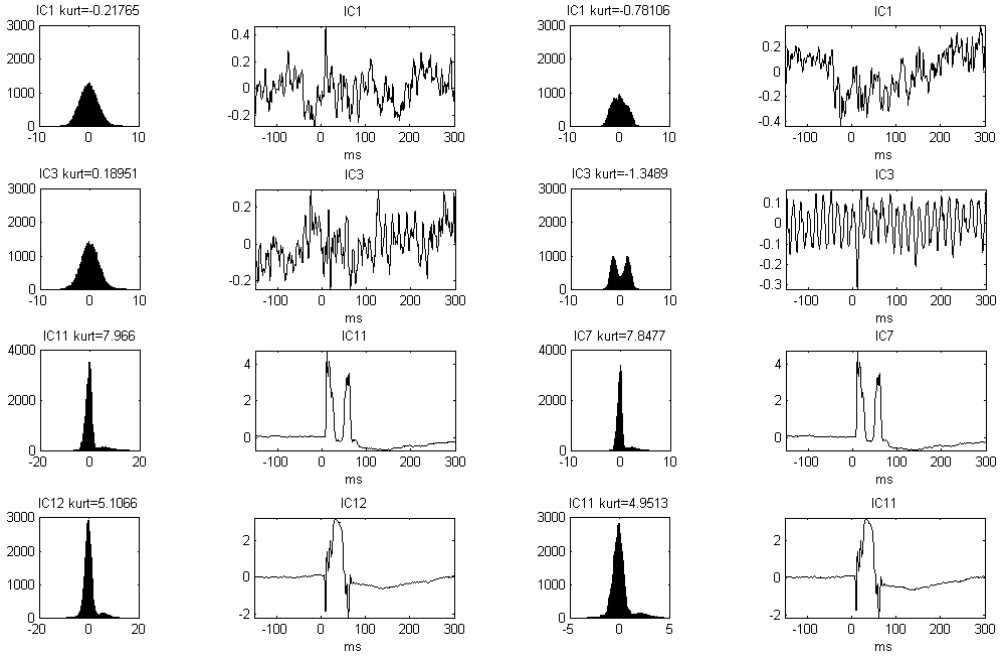

(a) (b)

Figure B.13 Comparison between the estimates of the background noise (rows 1, 2 and 3) and the CI artifact (rows 4 and 5) using (a) *Infomax* and (b) *Ext-Infomax* for S5-St3; this subject has been using his CI for more than 5 years. The principal difference between both algorithms is the estimate of the background noise; it was no possible to identify a clear AEP neither with *Infomax* nor *Ext-Infomax*.

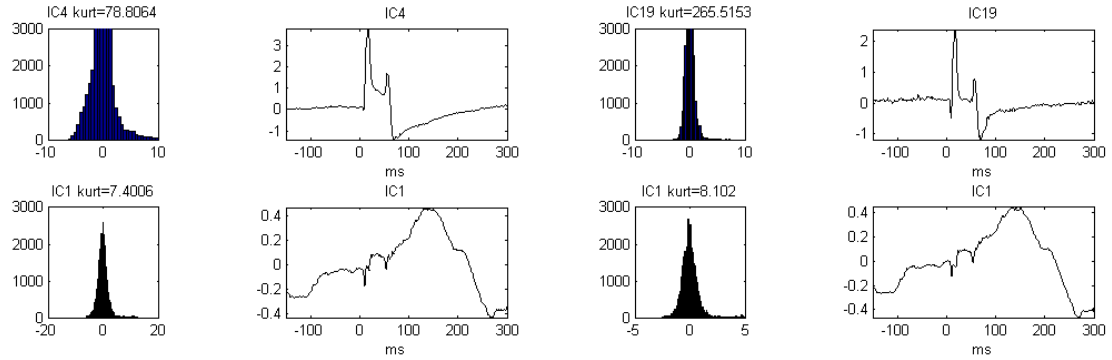

(a) (b)

Figure B.14 Comparison between the estimate of the CI artifact (row 1) and the AEP (row 2) using (a) *Infomax* and (b) *Ext-Infomax* for S6-St1; this subject has been using her CI for 2.5 years. Some differences can notice between the estimates of the CI artifact components; the estimate associated with the AEP is essentially the same for both algorithms.

Appendix C. Separability matrix values

This appendix shows the changes of the separabilty matrix in accordance with the increasing of τ. Significant changes in the structure of the matrix can be observed between τ=0...1 and τ=0...5 in most of the recordings. After those values the structure of the separability matrix remains almost without changes but the separability values are lower, with the lowest value at τ=0...20. In normal hearing children, the one dimensional subspaces correspond to noise whilst the high dimensional subspaces are related to components of the AEPs. In children with CIs one dimensional subspace is related to the CI artifact and noise whilst high dimensional subspace can be associated with the AEP. Chapter 5 includes the waveform and topographic maps of relevant ICs from both normal hearing children and children with CIs.

Normal hearing children

Subject ad. τ=0...1

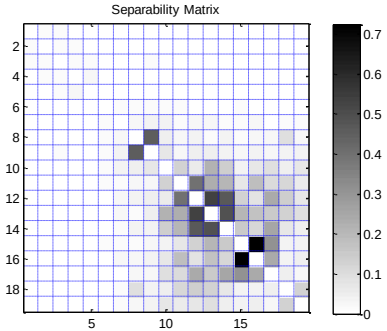

τ=0...5

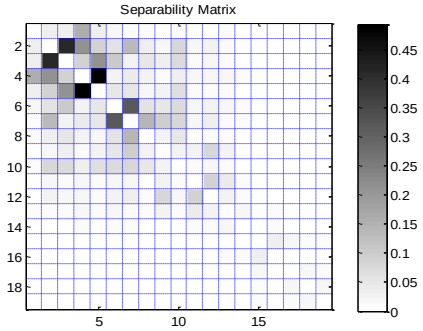

τ=0...15

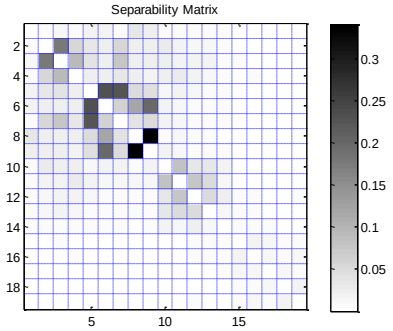

τ=0...20

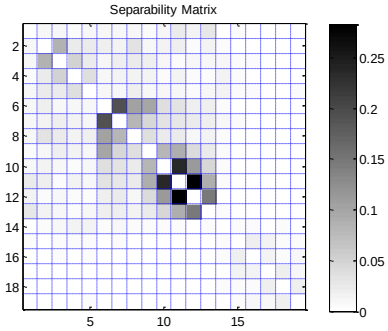

Subject al τ=0...1

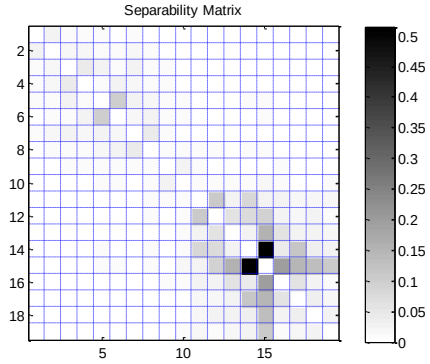

τ=0...5

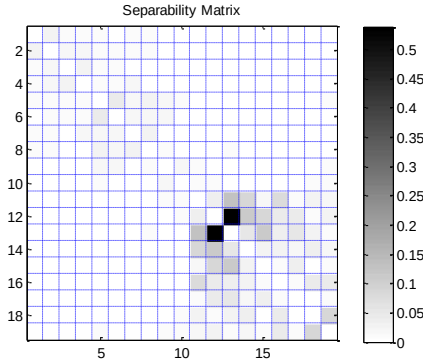

τ=0...15

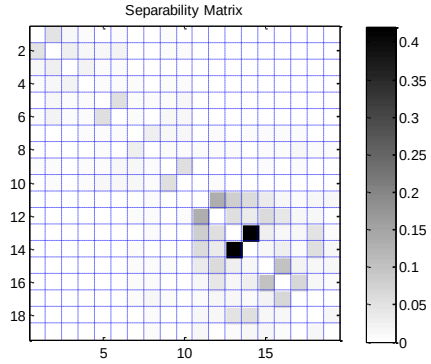

τ=0...20

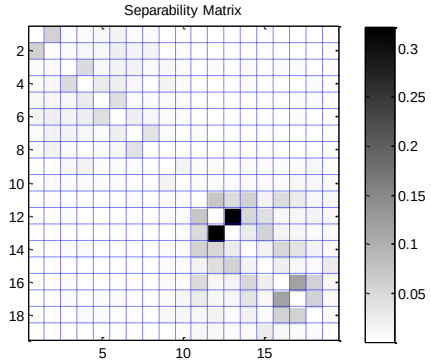

Subject an τ=0...1

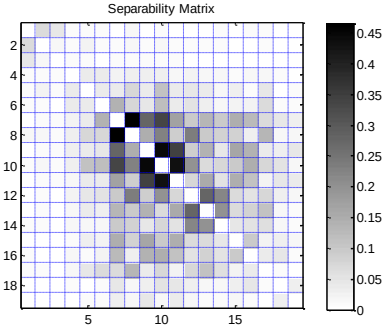

τ=0...5

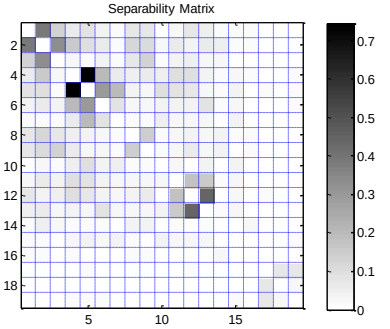

τ=0...15

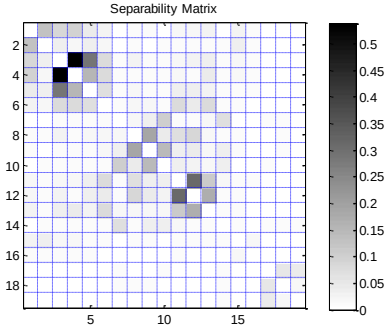

τ=0...20

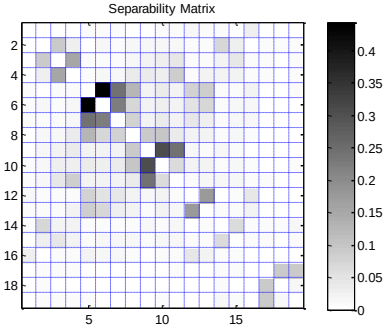

Subject ax τ=0...1

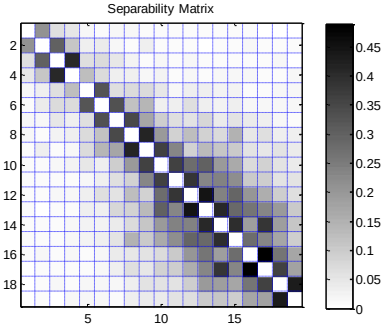

τ=0...5

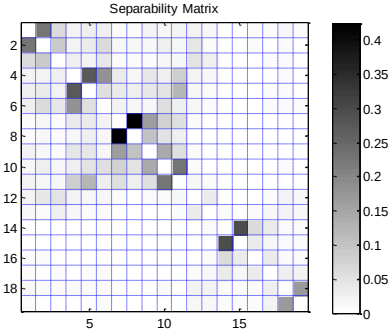

τ=0...15

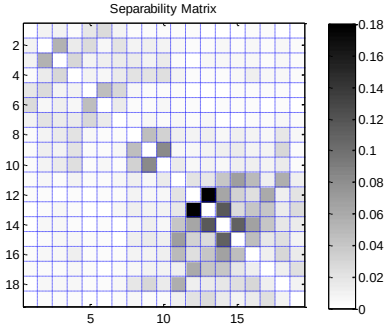

τ=0...20

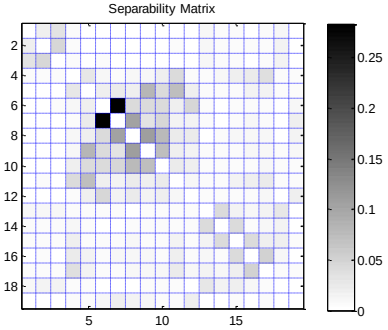

Subject ax τ=0...1

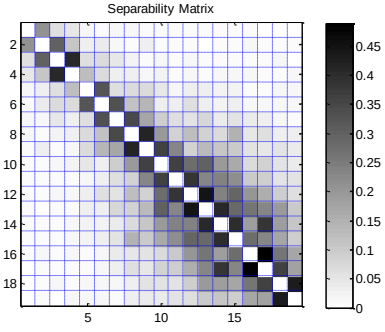

τ=0...5

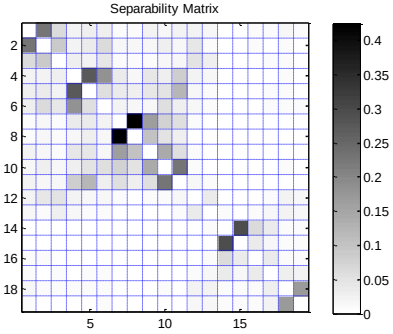

τ=0...15

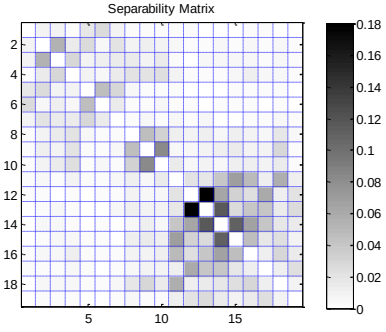

τ=0...20

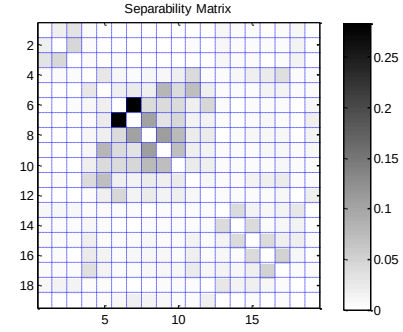

Subject bf τ=0...1

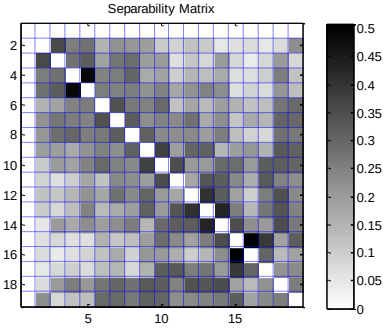

τ=0...5

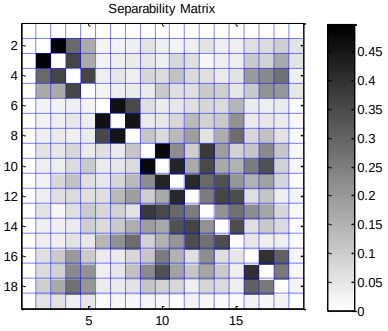

τ=0...10

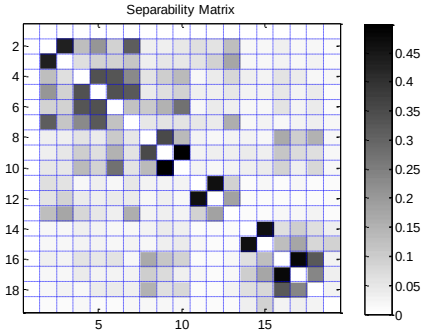

τ=0...20

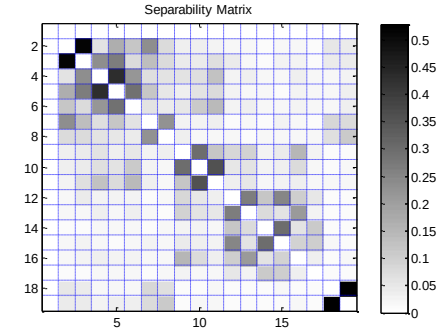

Subject cc τ=0...1

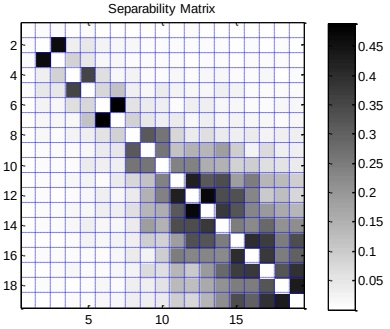

τ=0...5

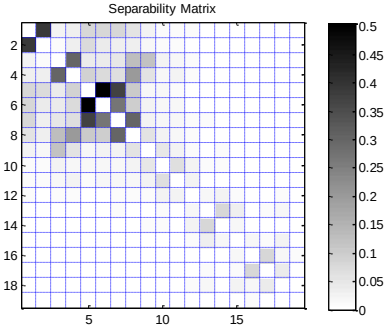

τ=0...15

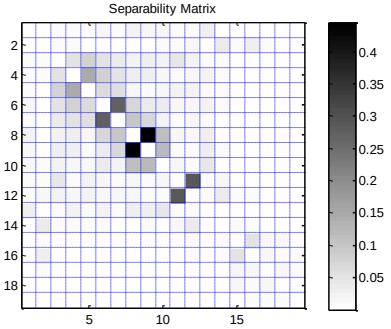

τ=0...20

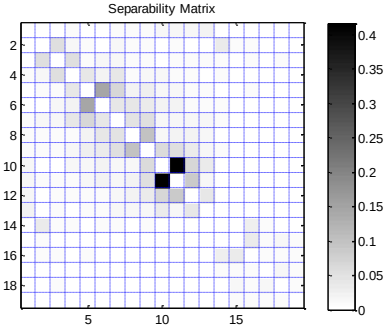

Subject dt τ=0...1

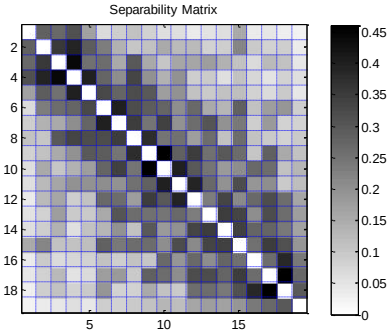

τ=0...5

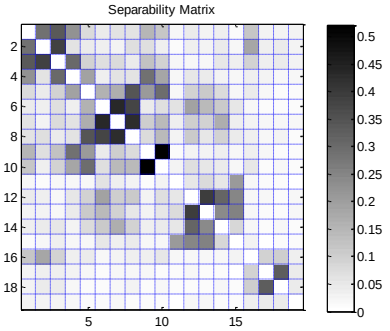

τ=0...15

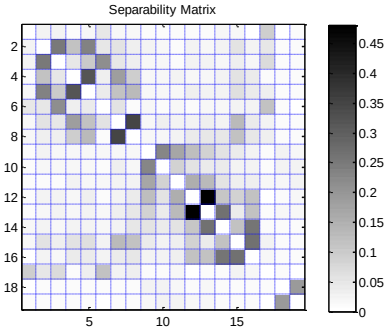

τ=0...20

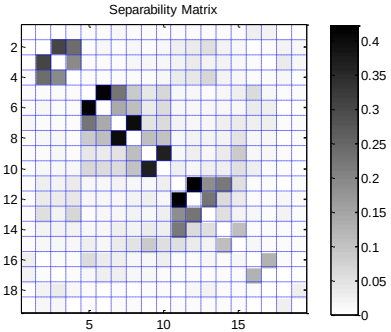

Subject ed τ=0...1

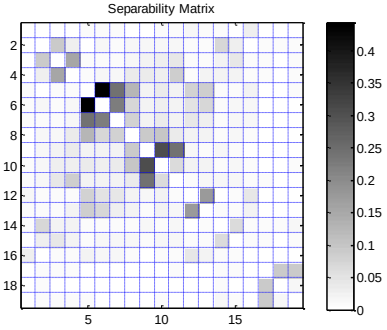

τ=0...5

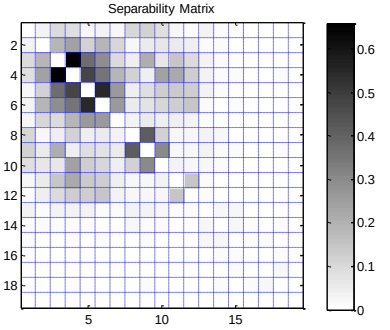

τ=0...15

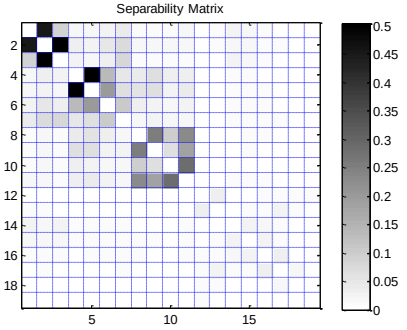

τ=0...20

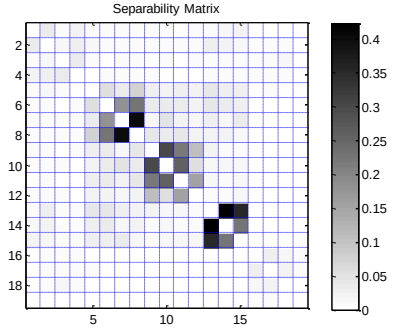

Subject fc τ=0...1

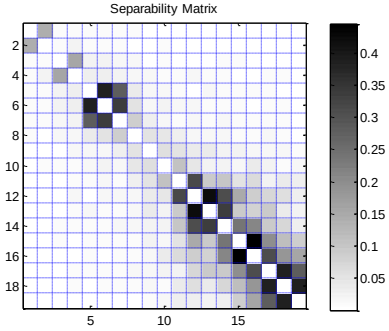

τ=0...5

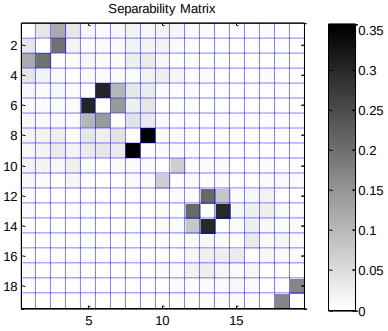

τ=0...15

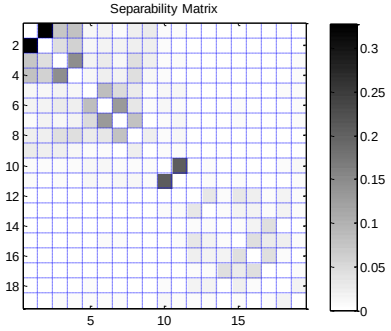

τ=0...20

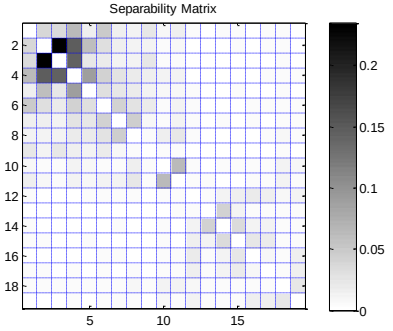

Subject iv τ=0...1

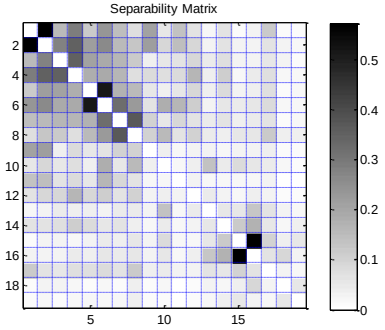

τ=0...5

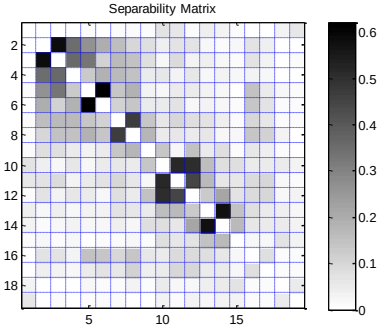

τ=0...15

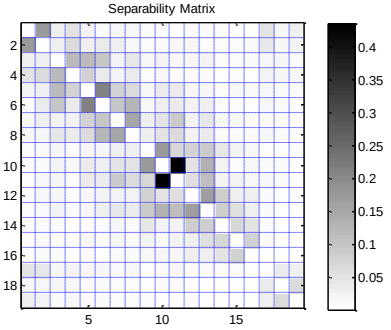

τ=0...20

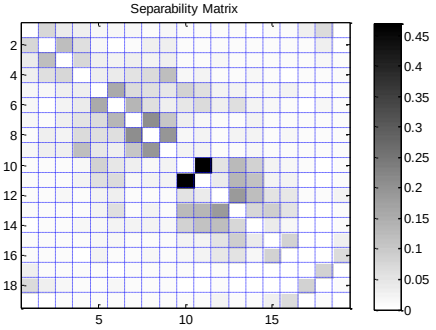

Subject jg τ=0...1

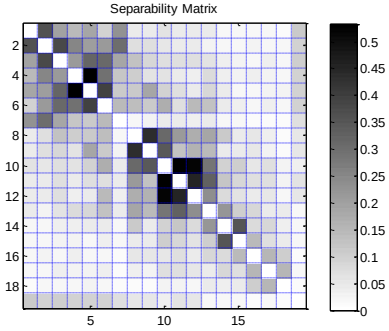

τ=0...5

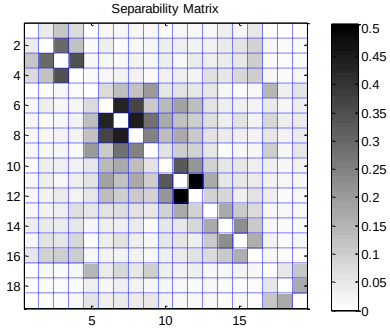

τ=0...15

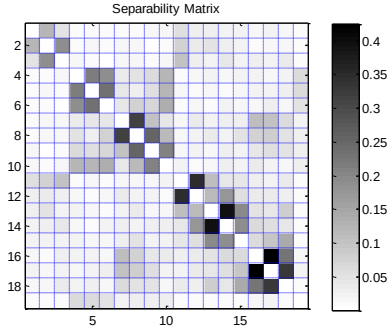

τ=0...20

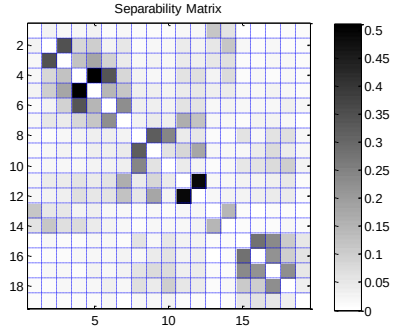

Subject kc τ=0...1

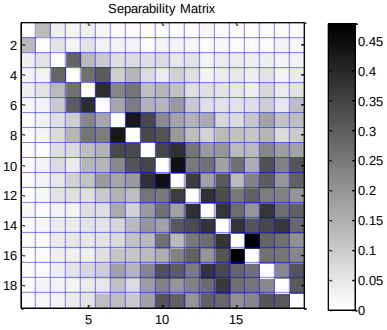

τ=0...5

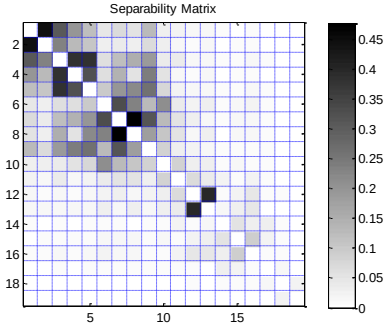

τ=0...15

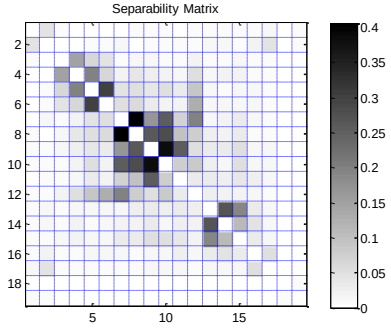

τ=0...20

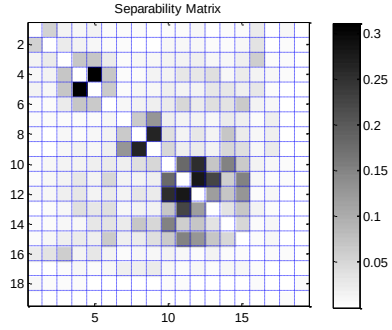

Subject mar2 τ=0...1

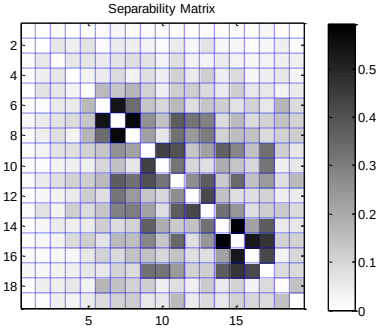

τ=0...5

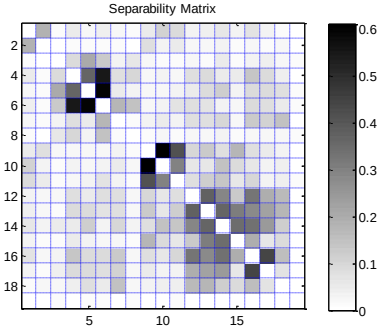

τ=0...15

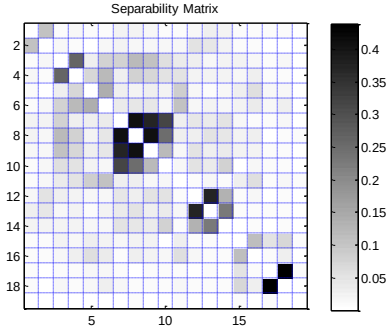

τ=0...20

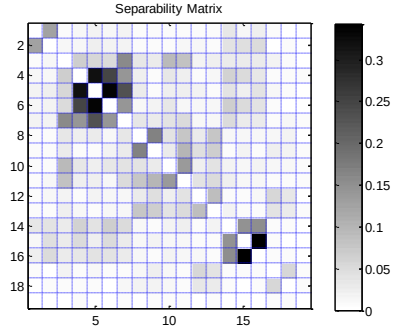

Subject mp τ=0...1

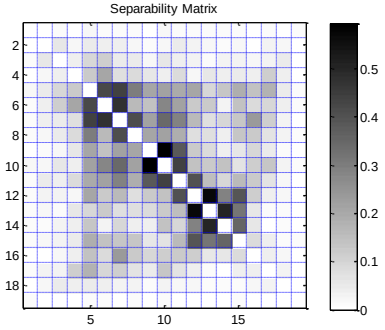

τ=0...5

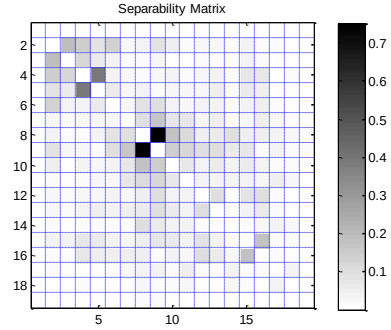

τ=0...15

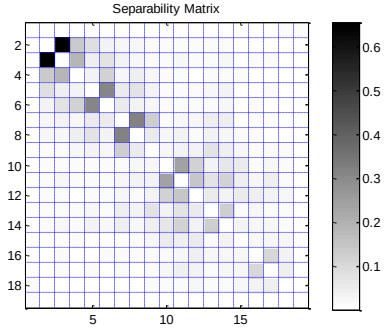

τ=0...20

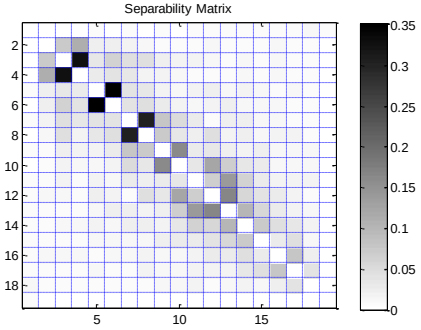

Subject nan τ=0...1

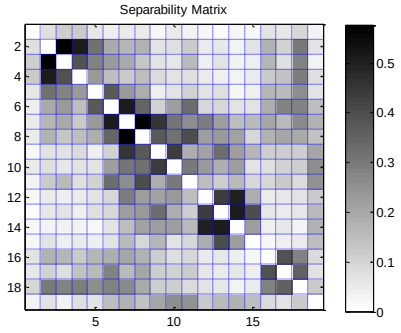

τ=0...5

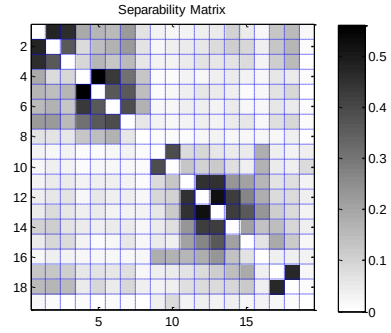

τ=0...15

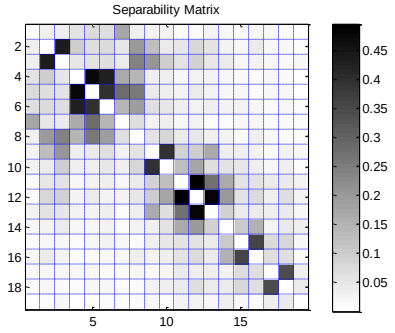

τ=0...20

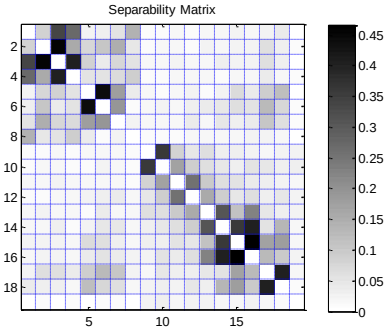

Subject of τ=0...1

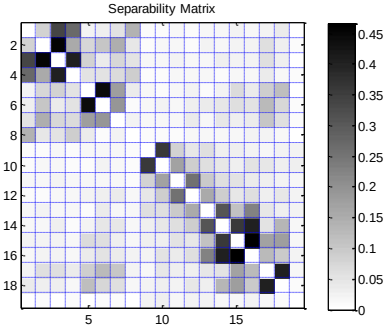

τ=0...5

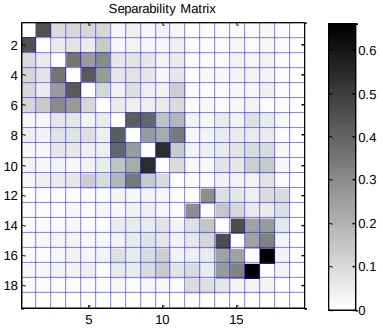

τ=0...15

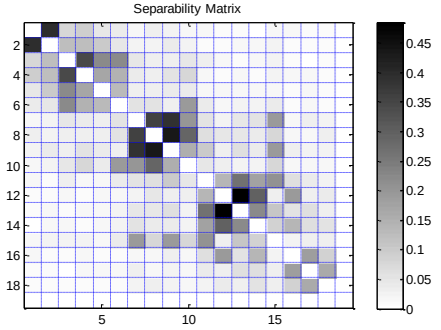

τ=0...20

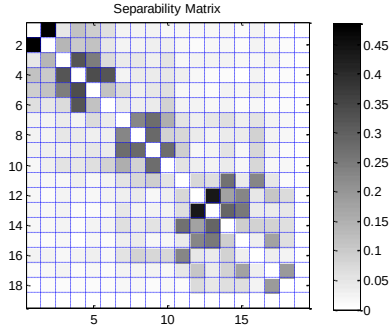

Subject pf τ=0...1

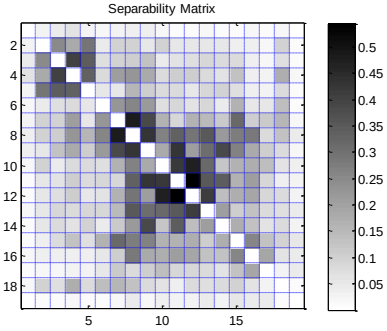

τ=0...5

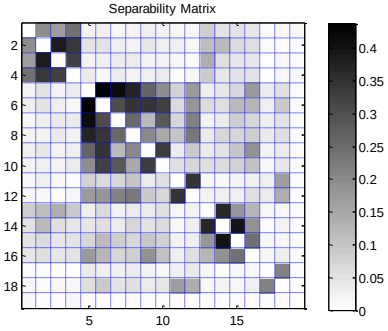

τ=0...15

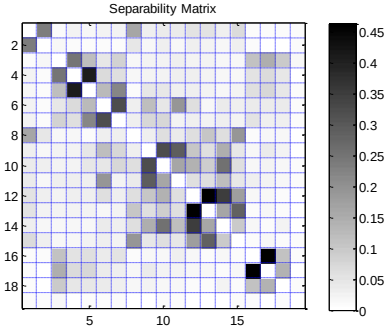

τ=0...20

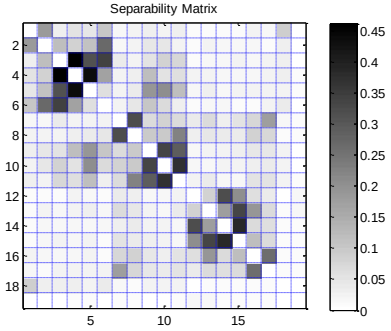

Subject st τ=0...1

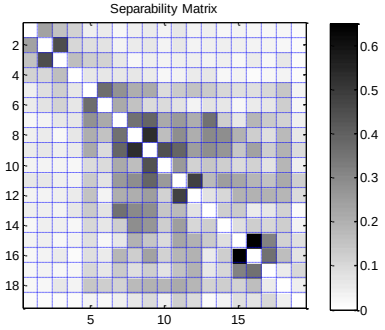

τ=0...5

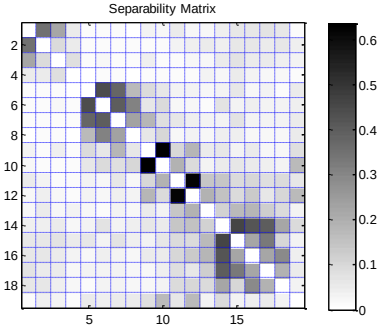

τ=0...15

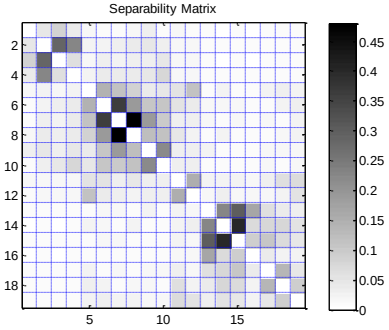

τ=0...20

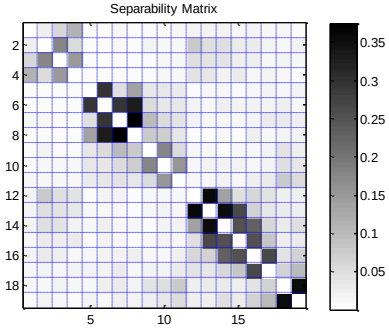

Subject ug τ=0...1

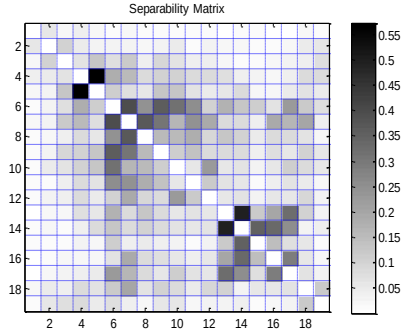

τ=0...5

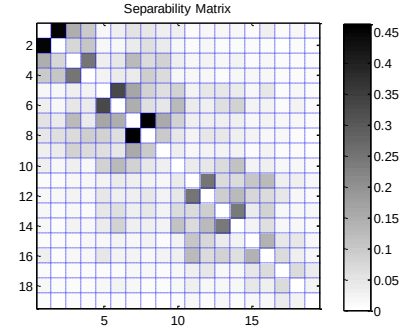

τ=0...15

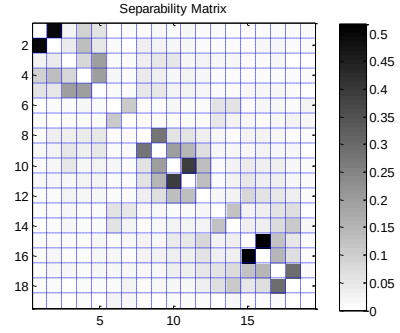

τ=0...20

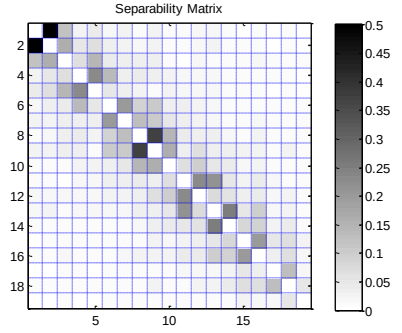

Subject xal τ=0...1

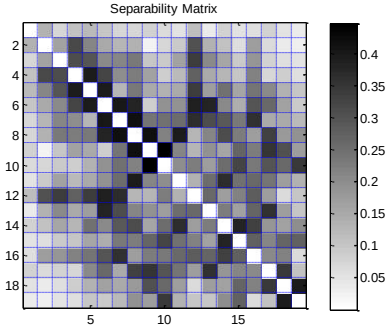

τ=0...5

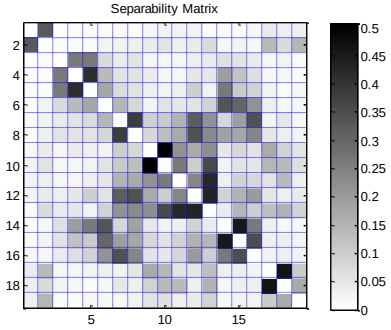

τ=0...15

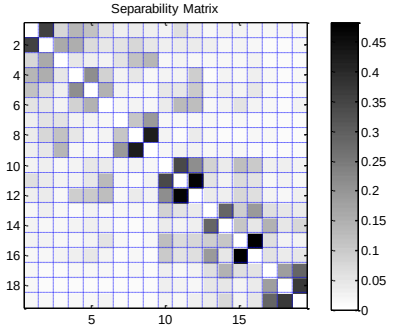

τ=0...20

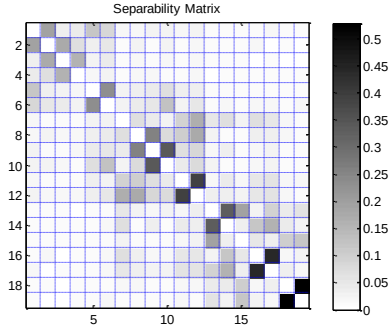

Children with CIs

S1-St1 τ=0...1

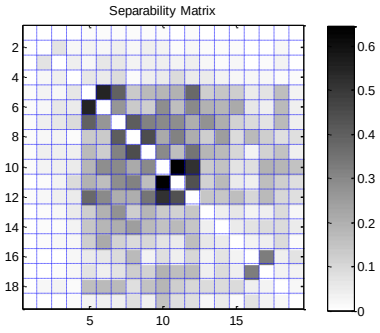

τ=0...5

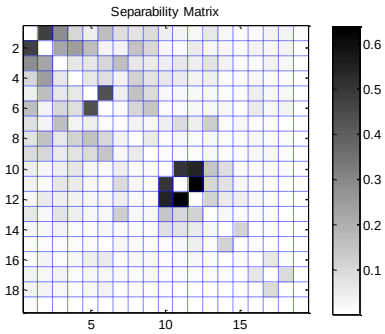

τ=0...15

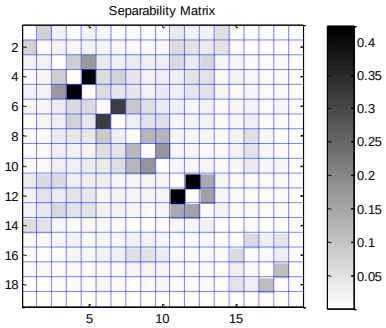

τ=0...20

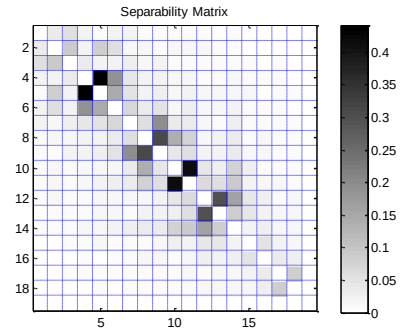

S1-St2 τ=0...1

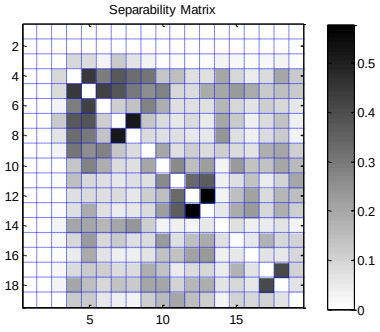

τ=0...5

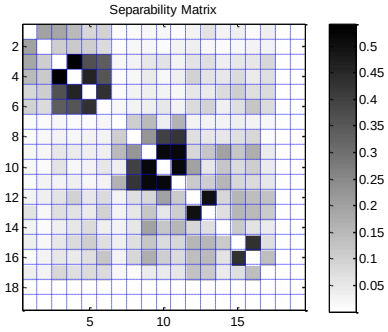

τ=0...15

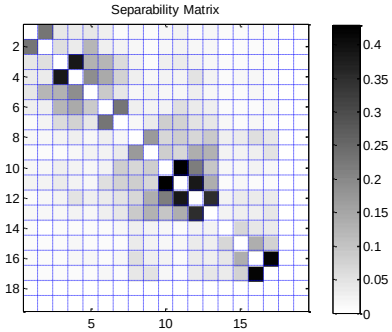

τ=0...20

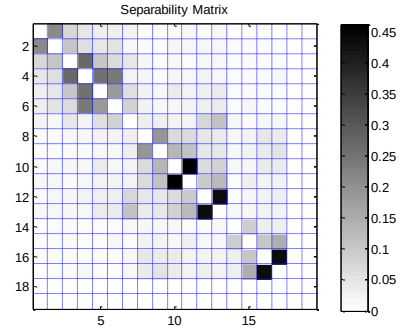

S1-St3 τ=0...1

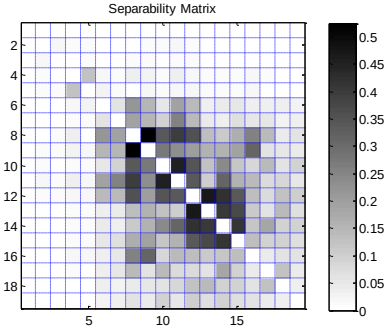

τ=0...5

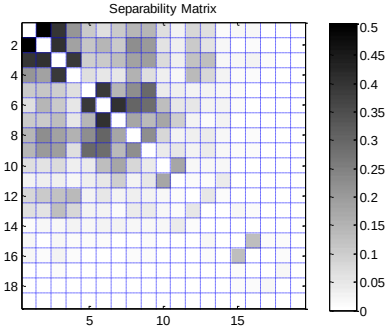

τ=0...15

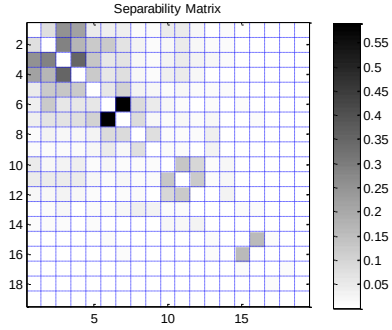

τ=0...20

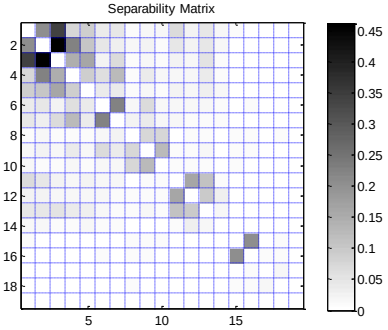

St2-St1 τ=0...1

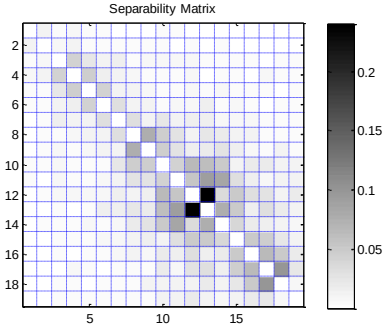

τ=0...5

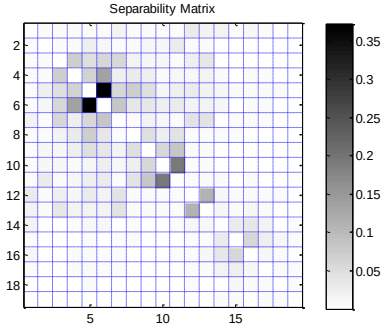

τ=0...15

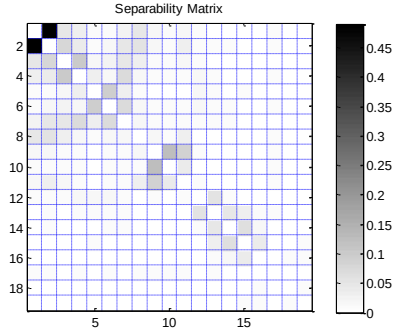

τ=0...20

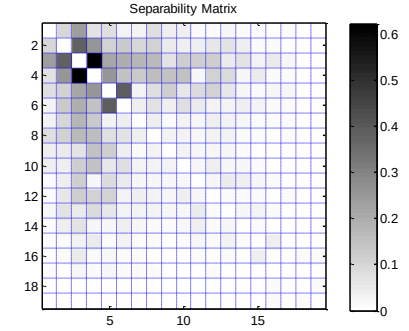

St3-St1 τ=0...1

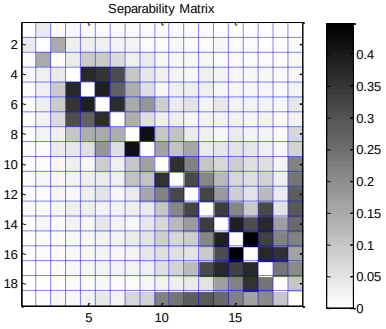

τ=0...5

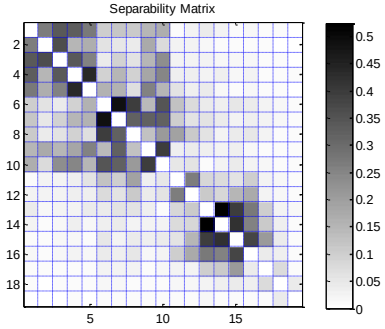

τ=0...15

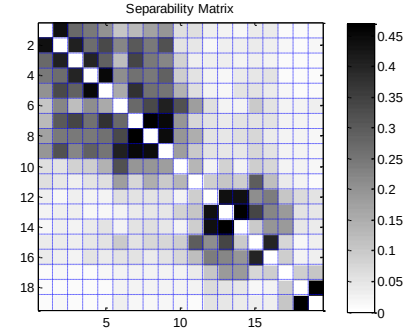

τ=0...20

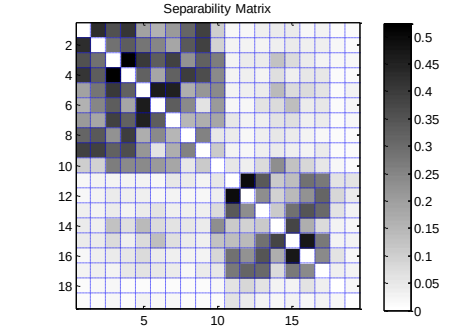

St3-St2 τ=0...1

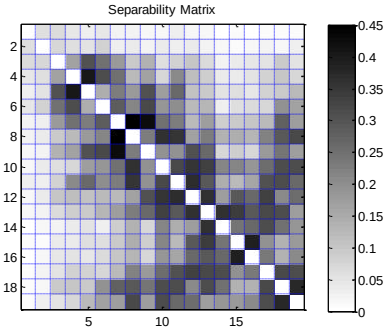

τ=0...5

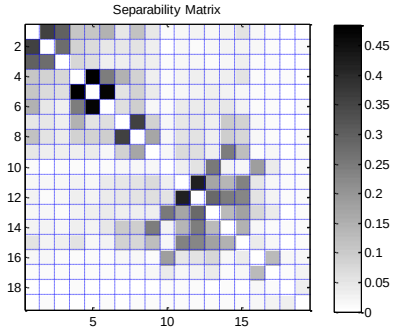

τ=0...15

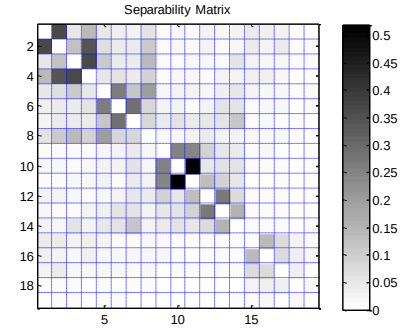

τ=0...20

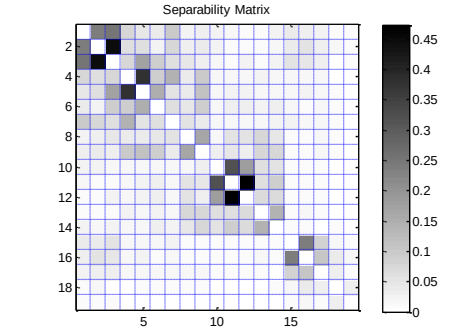

St3-St3 τ=0...1

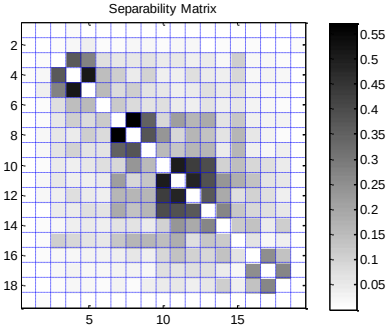

τ=0...5

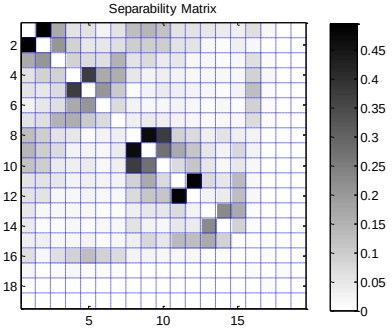

τ=0...15

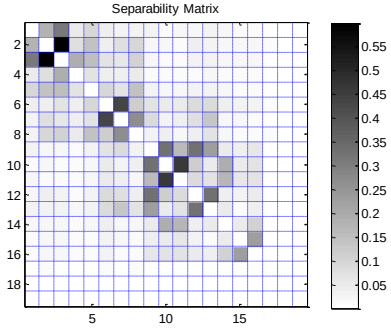

τ=0...20

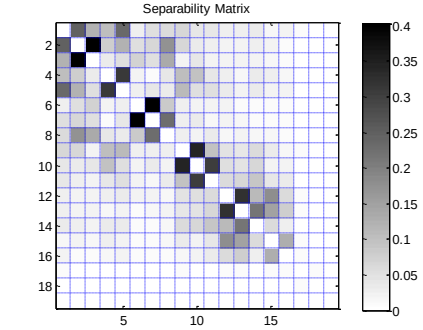

St4-St2 τ=0...1

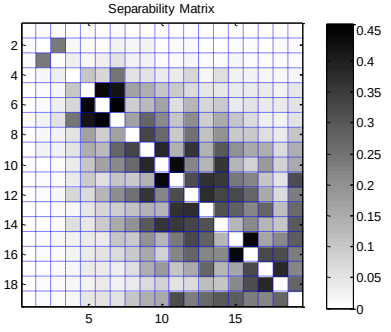

τ=0...5

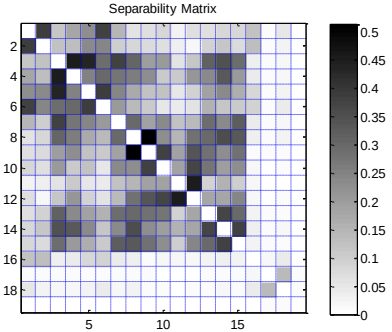

τ=0...15

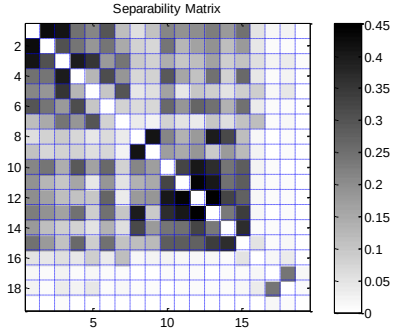

τ=0...20

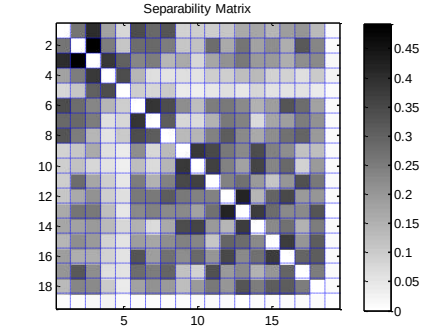

St5-St1 τ=0...1

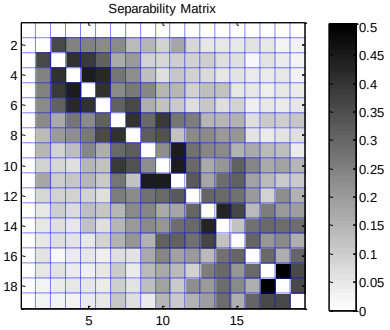

τ=0...5

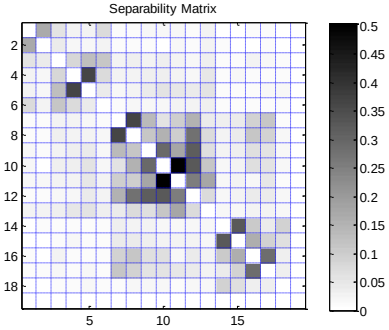

τ=0...15

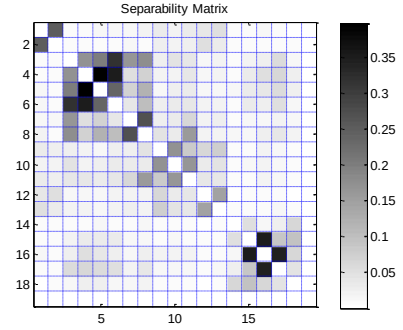

τ=0...20

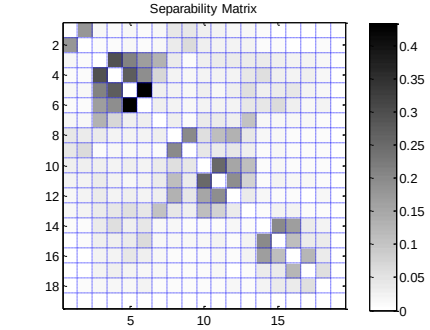

S5-St2 τ=0...1

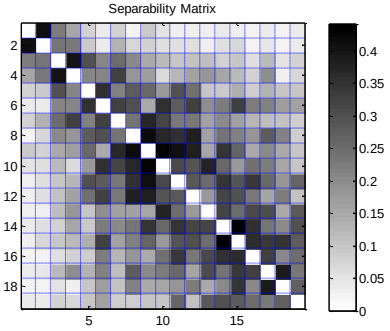

τ=0...5

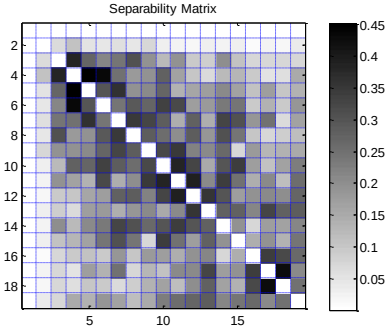

τ=0...15

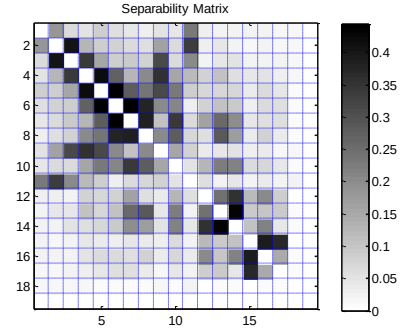

τ=0...20

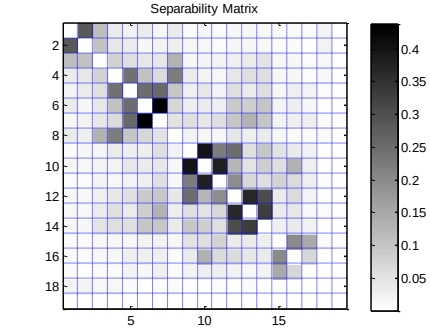

S5-St3 τ=0...1

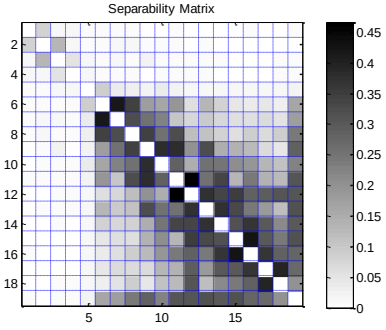

τ=0...5

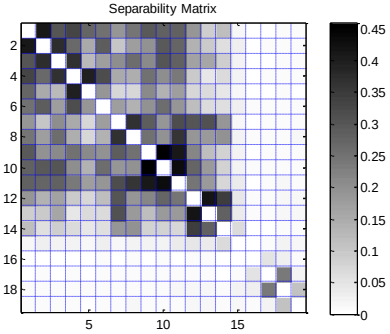

τ=0...15

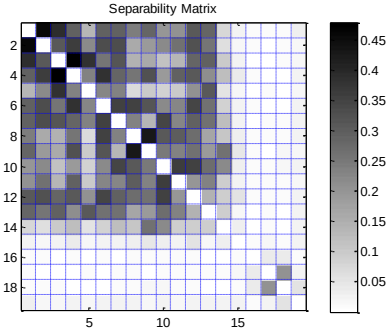

τ=0...20

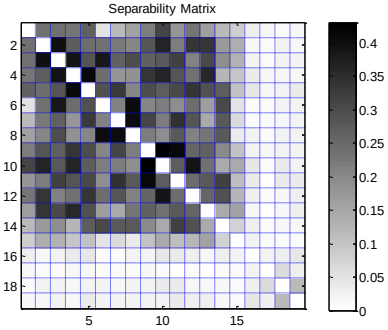

S6-St1 τ=0...1

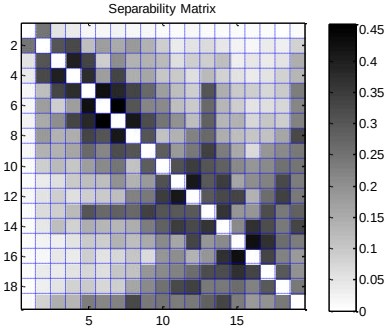

τ=0...5

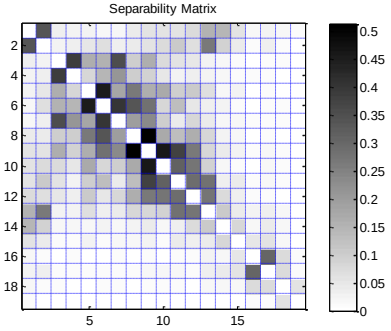

τ=0...15

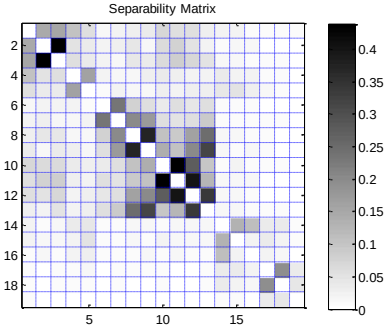

τ=0...20

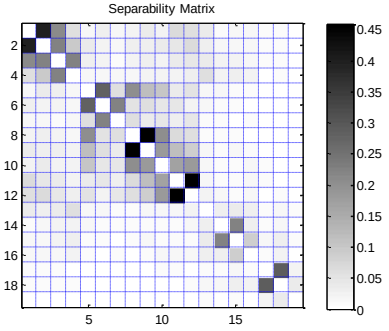

Appendix D Separability matrixes using three ICA algorithms

Normal hearing children

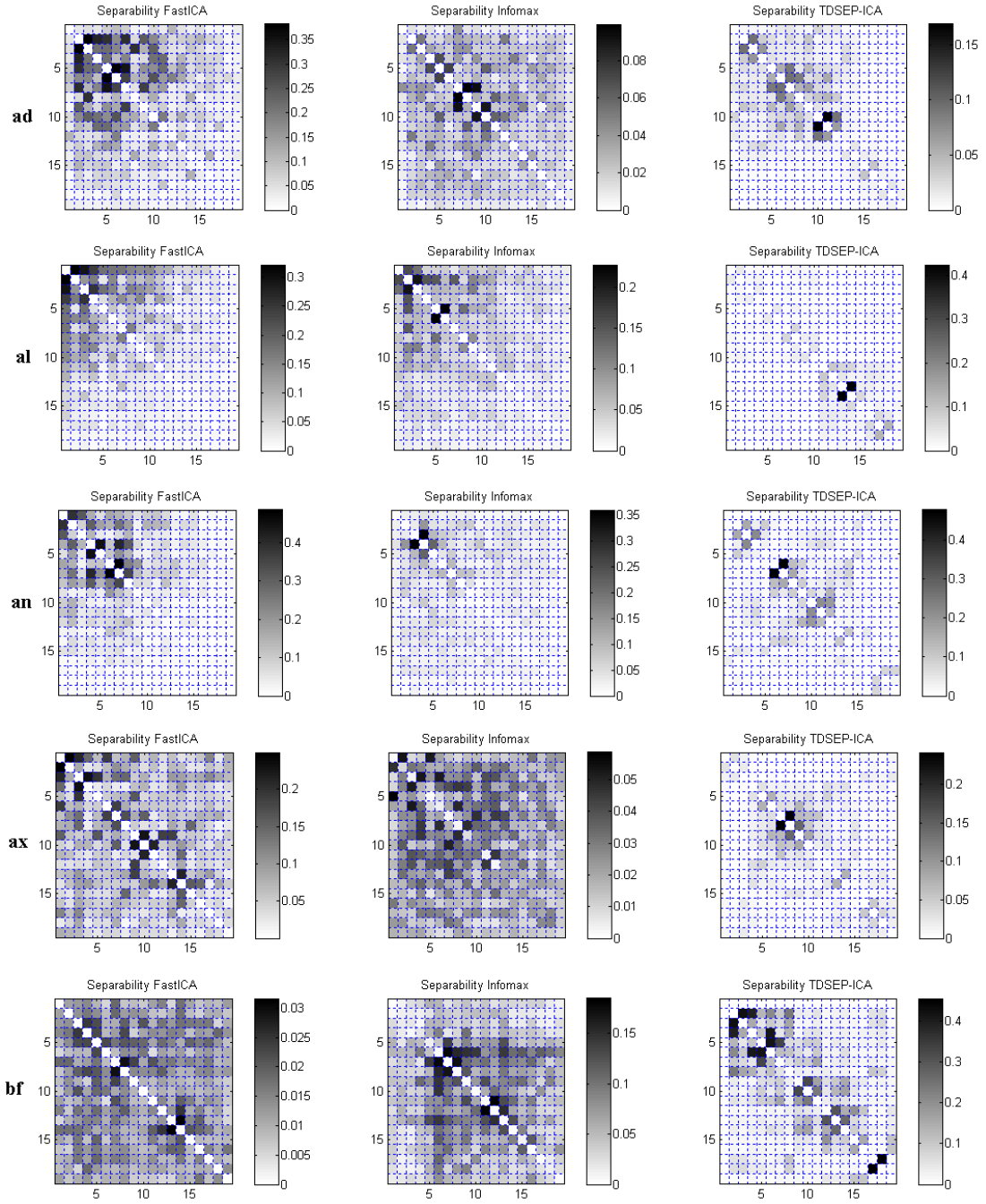

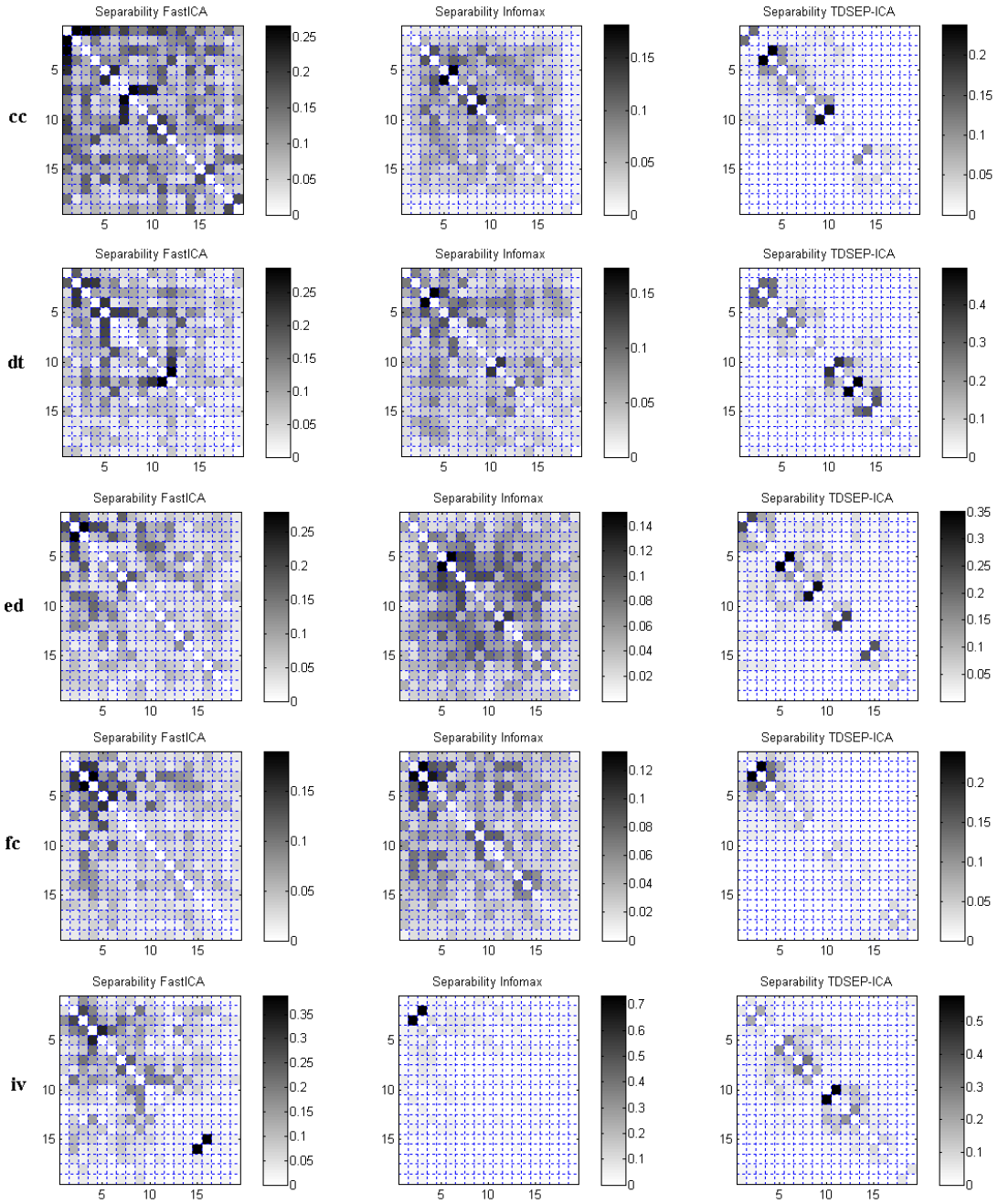
cc
dt
ed
fc
iv
Separability FastICA
Separability Infomax
Separability TDSEP-ICA

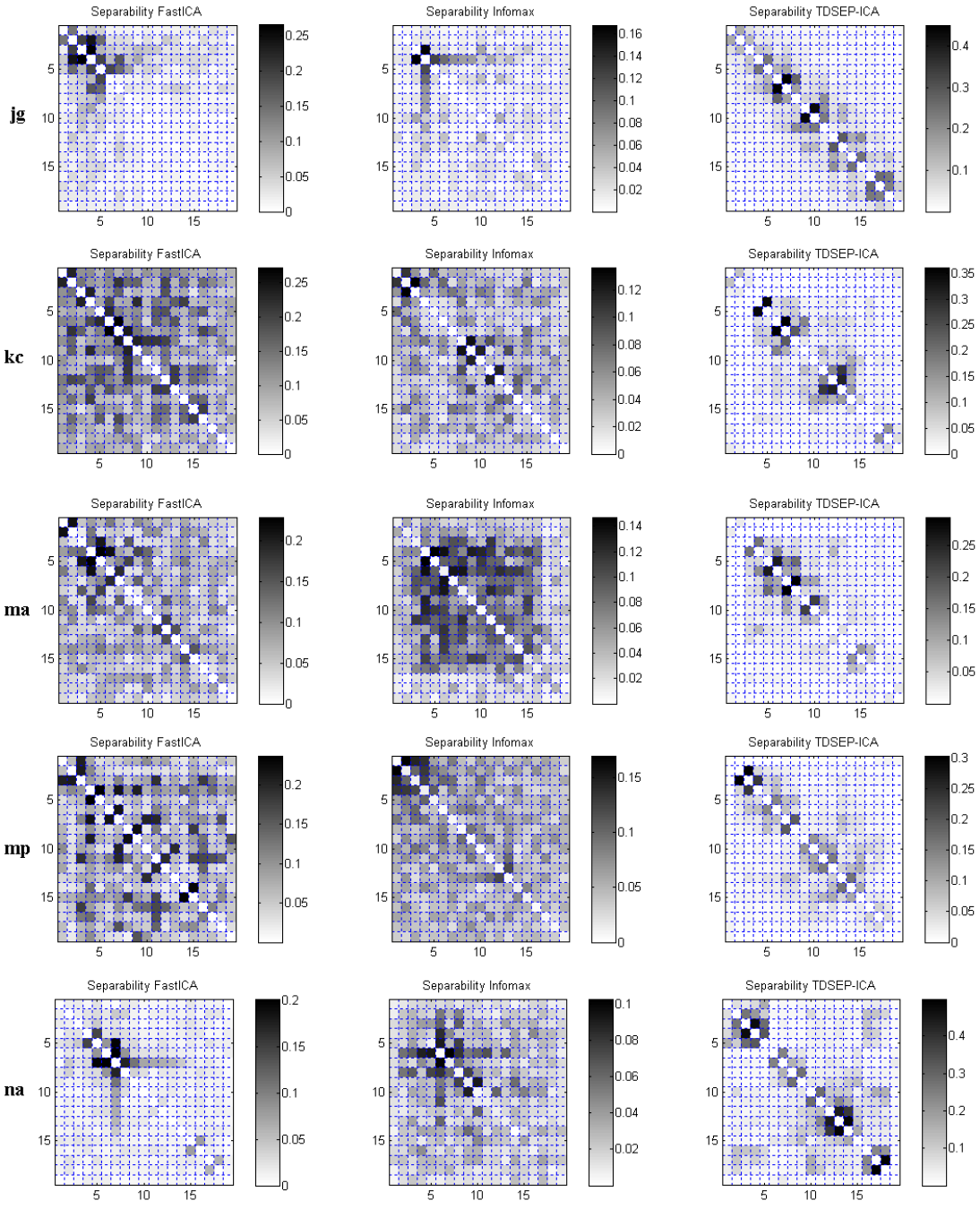
jg
Separability FastICA
Separability Infomax
Separability TDSEP-ICA
kc
Separability FastICA
Separability Infomax
Separability TDSEP-ICA
ma
Separability FastICA
Separability Infomax
Separability TDSEP-ICA
mp
Separability FastICA
Separability Infomax
Separability TDSEP-ICA
na
Separability FastICA
Separability Infomax
Separability TDSEP-ICA

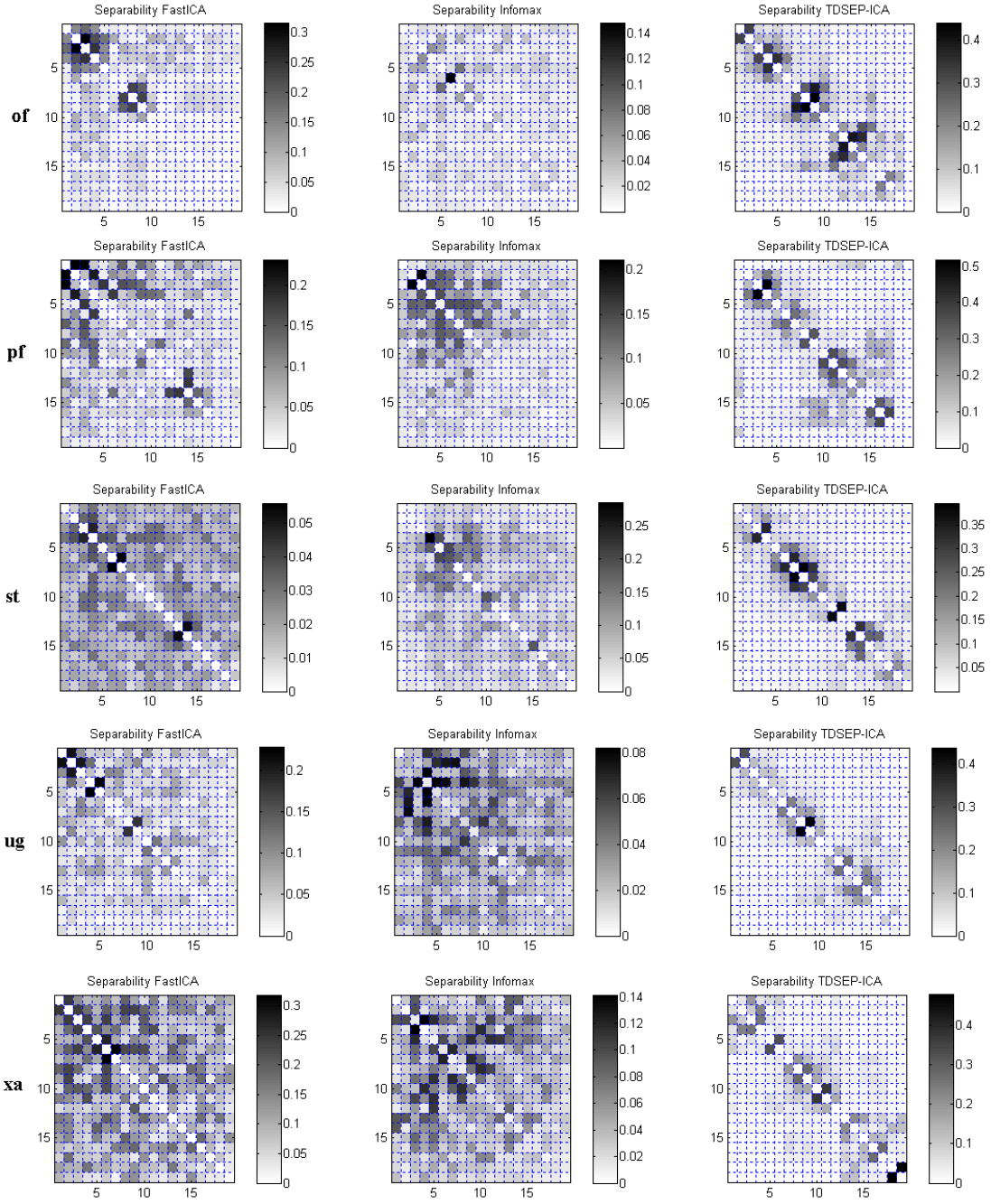
of
pf
st
ug
xa
Separability FastICA
Separability Infomax
Separability TDSEP-ICA

Children with CIs

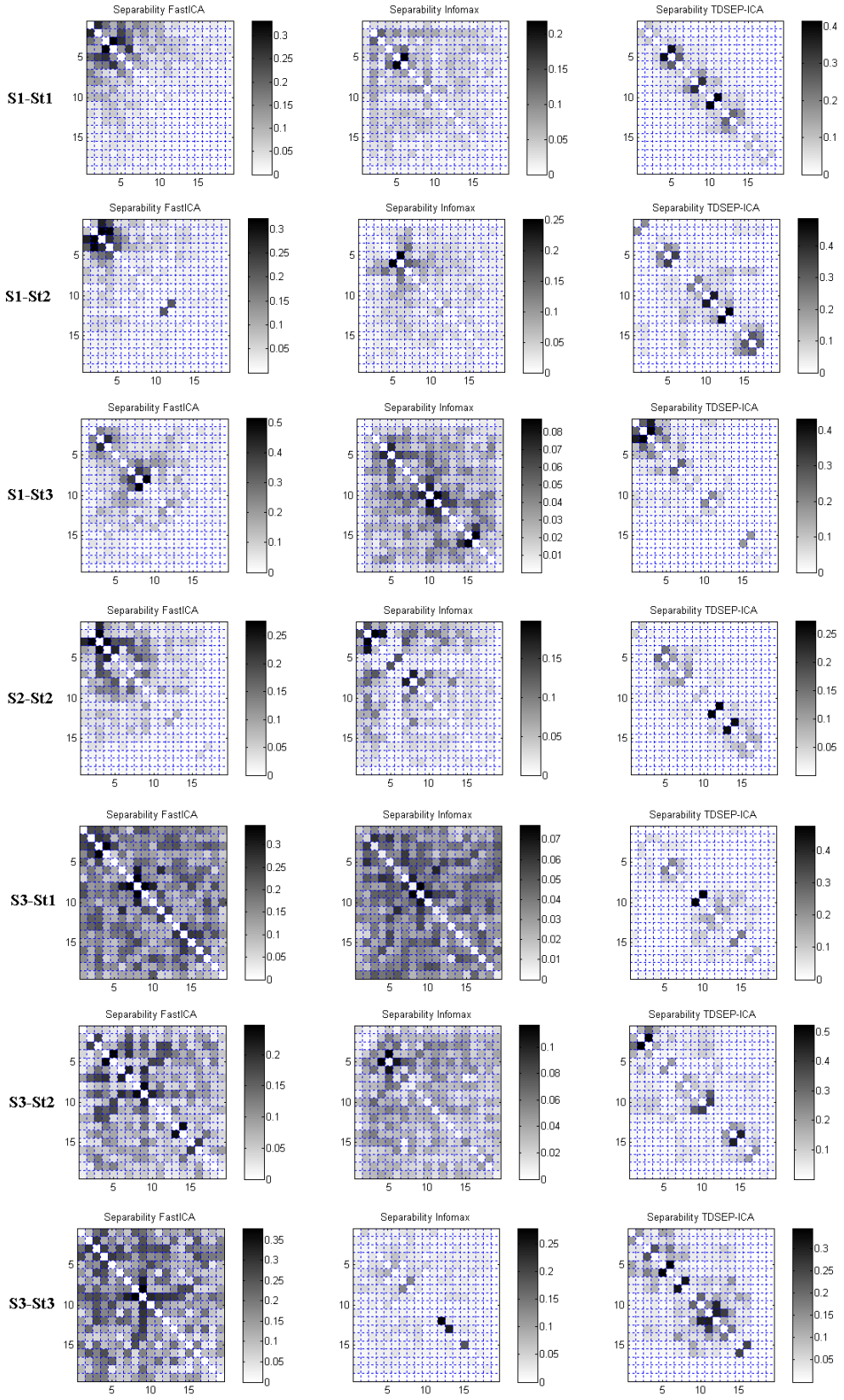

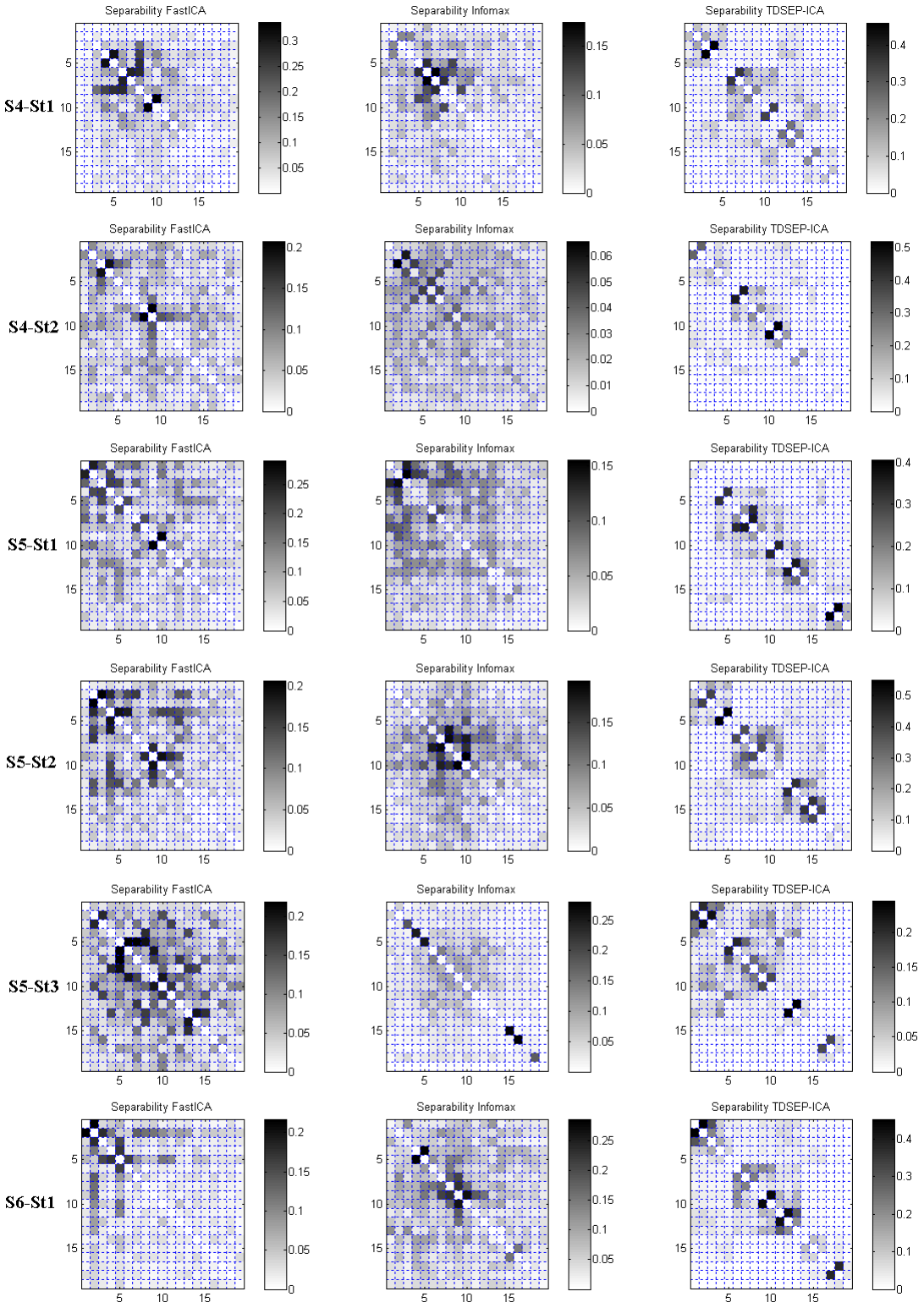
S4-St1
Separability FastICA
Separability Infomax
Separability TDSEP-ICA
S4-St2
Separability FastICA
Separability Infomax
Separability TDSEP-ICA
S5-St1
Separability FastICA
Separability Infomax
Separability TDSEP-ICA
S5-St2
Separability FastICA
Separability Infomax
Separability TDSEP-ICA
S5-St3
Separability FastICA
Separability Infomax
Separability TDSEP-ICA
S6-St1
Separability FastICA
Separability Infomax
Separability TDSEP-ICA

Appendix E. ICs recovered using *TDSEP-ICA* with time delays up to 90.

This appendix includes the ICs recovered using *TDSEP-ICA* with a time delay higher than 20, up to 90. Recordings from two children with CIs are included; the ICs recovered do not have significant differences.

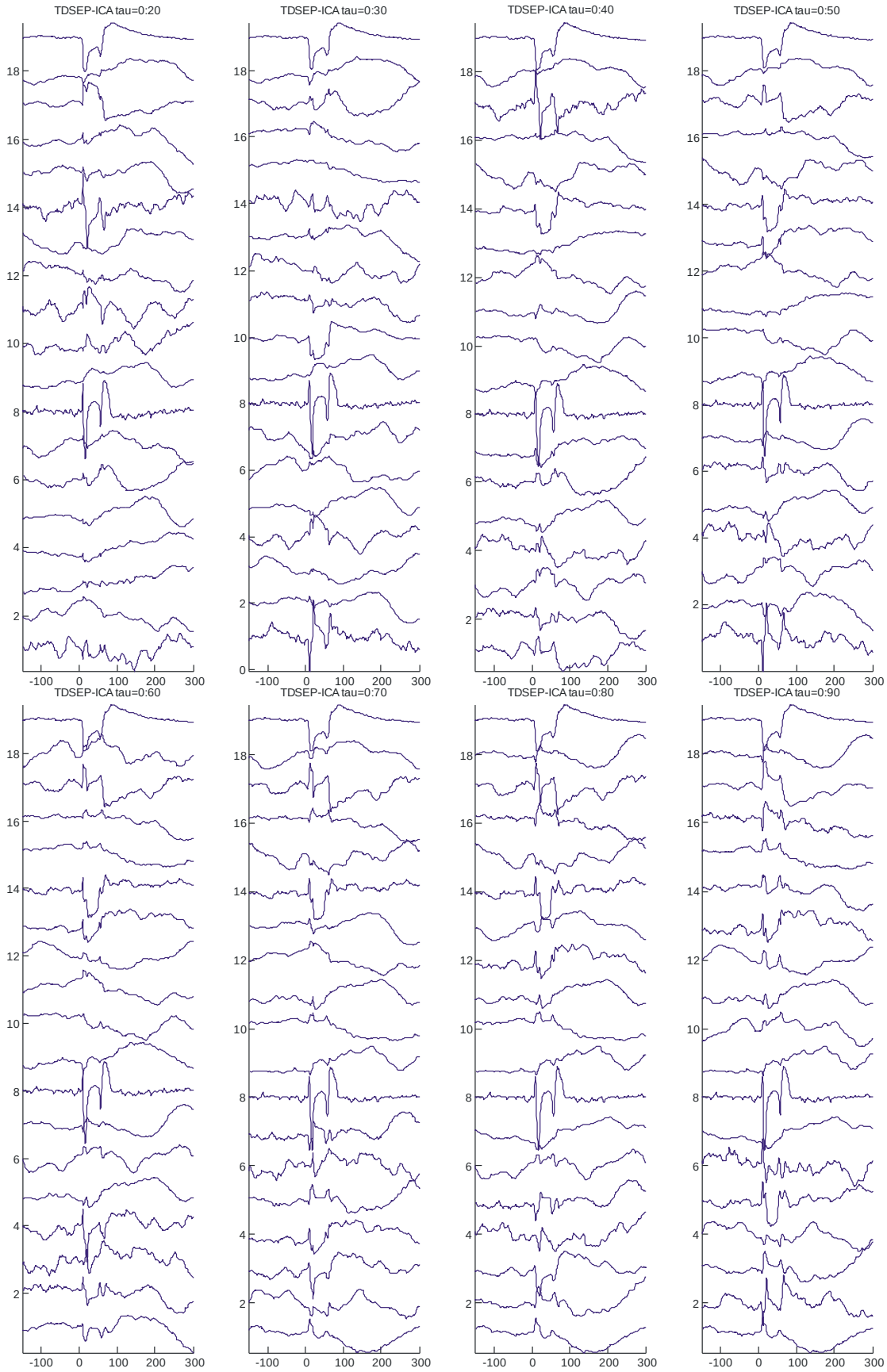

Figure E.1 Recording S5-St1, (female CI user), ICs recovered by *TDSEP-ICA* with time delays higher than 20.

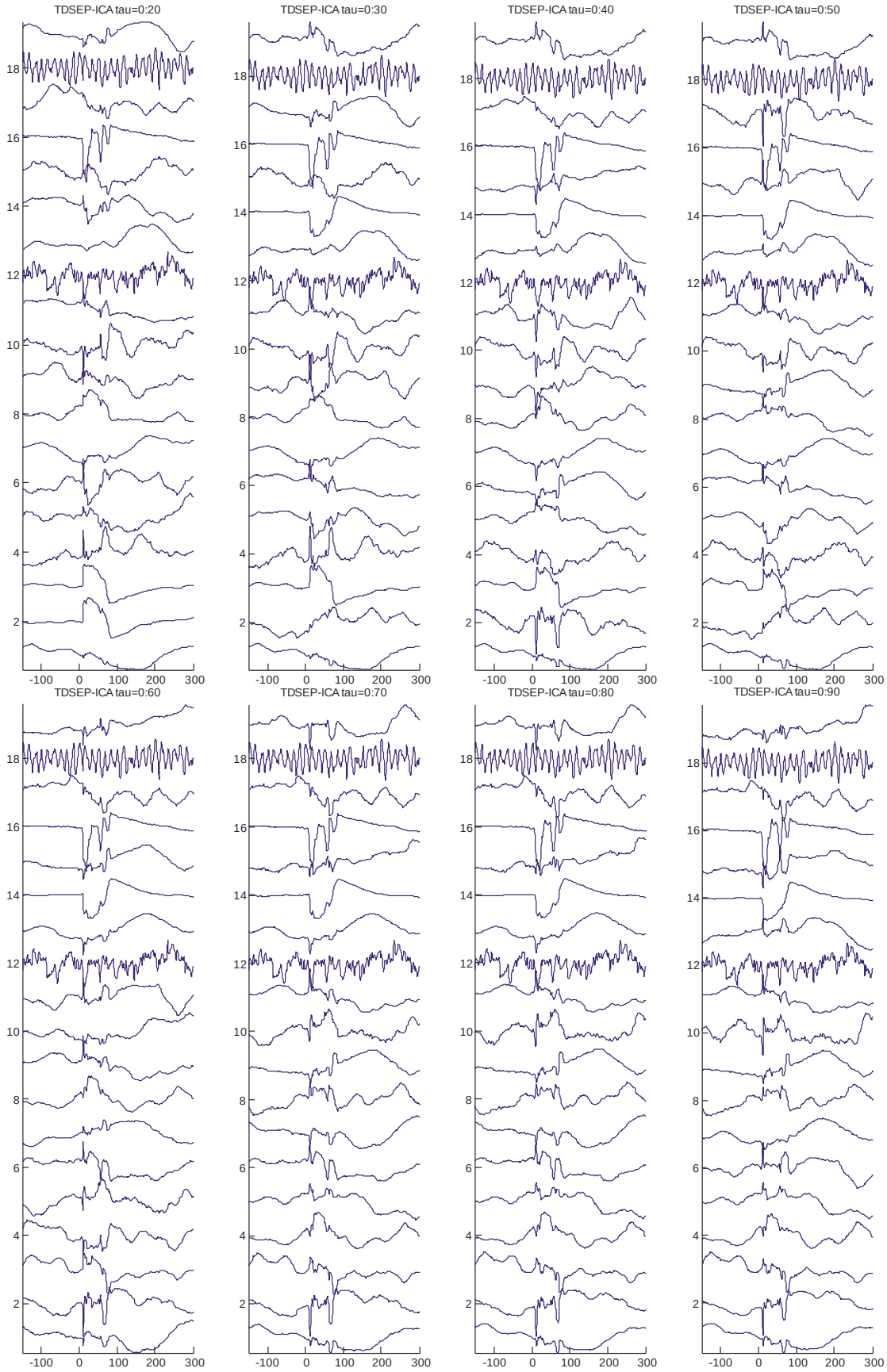

Figure E.2 Recording S3-St3, (male CI user), ICs recovered by *TDSEP-ICA* with time delays higher than 20.

Appendix F. *SIR* index values

Table F.1. *SIR* index values for basal recordings (without acoustic stimulation) using the AEP as reference signal. The *SIR* average for the three algorithms is $SIR_{average}$=0.65946±0.084521

Basal recordings	*FastICA*	*Ext-Infomax*	*TDSEP-ICA*
1	0.73	0.42	0.69
2	0.55	0.78	0.98
3	0.42	0.48	0.30
4	0.49	0.65	0.51
5	0.47	0.58	0.45
6	0.49	0.34	0.51
7	0.62	1.21	1.47
8	0.39	0.71	0.68
9	0.78	0.35	0.46
10	0.85	0.84	0.33
11	1.28	0.54	2.80
12	0.38	0.53	1.09
13	0.30	0.40	0.53
14	0.28	0.31	0.27
15	0.53	0.37	0.56
16	0.75	0.38	0.63
17	0.59	0.96	0.92
18	0.88	0.57	0.55
19	0.48	0.28	0.63
20	0.92	1.56	0.79
SIR	0.61±0.14	0.61±0.23	0.76±0.35

Table F.2. *SIR* index values for recordings from normal hearing children recordings using the CI artifact as reference signal. The *SIR* average for the three algorithms is $SIR_{average}$=0.515583±0.045662

NH recordings	*FastICA*	*Ext-Infomax*	*TDSEP-ICA*
1	0.46	0.46	0.49
2	0.56	0.34	0.30
3	1.02	0.56	0.69
4	0.22	0.18	0.33
5	0.14	0.14	0.15
6	0.59	0.59	0.57
7	0.76	0.75	0.35
8	0.17	0.18	0.16
9	0.72	0.73	0.31
10	0.26	0.38	0.72
11	0.98	0.38	0.37
12	0.94	1.31	0.55
13	0.29	0.48	0.41
14	0.21	0.36	0.32
15	0.54	0.57	0.38
16	0.57	0.60	0.29
17	0.37	0.51	0.68
18	0.75	1.12	0.93
19	0.57	0.40	0.26
20	0.56	0.41	0.26
21	0.56	0.62	0.84
22	0.87	0.63	0.84
SIR	0.55±0.27	0.53±0.28	0.46±0.23

Appendix G. Artifactual ICs and De-noised signals

The first part of this appendix includes the artifactual ICs identified in the recordings from children with CIs, using *TDSEP-ICA* (τ=0,1,2,…,20). The principal artifact recovered were those related to the CI artifact and noisy electrodes. The columns of the mixing matrix corresponding to those components were made zero to generate the de-noised signal. Additionally, both the original and the de-noised signal after removing those artifacts are shown. In most of the de-noised signal P_1 peak can be observed; those signals were used in source analysis of P_1.

Artifactual ICs

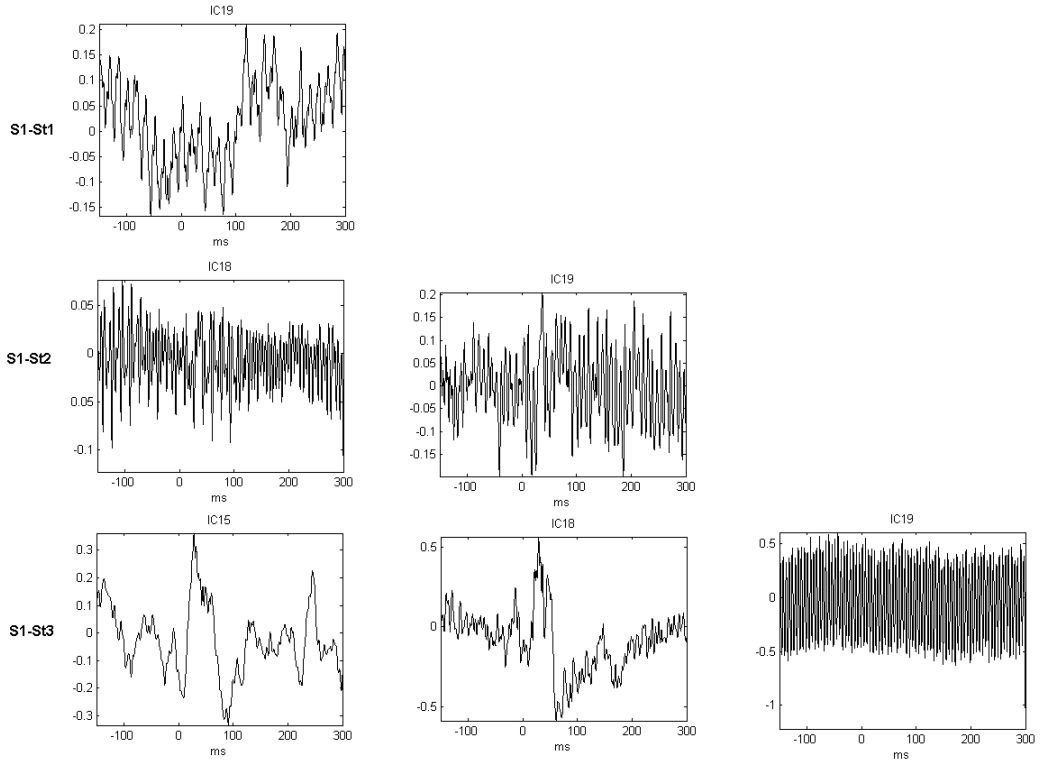

Figure G.1 Subject 1 (male, age of implantation: 8y 3m), in both recordings S1-St1 and S1-St2 the electrodes around the CI were not connected. The ICs removed correspond to noisy electrodes and with the CI artifact (S1-St3).

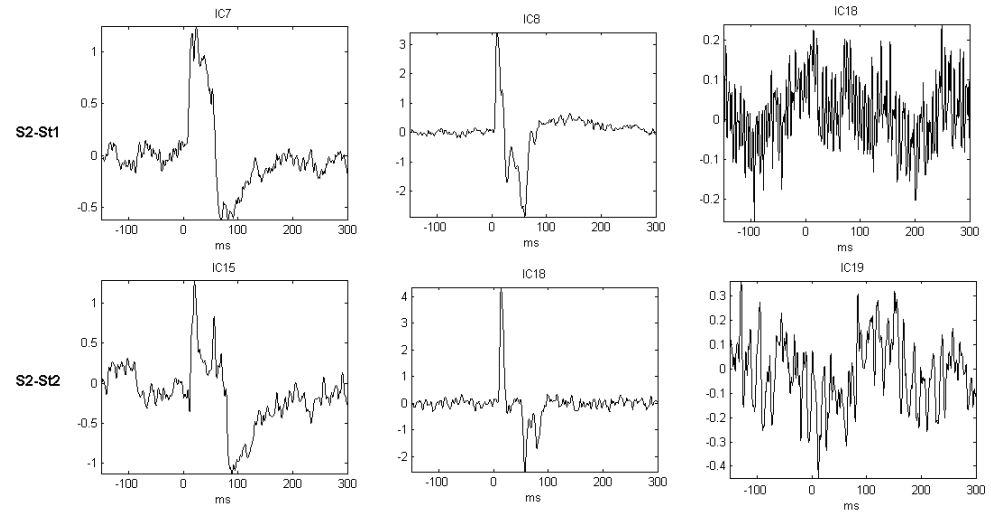

Figure G.2 In both recordings of subject S2 (female, age of implantation: 10y 5m), two components of the CI artifact and noisy electrodes were removed.

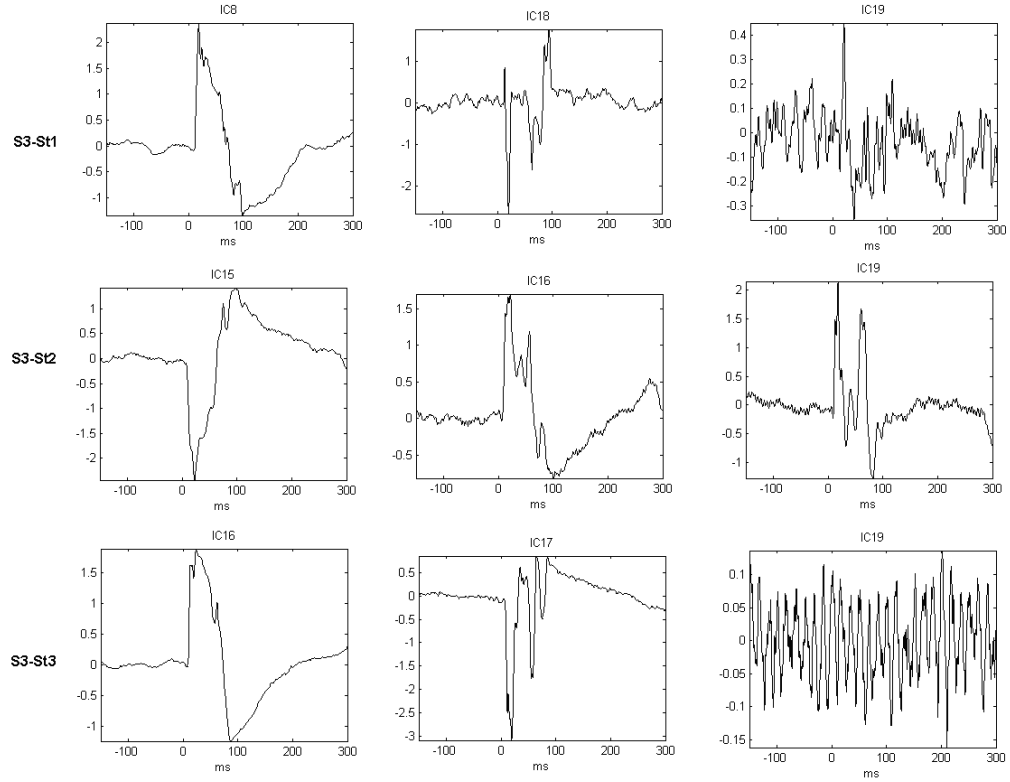

Figure G.3 Two or three components related to the CI artifact and noise were removed from the subject S3 recordings (male, age of implantation: 7y 1m).

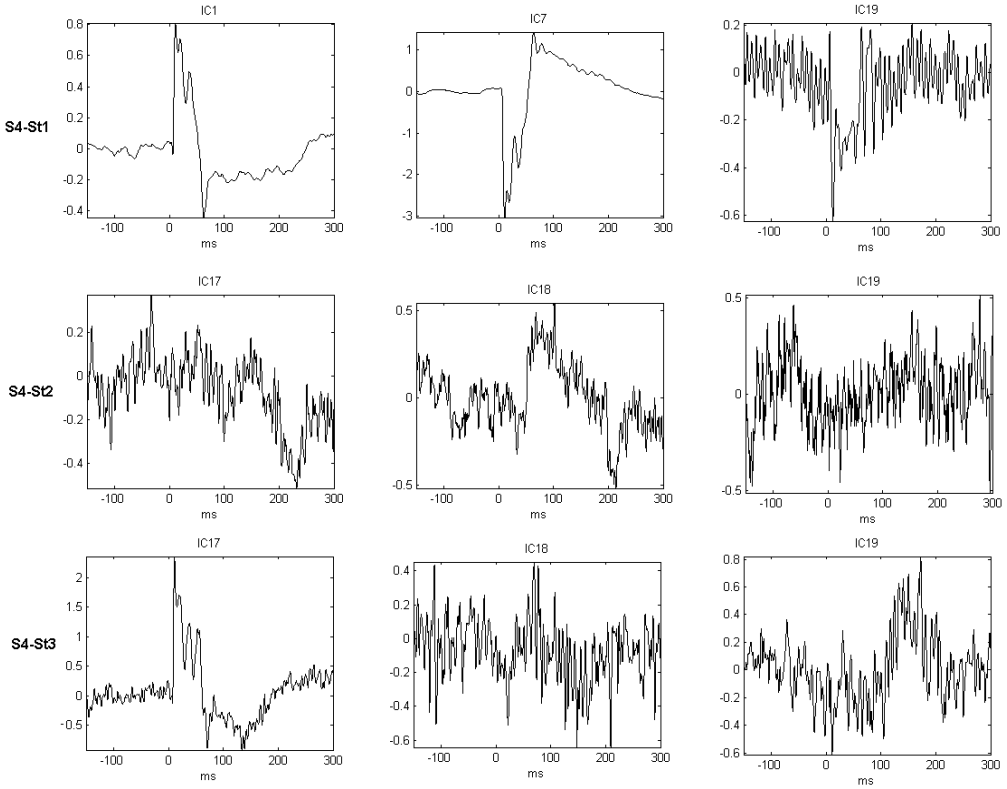

Figure G.4 In subject 4 (female, age of implantation: 3y 8m) the ICs related to the CI artifact and noise were removed from the original AEP signal.

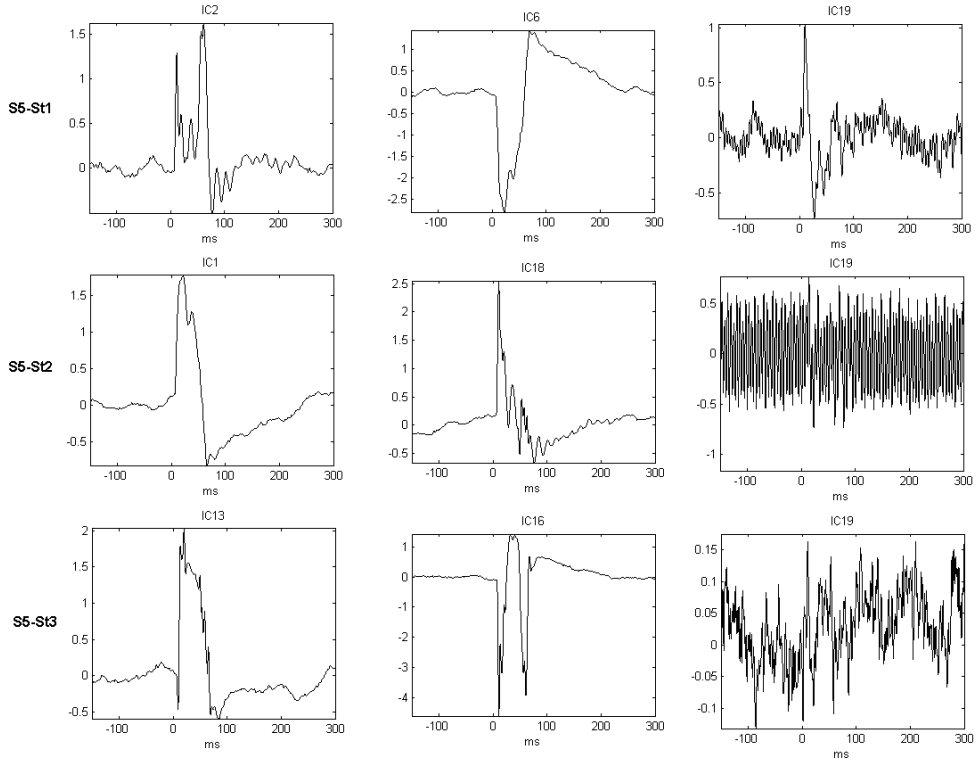

Figure G.5 From two to three components related to the CI artifact and noisy electrodes were eliminated from the AEP recording in subject S5 (male, age of implantation: 4y 5m).

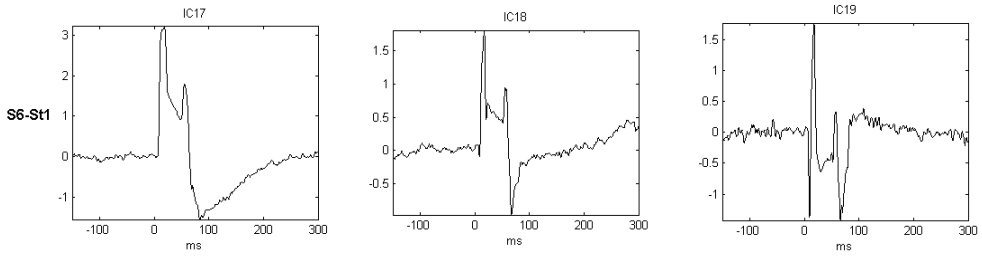

Figure G.6 Three ICs related to the CI artifact were removed from the AEP recordings in subject S6 (female, 4y 2m).

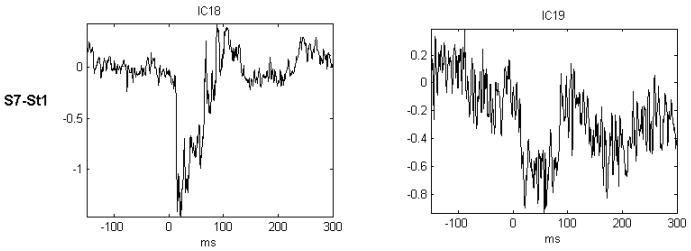

Figure G.7 ICs related to the CI and noisy electrodes were eliminated from the AEP recordings in subject S7 (female).

De-noised Signals

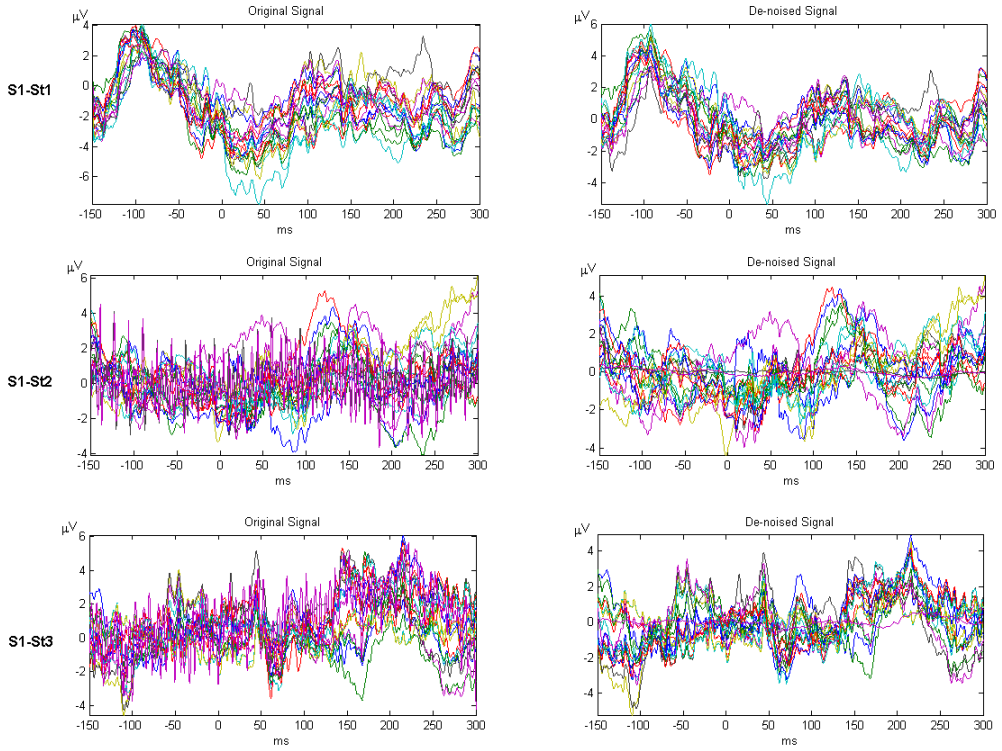

Figure G.8 Butterfly plots of both the original signal (left column) and the signal after removing the ICs associated with the CI artifact and noisy electrodes (right column). S1, male, recordings at 5 months , 1 year and 2 years and 6 months after implantation (St1, St2 and St3, respectively).

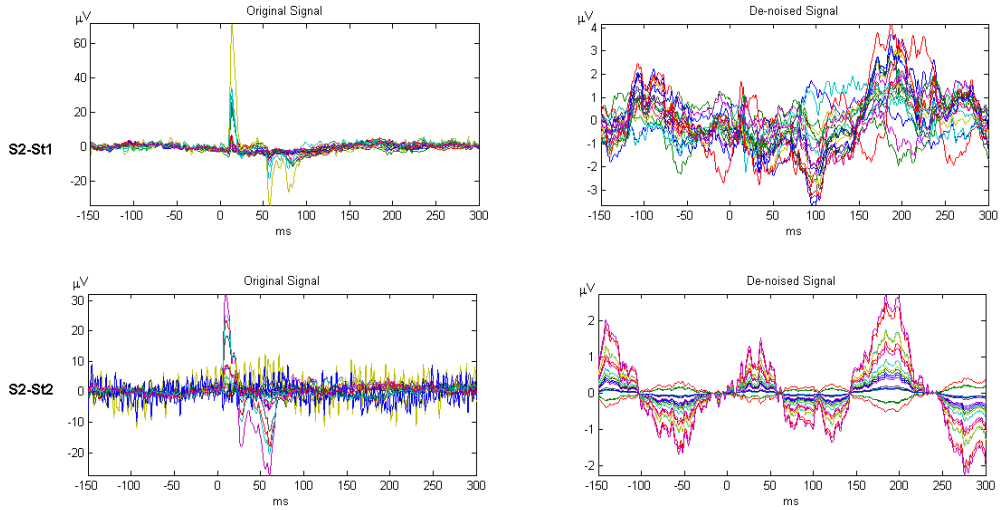

Figure G.9 Butterfly plots of both the original signal (left column) and the signal after removing the ICs related to two components of the CI artifact and noisy electrodes (right column). S2, female, recordings at 3 months and 9 months after implantation (St1 and St2, respectively).

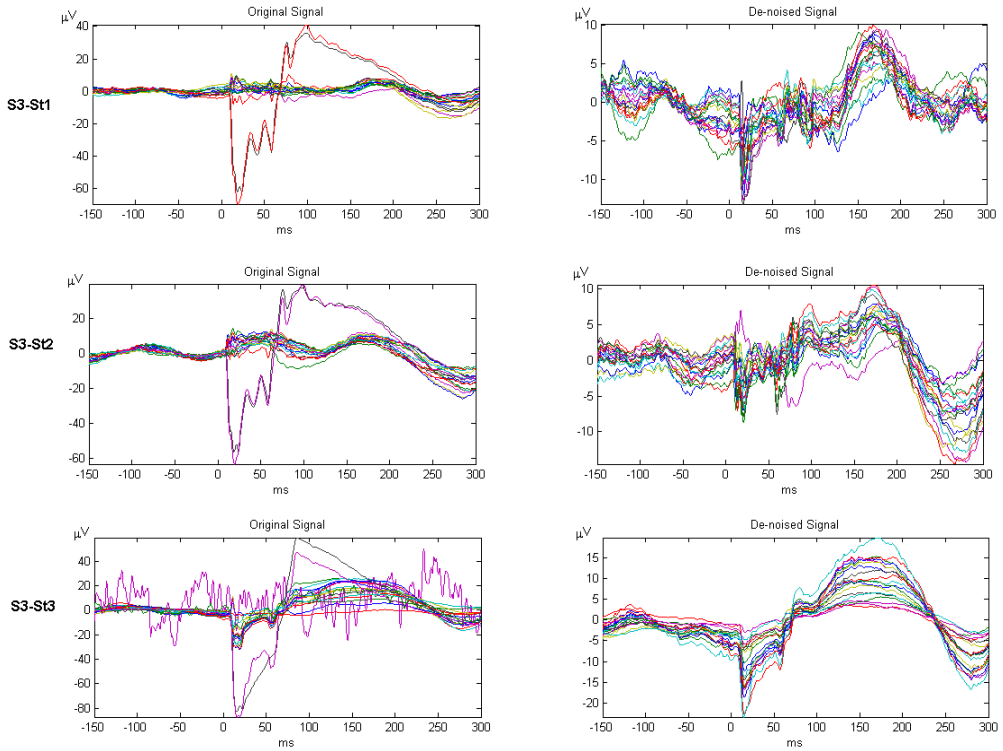

Figure G.10 Butterfly plots of both the original signal (left column) and the signal after removing the ICs related to two components of the CI artifact and noisy electrodes (right column). S3, male, recordings at 1 year, 1 year and 8 months and 5 year and 5 months after implantation (St1, St2 and St3, respectively).

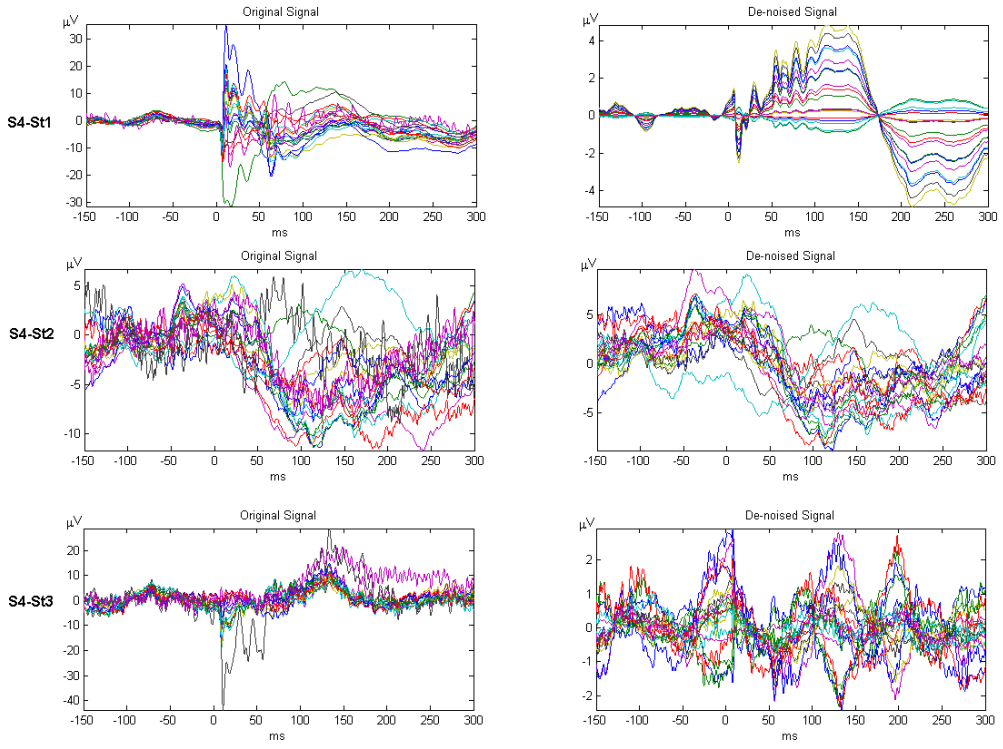

Figure G.11 Butterfly plots of both the original signal (left column) and the signal after removing the ICs related to two components of the CI artifact and noisy electrodes (right column). S4, female, recordings at 8 months, 1 year and 1 month and 1 year and 6 months after implantation (St1, St2 and St3, respectively).

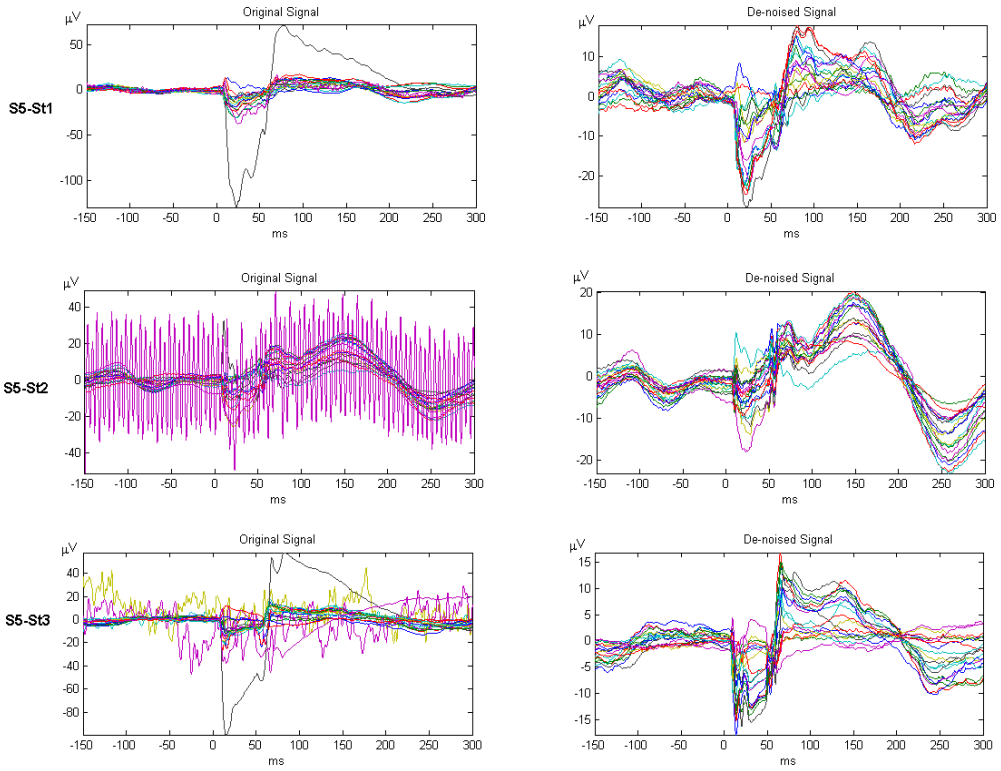

Figure G.12 Butterfly plots of both the original signal (left column) and the signal after removing the ICs related to two components of the CI artifact and noisy electrodes (de-noised signal, right column). S5, male, recordings at 1 year and 9 months, 2 year and 8 months and 5 years and 1 month after implantation (St1, St2 and St3, respectively).

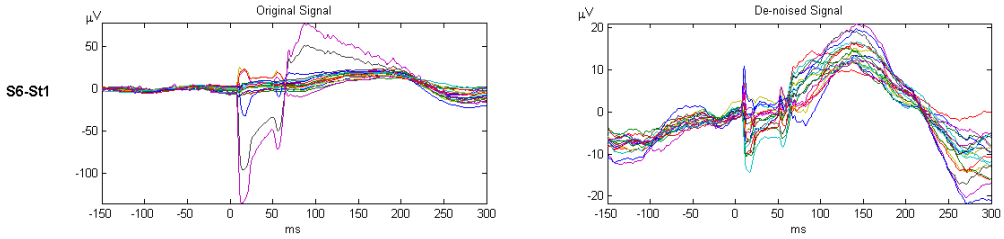

Figure G.13 Butterfly plots of both the original signal (left column) and the signal after removing the ICs related to two components of the CI artifact (right column). S6, female, recording St1 at 2 year and 5 months after implantation.

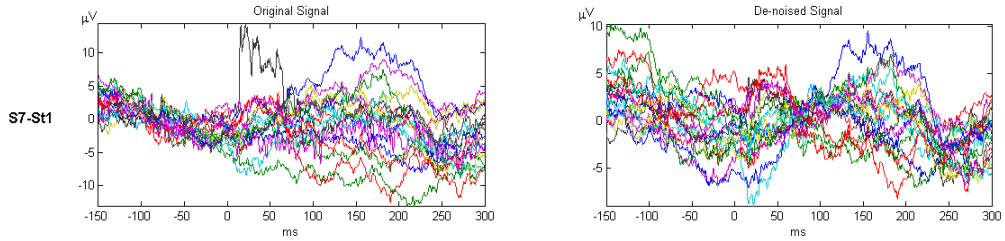

Figure G.14 Butterfly plots of both the original signal (left column) and the signal after removing the ICs related to one components of the CI artifact (right column). S7, female, recordings at 1 year and 4 months after implantation.

Appendix H. Publications arising from this research

Journal Paper

N. Castaneda-Villa, J.M. Cornejo, and C. J. James. "*Independent Component Analysis for robust assessment of auditory system maturation in children with cochlear implants*" Cochlear Implant International Journal. Published Online: Feb 2009.

N. Castañeda-Villa and C. J. James "*Independent component analysis for Auditory evoked potentials and cochlear implant artifact estimation: a comparison between High and Second order statistic algorithms*". (In preparation)

Conference papers

C.J. James and N. Castañeda-Villa. *"ICA of auditory evoked potentials of children with cochlear implants: component selection"*. 3rd International Conference MEDSIP 2006 Advances in Medical, Signal and Information Processing, 17-19 July, Glasgow, Scotland.

N. Castañeda-Villa and C. J. James. *"Objective source selection in Blind Source Separation of AEPs in children with Cochlear Implants"* 29th Annual International Conference of the IEEE Engineering in Medicine and Biology Society, 23-26 August 2007, Lyon France.

N. Castañeda-Villa and C. J. James. *"Differences in source analysis accuracy of AEP generators following FastICA and TDSEP-ICA de-noising"* 4th International Conference MEDSIP 2008 Advances in Medical, Signal and Information Processing, 14-16 July 2008 Santa Margherita Ligure, Italia.

N. Castañeda-Villa and C. J. James *"The selection of optimal ICA algorithm parameters for robust AEP component estimates using 3 popular ICA algorithms"* 30th Annual International Conference of the IEEE Engineering in Medicine and Biology Society "Personalized Healthcare through Technology" 20-24 August 2008 Vancouver, British Columbia.

Conference Abstracts

N. Castaneda-Villa, J.M. Cornejo-Cruz, and C. J. James. *"Assessment of the neurological maturation in children with CIs: Identification of AEPs by ICA"*. 10th International Conference on Cochlear Implants and Other Implantable Auditory Technologies, 10-12 April 2008, en San Diego, California, US (Poster).

N. Castaneda-Villa, J.M. Cornejo, P. Granados and C. Tirado. *"Cochlear implant fitting using middle latency auditory evoked potentials"* 11th International Conference on Cochlear Implants in Children, Charlotte NC, USA, 11-14 April 2008 (Oral Presentation)

N. Castañeda, C. James and J.M. Cornejo. *"Objective assessment of CI users by source analysis of LLAEPs peak P_1"* 12th International Conference on Cochlear Implants in Children, 17-20 June, 2009 Seattle, Washington.

References

[1] NeuroScan, "Synamps and STIM systems", *User Manuals*. Charlotte, NC, 2005.

[2] Polhemus, "3D Digitizer, high speed digitizer". *User manual*, Kaiserslautern, 2007.

[3] NeuroScan, "Curry, multi-modal neuroimaging and dipole source reconstruction" *User Manual*. Charlotte, NC, 2008.

[4] Brüel & Kjær," Precision sound level meter". *User manual*, Nærum, 2008.

[5] McConnell Brain Imaging Centre at the Montreal Neurological Institute," MRI brain datasets ", 2008.

[6] Electro-Cap Internationa Inc., "Electro-cap system", *Instruction manual*, Ohio, 2009.

[7] Cochlear," Cochlear Nucleus 24", *User manual*, Centennial, CO 2006.

[8] Advanced Bionics,"Clarion, Hi-Resolution Cochlear Implant", *User manual* Sylmar, CA, 2009.

[9] S. Amari, A. Cichocki, and H. Yang, "A new Learning Algorithm for Blind Source Separation", *Advances in Neural Information Processing Systems*, vol. 8, pp. 757-763, 2006.

[10] American Clinical Neurophysiology Society, "Guideline 8: Guidelines for recording clinical EEG on digital media," *J. Clin. Neurophysiol.*, vol. 23, no. 2, pp. 122-124, Apr.2006.

[11] American Clinical Neurophysiology Society, "Guideline 1: minimum technical requirements for performing clinical electroencephalography", *Am. J. Electroneurodiagnostic. Technol.*, vol. 46, no. 3, pp. 198-204, Sept.2006.

[12] American Clinical Neurophysiology Society, "Guideline 5: guidelines for standard electrode position nomenclature", *Am. J. Electroneurodiagnostic. Technol.*, vol. 46, no. 3, pp. 222-225, Sept.2006.

[13] American Clinical Neurophysiology Society, "Guideline 6: a proposal for standard montages to be used in clinical EEG", *Am. J. Electroneurodiagnostic. Technol.*, vol. 46, no. 3, pp. 226-230, Sept.2006.

[14] American Clinical Neurophysiology Society, "Guideline 9A: Guidelines on evoked potentials", *J. Clin. Neurophysiol.*, vol. 23, no. 2, pp. 125-137, Apr.2006.

[15] H. B. Barlow and J. D. Mollon, *The Senses*. Cambridge Cambridgeshire: Cambridge University Press, 1982.

[16] A. J. Bell and T. J. Sejnowski, "An information-maximization approach to blind separation and blind deconvolution", *Neural Comput.*, vol. 7, no. 6, pp. 1129-1159, Nov.1995.

[17] O. Bertrand, J. Bohorquez, and J. Pernier, "Time-frequency digital filtering based on an invertible wavelet transform: an application to evoked potentials", *IEEE Trans. Biomed. Eng*, vol. 41, no. 1, pp. 77-88, Jan.1994.

[18] J. R. Boston, "Spectra of Auditory Brainstem Responses and Spontaneous EEG", *IEEE Trans. Biomed. Eng*, vol. 28, no. 4 1981.

[19] A. P. Bradley and W. J. Wilson, "On wavelet analysis of auditory evoked potentials", *Clin. Neurophysiol.*, vol. 115, no. 5, pp. 1114-1128, May2004.

[20] C. Braun, S. Kaiser, W. E. Kincses, and T. Elbert, "Confidence interval of single dipole locations based on EEG data", *Brain Topogr.*, vol. 10, no. 1, pp. 31-39, 1997.

[21] R. F. Burkard, M. Don, and J. J. Eggermont, *Auditory Evoked Potentials. Basic principles and clinical applications* 2007.

[22] J. Cao, N. Murata, S. Amari, A. Cichocki, and T. Takeda, "Independent component analysis for single-trial MEG data decomposition and single-dipole source localization", *Neurocomputing*, vol. 49, pp. 255-277, 2002.

[23] J.-F. Cardoso, "Multidimensional Independent Component Analysis", Proceedings of ICASSP, pp. 1941-1944, 1998,.

[24] J.-F. Cardoso, "Blind Source Separation: Statistical Principles", Proceeding of the IEEE, vol 9 (10), pp. 2009-2025, 1998.

[25] J.-F. Cardoso, "Statistical principles of source separation", Proceeding of the SYSID, pp. 1837-184, 1997.

[26] J.-F. Cardoso and A. Soulomiac, "Blind beamforming for non Gaussian signals", *Proceeding of the IEEE*, vol. 140, pp. 362-370, 1993.

[27] N. Castaneda-Villa and C. J. James, "The selection of optimal ICA algorithm parameters for robust AEP component estimates using 3 popular ICA algorithms", *International Conference of the IEEE EMBS*, 2008.

[28] N. Castaneda-Villa and C. J. James, "Objective source selection in Blind Source Separation of AEPs in children with Cochlear Implants", *Conf. Proc. IEEE Eng Med. Biol. Soc.*, vol. 2007, pp. 6224-6227, 2007.

[29] Cichocki A, Amari S., Siwek K., Tanaka T, and Phan A H, "ICALAB Toolboxes", 2009.

[30] A. Cichocki and S. i. Amari, *Adaptive blind signal and image processing learning algorithms and applications*. Chichester: J. Wiley, 2002.

[31] P. Comon, "Independent component analysis –a new concept?", *Signal Processing*, vol. 36, pp. 287-314, 1994.

[32] Compumedics Neurosacan, *Curry User Manual multi-modal neuroimaging for Curry 6.* El Paso: 2007, pp. 1-258.

[33] R. J. Croft and R. J. Barry, "Removal of ocular artifact from the EEG: a review", *Neurophysiol. Clin.*, vol. 30, no. 1, pp. 5-19, Feb.2000.

[34] R. J. Croft and R. J. Barry, "EOG correction: which regression should we use?," *Psychophysiology*, vol. 37, no. 1, pp. 123-125, Jan.2000.

[35] B. N. Cuffin, "A method for localizing EEG sources in realistic head models", *IEEE Trans. Biomed. Eng*, vol. 42, no. 1, pp. 68-71, Jan.1995.

[36] B. N. Cuffin, "EEG localization accuracy improvements using realistically shaped head models", *IEEE Trans. Biomed. Eng*, vol. 43, no. 3, pp. 299-303, Mar.1996.

[37] B. N. Cuffin, "EEG dipole source localization", *IEEE Eng Med. Biol. Mag.*, vol. 17, no. 5, pp. 118-122, Sept.1998.

[38] Curry, "Multi-modal neuroimaging for Curry 6", Compumedics Neuroscan, El Paso, TX USA,2007.

[39] S. Debener, J. Hine, S. Bleeck, and J. Eyles, "Source localization of auditory evoked potentials after cochlear implantation", *Psychophysiology*, vol. 45, no. 1, pp. 20-24, Jan.2008.

[40] A. Delorme and S. Makeig, "EEGLAB: an open source toolbox for analysis of single-trial EEG dynamics including independent component analysis", *J. Neurosci. Methods*, vol. 134, no. 1, pp. 9-21, Mar.2004.

[41] M. F. Dorman, A. Sharma, P. Gilley, K. Martin, and P. Roland, "Central auditory development: evidence from CAEP measurements in children fit with cochlear implants", *J. Commun. Disord.*, vol. 40, no. 4, pp. 284-294, July 2007.

[42] G. H. Dunteman, *Principal components analysis*. Newbury Park: Sage Publications, 1989.

[43] B. Efron and R. J. Tibshirani, *An Introduction to Bootstrap*, Chapman & Hall/CRC, 1993.

[44] J. J. Eggermont and C. W. Ponton, "Auditory-evoked potential studies of cortical maturation in normal hearing and implanted children: correlations with changes in structure and speech perception", *Acta Otolaryngol.*, vol. 123, no. 2, pp. 249-252, Jan.2003.

[45] J. J. Eggermont, C. W. Ponton, M. Don, M. D. Waring, and B. Kwong, "Maturational delays in cortical evoked potentials in cochlear implant users", *Acta Otolaryngol*, vol. 117, no. 2, pp. 161-163, Mar. 1997.

[46] B. Everitt, *Cluster analysis*, 3rd ed. London: E. Arnold, 1993.

[47] M. Fuchs, J. Kastner, M. Wagner, S. Hawes, and J. S. Ebersole, "A standardized boundary element method volume conductor model," *Clin. Neurophysiol.*, vol. 113, no. 5, pp. 702-712, May 2002.

[48] M. Fuchs, M. Wagner, and J. Kastner, "Boundary element method volume conductor models for EEG source reconstruction", *Clin. Neurophysiol.*, vol. 112, no. 8, pp. 1400-1407, Aug 2001.

[49] M. Fuchs, M. Wagner, and J. Kastner, "Confidence limits of dipole source reconstruction results", *Clin. Neurophysiol.*, vol. 115, no. 6, pp. 1442-1451, June 2004.

[50] A. E. Geers, "Speech, language, and reading skills after early cochlear implantation", *Arch. Otolaryngol Head Neck Surg*, vol. 130, no. 5, pp. 634-638, May 2004.

[51] R. R. Gharieb and A. Cichocki, "Segmentation and tracking of the electro-encephalogram signal using an adaptive recursive bandpass filter", *Med. Biol. Eng Comput.*, vol. 39, no. 2, pp. 237-248, Mar. 2001.

[52] P. M. Gilley, A. Sharma, M. Dorman, C. C. Finley, A. S. Panch, and K. Martin, "Minimization of cochlear implant stimulus artifact in cortical auditory evoked potentials", *Clin. Neurophysiol.*, vol. 117, no. 8, pp. 1772-1782, Aug. 2006.

[53] A. L. Giraud, C. J. Price, J. M. Graham, and R. S. Frackowiak, "Functional plasticity of language-related brain areas after cochlear implantation", *Brain*, vol. 124, no. Pt 7, pp. 1307-1316, July 2001.

[54] A. L. Giraud, E. Truy, and R. Frackowiak, "Imaging plasticity in cochlear implant patients", *Audiol. Neurootol.*, vol. 6, no. 6, pp. 381-393, Nov. 2001.

[55] G. Gomez-Herrero, A. Gotchev, and K. Egiazarian, "Distortion Measures for Sparse Signals", *CompSysTech*, pp IIIB.9-1-9-6, 2005.

[56] A. D. Gordon, "A review of Hierarchical Classification", *Journal of the Royal Statistical Society*, vol. 150, no. 2, pp. 119-137, 1987.

[57] J. B. Green, W. W. Elder, and D. M. Freed, "The P1 component of the middle latency auditory evoked potential predicts a practice effect during clinical trials in Alzheimer's disease", *Neurology*, vol. 45, no. 5, pp. 962-966, May 1995.

[58] J. W. Hall, *Handbook of auditory evoked responses*. Boston: Allyn and Bacon, 1992.

[59] S. S. Haykin, *Unsupervised adaptive filtering*. New York: Wiley, 2000.

[60] P. He, G. Wilson, and C. Russell, "Removal of ocular artifacts from electro-encephalogram by adaptive filtering", *Med. Biol. Eng Comput.*, vol. 42, no. 3, pp. 407-412, May2004.

[61] P. He, G. Wilson, C. Russell, and M. Gerschutz, "Removal of ocular artifacts from the EEG: a comparison between time-domain regression method and adaptive filtering method using simulated data", *Med. Biol. Eng Comput.*, vol. 45, no. 5, pp. 495-503, May2007.

[62] L. H. Hemming, IEEE Electromagnetic Compatibility Society, and IEEE Antennas and Propagation Society, *Electromagnetic anechoic chambers: a fundamental design and specification guide*. Piscataway, NJ: IEEE Press, 2002.

[63] C. W. Hesse and C. J. James, "The FastICA Algorithm with Spatial Constraints", *IEEE Signal Processing*, vol. 12, pp. 792-795, 2005.

[64] J. Himberg, A. Hyvarinen, and F. Esposito, "Validating the independent components of neuroimaging time series via clustering and visualization", *Neuroimage.*, vol. 22, no. 3, pp. 1214-1222, July2004.

[65] J. Himberg and A. Hyvärunen, "ICASSO: software for investigating the reliability of ICA estimates by clustering and visualization", *NNSP*, pp 259-268, 2003.

[66] M. C. Hirsch and T. Kramer, *Neuroanatomy: 3D-stereoscopic atlas of the human brain*. Berlin: Springer, 1999.

[67] M. Hyde, "The N1 response and its applications", *Audiol. Neurootol.*, vol. 2, no. 5, pp. 281-307, Sept.1997.

[68] A. Hyvarinen, "New approximations of differential entropy for independent component analysis and projection persuit", *Advances in Neural Information Processing Systems*, vol. 10, pp. 273-279, 1998.

[69] A. Hyvarinen, P. O. Hoyer, and M. Inki, "Topographic independent component analysis", *Neural Comput.*, vol. 13, no. 7, pp. 1527-1558, July 2001.

[70] A. Hyvarinen and E. Oja, "Independent component analysis: algorithms and applications", *Neural Netw.*, vol. 13, no. 4-5, pp. 411-430, May 2000.

[71] A. Hyvarinen and E. Oja, "A fast Fixed-Point Algorithm for Independent component Analysis", *Neural Computation*, vol. 9, pp. 1483-1492, 1997.

[72] E. C. Ifeachor and B. W. Jervis, *Digital signal processing a practical approach*, 2nd ed. Harlow, England: Prentice Hall, 2002.

[73] C. J. James and N. Castaneda-Villa, "ICA of Auditory Evoked Potentials of children with Cochlear Implants: Component selection", MEDSIP, 2006.

[74] C. J. James and C. W. Hesse, "Independent component analysis for biomedical signals", *Physiol Meas.*, vol. 26, no. 1, p. R15-R39, Feb.2005.

[75] C. J. James and C. W. Hesse, "A Comparison of Time Structure and Statistically Based BSS Methods in the Context of Long-Term Epileptiform EEG Recordings", *Lecture Notes in Computer Science*, vol 3195, pp. 1025-1032, 2004.

[76] M. Jing and S. Sanei, "A novel constrained topographic independent component analysis for separation of epileptic seizure signals", *Comput. Intell. Neurosci.*, p. 21315, 2007.

[77] T. P. Jung, C. Humphries, T. W. Lee, S. Makeig, M. McKeown, V. Iragui, and T. Sejnowski, "Removing Electroencephalographic Artifacts: Comparison between ICA and PCA", *Neural Netw.*, vol. VIII, 1998.

[78] T. P. Jung, C. Humphries, S. Makeig, T. W. Lee, M. McKeown, V. Iragui, and T. Sejnowski, "Extended ICA Removes Artefacts from Electroencephalographic Recordings", *Advances in Neural processing Systems*, vol. 10, pp. 894-900, 1997.

[79] T. P. Jung, S. Makeig, C. Humphries, T. W. Lee, M. J. McKeown, V. Iragui, and T. J. Sejnowski, "Removing electroencephalographic artifacts by blind source separation", *Psychophysiology*, vol. 37, no. 2, pp. 163-178, Mar. 2000.

[80] T. P. Jung, S. Makeig, M. Westerfield, J. Townsend, E. Courchesne, and T. J. Sejnowski, "Removal of eye activity artifacts from visual event-related potentials in normal and clinical subjects", *Clin. Neurophysiol.*, vol. 111, no. 10, pp. 1745-1758, Oct.2000.

[81] A. Kanno, N. Nakasato, K. Nagamatsu, M. Iwasaki, K. Hatanaka, N. Murayama, and T. Yoshimoto, "Comparison of source localization for the P30m, P50m, and N100m peaks of the auditory evoked fields", *12th Int Conf on Biomagnetism*, pp 25-28, 2000.

[82] J. Katz, R. F. Burkard, and L. Medwetsky, *Handbook of clinical audiology*, 5th ed. Philadelphia: Lippincott Williams & Wilkins, 2002.

[83] L. Kaufman and P. J. Rousseeuw, *Finding groups in data an introduction to cluster analysis*. Hoboken, N.J: Wiley, 2005.

[84] A. S. Kelly, S. C. Purdy, and P. R. Thorne, "Electrophysiological and speech perception measures of auditory processing in experienced adult cochlear implant users," *Clin. Neurophysiol.*, vol. 116, no. 6, pp. 1235-1246, June2005.

[85] R. Kèonig, *The auditory cortex: a synthesis of human and animal research*. Mahwah, N.J: Lawrence Erlbaum Associates, 2005.

[86] A. Kraskov, H. Stogbauer, R. Andrzejak, and P. Grassberger, "Hierarchical clustering using mutual information", *Europhys. Lett*, vol. 70, no. 2, pp. 278-284, 2005.

[87] A. Kraskov, H. Stogbauer, and P. Grassberger, "Estimating mutual information", *Phys. Rev. E. Stat. Nonlin. Soft. Matter Phys.*, vol. 69, no. 6, June 2004.

[88] P. H. Laarne, M. L. Tenhunen-Eskelinen, J. K. Hyttinen, and H. J. Eskola, "Effect of EEG electrode density on dipole localization accuracy using two realistically shaped skull resistivity models", *Brain Topogr.*, vol. 12, no. 4, pp. 249-254, 2000.

[89] T. D. Lagerlund, F. W. Sharbrough, and N. E. Busacker, "Spatial filtering of multichannel electroencephalographic recordings through principal component analysis by singular value decomposition", *J. Clin. Neurophysiol.*, vol. 14, no. 1, pp. 73-82, Jan. 1997.

[90] T. D. Lagerlund, F. W. Sharbrough, C. R. Jack, Jr., B. J. Erickson, D. C. Strelow, K. M. Cicora, and N. E. Busacker, "Determination of 10-20 system electrode locations using magnetic resonance image scanning with markers", *Electroencephalogr. Clin. Neurophysiol.*, vol. 86, no. 1, pp. 7-14, Jan. 1993.

[91] T. W. Lee, M. Girolami, and T. J. Sejnowski, "Independent component analysis using an extended infomax algorithm for mixed subgaussian and supergaussian sources", *Neural Computation.* vol. 11, no. 2, pp 417-41, Feb.1999.

[92] P. Loizon, "Mimicking the human ear", *IEEE Signal Processing Magazine*, vol. 15, no. 5, pp. 101-130, 1996.

[93] S. Makeig, T. P. Jung, A. J. Bell, D. Ghahremani, and T. J. Sejnowski, "Blind separation of auditory event-related brain responses into independent components," *Proc. Natl. Acad. Sci. U. S. A*, vol. 94, no. 20, pp. 10979-10984, Sept. 1997.

[94] F. Meinecke, A. Ziehe, M. Kawanabe, and K. R. Muller, "A resampling approach to estimate the stability of one-dimensional or multidimensional independent components", *IEEE Trans. Biomed. Eng*, vol. 49, no. 12, pp. 1514-1525, Dec. 2002.

[95] A. M. Murro, J. R. Smith, D. W. King, and Y. D. Park, "Precision of dipole localization in a spherical volume conductor: a comparison of referential EEG, magnetoencephalography and scalp current density methods", *Brain Topogr.*, vol. 8, no. 2, pp. 119-125, 1995.

[96] R. Naatanen and T. Picton, "The N1 wave of the human electric and magnetic response to sound: a review and an analysis of the component structure", *Psychophysiology*, vol. 24, no. 4, pp. 375-425, July 1987.

[97] N. Nicolaou and S. Nasuto, "Comparison of Temporal and Standard Independent Component Analysis (ICA) Algorithms for EEG Analysis", *ICANN/ICONIP*, 2003.

[98] E. Niedermeyer and F. H. Lopes da Silva, *Electroencephalography, basic principles, clinical applications, and related fields*. Baltimore: Urban & Schwarzenberg, 1982.

[99] M. Nilsson, S. D. Soli, and J. A. Sullivan, "Development of the Hearing in Noise Test for the measurement of speech reception thresholds in quiet and in noise", *J. Acoust. Soc. Am.*, vol. 95, no. 2, pp. 1085-1099, Feb.1994.

[100] P. L. Nunez and R. Srinivasan, *Electric fields of the brain: the neurophysics of EEG*, 2nd ed. Oxford: Oxford University Press, 2006.

[101] C. Pantev, A. Dinnesen, B. Ross, A. Wollbrink, and A. Knief, "Dynamics of auditory plasticity after cochlear implantation: a longitudinal study", *Cereb. Cortex*, vol. 16, no. 1, pp. 31-36, Jan. 2006.

[102] C. Pantev, B. Ross, A. Wollbrink, M. Riebandt, K. W. Delank, E. Seifert, and A. Lamprecht-Dinnesen, "Acoustically and electrically evoked responses of the human cortex before and after cochlear implantation", *Hear. Res.*, vol. 171, no. 1-2, pp. 191-195, Sept. 2002.

[103] M. Pelizzone, "Auditory magnetic fields in cochlear-implant patients", *Physiol Meas.*, vol. 14 Suppl 4A, p. A81-A84, Nov. 1993.

[104] M. J. Peters and H. J. Wieringa, "The influence of the volume conductor on electric source estimation", *Brain Topogr.*, vol. 5, no. 4, pp. 337-345, 1993.

[105] T. W. Picton, S. Bentin, P. Berg, E. Donchin, S. A. Hillyard, R. Johnson, Jr., G. A. Miller, W. Ritter, D. S. Ruchkin, M. D. Rugg, and M. J. Taylor, "Guidelines for using human event-related potentials to study cognition: recording standards and publication criteria," *Psychophysiology*, vol. 37, no. 2, pp. 127-152, Mar. 2000.

[106] C. Ponton, J. J. Eggermont, D. Khosla, B. Kwong, and M. Don, "Maturation of human central auditory system activity: separating auditory evoked potentials by dipole source modeling," *Clin. Neurophysiol.*, vol. 113, no. 3, pp. 407-420, Mar. 2002.

[107] C. W. Ponton, M. Don, J. J. Eggermont, M. D. Waring, and A. Masuda, "Maturation of human cortical auditory function: differences between normal-hearing children and children with cochlear implants", *Ear Hear.*, vol. 17, no. 5, pp. 430-437, Oct. 1996.

[108] C. W. Ponton and J. J. Eggermont, "Of kittens and kids: altered cortical maturation following profound deafness and cochlear implant use", *Audiol. Neurootol.*, vol. 6, no. 6, pp. 363-380, Nov. 2001.

[109] C. W. Ponton, J. J. Eggermont, B. Kwong, and M. Don, "Maturation of human central auditory system activity: evidence from multi-channel evoked potentials," *Clin. Neurophysiol.*, vol. 111, no. 2, pp. 220-236, Feb. 2000.

[110] H. Pratt, D. Urbach, and N. Bleich, "Auditory brainstem evoked potentials peak identification by finite impulse response digital filters", *Audiology*, vol. 28, no. 5, pp. 272-283, 1989.

[111] S. Purdy and A. Kelly, "Cortical auditory evoked potential testing in infants and young children," *The New Zealand Audiological Society Bulletin*, vol. 11, pp. 16-24, 2001.

[112] S. C. Purdy, A. S. Kelly, and P. R. Thorne, "Auditory evoked potentials as measures of plasticity in humans", *Audiol. Neurootol.*, vol. 6, no. 4, pp. 211-215, July 2001.

[113] T. Rosburg, N. N. Boutros, and J. M. Ford, "Reduced auditory evoked potential component N100 in schizophrenia--a critical review", *Psychiatry Res.*, vol. 161, no. 3, pp. 259-274, Dec. 2008.

[114] J. T. Rubinstein, "How cochlear implants encode speech", *Curr Opin Otolaryngol Head Neck and Surg*, vol. 11, pp. 16-24, 2005.

[115] J. Sarvas, "Basic mathematical and electromagnetic concepts of the biomagnetic inverse problem", *Phys. Med. Biol.*, vol. 32, no. 1, pp. 11-22, Jan. 1987.

[116] C. J. Scarff, J. C. Dort, J. J. Eggermont, and B. G. Goodyear, "The effect of MR scanner noise on auditory cortex activity using fMRI", *Hum. Brain Mapp.*, vol. 22, no. 4, pp. 341-349, Aug. 2004.

[117] C. J. Scarff, A. Reynolds, B. G. Goodyear, C. W. Ponton, J. C. Dort, and J. J. Eggermont, "Simultaneous 3-T fMRI and high-density recording of human auditory evoked potentials", *Neuroimage.*, vol. 23, no. 3, pp. 1129-1142, Nov. 2004.

[118] A. Sharma, M. F. Dorman, and A. Kral, "The influence of a sensitive period on central auditory development in children with unilateral and bilateral cochlear implants", *Hear. Res.*, vol. 203, no. 1-2, pp. 134-143, May2005.

[119] A. Sharma, K. Martin, P. Roland, P. Bauer, M. H. Sweeney, P. Gilley, and M. Dorman, "P1 latency as a biomarker for central auditory development in children with hearing impairment", *J. Am. Acad. Audiol.*, vol. 16, no. 8, pp. 564-573, Sept.2005.

[120] L. Stanberry, R. Nandy, and D. Cordes, "Cluster analysis of fMRI data using dendrogram sharpening", *Hum. Brain Mapp.*, vol. 20, no. 4, pp. 201-219, Dec.2003.

[121] H. Stogbauer, R. Andrzejak, A. Kraskov, and P. Grassberger, "Reliability of ICA Estimates with Mutual Information", *Lecture Notes in Computer Science*, pp. 209-216, 2004.

[122] M. A. Svirsky, A. M. Robbins, K. I. Kirk, D. B. Pisoni, and R. T. Miyamoto, "Language development in profoundly deaf children with cochlear implants", *Psychol. Sci.*, vol. 11, no. 2, pp. 153-158, Mar. 2000.

[123] A. C. Tang, B. A. Pearlmutter, N. A. Malaszenko, and D. B. Phung, "Independent components of magnetoencephalography: single-trial response onset times", *Neuroimage.*, vol. 17, no. 4, pp. 1773-1789, Dec. 2002.

[124] A. C. Tang, M. T. Sutherland, and C. J. McKinney, "Validation of SOBI components from high-density EEG", *Neuroimage.*, vol. 25, no. 2, pp. 539-553, Apr. 2005.

[125] N. V. Thakor, X. R. Guo, Y. C. Sun, and D. F. Hanley, "Multiresolution wavelet analysis of evoked potentials", *IEEE Trans. Biomed. Eng*, vol. 40, no. 11, pp. 1085-1094, Nov. 1993.

[126] H. G. Van, B. Vanrumste, M. D'Have, W. R. Van de, I. Lemahieu, and P. Boon, "Influence of measurement noise and electrode mislocalisation on EEG dipole-source localisation", *Med. Biol. Eng Comput.*, vol. 38, no. 3, pp. 287-296, May 2000.

[127] B. Vanrumste, G. Van Hoey, R. Van de Walle, P. Van Hese, M. D'Havé, P. Boon, and I. Lemahieu, "The Realistic versus the spherical head model in EEG Dipole Source Analysis in the presence of noise", *Proceedings-23rd Annual Conference-IEEE/EMBS*, 2001.

[128] R. Vigario, J. Sarela, V. Jousmaki, M. Hamalainen, and E. Oja, "Independent component approach to the analysis of EEG and MEG recordings", *IEEE Trans. Biomed. Eng*, vol. 47, no. 5, pp. 589-593, May 2000.

[129] R. N. Vigario, "Extraction of ocular artefacts from EEG using independent component analysis," *Electroencephalogr. Clin. Neurophysiol.*, vol. 103, no. 3, pp. 395-404, Sept. 1997.

[130] M. D. Waring, C. W. Ponton, and M. Don, "Activating separate ascending auditory pathways produces different human thalamic/cortical responses", *Hear. Res.*, vol. 130, no. 1-2, pp. 219-229, Apr. 1999.

[131] K. Whittingstall, G. Stroink, L. Gates, J. F. Connolly, and A. Finley, "Effects of dipole position, orientation and noise on the accuracy of EEG source localization", *Biomed. Eng Online.*, vol. 2, p. 14, June 2003.

[132] J. L. Wunderlich and B. K. Cone-Wesson, "Maturation of CAEP in infants and children: a review", *Hear. Res.*, vol. 212, no. 1-2, pp. 212-223, Feb. 2006.

[133] J. L. Wunderlich, B. K. Cone-Wesson, and R. Shepherd, "Maturation of the cortical auditory evoked potential in infants and young children", *Hear. Res.*, vol. 212, no. 1-2, pp. 185-202, Feb. 2006.

[134] F. G. Zeng, A. N. Popper, and R. R. Fay, *Cochlear implants: auditory prostheses and electric hearing*. New York: Springer, 2004.

[135] A. Ziehe and K. R. Muller, "TDSEP- an efficient algorithm for blind separation using time structure", ICANN, pp. 675-680, 1998.